Hydrodynamic modelling of sediment transport and bedform formation on the NW Irish shelf

By

Will Evans
B.Sc. (hons), Marine Science, University of Ulster, 2011

Thesis submitted for the degree of Doctor of Philosophy

School of Environmental Sciences
Faculty of Life and Health Sciences
University of Ulster
Coleraine

May 2018

I confirm that the word count of this Thesis is less than 100,000 words

Table of Contents

Acknowledgements

I would like to extend my gratitude to my Ph.D. supervisors, Dr. Sara Benetti and Prof. Derek Jackson for their constant support and assistance throughout this research project. I could not have carried out this work without their understanding, expertise and open-door policy. I would also like to thank Dr. Rory Quinn for kindling my interest in marine mapping at an undergraduate level and providing an honest but supportive sounding board throughout my research. I have been influenced and educated by many individuals throughout my studies, Dr. Aggie Georgiopolou, Dr. Ruth Plets and Dr. Marianne O'Connor have all contributed to my decision to undertake this Ph.D. and aided me in seeing it through to completion. Thanks also to Dr. Chris McGonigle and Jay Calvert, who have provided me with constant friendship, support and perspective on what I am trying to achieve with this research. This project was funded by the Department of Education and Learning, with additional funding obtained from the International Association of Sedimentologists postgraduate grants (2012) and Ulster's Environmental Science Research Institute (2012). Special thanks must be extended to the Marine Institute, Ireland and its personnel, both afloat and ashore. Further to providing a wealth of datasets, the awarding of a Shiptime Grant (2013) and Networking Grant (2012) significantly aided the development of my research in the field of sediment dynamics. Suzie Clarke of Danish Hydraulic Institute, UK (DHI) deserves special mention, with unparalleled patience she guided me through hydrodynamic modelling complications. In tandem with this I would also like to thank Dr. Colin Anderson,

who maintained the HPC and enabled my software to utilise this resource to the full.

Without the help, financial support and encouragement of my mother and late father, my decision to pursue my interest in the marine environment would simply not have been possible.

I dedicate this work to my late father, William Snr.

Summary

Much of our knowledge of sediment transport on the northwest Irish shelf was hypothesised in the 1970's with limited resources and without the benefit of modern seafloor mapping equipment and techniques (Kenyon and Stride, 1970). Utilising existing and newly generated data sets, this research focuses on modern sediments located on the north Irish shelf between 54º - 56ºN the aim of which is to establish connections between bedform morphology, sediment distribution and modelled hydrodynamics in order to describe sediment transport processes from a shelf to bedform scale.

Interrogation of multibeam echosounder data has enabled classification of 8 depositional and 2 erosional bedform types (Evans et al., 2015). Many of these bedforms overlap those glacial formations identified in previous research (Benetti et al., 2010b, Dunlop et al., 2011, O'Cofaigh et al., 2012).

Classification of backscatter data has identified 5 sedimentary classes across the shelf, with gravel dominating the inshore areas and large soft sediment deposits concentrated in proximity to moraine features and areas of bathymetric lows.

These mapping techniques applied alongside outputs from a sediment transport specific, hydrodynamic model created as part of this research, have led to a number of novel findings and challenges to existing research.

The location of bedload parting zones presented by (Belderson et al., 1982) are challenged and a new location suggested based on bedform distribution, bedform geometry and modelled current data.

It is also proposed that bedforms south of the Malin Deep in 130 m water depth, previously described as ‘active’ by (Dunlop et al., 2011) , are relict in nature due to insufficient flow velocities in the area to mobilise the sediments of which they are comprised (Terwindt and Brouwer, 1986).

It is hypothesised that a change in orientation of identified sediment lineations is a sedimentary record of the point of incursion onto the Irish shelf by the European Slope Current (ESC), a longstanding oceanographic feature (Fernand et al., 2006, White and Bowyer, 1997). This change of orientation occurs ~55º30’N and correlates with literature on the ESC, model and oceanographic data (Souza et al., 2001).

On a bedform scale, repeat bathymetric surveys have revealed a wide range of sediment wave migration rates. Utilising a new ESRI Arc GIS based technique, these rates were accurately measured across the shelf with highest rates of ~ 8 m yr^{-1} displayed by giant sandwaves 14 km north of Malin Head. Through analysis of repeat survey data, these same waves display a rotary migration pattern. Located on an offshore tidal sandbank (Caston, 1972), sandwaves rotate around a central point, driven by currents connected to a nearby tidal sound (Sanay et al., 2007). It is hypothesised that these currents are the primary means of soft sediment retention in an otherwise gravel dominated area of shelf (Williams et al., 2000, Zhu and Chang, 2000).

The multidisciplinary approach adopted by this research, including bathymetric, backscatter, sedimentary, seismic and hydrodynamic model data, reveals new approaches to examining and insights into the sediment transport processes on the northwest Irish shelf.

Abbreviations

ADCP	Acoustic Doppler Current Profiler
ARA	Angular Response Analysis
AVG	Angle Varied Gain
BIIS	British Irish Ice Sheet
BPI	Bathymetric Position Indices
CTD	Conductivity Temperature Depth
DHI	Danish Hydraulic Institute
EEZ	Economic Exclusion Zone
EMODNET	European Marine Observation and Data Network
ESC	European Shelf Current
GIS	Geographic Information System
GSI	Geological Survey of Ireland
HPC	High Powered Computer
IHO	International Hydrographic Organisation
INFOMAR	INtegrated mapping FOr the sustainable development of Ireland's MArine Resource
INSS	Irish National Seabed Survey
JIBS	Joint Irish Bathymetric Survey
MBES	MultiBeam Echo Sounder
MESH	Mapping European Seabed Habitats
ROMS	Regional Ocean Modeling System
RV	Research Vessel
STABLE	Sediment transport & Boundary Layer Equipment

Notes on access to contents

I hereby declare that with effect from the date on which the thesis is deposited in the Research Office of the University of Ulster, I permit

- The librarian of the university to allow the thesis to be copied in whole or in part without reference to me on the understanding that such authority applies to the provision of single copies made for study purposes or for inclusion within the stock of another library.

The thesis to be made available through the Ulster Institutional Repository and/or EThOS under the terms of the Ulster eTheses Deposit Agreement which I have signed.

It is a condition of use of this thesis that anyone who consults it must recognise that the copyright rests with the author and that no quotation from the thesis and no information derived from it may be published unless the source is properly acknowledged.

Chapter 1 – Introduction

1.1 Investigation of sediment transport in the marine environment

Our knowledge of sediment transport in the marine environment has been derived from a combination of field measurements (Allen, 1965, Kenyon and Stride, 1970), laboratory experiments (Folk, 1954), numerical models (Hjulstrom, 1935, Shields, 1936) and governing equations from other areas of research (Lewis, 1980).

Several factors are known to influence the initiation of sediment transport. The characteristics of the sediment should be considered, including; grain size, density, packing, sorting and shape. Likewise, the fluid itself should be taken into account with density, viscosity, velocity and turbulence all having an effect on sediment transport ability (Miller et al., 1977, Shields, 1936). As a fluid moves over sediment, it exerts a frictional force. When the correct combination of the above factors is reached, particles of sediment will reach a ‘threshold’ point and begin to move (Hjulstrom, 1935). Through the work of (Hjulstrom, 1935), (Shields, 1936), (Miller et al., 1977), (Wilcock, 1993) and others, it is possible to place a value on the friction or stress required to mobilise a sediment of known size.

This bed stress value can be calculated using the following equation (Shields, 1936).

$$\tau_c = \frac{1}{2}\rho f_c V^2$$

τ_c = bed shear stress (N/m2)

ρ = density of fluid (kg/m3)

V = mean current velocity (m/s)

f_c= current friction factor (composed of water depth and bed roughness)

Values can then be compared to derived tables such as that created by (Julien, 2002) below (Fig 1.1).

Particle classification name	Ranges of particle diameters		Shields parameter (dimensionless)	Critical bed shear stress (τ_c) (N/m^2)
	φ	mm		
Coarse cobble	-7 – -8	128 – 256	0.054 – 0.054	112 – 223
Fine cobble	-6 – -7	64 – 128	0.052 – 0.054	53.8 – 112
Very coarse gravel	-5 – -6	32 – 64	0.05 – 0.052	25.9 – 53.8
Coarse gravel	-4 – -5	16 – 32	0.047 – 0.05	12.2 – 25.9
Medium gravel	-3 – -4	8 – 16	0.044 – 0.047	5.7 – 12.2
Fine gravel	-2 – -3	4 – 8	0.042 – 0.044	2.7 – 5.7
Very fine gravel	-1 – -2	2 – 4	0.039 – 0.042	1.3 – 2.7
Very coarse sand	0 – -1	1 – 2	0.029 – 0.039	0.47 – 1.3
Coarse sand	1 – 0	0.5 – 1	0.033 – 0.029	0.27 – 0.47
Medium sand	2 – 1	0.25 – 0.5	0.048 – 0.033	0.194 – 0.27
Fine sand	3 – 2	0.125 – 0.25	0.072 – 0.048	0.145 – 0.194
Very fine sand	4 – 3	0.0625 – 0.125	0.109 – 0.072	0.110 – 0.145
Coarse silt	5 – 4	0.0310 – 0.0625	0.165 – 0.109	0.0826 – 0.110
Medium silt	6 – 5	0.0156 – 0.0310	0.25 – 0.165	0.0630 – 0.0826
Fine silt	7 – 6	0.0078 – 0.0156	0.3 – 0.25	0.0378 – 0.0630

Fig 1.1 Table relating sediment classification, grain size (mm of phi) and bed stress (τ_C) in N/m^2 required to initiate transport (Julien, 2002).

A number of empirical curves have also been created in an attempt to better visualise these thresholds. The curve present here by (Hjulstrom, 1935) is an example of this, illustrating the flow velocity (cm/s) required to initiate transport of given sediments (Fig. 1.2).

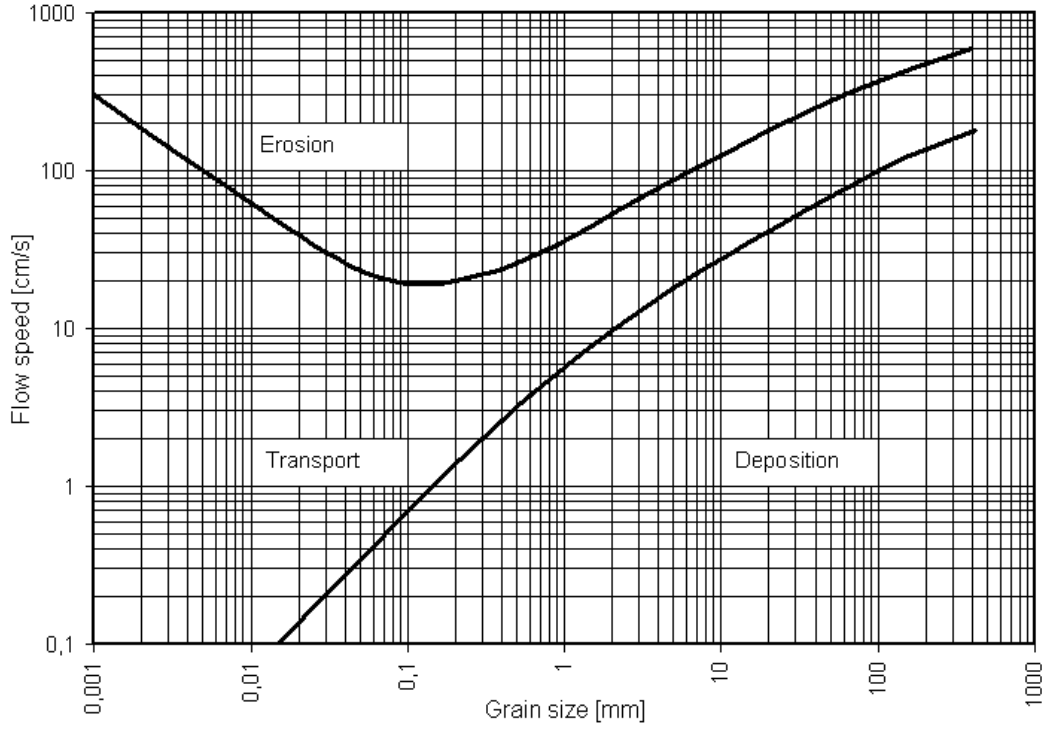

Fig 1.2 Hjulstrom Curve designed to visualise the relationship between grain size (mm) and flow speed (cm/s). The cohesive properties of silts and clays (0.001 – 0.064 mm) require increased energy to initiate erosion when compared to larger, non-cohesive sediments (Hjulstrom, 1935).

Once this threshold is reached, marine sediments are known to move either as bedload or as suspended load. Bedload typically occurs in sands and gravels and manifests itself as particles rolling, sliding or by saltation (Bartholdy et al., 2010c). Silts and clays are most often transported as suspended load, either held in the water column by turbulence or as a dissolved water constituent (Lefebvre et al., 2014).

How this transport generates the range of bedforms identified in shelf environments is part of a dynamic balance between available sediments, tidal currents and in some cases wave energy (Cataño-Lopera and García, 2006). Not unlike dune formation processes in rivers, marine bedform development is initiated by transport of several grains into a patch just several grains higher

than the surrounding sediment (Perillo et al., 2014). This change in morphology is referred to as a pertubation by (Besio et al., 2008a). As water flows around this pertubation a recirculation cell is created. When net transport of sediment is directed towards this perturbation, a crest is formed. This crest grows in amplitude, is manipulated by hydrodynamic conditions and a bedform is formed (Besio et al., 2008a, Gerkema, 2000, Perillo et al., 2014).

(Allen, 1965) placed this theory into a marine sediment wave context in his description of how particles move across a typical sand wave. Grains are forced upslope on the stoss side of the wave due to current velocity and resulting friction (Fig. 1.3). Upon crossing the crest, flow velocity drops, causing the sediment to accumulate on the lee side, either avalanching down the wave face or by settling out of suspension down current (Bartholdy et al., 2010a, Cataño-Lopera and García, 2006, Mazumder, 2003).

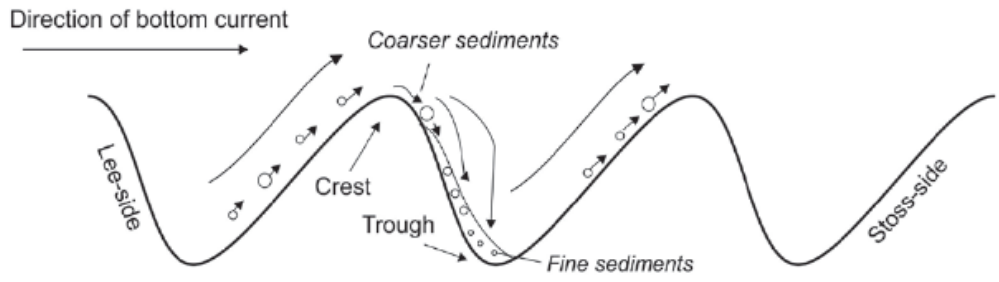

Fig. 1.3 Adapted from (Allen, 1965). Migration of sediment grains up the stoss slope and deposition on the lee side. Note coarser grains travel less distances down the lee slope than finer sediments.

The theory of sediment transport and genesis of bedforms serve as a foundation for shelf sediment surveys and the analysis of the data they generate.

Investigations into the distribution of seafloor sediments began in the Victorian era, when bathymetric soundings with leaded line (Mayer, 2006, Quinn and

Boland, 2010) were supplemented by attempts to recover seafloor samples to document seafloor sediment differences on navigational charts. Over a century, advances in marine acoustics, driven by military needs during the world wars, prompted modern pioneering surveys in shallow shelf environments (Lurton, 2002, McGonigle et al., 2009, Quinn, 2000). As a result, a more complete picture of shelf bathymetry, sediment distribution and bedform formations was developed. At the forefront of shelf-scale sedimentary investigations was the use of acoustic side scan sonar to map seafloor morphology, identify bedforms and classify sediment distributions around the UK and Ireland (Belderson et al., 1982, Kenyon and Stride, 1970). This globally significant work greatly advanced the understanding of sedimentary processes on modern day shelves by establishing key models and supporting evidence, illustrating mechanisms for seafloor mobility. This pioneering work describing sedimentary deposits and making deductions regarding the relationship between bedform asymmetry, grain size, current flow and transport pathways still forms the basis for modern day sedimentary shelf science (Barnard et al., 2013, Van Landeghem et al., 2009b). The bedform matrix diagram (Belderson et al., 1982) classifies the various sedimentary formations and links them directly to bottom current regime (Fig. 1.4).

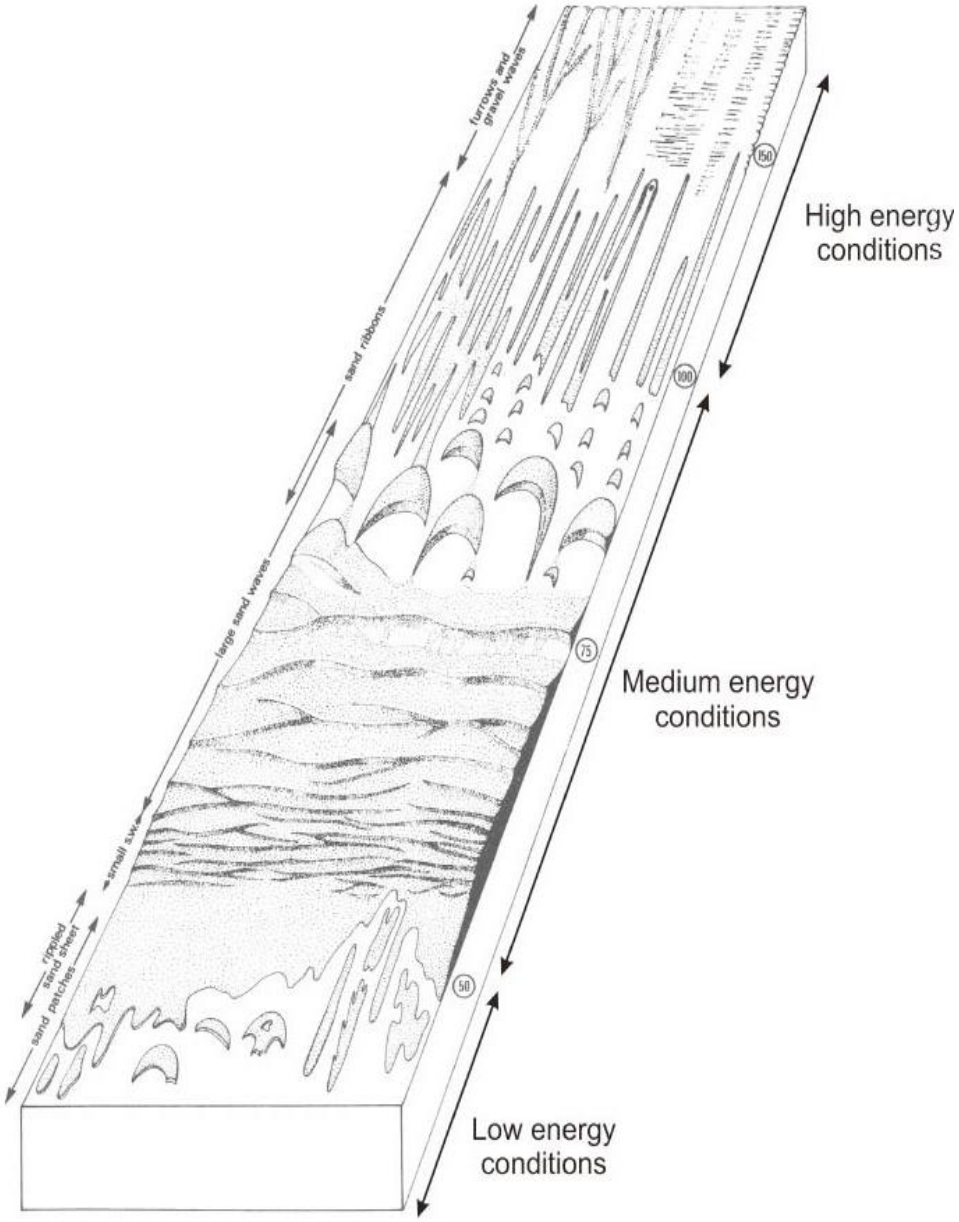

Fig. 1.4 (Belderson et al., 1982) bedform matrix. Bedforms created by currents on the continental shelf and related to mean spring peak near-surface currents in cms^{-1} (circles)

The orientation and shape of these bedforms was revealed to be key in understanding migration rate and direction, with asymmetry of shape being one of the central measures. Bedform asymmetry is described as the variation in ratio between a gently sloping, longer stoss slope and a steeper, shorter lee slope (Fig. 1.5). As discussed in relation to the theory of sediment transport, movement typically follows a stoss to lee direction with a steeper lee angle

suggesting high mobility (Allen, 1965, Belderson et al., 1982, Caston, 1972), a model which is continually re-evaluated and refined (Knaapen et al., 2005, Lobo et al., 2000, Van Landeghem et al., 2012). Steeper slopes generate higher transport rates due to increased volumes of sediment entering suspension at the crest (Bartholdy et al., 2010c, Lefebvre et al., 2014). Equal length (symmetrical) and gently-angled wave slopes thus indicate a low mobility rate (Ferret et al., 2010, Van Landeghem et al., 2012).

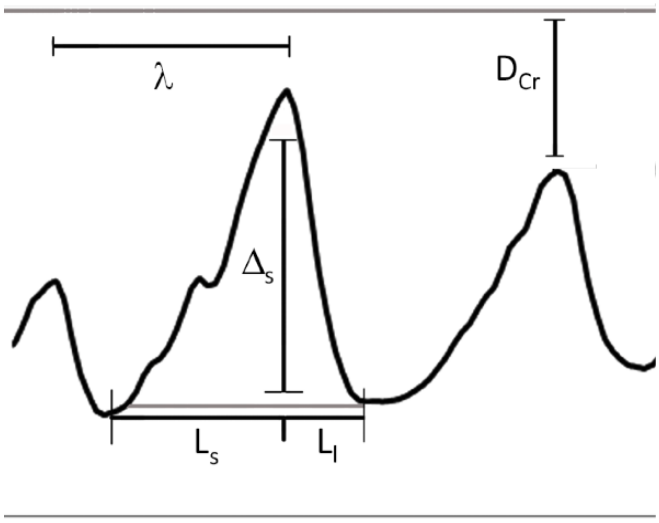

Fig. 1.5. Diagram of commonly used description for bedform geometry.
λ = Wavelength, Δ_s = wave height, L_s = stoss slope, L_l = lee slope, D_{cr} = crest depth.

While these early investigations helped inform the basic principles of bedform development, as technology and seagoing capability has improved, so has the quality of seafloor data and how it is interpreted. While side scan instruments are still used to great effect (Wewetzer, 1999), modern marine investigations typically utilise a suite of state of the art instruments to gather a complete picture of the seafloor. Modern hydrographic standard surveys often adopt multibeam echosounder (MBES) as primary equipment in collecting depth data,

resulting in the most complete and robust charts (Barnard et al., 2013, Li and King, 2007, McGonigle et al., 2009, Plets et al., 2011, Shaw et al., 2014). MBES enables swath coverage of tracts of seafloor, covering greater area in a lot more detail than single point echosounder data (Brown and Blondel, 2009, Marks and Smith, 2009). This creates multiple soundings over an area (controlled by vessel speed, water depth, beam width and acoustic amplitude) resulting in a high-resolution image of the seafloor with an up to centrimetric resolution depending on weather conditions at time of survey and the type of system used. The high accuracy of MBES in both the horizontal and the vertical has resulted in the instrument's increased use as a method to study and monitor the seafloor, either to measure movement or to confirm a stable sedimentary environment (Knaapen et al., 2005, Knaapen and Hulscher, 2002, Ma et al., 2014, Németh et al., 2002). It can therefore be argued that the results of a single survey have limited value in fully understanding a mobile sediment environment and they are only valid at time of survey (Barrie and Conway, 2014). By conducting sequential surveys, time-lapse imagery of the seafloor can be generated. Repeat survey reveals differences in seafloor bathymetry, direction and rate of bedform migration and a means of quantifying net accretion or erosion of substrates provided all surveys are corrected to the same datum (Barrie et al., 2009, Knaapen and Hulscher, 2002, Van Landeghem et al., 2012). This technique has proved particularly useful when considering sediment mobility and scouring around installations such as pipelines or piers (Morelissen et al., 2003, Schmitt et al., 2007). It has also been adopted as a method to confirm the direction and rate of sediment wave movement, acting as a check on asymmetry-based assumptions (Barnard et al.,

2013, Van Landeghem et al., 2009b, Van Landeghem et al., 2012). In situ techniques have been employed to monitor changes in seafloor such as the Sediment Transport and Boundary Layer Equipment (STABLE) lander, which has proved highly effective in calculating turbulence and bedstress in coastal waters (Huthnance et al., 2002). Likewise other seafloor mounted methods have used noise in acoustic signal to monitor concentrations of suspended sediment to give indication of transport potential (Betteridge et al., 2008). Equipment such as STABLE is, however, expensive, data cannot be monitored until the instruments are recovered, and in energetic environments there is the potential for damage or loss when mooring specialised instruments. This risk and the ability to monitor data quality on the fly are just two reasons repeat MBES surveys have come to the fore in the field of seafloor monitoring.

The result of these advances in technology and techniques with which to investigate marine sediments is that previous work in the field can be challenged and improved. An update to Belderson's bedform matrix is one such improvement. Including the bedforms identified in Belderson et.al., 1982, Stow et. al., 2009 improves the matrix by including bedform formation as a function of grain size (mm) and flow velocity ms^{-1} (Fig. 1.6). Derived from 69 different investigations, this improved matrix utilises data unavailable to Belderson et. al., 1982 in the 1970's.

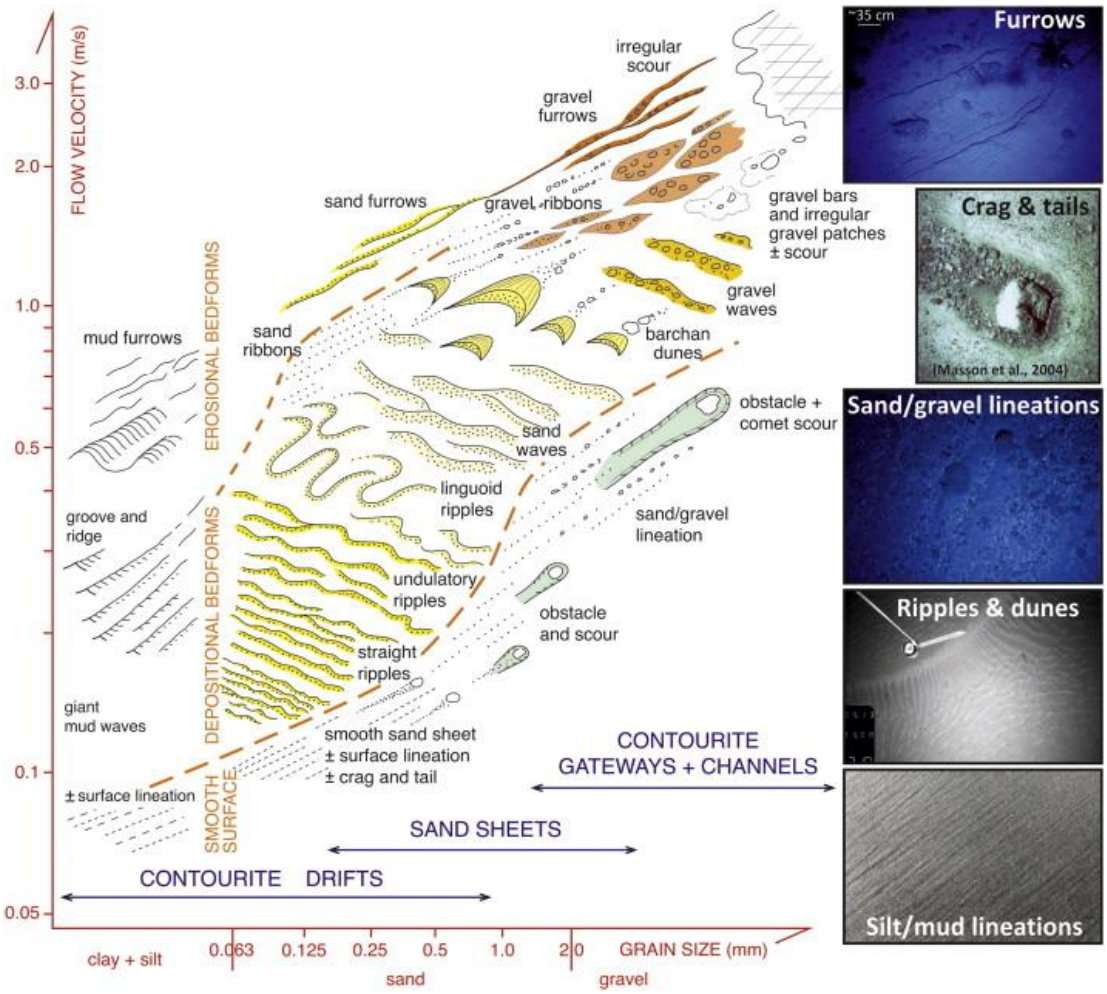

Fig. 1.6 (Stow et al., 2009) bedform velocity matrix representing bedforms occurrence under specific near seafloor velocities (m/s) and grain size (mm).

As further studies into sediment transport are conducted, resulting in more comprehensive data, early assumptions on seafloor mobility are being challenged. One such assumption is the direction of bedform migration based on asymmetry. Through use of repeat MBES in the Irish Sea, (Van Landeghem et al., 2012) demonstrated that 18% of over 200 sediment waves surveyed, moved in the direction of their stoss slope rather than the expected lee direction (reversed – asymmetry migration). Antidunes do present an example of the this process however these form in fast flow, with large Froude numbers (Kennedy,

2006) well in excess of those measured by (Van Landeghem et al., 2012). While possible causes such as internal feedback between waves or influence of superimposed sediment waves were suggested, it is accepted that further research is required to fully explain how reversed – asymmetry migration can occur in the Irish Sea environment.

Interestingly many of these early surveys, through to the state-of-the-art mapping programs, have occurred in UK and Irish waters due to a relatively shallow shelf environment and variable tidal currents. These surveys have helped to inform some of the shelf sedimentary processes in the region.

An advantage in utilising MBES is the capability to measure the strength of signal return (dB) from the seafloor, known as backscatter. Differing seabed sediments affect the strength of signal return by absorbing or reflecting acoustic energy to varying extents (Fig. 1.7). The variance in this response can give indication of grain size, sound speed, density, porosity and volume of the seafloor sediments (Brown and Blondel, 2009). At a basic level, rocky areas provide high-energy returns while soft muds absorb the signal energy, creating a low backscatter return (Blondel and Gómez Sichi, 2009, Fonseca et al., 2009, Lamarche et al., 2011, Sacchetti et al., 2011). Two main approaches to the processing of this signal return are feature-based image analysis and examination of relationships between acoustic response and ground-truthed measurements (geoacoustic) (Brown and Blondel, 2009). As computational capability increases, use of specialist software packages to undertake processing and classification of backscatter data is increasingly common (McGonigle and Collier, 2014). This is not without issue and image-based analysis software such as ESRI ArcGIS and QTC Multiview can be thought to

be a less accurate means than feature-based approaches to analyse acoustic response due to the averaging of responses across the data set during processing. The angular response of backscatter acoustic signal can be processed by software programs like CARIS and Geocoder and applied to a standardised model, generating an anticipated sediment type at a specific point (McGonigle et al., 2010b, Rzhanov et al., 2012). Angular response can, however, be affected by a number of factors including data quality and environmental influences. As a result, there are increasing uses for a combination of signal and image-based analysis to fully interrogate backscatter data sets (Hasan et al., 2012). By collecting sediment samples in an area of backscatter coverage, it is possible to further refine this relationship by correlating grain size with acoustic response. By using grain size to ‘train’ classification of backscatter response, data from only a few sampling stations can inform sediment distribution across a large area. This can prove an invaluable method to infer sediment distribution in areas where ground truth data is unavailable (Goff et al., 2000, McGonigle and Collier, 2014)

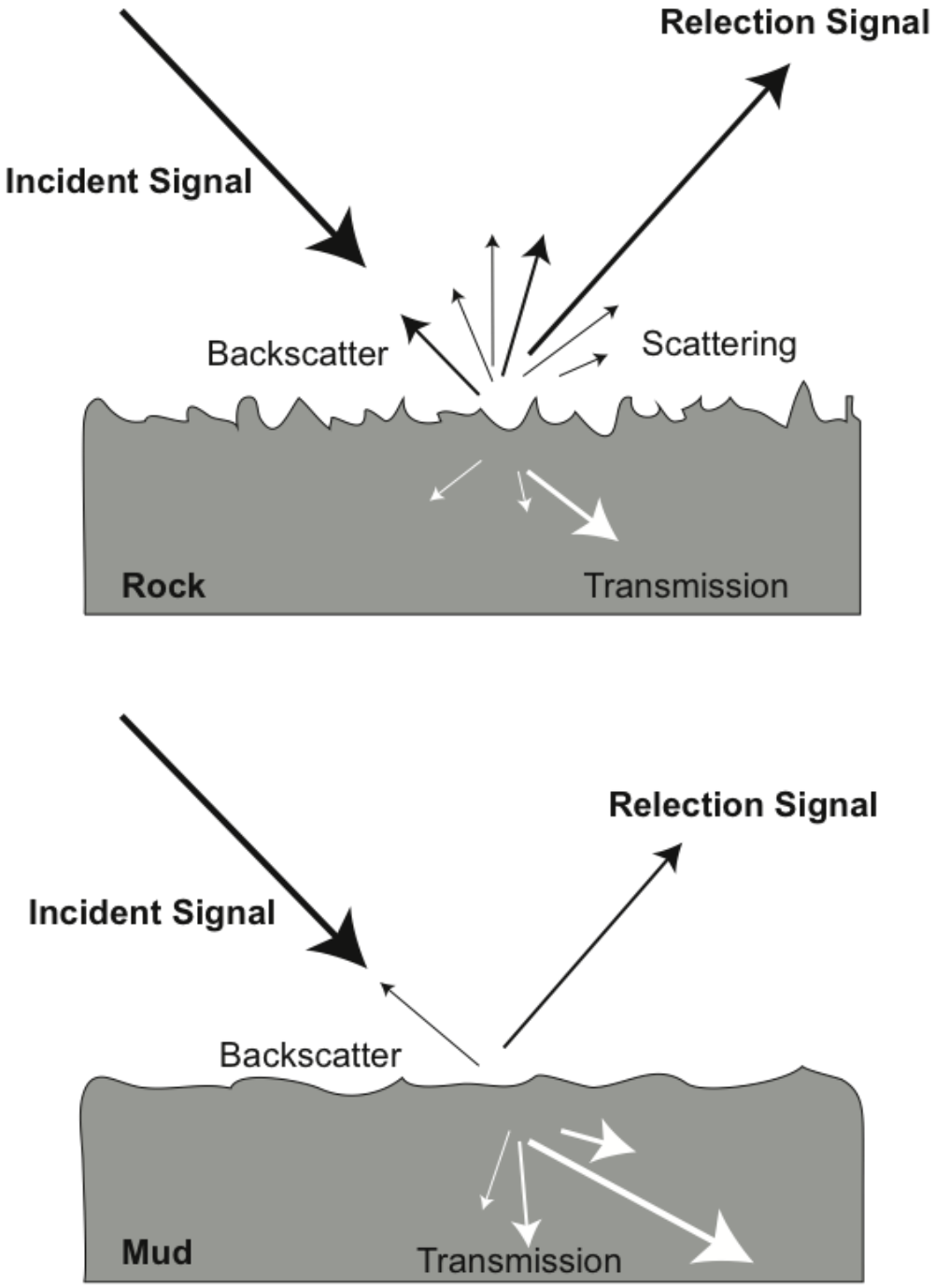

Fig. 1.7 Differing backscatter response to variation in sediment type. Typically, rugose rock surfaces create increased scattering. The hard surface promotes reflection with little transmission into substrate. The result is a high backscatter response. Mud, typically smooth surfaced and soft in composition enhances transmission resulting in little scattering, poor reflection and low backscatter responses.

The mobilisation costs of scientific vessels, the difficulties associated with equipment deployment and recovery and inaccessibility of some study areas coupled with advances in computational ability have led to the increasing use of numerical modelling as an alternative to field measurements in the marine environment (Gunn and Stock-Williams, 2013, Staneva et al., 2009). Ability to forecast oceanographic processes have enabled identification of upcoming storm-surge and tidal events, changes in future water temperature and other key parameters (Shan et al., 2011, Sheng and Yang, 2010). Hindcasting of this data has also key to oceanographic research enabling analysis of globally significant changes over time, such as palaeotidal ranges and sea level or sea temperature changes (Brooks et al., 2008, Ward et al., 2015). Global ocean models have been in existence since the early 80's, increasing in realism as computational power has developed. While these models provide an excellent overview of large-scale phenomenon such as El Niño or the North Atlantic Oscillation, it has long been recognised that it is the shelf and coastal regions that are the centres of biological productivity, chemical cycling and socio-economic importance and that these models are not adequate to show oceanographic variability at the required scale (Staneva et al., 2009, Wu et al., 2011, Young et al., 2011).

As a result, the development of coastal modelling has come to the fore, with resolutions of <1 km within confined bays and inlets. These regional models have also undergone a period of evolution as software, hardware and our understanding of hydrodynamics have improved. With a need to accurately resolve complex coastline and bathymetry, terrestrial runoff and other key factors, these coastal models represent a smaller domain but typically have

much higher computational requirements than coarse resolution global models (Staneva et al., 2009).

It is on these coastal scales (and smaller) that hydrodynamic models are utilised to assess sediment transport and similarly to large-scale models, this is often due to unfeasible collection of field data. Typically sediment transport models have a specific, localised focus and these can include dispersal of contaminants (Callaway et al., 2011a), smothering of commercially important fishery grounds (Liu and Huang, 2009), accretion or erosion often objects such as piers and pipelines (Morelissen et al., 2003) or the effects of human interference with natural currents by introducing structures for marine renewables (Thiébot et al., 2015). Central to these simulations is the ability to calculate both bed load transport, through bed stress and suspended transport, by flow velocity (Wu et al., 2011). As discussed, bed stress τ_c (N/m^2) controls the intensity and pathway of bed transport and is a function of fluid density ρ (kg/m^3), mean current V (m/s) and current friction f_c. Current friction is controlled by water depth and bed roughness. These inputs are typically generated within a hydrodynamic simulation itself (unless otherwise specified) with the exception of bed roughness, which must be provided as an external input in order to improve accuracy of model outputs.

Many of these methods of investigating the seafloor have been applied to mapping programs globally (Dong et al., 2011, Ferrini and Flood, 2005, Schimel et al., 2015, Shaw et al., 2014, Zhu and Chang, 2000). These have not only provided an excellent baseline for future scientific studies, but also an insight into sediment transport processes across the shelf.

1.2. Recent mapping on The Irish Continental Shelf

The Irish National Seabed Survey (INSS), a joint venture between the Marine Institute Ireland (MI) and the Geological Survey of Ireland (GSI), began in 2000 and started with the outer margins of Ireland's Economic Exclusion Zone (EEZ) and worked inshore to the 200m contour. Split into three zones, 'Deep Water (435,000 km^2), 'Near Shore' (30,500 km^2) and 'Coastal' (3000 km^2), this €32 million project required significant resource to complete (www.gsiseabed.ie).

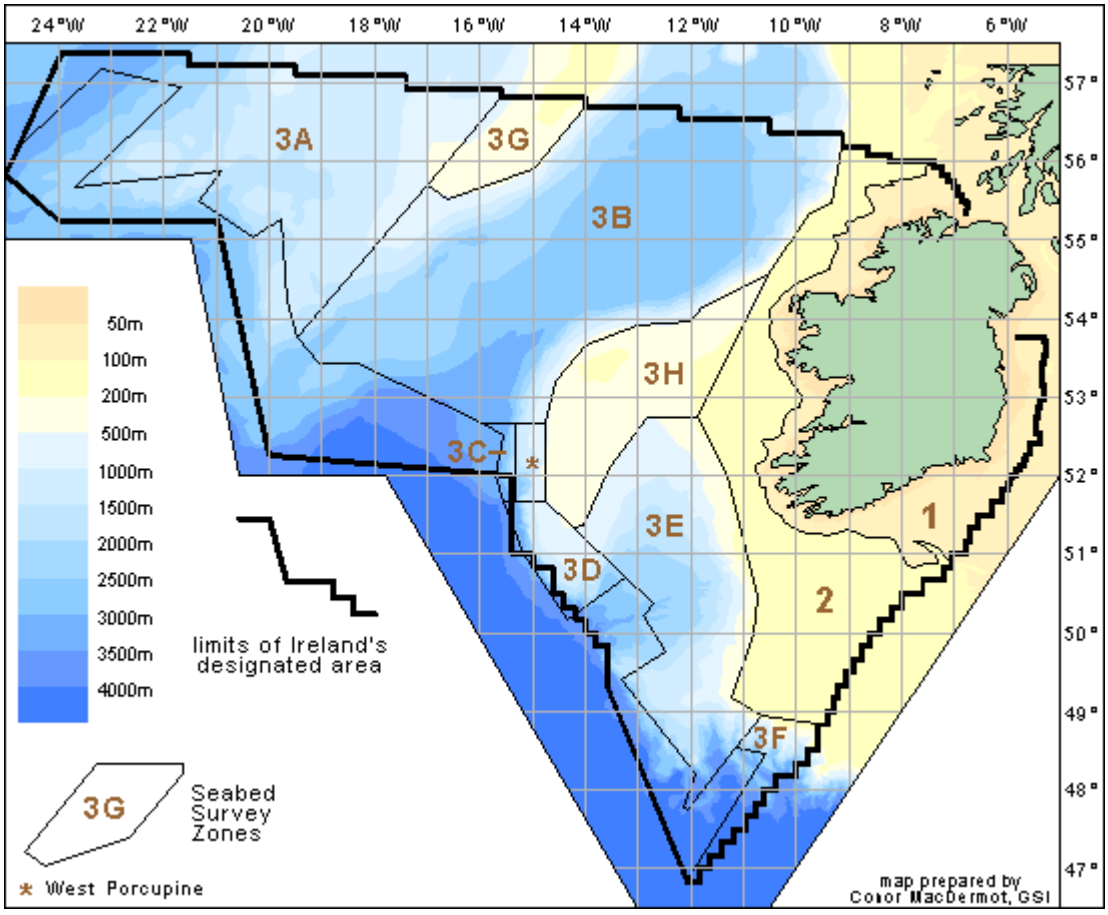

Fig. 1.8. Deep water (3), Nearshore (2) and Coastal zones (1) mapped during INSS survey. Mapping of area 1 has continued through the INFOMAR program and is still in progress.

This survey included not just MBES data, but also magnetic and gravity readings, shallow seismics, Conductivity Temperature Depth (CTD) measurements of the water column, sidescan imaging and seabed ground truthing samples. The result is an excellent baseline dataset, which has encouraged development in the field of marine science, as well as revealing many untapped resources contained within Ireland's offshore EEZ. While the INSS achieved coverage of 81% of Irish waters, it was identified that a successor program would be required to map the commercially significant inshore waters and embayments.

As a result, in 2006, the INtegrated mapping FOr the sustainable development of Ireland's MArine Resource began. Similar to the INSS, a range of methodologies and equipment are utilised as part of INFOMAR's ongoing survey. Due to the nature of MBES survey methods and narrowing swath widths in shallower water depths, this program was a great deal more labour intensive despite covering a smaller (125,000 km^2) area (www.infomar.ie, 2016).

The resulting data has also been utilised by associated projects such as the European Marine Observation and Data Network (EMODNET) and the Mapping European Seabed Habitats (MESH) programs. The most significant of these associated projects to this thesis is the Joint Irish Bathymetric Survey (JIBS). This joint project between the Maritime Coastguard Agency, Marine Institute and Northern Ireland Environment Agency was funded by INTERREG IIIA and was intended to provide a baseline bathymetric dataset to not only update hydrographic charts of the area but also as a resource for multiple stakeholders such as maritime archaeologists and marine renewable engineers. Spanning April 2007 to October 2008, the JIBS survey achieved full coverage multibeam

data up to 3 nautical miles offshore between Fanad Head (Co. Donegal, Republic of Ireland) and Torr Head (Co. Antrim, Northern Ireland) (Westley et al., 2011).

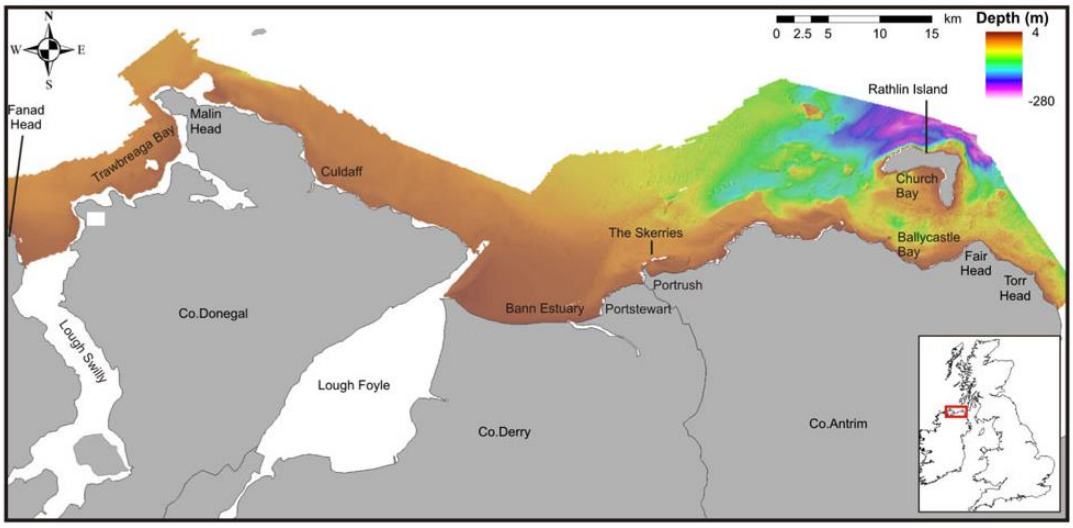

Fig.1.9. Bathymetric data from JIBS survey. Stretching from Fanad Head in the west to Torr Head in the east, depths range from <10m to 280m. Figure modified from (Westley et al., 2011).

This data revealed a wealth of bedforms, shipwrecks, geological structures and insight into archaeologically significant submerged landscapes (Plets et al., 2011, Westley et al., 2011). It has also been utilised as a baseline dataset for site selection of potential marine renewable engineering projects (Rourke et al., 2010). The north Irish shelf is the north westerly extreme of the European shelf margin with the Atlantic Ocean. Flanked by the Rockall Trough to the west, and the Malin Deep to the north (Fig. 1.10), the shelf extends east to the Scottish coast and the narrow North Channel entrance to the Irish Sea (Dunlop et al., 2011, O'Cofaigh et al., 2012, Xing and Davies, 1998). MBES mapping programmes have revealed detailed insight into the variability in depth across the study area. To the west, depth ranges down to 200 m at the shelf break, where a steep decline in bathymetry reaches maximum water depths of ~3000

m in the Rockall Trough (Sacchetti et al., 2011). To the north, a less marked decline into the Malin Deep extends down to 250 m water depth (Szpak et al., 2012). Moving east towards the Scottish Hebrides, the shelf narrows (<15 km) (Cooper et al., 2002) and water depth varies reaching a maximum of 250 m close to the North Channel. The waters surrounding Ireland also contains a multitude of islands, 27 of which are on the north Irish shelf (www.infomar.ie, 2016). These islands present not only an often dramatic change in bathymetry, but also a controlling factor on localised currents (Pingree and Maddock, 1979, Rourke et al., 2010).

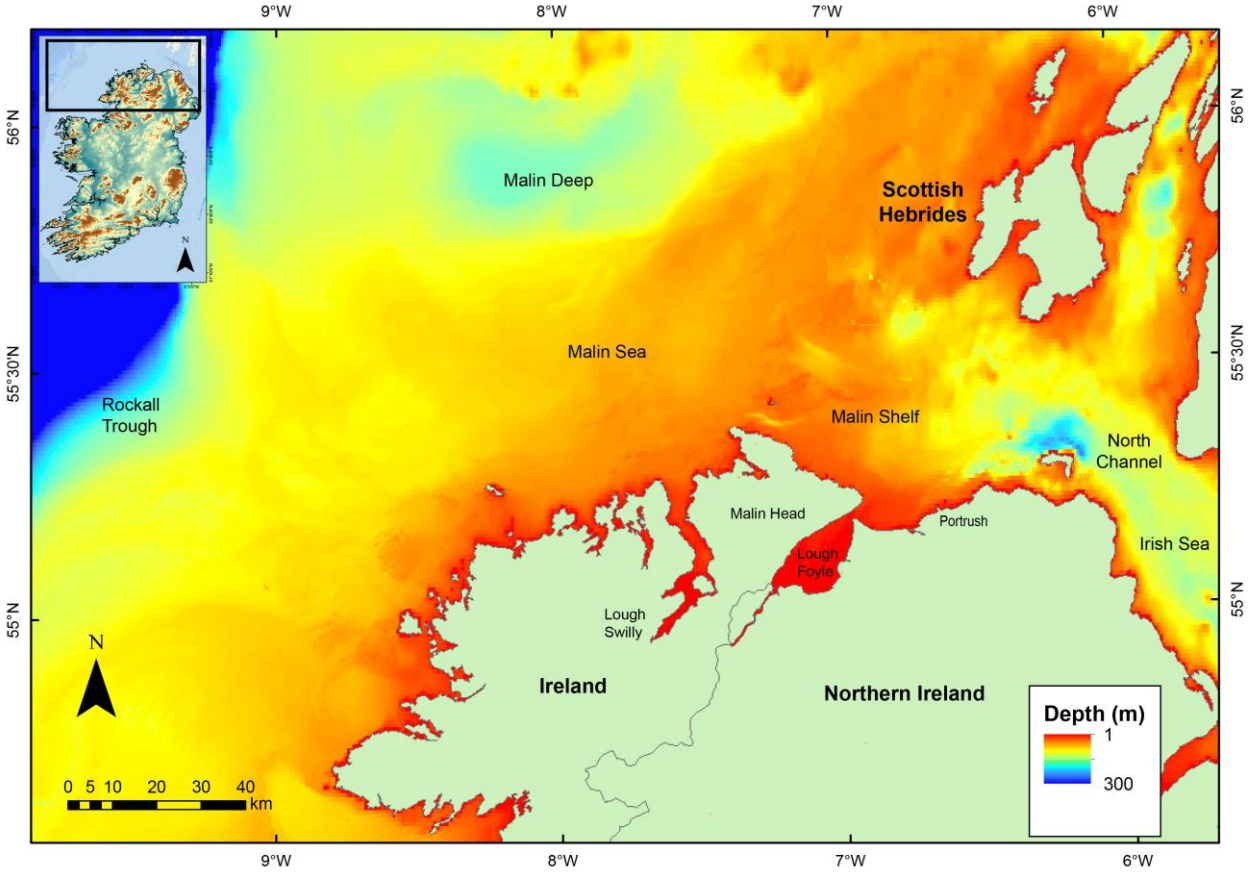

Fig.1.10. Extent of study area on the north Irish shelf. The shelf break to the west is marked by a sharp increase in bathymetry. The narrow North Channel and Irish Irish Sea are included to provide context to hydrodynamic regime discussion. Bathymetry is derived from INSS, INFOMAR and GEBCO data sets (www.gsiseabed.ie, www.infomar.ie, 2016, IOC et al., 2003)

The high resolution of these data sets has also revealed previously unidentified features on the seafloor including glacial formations, which have significant effect on seafloor morphology across much of the shelf. The identification and orientation of these glacial features is key to the reconstruction of the British Irish Ice Sheet extent and has revealed an extensively glaciated shelf on which ice coverage extended to the shelf break (Benetti et al., 2010b, Dunlop et al., 2011, O'Cofaigh et al., 2012, Sacchetti et al., 2012). The result is a large volume of glacial material distributed widely across the shelf. During analysis of geophysical data for glacial features, modern, potentially active sediments and bedforms were also identified (Dunlop et al., 2010). Grouped into sand ribbons, sand patches and sediment waves, these ‘modern’ bedforms were assumed to be active (Dunlop et al., 2010).

1.3 North Irish Shelf Sediment Transport

As with the oceanographic investigations on the north and west Irish shelf, sediment transport research in this area has been sparse in comparison to other Irish waters. The early work of (Kenyon and Stride, 1970) represents the only sediment transport study which encompasses the entire study area presented here. This extensive survey mapped distribution of bedforms, primarily sand ribbons and sand patches on the north Irish shelf. The orientation of the majority of these bedforms enabled the identification of a bed parting point north of Lough Swilly with an easterly migration pattern west of this point. To the west, pathways are less well defined but generally follow the coastline and depth contours. As noted previously, not all bedforms matched the principle

tidal current regime and were identified as relict feature from previous tidal conditions or having an additional formative parameter(s). Lastly, it was suggested that the combination of currents and bedforms meant that sandy sediments were accumulating and trapped on the Malin Shelf (Kenyon and Stride, 1970). Other comments on transport potential mechanisms come from investigations focused on other fields such as ice sheet advance and retreat research. These are typically based on assumptions derived from bedform asymmetry, e.g. the classification of ‘active’ bedforms on the southern edge of the Malin Deep by (Dunlop et al., 2011). While there have been numerous sediment transport studies in the inshore relating to areas of soft coastline, some of which discuss an offshore sediment budget, recent shelf scale studies have been limited to the hydrodynamic simulations of (Davies and Xing, 2002). As a result, knowledge of sediment transport on a shelf scale is limited.

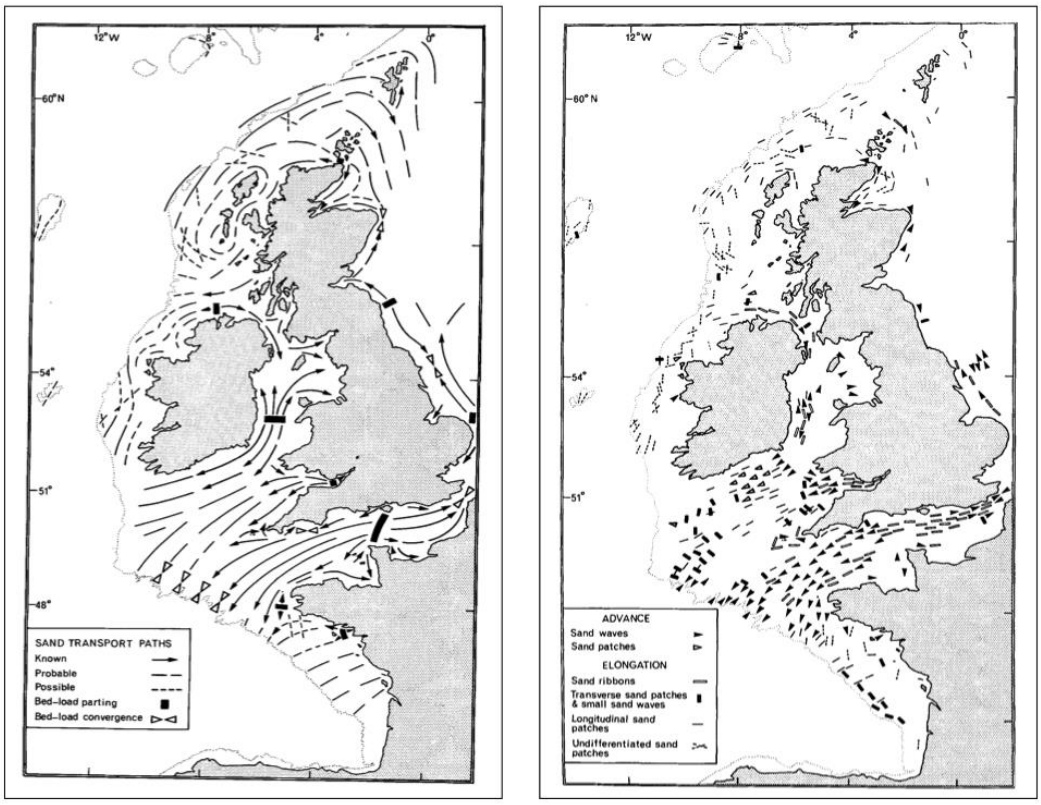

Fig, 1.11. (Belderson et.al., 1982), (A) Generalised transport paths based on tidal data and bedform geometry. Note the Bed-load parting occurrence on the north Irish shelf. (B) Classification of bedforms identified in side scan sonar data. Orientation of symbols indicates inferred direction of advance based on bedform asymmetry.

Many of the scientific cruises on the north Irish shelf collected backscatter and sedimentary data as part of their research campaigns. The result is full coverage, backscatter data complimented by a wide distribution of point sedimentary data with which to infer surface sediment composition. As a consequence, backscatter data has revealed distribution of hard and soft sediment across the entire shelf, albeit without defining the sediment composition. Much of the backscatter response across the shelf is high, suggesting exposed bedrock, pebbles and gravels are prevalent. Localised patches of low response do occur. These softer sediments are confined to the Malin Deep area, a large bathymetric depression occurring around 55º20’N, and isolated patches to the southwest of the study area.

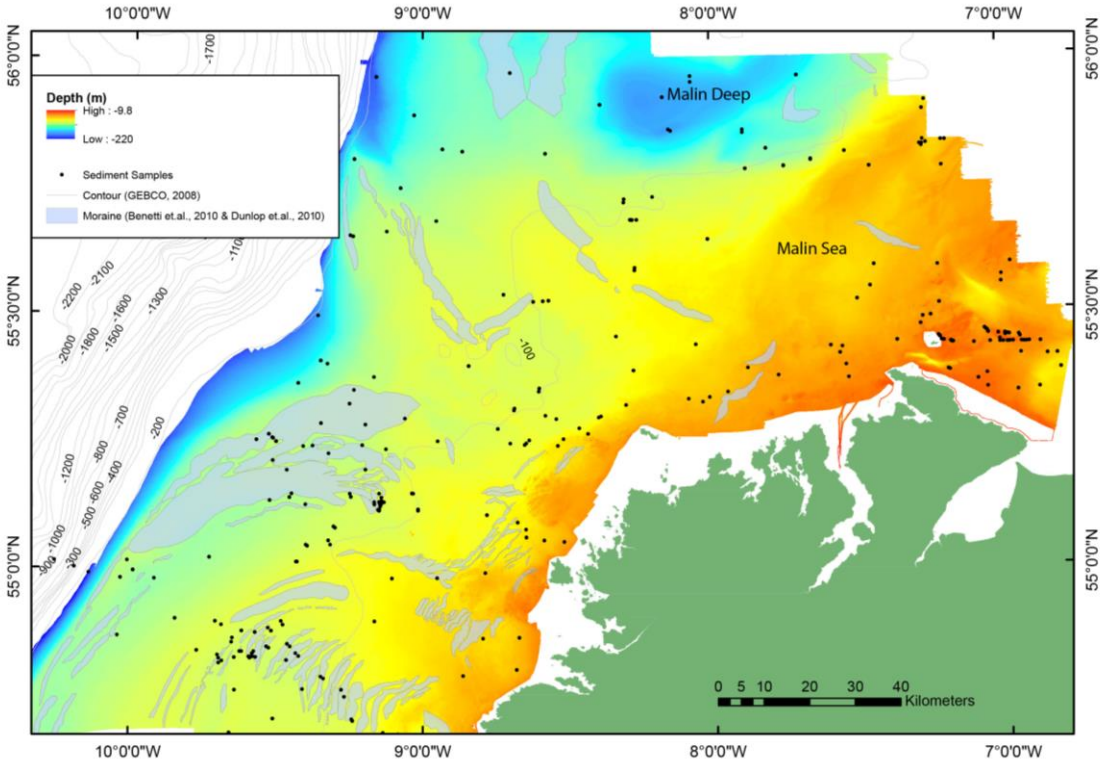

Fig. 1.12. Bathymetric map of the north west Irish shelf with depths ranging <10 m inshore to 220m at the shelf break. Distributions of main glacial moraines are included for context. Location of sediment samples used for backscatter classification are also indicated.

Due to the nature of backscatter data, only the seafloor surface component of the signal is insonified which can result in underlying sediments becoming masked by a thin drape of differing grain size (Goff et al., 2000, McGonigle et al., 2009). As a result, the acoustic response you may associate with the glacial sediments of a large moraine, typically comprised of tightly packed diamict, may be masked by a drape of modern sandy sediments. On such a heavily glaciated margin it is important to consider the interaction of modern sediments with underlying glacial formations, especially if these interactions modify key indicators of ice sheet progression or regression (Dunbar et al., 1985).

1.4 Oceanography and hydrodynamics

Measuring hydrodynamic forces and oceanographic processes that occur across the Irish shelf is complicated by the highly energetic nature of the NE Atlantic (Cooper et al., 2004, Lozano et al., 2004), making the deployment of vessels and equipment hazardous. The tidal range in north Irish shelf range is from microtidal (<2 m) to mesotidal (<4 m) and are dominated by the M2 and S2 phases (Cooper et al., 2004, Uehara et al., 2006). These tidal ranges coupled with frequent storms, mean that this part of Irish coastline is exposed to high energies of 10^{11}- 10^{12} J/m/y (Jackson et al., 2005).

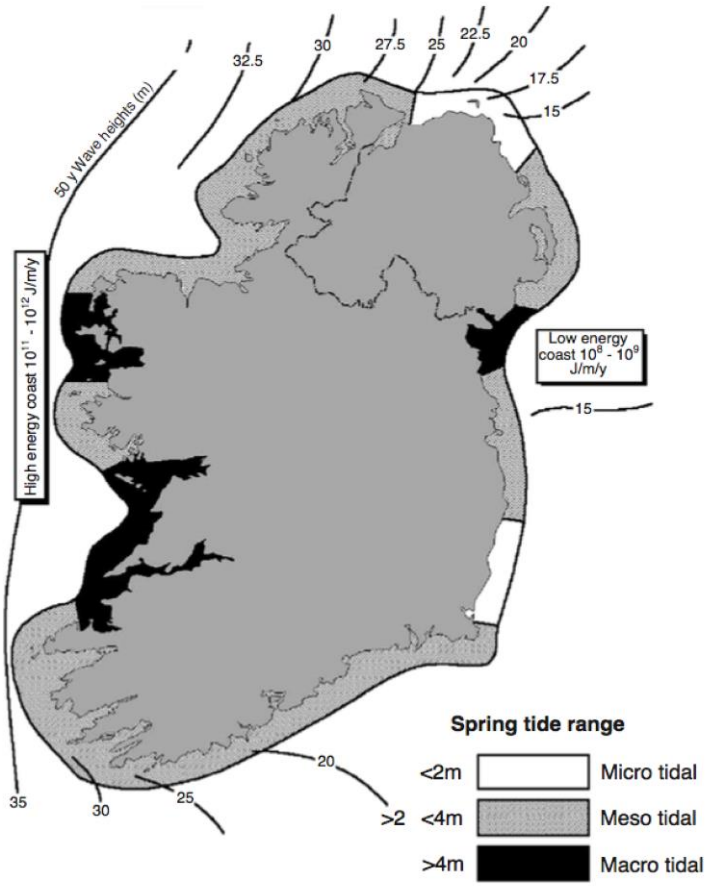

Fig. 1.13 Distribution of tidal ranges (m), wave heights (m) and energy (J/m/y) around the Irish coast. Adapted from (Jackson et al., 2005). The study area largely experiences Mesotidal ranges <4 m.

As a result, investigations into the oceanography of the waters north and west of Ireland historically have been significantly fewer, lower in resolution and constrained by seasonality in comparison to other Irish shelf regions (McMahon, 1995, White and Bowyer, 1997). The result is a lack of detailed understanding of shelf processes on the west and north Irish shelf (Raine, 2014). The *in situ* Conductivity Temperature Depth (CTD) transects from sampling campaigns in the early 90's did however reveal a strong thermohaline front separating coastal and oceanic waters on the shelf (McMahon, 1995). From year round sampling it also became apparent that seasonality has significant effects on the shelf's hydrodynamic regime (Pingree et al., 1999). This requirement for higher resolution, inter-seasonal data, coupled with the adverse weather conditions in winter months, resulted in a reliance upon remote sensing to study oceanographic conditions in the area (Fernand et al., 2006; Inall et al., 2009; Pingree & Sinha, 1999). The Langrangian and Eularian floats, CTD's and Acoustic Doppler Current Profilers (ADCP's) utilised in these various campaigns presented a more complete picture of oceanographic processes on the Irish Shelf. (Fernand et al., 2006) attributed between 13-25% of surface flows to wind forcing, highlighting the influence of tides and long standing current regime on water movement in the area. However, it is also clear that the complexity of coastline on the west and north coast of Ireland, including outlying islands, creates significant localised effects on water transport which are difficult to quantify in a large scale investigations (Pingree and Maddock, 1979).

Aside from seasonal variation, the most prominent oceanographic feature associated with the western Irish shelf is the European Slope Current (ESC). Described as a relatively warm and saline flow (Hill and Mitchelson-Jacob,

1993), the ESC was first described in oceanographic studies without being recognised as a current (Booth and Meldrum, 1987, Gowen et al., 1998), or identified as a permanent feature on the shelf (McMahon, 1995). As a result, the ESC received little attention until the late 1990's (White and Bowyer, 1997).

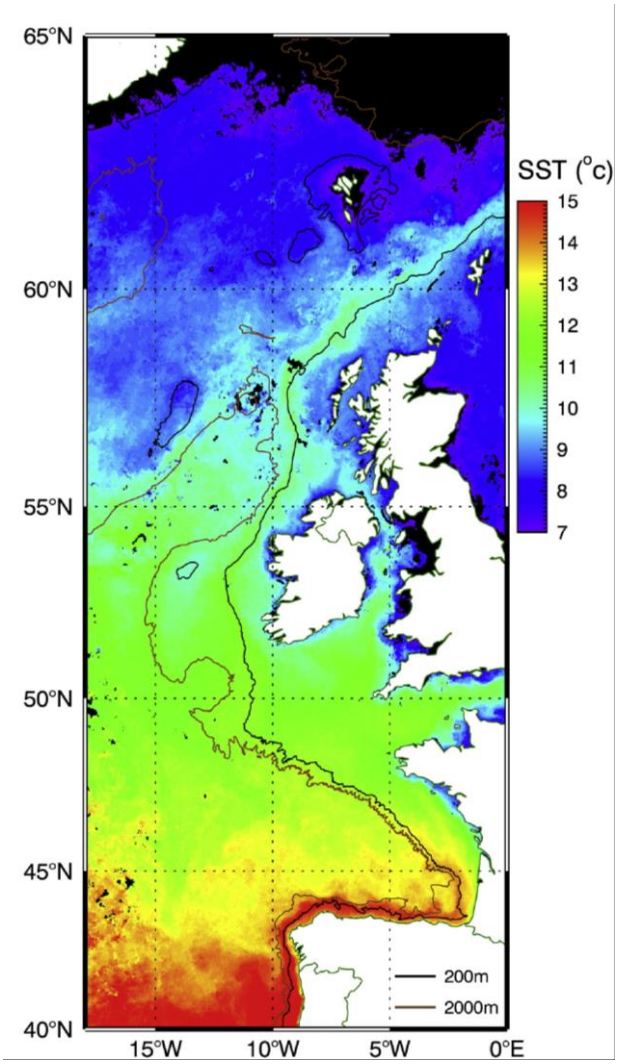

Fig. 1.14 The extent of the European Slope Current evidence by sea surface temperature in ºC (SST). The flow (green) can be seen following the shelf break along the west of Ireland and extending north onto the Hebridean Shelf. Modified from (Xu et al., 2015).

As frequency and resolution of seagoing investigations increased west of Ireland, further knowledge of the ESC was developed. This poleward moving current flows towards the Norwegian Sea and closely follows the shelf edge west of Ireland for some 1600 km (Fig. 1.14) with increasing current speeds in

excess of 0.66 ms^{-1}(Inall et al., 2009, Pingree and Le Cann, 1989, Pingree et al., 1999). (White and Bowyer, 1997) noted that this northward movement, coupled with bathymetry, creates a mean offshore current component, impacting sections of the shelf in proximity to the shelf break. This has particular significance for offshelf / downslope processes. Intrusions of this current onto the north Irish shelf are also documented (Fig. 1.15). These intrusions typically occur between 55ºN and 56ºN and in winter months (Souza et al., 2001). The result is a current with the potential to have influence on cross shelf fluxes (Huthnance, 1995) and act as a rapid transport mechanism (Fernand et al., 2006).

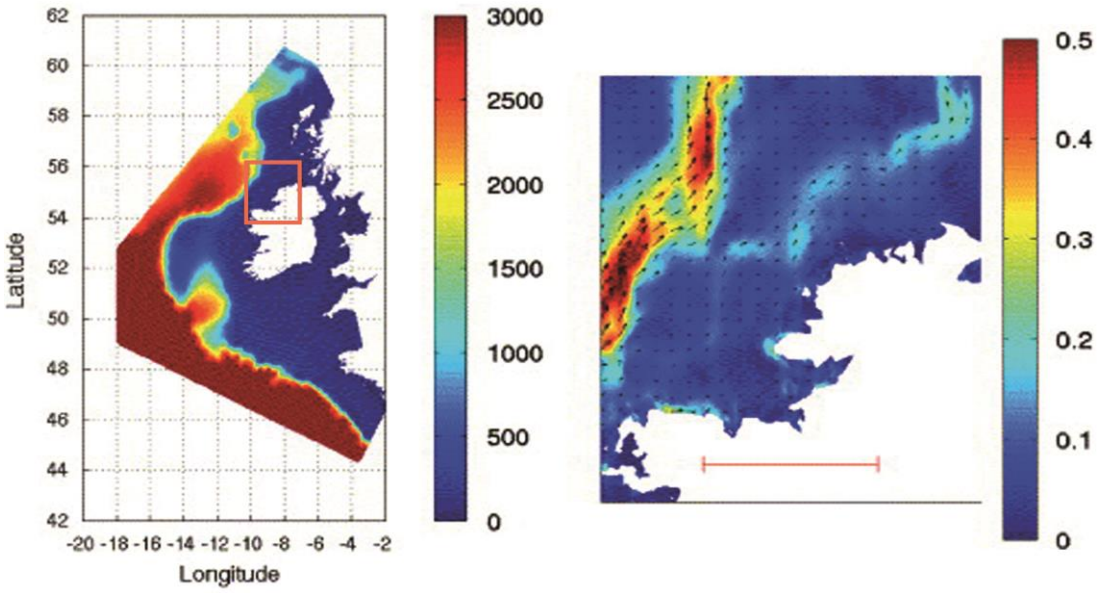

Fig. 1.15 Location of example and bathymetry in metres (left). Intrusion of the ESC onto the shelf illustrated by the light blue band ~ 0.2 m/s (right). Adapted from (Lynch et al., 2004).

While these investigations improve our understanding of shelf oceanographic processes and the resulting data provides a means with which to validate and calibrate satellite imagery and hydrodynamic model outputs, there is still much to learn. When compared to heavily studied areas such as the Irish Sea, it is

clear a more complete understanding of oceanographic processes off the west coast of Ireland is still being developed. The methods of remote sensing employed in many of the studies mentioned typically concentrate on the upper layers of the water column and as such do not provide some of the key information required when considering near seabed processes. Likewise, while many plankton, CTD and hydrodynamic model investigations on the north Irish shelf generate data from the entire water column, the focus of these studies has rarely been on the boundary layers adjacent to seafloor. As a result, there is a lack of definitive understanding of the formative processes creating some of the habitats and features we see on the present-day seafloor.

Several areas in Irish territorial waters proved both challenging and of great interest to modellers, in particular the Irish Sea and the ebb and flow of its tidal streams. Early attempts to model hydrodynamics conditions in Irish waters were 2 dimensional and coarse in resolution, so, while allowing numerical analysis of flows at a particular height in the water column, elements such as turbidity, bed stress and vertical currents could not be examined (Davies, 1994; Xing & Davies, 1996). These early models did however illustrate the importance of tidal phases in coastal waters, in particular, the influence of the M2 and M4 tidal harmonics around Ireland (Sinha & Pingree, 1997). When Young et al. (2000) successfully simulated the complex hydrodynamics of the North Channel using a 3-dimensional model, numerical analysis of water flows began to show full potential for accurately recreating real-world conditions. In an Irish context similar 3D models have since been employed by different research disciplines to examine complex, shelf edge flows, mixing and internal waves (Xing and Davies, 2001) and have identified a seasonal current circulation which has

since been linked to the transit of anadromous fish, spawning cycles of commercially important species and the appearances of harmful algal blooms during the summer months (Lynch et al., 2004). They have also been applied to analyse factors driving suspended sediment transport across the shelf (Davies and Xing, 2002).

1.5 Investigation Rationale

In this thesis, existing knowledge of shelf processes, as well as new and historic data sets, are utilised in a range of methods designed to improve understanding of sediment transport processes on the northwest Irish shelf. These methods include:

- The classification of the seafloor sedimentary bedforms according to existing nomenclature (Folk, 1954, Stow et al., 2009);
- The classification of acoustic backscatter data for the extrapolation of sediment distribution across the shelf (Goff et al., 2000);
- Hydrodynamic models of varying scales and resolutions (Young et al., 2011);
- Monitoring of the seafloor depths over the time to measure possible significant changes in sediment transport (Knaapen et al., 2005).

While a range of glacial formations on the shelf have been identified, many of the modern bedforms have not been classified (Benetti et al., 2010b, Dunlop et al., 2010, O'Cofaigh et al., 2012). Allocating a classification scheme to bedforms not only applies a standard nomenclature to the formation but also allows inferences to be made as to the feature's formative processes (Belderson et al., 1982, Li and King, 2007, Van Landeghem et al., 2009b). These include

suggestions as to the grain size of sediments and speed of water flow near the seabed. By mapping these classifications on a shelf scale it then becomes possible to make inferences as to current flow direction, energy and sediment type across a much larger area than for which field data exists (Li et al., 2012). The extensive backscatter coverage off the north Irish coast gives useful insight into the distribution of soft and hard surficial sediments. This data however fails to relate this acoustic response (in decibels) to a range of specific grain sizes, e.g. an acoustic response of -80 dB will not always identify the same grain size of mud across the entire shelf. This is due to a range of factors including instrument setup, angle of insonification or water column properties such as density. The result is that the same sediment grain size may produce a range of dB responses, with better quality data and consistent survey techniques providing a less variation in response (Lamarche et al., 2011). It is for this reason that the sediment samples distributed across a study area are used to ground truth the backscatter response. This enables the creation of a more accurate surface sediment map relating to sediment fractions (Goff et al., 2000, McGonigle and Collier, 2014). This allows interpretations from bedform classification and mapping to be further developed. With more specific knowledge of grain size, the velocities and bed stresses required to initiate and maintain sediment transport may be better constrained (Thiébot et al., 2015, Wu et al., 2011). To calculate bedstress, hydrodynamic models require bed roughness as an input for simulation calculations. Models not concerned with near seafloor process will typically apply a single averaged roughness value across the simulation domain. However, to insure optimum accuracy of sediment transport model calculation of bedstress, input values of grain size (or

bed roughness) and their spatial variation is key (Davies and Xing, 2002), As such, backscatter classification is often important in devising a sediment transport specific hydrodynamic model (Liu and Huang, 2009).

A model originally designed to investigate internal tide by (Xing and Davies, 1998), was modified to analyse suspended sediment potential by increasing vertical layers in the near bed zone by (Davies and Xing, 2002). This modified hydrodynamic model developed by (Davies and Xing, 2002) provides insight into suspended sediment transport processes both across and off the Malin shelf, however it is accepted that the model lacks the detailed description of sediment types over the region and as a result is restricted to assessing the mobility of just two defined grain sizes . (Davies and Xing, 2002) study is also restricted to a single cross-section of shelf at 57ºN, restricting ability to analyse transport across the entire shelf. While the entrance to the North Channel has been extensively modelled, the north and northwest Irish shelf have not experienced the same level of interest (Knight and Howarth, 1999, Xing and Davies, 1996, Young et al., 2000).

Hydrodynamic models encompassing this area have been large scale, with resolutions larger than 1.5 km and often with an emphasis on the upper layers of the water column (Dabrowski et al., 2014, Lynch et al., 2004). It is therefore necessary to develop a shelf scale, hydrodynamic model with sediment transport as the focus. Building on the work of (Davies and Xing, 2002), increased vertical resolution in the boundary layer should be included. The model mesh should also be capable of resolving complex coastline and offshore islands due to their significant effects on local currents. Ideally the model should also be able to take advantage of the high-resolution bathymetric

data and should incorporate spatially varying roughness based on grain size distribution. The resulting simulation outputs can then be used to calculate areas of potential sediment transport, confirm inferences on bedform migration based on asymmetry and identify bedforms which are no longer active (Bøe et al., 2009, Terwindt and Brouwer, 1986, Ferrini and Flood, 2005). Given the range of hydrodynamic investigations in the area and the types of software used, the creation of a sediment specific model as part of this research was required. Several factors were taken into account during this selection process. Due to budget the software, support and training were required to be low cost. Sediment transport specific modules were required to enable analysis of appropriate data. A flexible, 3D mesh was required to accurately represent the complex coastline and bathymetry of the study area. Lastly there was a requirement due to inexperience in hydrodynamic modelling, for the software to be user friendly. After assessing multiple models on these attributes, Mike by DHI was selected as the software package to model sediment transport related hydrodynamic forces on the nor Irish shelf.

It is understood that while MBES surveys are an accurate method with which to map the seafloor, in areas of high sediment mobility these data can quickly become obsolete (Knaapen and Hulscher, 2002). While these data may provide a baseline from which to infer mobility through analysis of seafloor morphology and bedform geometry, the rate of movement can only be speculated on. By generating multiple data sets over a time period, this mobility can be better quantified (Knaapen et al., 2005). Repeat MBES surveys can provide key insights into the migration patterns of bedforms and rate of crest displacement. This movement may then be related to flow regime to infer future migration

pathways, or to hindcast location and provenance of bedform sediments by reconstruction of transport pathways (Barrie et al., 2009).

1.6 Objectives

This study utilises a multidisciplinary approach to improve knowledge of sedimentary distribution, bedform formation and potential mobility of sediments on the north Irish shelf. By building upon the early work of Belderson, Keyon and Stride (Belderson et al., 1982, Kenyon and Stride, 1970), and adopting modern techniques for predicting and quantifying seafloor change, this research focuses on the application of existing data sets to modern sedimentary processes and fills knowledge gaps through acquisition and interpretation of new datasets for the Irish shelf. To this end, high resolution data from MBES, sediment grabs and hydrodynamic models have been combined with insights from previous research into the seafloor on the Irish shelf to provide a more complete analysis of shelf sediments and their mobility.

The overall scientific goal of this PhD is to map shelf sediments and bedforms, identifying potential mobility and migration patterns to further inform our understanding of shelf sedimentary processes.

Specific objectives of this PhD research are:

- To map and classify the range of non-glacial sedimentary bedforms on the north Irish shelf utilising MBES and seismic data with a focus on the potential mobility of these features.

- To analyse backscatter data in conjunction with sediment samples and records in order to establish sediment distribution across the shelf.

- To generate a hydrodynamic model capable of simulating near seabed forces relating to sediment transport at a range of resolutions appropriate to features of interest.

- To establish connections between bedform morphology, sediment distribution, modelled hydrodynamics and rate of seafloor change over time.

- To describe sediment transport processes from a shelf to bedform scale, examining validity of existing assumptions on bedform formation, mobility and the conditions governing shelf sediment distribution and movement.

1.7 Thesis structure and chapter introduction

This PhD thesis comprises 4 research chapters, which have been published or are to be submitted to international peer-reviewed journals. Each chapter was written as a stand-alone paper, however they are organised to illustrate an evolution of research understanding throughout the thesis. This occurs at two scales, one covering large shelf-wide processes, the other focusing on individual bedforms. These chapters also show progression from the utilisation of existing data and hydrodynamic models, through to the collection of new field data and the development of a bespoke model for this research. Each chapter addresses at least one of PhD objectives and contains an extensive discussion relating to the specific results presented in that chapter. Thus, some repetition among chapters, particularly in relation to regional setting, methods and scientific rationale, is unavoidable. Some of these papers are published or submitted with co-authors. Co-authorship acknowledges a combination of financial support, provision of data or research cruise collaboration. Whilst valuable support came from co-authors with regard to editorial and organisational feedback; all writing, analyses and exploration of discussion points for the completion of this thesis are entirely the responsibility of this author.

An additional chapter provides an overview of the work and integrates the results of the previous chapters while a final chapter outlines the key conclusions and suggests future work.

Chapter 2: Bedforms on the northwest Irish Shelf: indication of modern active sediment transport and over printing of paleo-glacial sedimentary deposits.

Evans W., Benetti S., Sacchetti F., Jackson D., Dunlop P., Monteys X. (2015). *Bedforms on the northwest Irish Shelf: indication of modern active sediment transport and interaction with paleo-glacial sedimentary deposits.* Journal of Maps, 11(4), p. 561-574

doi: 10.1080/17445647.2014.956820

Chapter 2 presents historic MBES and sedimentary data from the INSS survey. While these data have previously been analysed for evidence of submerged glacial landforms and sediments (Benetti et al., 2010b, Dunlop et al., 2011, O'Cofaigh et al., 2012), no specific interpretation on surficial sediments and bedforms has been carried out in these previous studies. This chapter highlights how some of the GIS (Geographical Information Systems) mapping techniques can be used on multibeam bathymetric and backscatter data to chart sediment distribution and classify bedforms at the seafloor. The results include a map of 5 main shelf sediment types derived from 20 m-resolution MBES backscatter data and grab-sample sedimentary data. In addition, 8 depositional and 2 erosional bedform types are identified and described in detail. The combination of bedform geometry, sedimentary composition and knowledge of prevailing shelf currents has allowed inferences to be made on the mobility of the mapped features. Together with the backscatter classification, this enables a comprehensive discussion of modern shelf sedimentary processes and how they may interact with underlying glacial

features. As a result, this chapter creates the background datasets and working hypotheses for the remaining chapters.

Chapter 3: Bedform migration on a high-energy coast: examples from the north Irish shelf.

Evans, W., Benetti, S., Sachetti, F., Jackson, D., Lyons, K. *Bedform migration on a high-energy coast: examples from the north Irish shelf* (Submitted to Earth Processes and Landforms).

In Chapter 3 the results of repeat bathymetric surveys at selected sites on the north Irish coast are presented. These surveys include MBES data from the JIBS project, several University of Ulster's student training cruises and 138 km^2 coverage gathered at the two specific study sites by the author as part of the Irish National Development Plan Shiptime Grant Awards. Time lapses ranging between 2 and 9 years were analysed for change in both the horizontal (2 m resolution) and the vertical (+/- 50 cm confidence). Sediment wave crest displacements were measured to quantify horizontal sediment movement; while surface difference models gave indication of net sediment transport at each site. High-resolution (1 m) backscatter data coupled with an intensive sediment sampling strategy enabled the generation of sediment distribution charts for the area at an unprecedented scale. Rates of movement and sediment type were then integrated with hydrodynamic data from the Marine Institute of Ireland's Regional Ocean Model (ROMS) to allow initial inferences to be made as to the

forcing factors acting upon these bedforms. These are tested in the following chapters by *ad-hoc* hydrodynamic modelling.

Chapter 4: Hydrodynamic modelling of bedform formation and sediment transport: insights into modern and relict bedforms.

Evans, W., Benetti, S., Jackson, D., Lyons, K., Dabrowski, T. *Hydrodynamic modelling of bedform formation and sediment transport: insights into modern and relict bedforms*.

Chapter 4 focuses on simulated outputs from the hydrodynamic model Mike by DHI, which was developed as part of this research. To meet the requirements of the model setup, simulation domain encompasses areas of the Rockall Trough, Malin Sea, Inner Hebrides and approaches to the Irish Sea. In contrast to many previous models within this area, the simulation methodology outlines a setup bias towards resolving flows in the seafloor boundary zone. These outputs, flow velocity and bed stress are then examined in relation to the sediment distribution and bedform morphologies discussed in Chapter 2. In general, lower flow velocities coincide with decreased grain size across the model domain with increased flow in inshore areas potentially accounting for the prevalence of coarser material. The simulated hydrodynamic forces corroborate well with bedform classifications in Chapter 2, with less mobile, rounded crest sediment waves typically undergoing periods of lower energy exposure than those interpreted as more active. Simulations over bedforms identified as potentially relict suggest that hydrodynamic forces are not elevated enough to initiate or maintain transport of sediments in these areas.

Chapter 5: Integration of high-resolution hydrodynamic modelling and time-lapse bedform migration on the north Irish shelf.

Evans, W., Benetti, S., Jackson, D., Clarke, S., Sacchetti, F, Lyons, K. *Integration of high-resolution hydrodynamic modelling and time-lapse bedform migration on the north Irish shelf*.

In this research chapter bedform migration rates measured in Chapter 3 are combined with a high resolution (2 m) computational mesh adapted from the model in Chapter 4 to enable analysis of the relationships between current flow and sediment transport over two selected areas. Area A is located between 7º19W and 6º51W in waters ranging from 20 m to 50 m deep. The bedform of interest comprises of a series of giant sandwaves reaching amplitudes of 20 m and is composed of coarse sand. In this area, high resolution modelling provides insights into flow agreement with sandwave asymmetry, examines causes for breakdown in crest profile, identifies the pivot point around which these sediment waves appear to rotate and explores the relationships between flow and measured migration rates (up to 7.7 m yr^{-1}). Area B, located between 6º30W and 6º45W extends up to 9 km offshore and is characterised by a range of sediment waves centred around a rocky reef known as ‘The Ridges’. There are a wide range of sediment types and migration rates in this area. High-resolution model data reveals most sediments may be mobilised during periods of peak hydrodynamic energy but not during peak conditions. While bidirectional flow occurs across the site, it is the directionality of these peak

flows that are suggested as the primary factor controlling migration throughout the area.

Chapter 6: Discussion

In this chapter, the main findings from the 4 research chapters are developed and discussed. Sedimentary records of oceanographic currents are presented, previous locations of sediment pathways are challenged, bedforms in unique hydrodynamic environments are identified and assessments of bedforms as relict or active are made. This necessitates the inclusion of relative sea level research for the north Irish shelf. These discussions are supported not only by the data created as part of this research, but through comparison to investigations carried out in similar shelf environments.

Chapter 7: Conclusions

Chapter 7 draws together the key outcomes of the research that have been developed through the 4 research chapters and discussion. Some implications for marine stakeholders on the north Irish coast have been suggested and avenues of potential further work have been identified.

Chapter 2 – Bedforms on the northwest Irish Shelf: indication of modern active sediment transport and overprinting of paleo-glacial sedimentary deposits

Evans, W., Benetti, S., Sacchetti, F., Jackson, D.W.T., Dunlop, P., Monteys, X., 2014. Bedforms on the northwest Irish Shelf: indication of modern active sediment transport and overprinting of paleo-glacial sedimentary deposits. Journal of Maps (2014)

Available online at:

http://dx.doi.org/10.1080/17445647.2014.956820

2.1. Introduction

Irish territorial waters have long been of interest to researchers in the field of oceanography and marine sedimentology (Van Landeghem et al., 2009b). The high energy wave climate and combination of outlying islands and complex coastline have created some of the highest current velocities in western Europe (Rourke et al., 2010). It is therefore of little surprise that early investigations into sediment dynamics on this shelf identified sedimentary bedforms varying in composition, amplitude and morphology (Kenyon and Stride, 1970). Recent efforts to map Ireland's Economic Exclusion Zone (EEZ) using modern multibeam technology and other techniques have provided further detail as to the type and distribution of these formations. This detail has provided the baseline dataset for much of the research in this thesis.

Given the extent of the Ireland's EEZ, a realistic evaluation of the country's underwater resources required significant effort. This resource mapping took the form of the Irish National Seabed Survey (INSS, 1999—2005), which was carried out to International Hydrographic Organisation standard 1A (IHO, 2008). This programme utilised a variety of marine survey techniques, including multibeam echosounder (MBES) bathymetry and backscatter, sediment ground truthing, and sub-bottom profiling which provide primary datasets for this research. The survey has produced high resolution, ground-truthed, bathymetric and backscatter datasets, encompassing much of the Irish territorial waters, allowing insight into shelf geomorphology to a level of detail and certainty previously not possible. On the northwest Irish shelf, landforms interpreted as having glacigenic origin, mainly moraines, drumlins and iceberg scours, have been previously mapped, providing new insights into the extension and retreat of the former British Irish Ice Sheet (Benetti et al., 2010b, O'Cofaigh et al., 2012). While these large-scale, glacial deposits are an important element of the seafloor architecture; they are relict features and therefore provide no information on modern day shelf processes in this area. To understand contemporary shelf sedimentary processes, bedforms such as sand waves must be mapped and examined, as they can provide vital information on current and tidally-induced sediment movements (Bøe et al., 2009). The main map (Fig. 2.11) presented here at 1:225,000 scale shows the spatial distribution of the main bedforms on the northwest Irish shelf. This and other figures will be used to discuss the sedimentary processes that operate on the shelf at a variety of spatial scales.

2.2. Data and Methodology

2.2.1 Multibeam Bathymetry and backscatter

Multibeam data used in the creation of this map were acquired during 12 separate surveys between 2003 and 2005 aboard R.V. Celtic Explorer as part of the INSS programme (Fig. 2.2a). The Simrad EM1002 system was used for acquisition, operating at frequencies between 93 kHz and 95 kHz. This unit utilises 111 beams typically configured at a fixed angular coverage between 55° and 70°, dependant on water depth. In optimum conditions, the EM1002 is capable of resolutions in the order of centimetres. However, the variations in weather conditions during the surveys from which this data was derived can adversely affect MBES quality. As part of post processing, the Marine Institute determined a resolution of 10 m was the most realistic grid size obtainable from swath surfaces taking into account data quality. This resolution allows removal of spikes and other issues related to relatively poor data quality in some surveys yet is sufficient to map many of the large and medium scale landforms on the shelf and so was adopted for use in this investigation. On board navigation systems compensated fully for pitch, heave and heading. Sound velocity profiles (Fig. 2.1) and tidal gauges were also utilised to take into account water density variation and tidal corrections to allow for how these variations effect the accuracy of bathymetry measurements and to maintain IHO 1A standards (IHO, 2008).

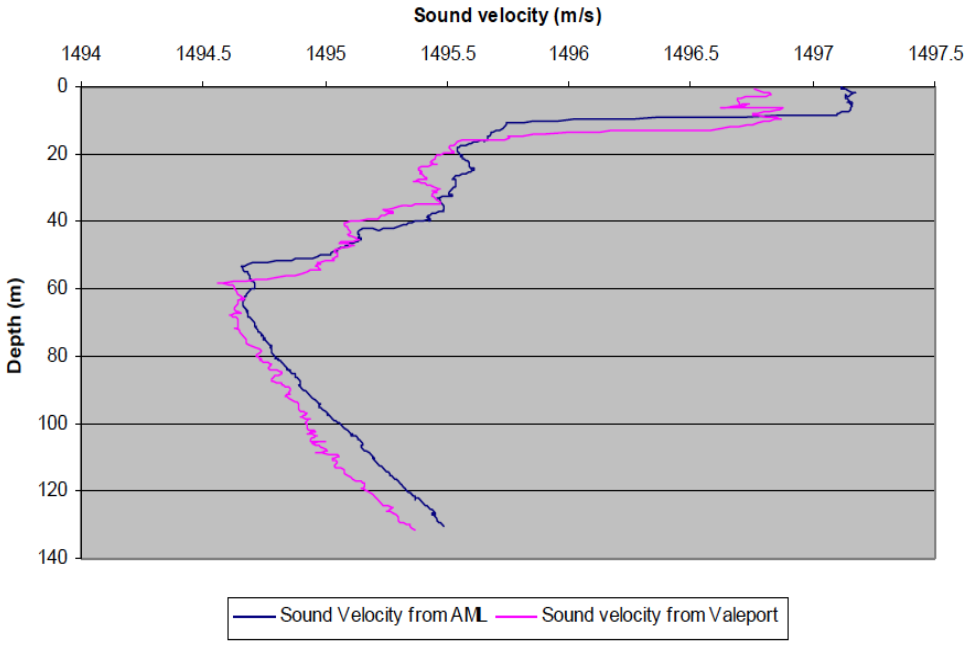

Fig. 2.1. Measurements acquired by AML Oceanographic and Valeport sound velocity profiler at sediment furrows shown in Fig. 2.9. Sound velocity varies rapidly between 0 m and 20 m. There is a steady decrease in velocity down to 60 m, this is the limit of the pycnocline. In depths beyond 60 m, velocity increases, most likely due to increased density and decreased temperature. In a well-mixed environment, less variation in sound velocity would be observed.

These measurements are particularly important in summer months where stratification of water densities is known to occur on the Irish north coast due to reduced wave energy (Gowen et al., 1998). Both bathymetric and backscatter values were derived from the acquired data and were processed at the Marine Institute Ireland initially with Caris HIPS & SIPS v5.3. Elements of this work represent an attempt to improve this backscatter data, with further processing carried out using Caris HIPS & SIPS v7.1 at University of Ulster. The result is an improvement in the quality of backscatter mosaic for sediment classification. The resultant datasets were gridded to 10 m resolution and imported into IVS Fledermaus v7.0. A vertical exaggeration of 6 was utilised to assist visualisation of bedforms and a range of azimuths and shading settings were employed to

avoid azimuth bias. Profiling tools were also used to gather values for the geometric properties of features such as wavelength and amplitude. Raster grids were imported into ESRI ArcGIS v10.1 to enable mapping, further interrogation, and ease of data set integration.

Backscatter derived from MBES signal is important when considering the physical properties of the seafloor. It displays variation in sediment hardness and can aid identification of features observed in bathymetric data (Lamarche et al., 2011). As the backscatter data has been extracted from MBES data collected on different surveys, the mix of weather conditions, depths and system configurations at time of survey can have a marked effect on the outputs from any processing methodology (McGonigle et al., 2010b). Artefacts remaining in the backscatter mosaics reflect the difficulties in compensating for this. Data were processed using the Geocoder algorithm in CARIS HIPS & SIPS v7.1 (Fonseca et al., 2009). Raw backscatter images were processed into Georeferenced Backscatter Rasters (GeoBaRs) to allow initial viewing and image quality assessment of data. GeoBaRs also allow the correction of artefacts across an entire data set, rather than on a line by line basis. This is useful when considering the range of surveys and system configurations previously mentioned. Adaptive Angle Varied Gain (AVG) was applied to normalise gain across the data to correct ‘banding’ and angular artefacts while a moderate despeckle setting was applied to reduce image noise. dB histograms were then modified using the software’s auto-adjust script, and lines mosaiced using a blending algorithm and exported into IVS Fledermaus 7.1 and ESRI ArcGIS v10.1 in gridded formats.

2.2.2 Sediment Samples

The Geological Survey of Ireland (GSI) sediment database is a collation of sediment descriptions gathered as part of multiple cruises in Irish waters, using a variety of sampling methods. 466 entries from the database relevant to the study area were extracted, converted to UTM 29N co-ordinates and imported into ESRI ArcGIS v10.1. Recorded sediment sample descriptions include data from a range of grabs and corers, as well as visual interpretation from video transects. These entries are included in the GSI database and it is assumed that the information provided was collected using appropriate geological methods and have been properly logged, taking into account the effects of wind, tide and other factors on sampling location accuracy.

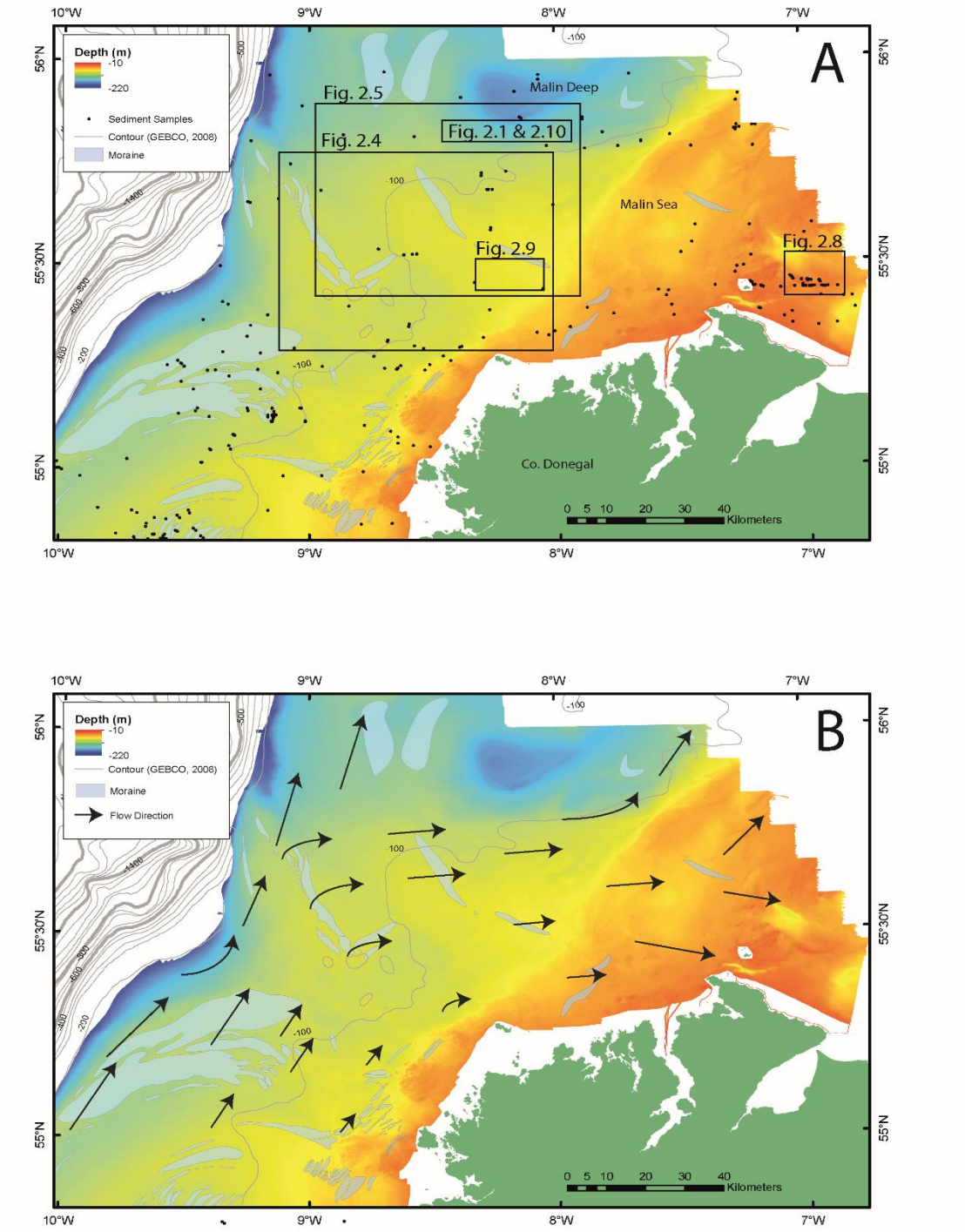

Fig. 2.2. (a) Bathymetric map of the northwest Irish shelf gridded at 10 m resolution. Distribution of glacial moraines from (Benetti et al., 2010b) and (Dunlop et al., 2010) are shown. Sediment sample locations used for backscatter classification are indicated. Remaining figure locations are included for context. (b) Bathymetric map with arrows illustrating residual flow direction in top 30 m gathered by floats (Fernand et al., 2006) and simulated using numerical modelling (Lynch et al., 2004, Xing and Davies, 2001). Higher velocity flows are indicated by longer arrows and are evident close to the shelf break.

2.3 Geophysical Data Processing

2.3.1 Bathymetric Derivatives

Elements of the Benthic Terrain Modeler (Wright et al., 2012) for ArcGIS v10.1 were used to further investigate the complexity and geomorphology of the survey area. Slope angle (degrees 0°- 90°) and aspect (downslope direction expressed as compass points) were calculated. A rugosity chart was then produced to give an overview of the variance in slope and aspect in one single measure, scaling from 0 (no variation) to 1 (complete variation). These charts provided inputs for additional analysis of seafloor geomorphology utilising Bathymetric Position Indices (BPI). BPI is a second-order derivative of the bathymetry and defines elevation relative to the entire MBES data set. It defines flat areas (zero values), elevations (positive values) and depressions (negative values) in terms of relationship to the sections of seafloor nearby rather than as part of a continuous scale (Micallef et al., 2012). BPI is typically calculated at both broad and fine scales (Fig. 2.3) and then standardised to allow for comparison of outputs (Plets et al., 2012). The area and resolution of the MBES data used dictated broad-scale BPI values of 25 m (inner ring radius) and 50 m (outer ring radius) to create a suitable scale factor of 1250 to analyse large shelf features such as moraines.

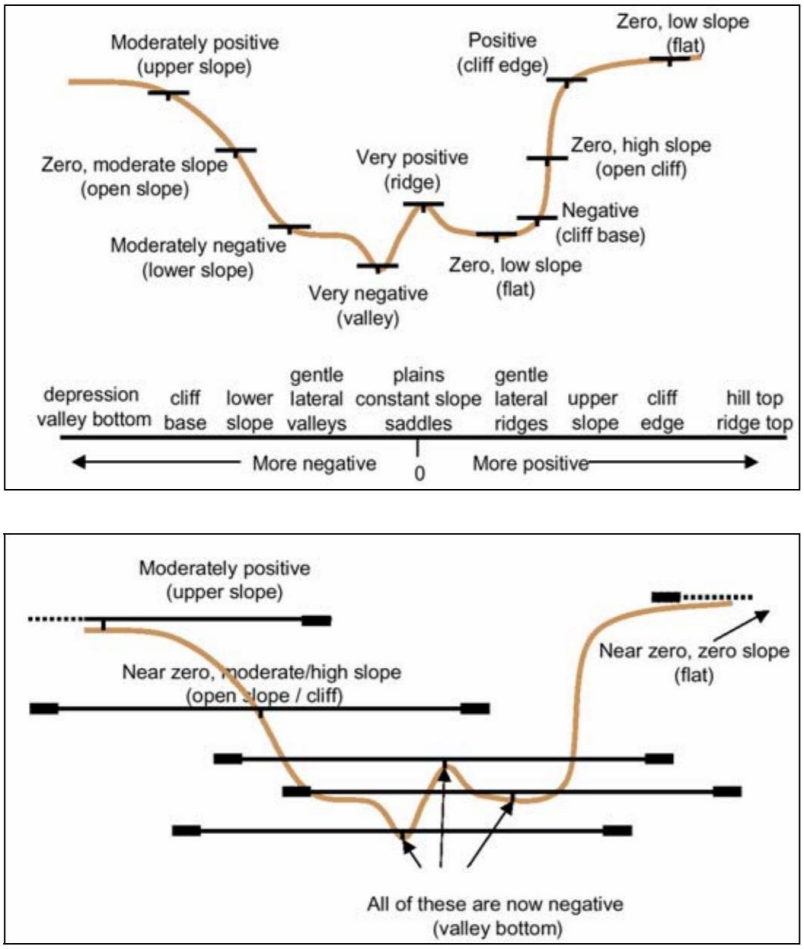

Fig. 2.3. Diagram illustrating the uses of both fine (upper) and broad (lower) scale BPI to identify seafloor features. In the case of the northwest Irish shelf, fine scale BPI was used to identify individual sandwave crests while on a broad scale, larger features such as moraines were highlighted (Verfaillie et al., 2007).

Fine-scale BPI was adjusted to 4 m (inner) and 6 m (outer) resulting in a scale factor of 400 which is better suited to identifying smaller features such as individual sediment waves. These data have been utilised during the mapping and classification of bedforms, allowing crest lines to be more accurately defined and mitigating azimuth bias that may occur with bathymetric data of this type.

2.3.2 Backscatter classification and ground-truthing

Classification of backscatter was carried out to map sediment distribution on the shelf by combining information from sediment samples and acoustic response. Like BPI, backscatter signal may also be used to inform geomorphological mapping, for example, when defining a sandy, low response bedform, surrounded by harder high backscatter substrates. In these instances, bedform boundaries are much more clearly defined and thus can be digitised more accurately. It can also highlight bedforms that are not immediately obvious in bathymetric data, such as thin sand patches draped over bedrock (Goff et al., 2000). Backscatter classification is key to the interpretation of shelf wide formations and is the best way to infer sediment distribution between sample locations (Lamarche et al., 2011, McGonigle and Collier, 2014).

Initial attempts to conduct a signal-based classification, based on raw data and processed in software such as Fledermaus FMGT, were unsuccessful. As previously stated, issues with inconsistency across data sets which cover the survey area were compensated for by processing and mosaicing into backscatter images. Signal based classification relies on good quality raw data to provide a realistic interpretation of sediment characteristics (Brown et al., 2011, McGonigle et al., 2010a, Rzhanov et al., 2012). This level of quality was not present in the raw data collected and and for this reason, an image based approach was adopted.

The validity of unsupervised classification of backscatter (and similar image based data) has been queried due to uncertainty of the number of classifications, or clusters, which should be used. A common approach to image based marine habitat mapping is to combine this unsupervised classification

with a ‘signature’ based approach which provides a supervised element to the process and accounts for the clustering issue (Stephens and Diesing, 2014). This approach has been adopted in this research as it is has proven to be an effective method for image-based classification in a habitat mapping context. (Varela et al., 2008) and (Shanmugam et al., 2003) utilised an isocluster classification process to map terrestrial habitat types to great effect, particularly in coastal dune environments. Maximum likelihood classification approach to classification has been used to great effect in the marine environment (Ierodiaconou et al., 2011), in Venice lagoons to investigate sponge/sediment relationships (Gavazzi et al., 2016) and in the Irish Sea to map habitat type in commercially significant fishing grounds (Calvert et al., 2015).

Utilising these proven approaches to classification, an ArcGIS spatial analyst routine ‘isocluster unsupervised classification’ was used to create a signature file containing 5 classes. A ‘maximum likelihood’ classification from the ArcGIS ‘multivariate analysis’ toolbox then used this signature file to classify the backscatter response data into clusters with some linear artefacts included due to the automated process for digitisation. These occur at the boundary of survey legs and are related to changes in equipment settings. These clusters were then manually assigned a sediment type based on ground truth data obtained from the Geological Survey of Ireland’s sediment database.

2.4 Results

Bedforms identified on the seafloor have been mapped based on geometry, sedimentary composition and backscatter response and have been classified based on these measurements using existing research (Barnard et al., 2013, Cataño-Lopera and García, 2006, Knaapen et al., 2005, Van Landeghem et al., 2009b). These bedforms were then further grouped as depositional or erosional features. While it is recognised that bedforms fall within a continuum of morphologies which change depending on sediment type, flow velocity and other factors, these groupings are often examined when considering the formative forces creating each bedform type (Hanquiez et al., 2007b, Stow et al., 2009, Wynn and Stow, 2002). This is particularly useful in a shelf sediment transport context as it also allows inferences to be made as to the hydrodynamic flows which are driving the formation and movement of the bedforms (Kuijpers et al., 2002, Masson et al., 2004). Depositional bedforms, such as barchan dunes and sand ribbons, and erosional features in the form of furrows and lineations have been identified. The current velocities which these beforms are associated with are also discussed (Belderson et al., 1982, Hanquiez et al., 2007b, Stow et al., 2009). Bathymetric derivatives have been utilised to further verify classifications made based on morphology and to mitigate user error due to azimuth bias.

2.4.1 Elevation

Shelf-wide Bathymetric Position Index (BPI) (Fig. 2.4), displays areas of elevation, depression and flatness. Areas of elevation and depression in close proximity identify parts of the shelf with increased rugosity. This may be in the

form of bedforms or exposed bedrock. It also highlights offshore small-scale anomalies across the shelf, some of which have been identified using 3D visualisation software as shipwrecks (Brady et al., 2012, Plets et al., 2011). BPI was particularly useful for mapping sedimentary features on northwest Irish shelf as it allowed the detection of features at a range of scales. This approach also represents the first steps of an automated approach to object and bedform identification across this area of seafloor. Large-scale seafloor architecture (e.g. moraines) is visualised, as well as smaller scale features, such as the mapped sand ribbons (Fig. 2.4). Individual crests and troughs of sandwaves are also defined. This enabled measurement of wavelength and to accurately digitise crestlines in ArcGIS 10.1. This means of crest detection also form the preliminary steps of an automated approach to measuring migration detailed in Chapter 3 of this thesis.

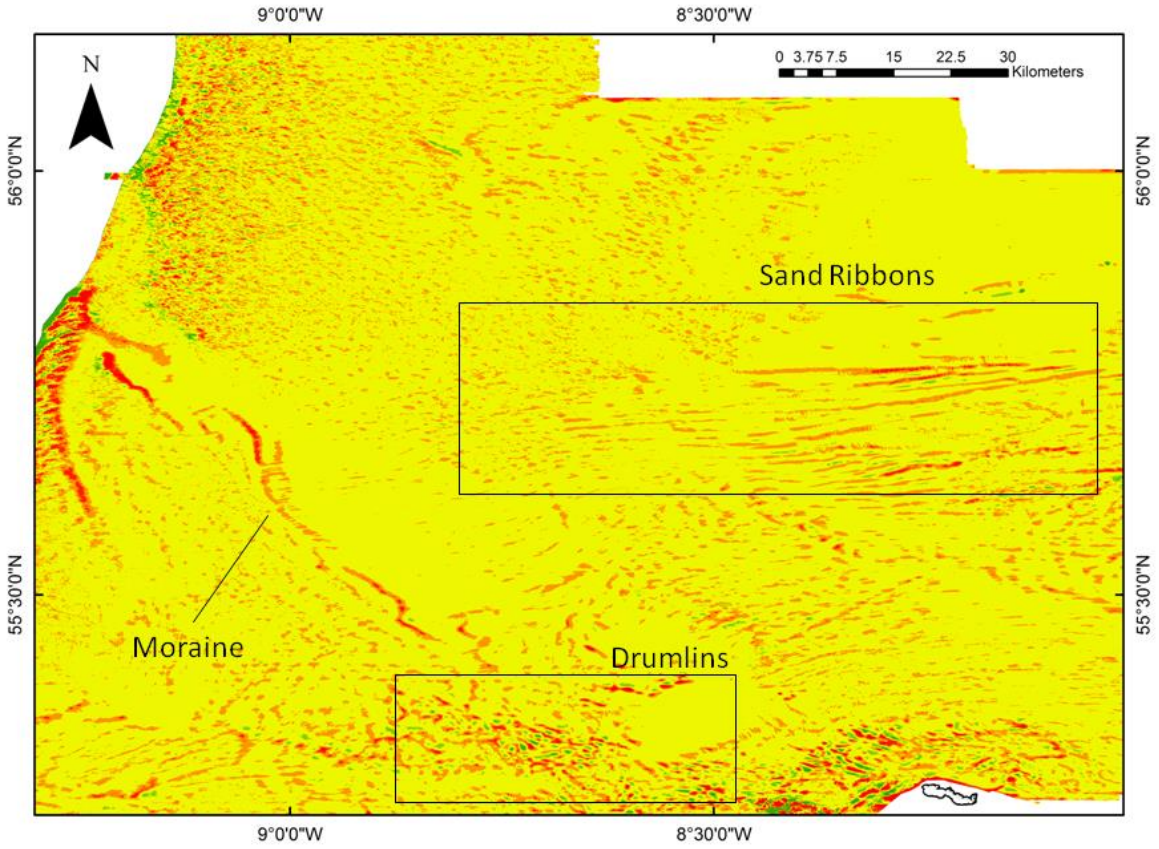

Fig. 2.4. Broad scale BPI as a means to identify features on a shelf scale. Green colouration represents area of relative depression while red illustrates elevation. Sand ribbons, drumlins and a large moraine are illustrated. White areas define sections of seafloor beyond survey coverage.

2.4.2 Sediment distribution

Backscatter mosaics give good indication of the variability of substrate hardness across the shelf. Soft sediments are characterised by dark coloured, low backscatter values. High backscatter values, brighter in colour, correspond to harder substrates such as coarse-grained sand, gravel and bedrock (Figs. 2.5 and 2.6).

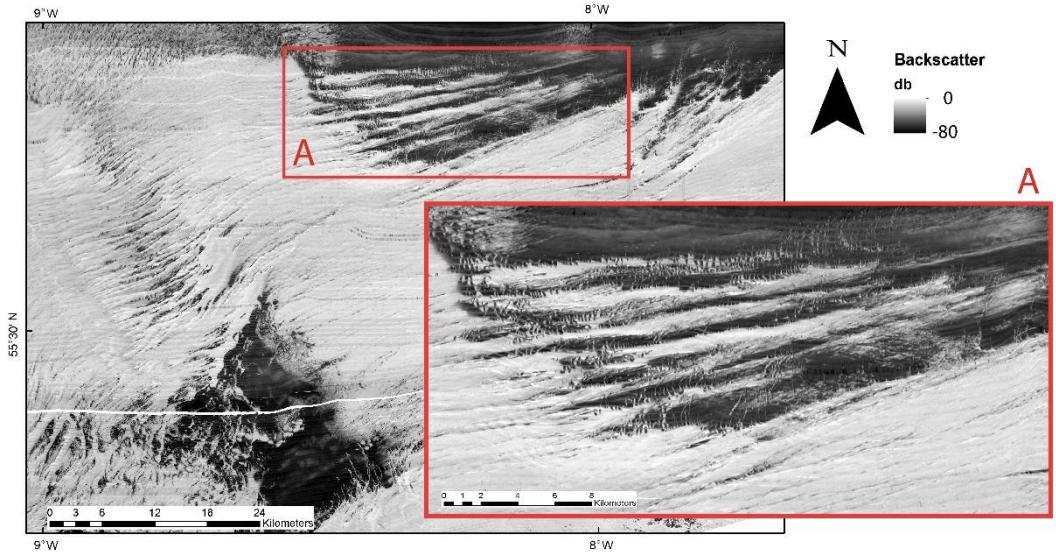

Fig. 2.5. Example of backscatter response to differing surface sediments. Soft sediments, muds and fine sands are characterised by dark coloured, low backscatter values. Light coloured, high backscatter response indicates hard material, typically gravels, cobbles and bedrock. This is the typical response across the shelf with soft sediments occurring in localised pockets. Backscatter imagery indicates that the erosional processes that have created furrows have revealed coarser material (light) underlying the dark coloured sand ribbons (inset).

This research represents the latest in a series of attempts to generate a sediment classification map for the north west Irish shelf. As previously stated the reduced backscatter data quality and range of equipment used has meant this section of shelf has proved particularly challenging to classify on a large scale resulting in only bays and single surveys having been processed by the GSI (F.Sachetti 2014, pers. comm). Much of the shelf is composed of gravelly coarse sand and gravel. Exposed bedrock closer to the shore is also classified as gravel with pebbles due to similarities in their backscatter response. The fact that exposed bedrock and gravelly material is prevalent water depths shallower than 50 m is unsurprising given the increased hydrodynamic energies and storm processes associated with shallower water environments of the northwest Irish shelf (Dodet et al., 2010, Fernand et al., 2006).

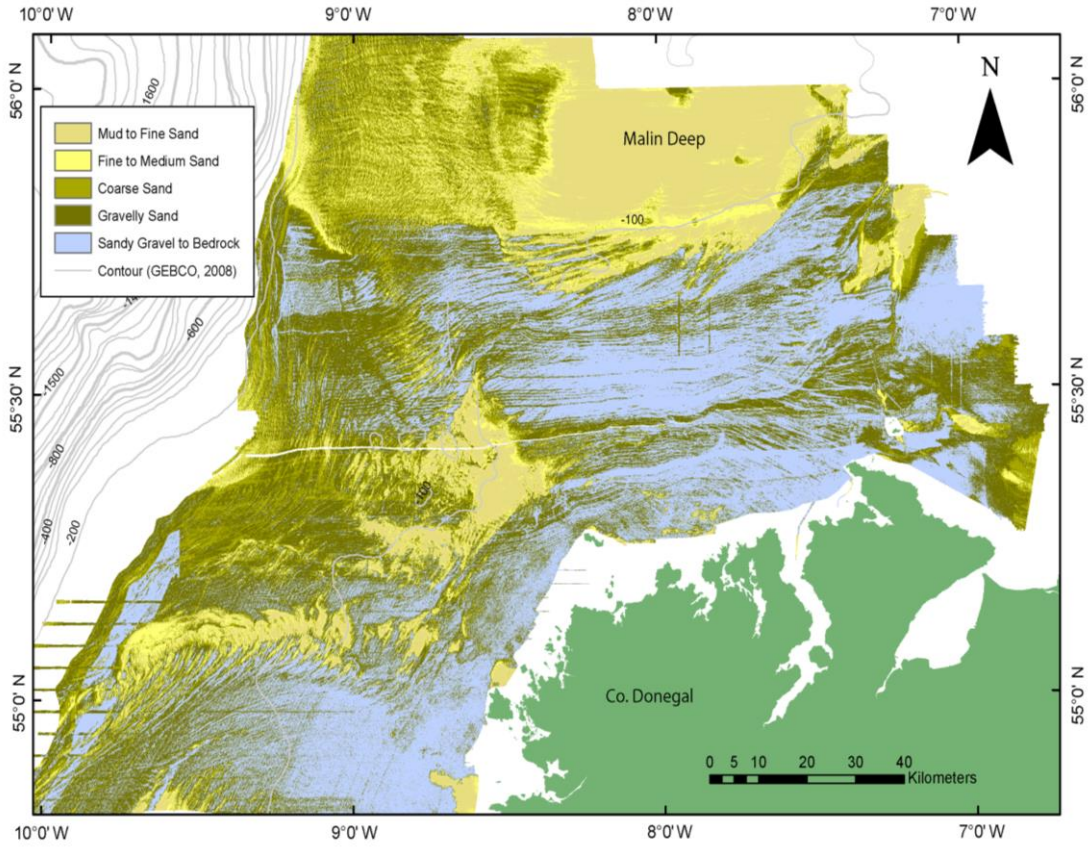

Fig. 2.6. Classification of backscatter data carried out in ArcGIS 10.1 using 466 sediment sample sites for ground-truthing. Muds and fine sands are confined to deep water and bathymetric depressions. Gravels and coarser material dominate much of the shelf with medium and coarse sands comprising many of the bedforms mapped. Distribution of these sediments can also be linked to the moraines illustrated in Fig. 2.2.

Muds, silts and fine sands are the next most prevalent sediment classification type with the most northerly section of the study area, the Malin Deep, exemplifying a typical backscatter response to these soft sediments (Fig. 2.5). On a shelf-wide scale, silt and fine sand are not evenly distributed across the entirety of the study area, but are instead confined to depressions, such as the Malin Deep and another smaller area on the mid-shelf at 55°20'N (Fig. 2.6). It is likely that a local increase in water depth at these locations creates much weaker hydrodynamic conditions close to the seafloor, allowing finer sediments to settle of out suspension in these areas or not to be winnowed away

(Berelson, 2001). Fine and medium grained sands, which comprise sand patches and sand waves, are more widely distributed. A large collection of sand patches is easily identifiable in the southwest of the study area, spanning from the shelf break to 15 km off the Co. Donegal coast at 55°05'N (yellow patches in Fig. 2.6). Other patches of fine and medium grain sands occur as isolated bedforms and are concentrated in the northeast between 7°19'W and 6°48'W. Also apparent are linear features of varying sediment composition running north-south parallel to the shelf edge, sweeping round to the northeast at 55°30'N, where they gain in width and amplitude.

(Dunlop et al., 2010) identified these wider, light coloured streaks as sand ribbons (Fig. 2.5). Closer inspection reveals these ribbons do not present a uniform acoustic response and appear to be striped by coarser high backscatter sediments (Fig. 2.5 inset). As a result, the classification of these formations as a traditional stand ribbon (Belderson et al., 1982, Daniell, 2015, Stow et al., 2009) may be open to challenge, particularly given that this striping occurs perpendicular to the suggested along ribbon deposition direction. Interestingly many of the glacial features identified in previous mapping of the area (Benetti et al., 2010b, O'Cofaigh et al., 2012) are not apparent in the backscatter classification. Backscatter response is based on the surface sediments only, suggesting that these glacial features are draped by more modern sediments, masking the signatures of typical glacial sediments.

2.4.3 Bedforms

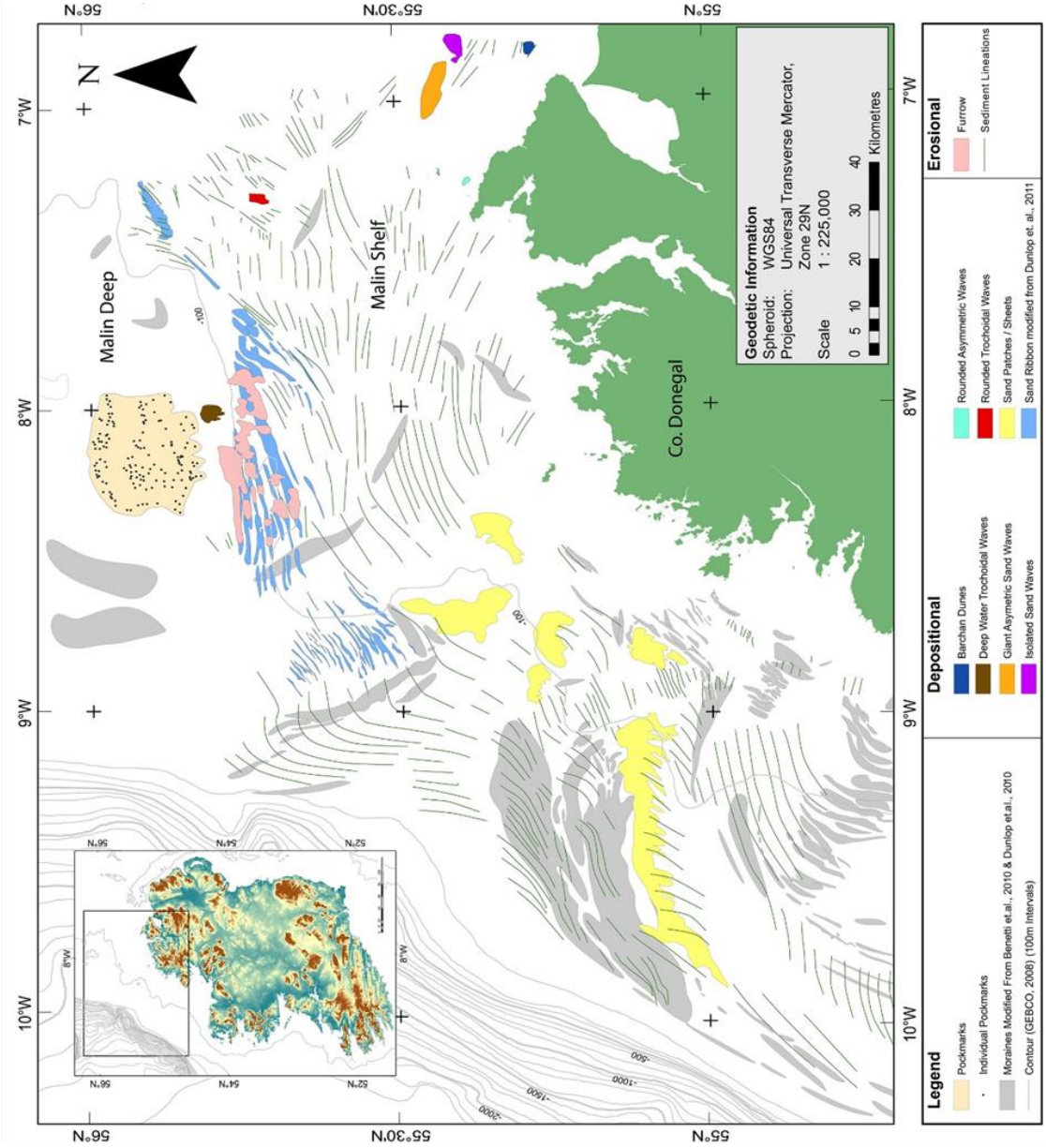

Fig. 2.7. Chart illustrating the classification and distribution of bedforms across the northwest Irish shelf. including moraines identified by (Benetti et al., 2010b) and (Dunlop et al., 2011). Bedforms identified as part of this research can be seen overlapping these moraines, White areas indicate areas where modern depositional and erosional bedforms were not mapped.

2.4.3.1 Depositional Bedforms

Sediment Waves

Sediment waves are confined to a small number of areas on the northwest Irish shelf, with most occurring in the Malin Sea between 7°19'W and 6°48'W. Sediment waves have been measured for amplitude, wavelength and slope length and angle, following the methodology of (Van Landeghem et al., 2009b). Measurements are compiled in Table 1. The observed variations in amplitude and asymmetry aided classification of sediment waves into: trochoidal, asymmetric, rounded and isolated waves and barchan dunes.

			Average					
	Amplitude (m)	Stoss Angle (°)	Stoss Length (m)	Lee Angle (°)	Lee Length (m)	Ratio Stoss / Lee	Wavelength (m)	Depth (m)
Barchan Dunes	3.0	2.0	85.9	3.8	49.3	1.74	135.1	48 - 50
Deeper Water Trochoidal Waves	1.0	1.4	42.5	1.2	41.8	1.02	84.3	126 - 134
Rounded Trochoidal Waves	1.4	0.6	130.4	0.4	113.0	1.15	243.4	58 - 61
Giant Asymmetric Waves	13.8	3.4	222.3	7.6	104.1	2.14	326.4	24 - 50
Isolated Waves	2.9	2.9	77.6	4.3	46.5	1.66	124.1	55 - 67
Rounded Asymmetric Waves	2.1	2.7	53.6	2.2	32.8	1.63	86.3	29 - 42

Table 2.1. Average geometries of six classified bedform types on the northwest Irish Shelf.

Due to the nature of their high amplitude, even in a global context (Bøe et al., 2009, Fenster et al., 1990), the giant asymmetric waves that occur in 30 m water depth at 55°26'N, 6°58'W are most striking. They reach amplitudes of greater than 20 m and have average wavelengths of 326 m (Fig. 2.8).

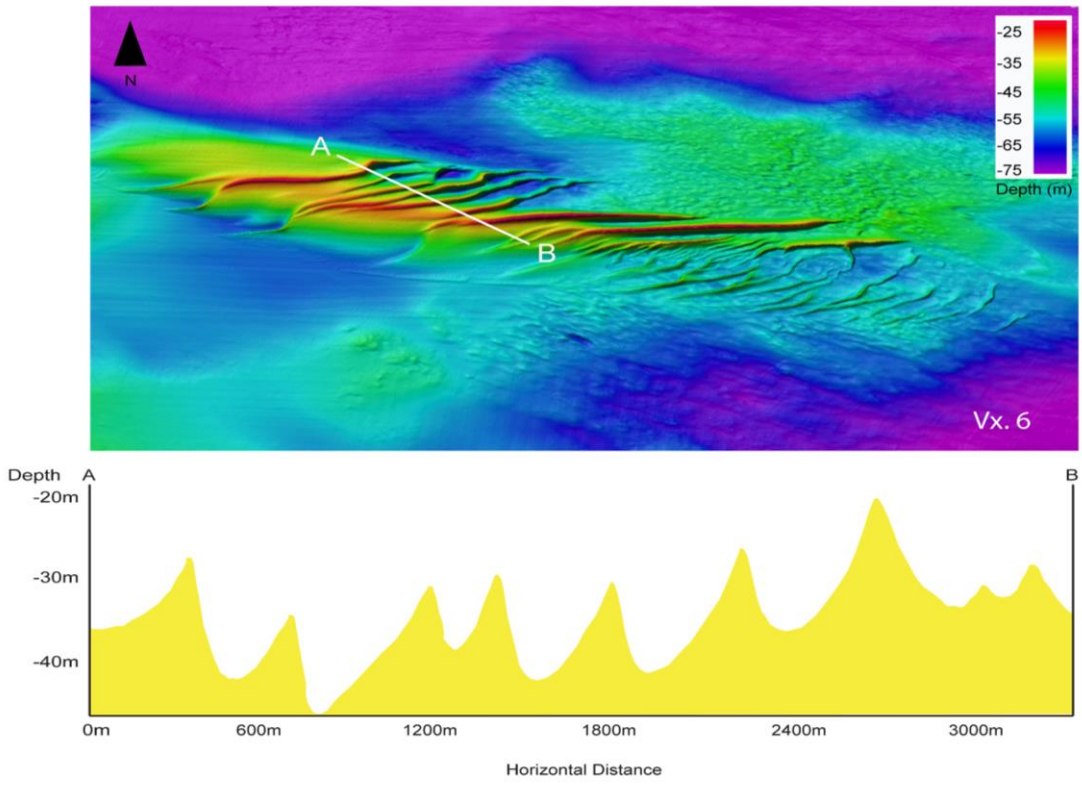

Fig. 2.8. Oblique MBES data view of Giant asymmetric waves situated in 30 m – 40 m water depth. Crests are sinuous in form and are typically aligned southwest- northeast. Extended view around the assemblage is included to contextualise the isolation of the bedform on the inner shelf. Image width at base is 11 km. The topographical profile reveals sharp crested, high amplitude waves with longer, stoss slopes on the northwest side of the formation. This suggests migration in a southeast direction. Bedform location illustrated in Figs. 2.2a and 2.7.

Wave crests are sinuous in form and up to 5 km long. Sediments retrieved from the wave crests and slopes show the waves are composed of medium to coarse, golden coloured sand with a shell component between 5 and 10%. Grabs taken in wave troughs and to the periphery of the formations were composed mostly of gravel with a smaller amount of coarse sand. These sand waves display the significant asymmetry (the difference in length of lee and stoss slope) associated with mobile formations of this type, suggesting migration in a southeast direction (Barnard et al., 2013, Belderson et al., 1982, Knaapen et al., 2005).

Twelve km southeast of these giant asymmetric waves, a field of barchan dunes is situated in 40 m water depth. Slightly crescentic in form, these features reach maximum amplitudes of 5 m and have typical wavelengths of 135m. Backscatter classification (Fig. 2.6) suggests the bedforms consist of medium to coarse sand and are surrounded by gravel. This composition and bedform geometry lead them to be classified as barchan dunes (Kuijpers et al., 2002, Van Landeghem et al., 2009b). These bedforms are associated with sediment-starved environments and are an excellent indicator of net sediment movement, which bedform asymmetry suggests is in a southeast direction (Belderson et al., 1982).

Isolated sand waves have also been identified six km east of the giant asymmetric waves (Fig. 2.7). Situated in 60 m to 65 m of water, these waves reach amplitudes of 4 m and exhibit some scouring at crest edges. Asymmetry of these isolated waves is of opposite orientation to both the barchan dunes and giant asymmetric waves. This suggests a difference in the prevailing hydrodynamic currents in this area to the northwest.

Other sediment waves have been classified based on crest form, rounded or sharp, and wave form, trochoidal or asymmetric (Table 1 & Fig. 2.7). Trochoidal or symmetrical waves can be caused by a bedform undergoing equal periods of tidal energy from opposing directions. In these cases, waves typically maintain a sharp crest form, flexing back and forth with each change in tide (Barnard et al., 2013, Knaapen et al., 2005, Van Landeghem et al., 2009b). Another hypothesis for symmetry of bedform profile is a reduction in active sediment transport. This is typically applied to waves with a rounded crest and gently angles slopes (Cataño-Lopera and García, 2006, Knaapen et al., 2005, Van

Landeghem et al., 2009b). Factors such as bioturbation or gravity driven processes can lead to the breakdown of wave profile over prolonged periods of time if no mobilisation via currents occurs. It is suggested these processes contribute to a rounding of wave crests and collapsing of asymmetrical form (Belderson et al., 1982, Borsje et al., 2008, Le Hir et al., 2007). The latter is a probable mechanism for the formation of these symmetrical waves identified on the Malin Deep. Sediments in this area are thought to have been deposited by the Donegal and Barra fans during deglaciation in this area (Szpak et al., 2012). It is possible that these waves formed in the periods following this, and as water depth increased to present day (130 m), the hydrodynamic forces reduced, allowing gravity and biological processes to lead to a breakdown in wave profile. .

Sand Patches

Patchy distribution of sediment is visible in MBES data, but it is much more clearly represented in backscatter classification (Fig. 2.6). Occurring across the shelf these sediment patches display amplitudes of 1 m - 2 m above the surrounding seafloor. These ragged edged patches occur in larger accumulations closer to the shelf break than further inshore. These offshore patches consist of fine and medium sand and they are surrounded by gravel material. In waters shallower than 60 m, patches appear to be draped over exposed bedrock and are smaller in size and thickness. Composed of finer sand material than the offshore patches, a good example of an inshore sand patch is visible in the backscatter classification at 55º01N, 8º40’W (Fig. 2.6).

Elongated Ridges: Sand Ribbons

Elongated ridges between 300 m and 1200 m wide and extending for 16 km have been observed across the northwest Irish Shelf (Figs. 2.3, 2.7 & 2.10). The most pronounced of these ridges are 4 m in amplitude and occur south of the Malin Deep (55°43'N, 8°19'W) in 90 m water depth aligned parallel to the shelf gradient. Other subtler ridges continue further to the south and east of these and gradually decrease in amplitude. This morphology is consistent with previous mapping of sand ribbons carried out by (Dunlop et al., 2010) and on other shelf environments in Spanish (Hanquiez et al., 2007b) and Faroese (Masson et al., 2004) waters. Samples taken from the ridges confirm they are made of medium to coarse, dark coloured sand with a shell component between 10 and 20%. These bedforms are associated with high velocity currents (Belderson et al., 1982, Hanquiez et al., 2007b, Masson et al., 2004, Stow et al., 2009), with their orientation giving an indication of flow direction. This suggests that a long term, stable current is present on the shelf (Wynn and Stow, 2002), flowing parallel to the shelf slope similar to the flow patterns observed in Fig. 2.2b.

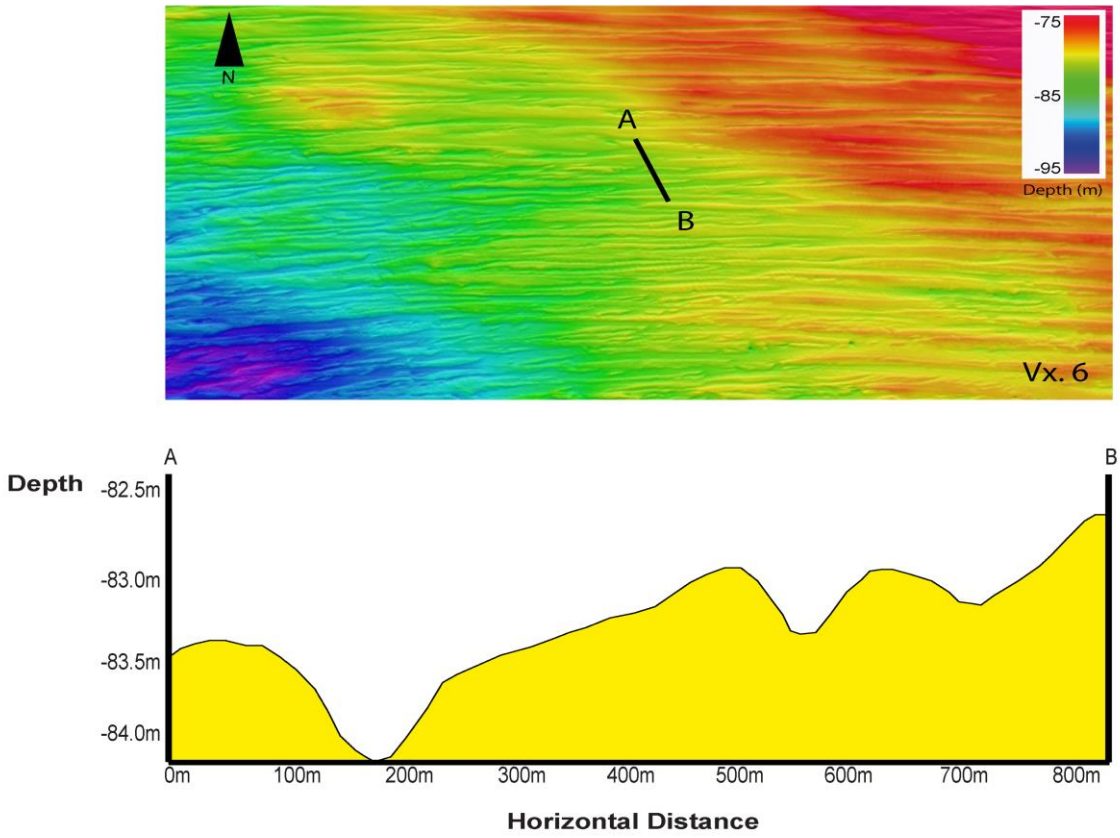

Fig. 2.9. MBES data displayed from an oblique view (image base measures 4.5 km). Sediment lineations are visible orientated west-east and aligned parallel to each other. Profile illustrates subtle profile of these features. Bedform location illustrated in Fig. 2.2a and 2.7.

2.4.3.2 Erosional Bedforms

Lineations

Subtle lineations (Fig. 2.9) have been identified in bathymetric data and are prevalent across the study area. Typically 0.5 m to 1 m in amplitude and 100m in width, these low-relief peaks and troughs occur parallel to each other and traverse larger, relict, glacial deposits. In the southwest portion of the study area, they are aligned southwest-northeast until a gradual change towards a west-east orientation is observed at approximately 55°30'N. This pattern is similar to the direction of simulated bottom currents modelled by (Lynch et al.,

2004)(Fig. 2.2b). Similar patterns are observed in seafloor sediments in the Gulf of Cadiz caused Mediterranean Outflow Water (MOW) (Hanquiez et al., 2007b) and in Faroe-Shetland gateway where bedforms change orientation with the currents of the Norwegian Sea Overflow Water (NSOW) (Masson et al., 2004). These streaks vary in composition from fine sand to gravel. Sandy material is concentrated over the large outer moraine and in proximity to the Malin Deep (Fig. 2.7). For much of the inner shelf this bedform is represented by coarser gravels. This wide range of grain sizes suggests a current of constant directionality is reworking any surficial sediments path of flow. While these features may be interpreted as either erosional or depositional (Stow et al., 2009), in this instance (and in agreement with literature), flow parallel orientation suggests sediment winnowing, substantiated by the formation of sand ribbons of increased fine sediment content at the downstream end of these lineations (Hanquiez et al., 2007b, Masson et al., 2004, Weaver et al., 2000). Thus, erosion is described as the primary formative force for these bedforms.

Furrows

Elongate, sinuous incisions (Fig. 2.10) appear on the southern edges of the Malin Deep (55°45'N, 8°18'W). These features are observed bisecting the large sand ribbons described in 2.4.3.1. of this chapter.

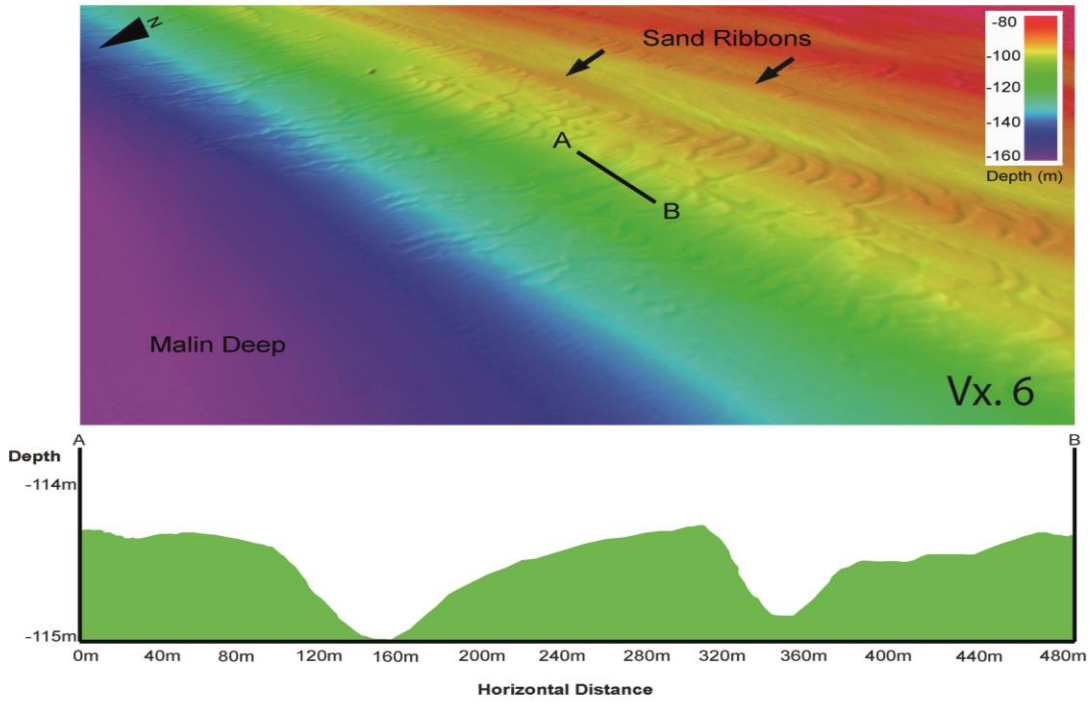

Fig. 2.10. Oblique view of furrows apparent in MBES data at southern edge of the Malin Deep. Aligned downslope and in a north-south direction these erosional features are slightly sinuous in shape. A vertical exaggeration of x6 has been applied to enhance visualisation of these subtle features. Sand ribbons described in 2.4.3.1 aligned northeast-southwest and parallel to shelf gradient are also visible. The horizontal distance at the base of this image is 5.2 km. The topographic profile indicates the dimensions of typical furrows at their mid-point. Bedform location illustrated in Fig. 2.2a and 2.7.

At the peak of the shelf slope, the widest furrows occur in ~105 m water depth, are 110 m wide and extend for over 1 km. They generally narrow downslope and in some cases close out. While no sediment samples were taken directly upon these features, backscatter data (Fig. 2.5) reveals the base of these features to be comprised of much coarser material than the sand ribbons. This suggests downslope, erosional processes have removed the finer sediments in these locations.

2.4.3.3. Other Features

Pockmarks

Circular depressions occur in the Malin Deep (175 m water depth) and are distributed across an area of ~400 km^2 (Fig. 2.7). These depressions have varying slope angles with depths ranging from 1 m to 4 m and diameters of up to 300 m. Sediment samples taken in the Malin Deep show that this large bathymetric depression is a trap for fine-grained sediments, primarily mud and silt with some fine sand. These features have been classified by (Szpak et al., 2012) as gas and pore water escape features or pockmarks and are found on similar coastal shelfs globally (Hovland and Judd, 1988, Hovland et al., 2005, King and MacLean, 1970, Paull et al., 2002, Szpak et al., 2012).

2.5 Discussion and Conclusions

The combination of bathymetric and backscatter analysis of the INSS multibeam data sets has revealed the complexity of seafloor morphology and sediment distribution on the northwest Irish shelf. Surficial sediments have been classified and their distribution mapped in detail. This investigation has identified some sediment waves presenting characteristics typical of mobile, active bedforms (Belderson et al., 1982, Barnard et al., 2013, Stow et al., 2009, Van Landeghem et al., 2012). These include shelf-wide sediment lineations and sand ribbons that are typical of continuous, stable and high-energy current regimes. Their orientation also correlates well with simulated flows modelled and measured (Fig. 2.2b) by (Davies and Xing, 2002) and (Lynch et al., 2004). These modern sediments partially bury and traverse relict, glacial deposits. Not

only does this mask the acoustic response of these glacial sediments but could also alter the apparent morphology of these features via infilling or overprinting. It is possible that these modern sediments are also interacting with these older, relict deposits through reworking. This is best illustrated by the large outer shelf moraine located between 55º0'N and 55º30'N. This suggested moraine has gently sloping crests, and wider dimensions and has a segmented arrangement that is uncharacteristic of other features mapped as moraines on the Irish shelf (Benetti et al., 2010b, O'Cofaigh et al., 2012). Concentration of sandy sediments contained within formations such as the lineations in proximity to glacial formations e.g. the large outer moraine, suggests that these winnowing processes also provide the source of many of these modern active sediments. It is likely that this process has been ongoing since the retreat of the British Irish Ice Sheet. Relative sea level models indicate a lowstand in the study area of -41 m ~ 14,500 B.P (Bradley et al., 2011, Brooks et al., 2008, Kuchar et al., 2012) with (Neill et al., 2010) predicting a tidal range of 8 m at this time. As a result, the bedforms on the northwest Irish shelf would have undergone a period of transgression and increased bed stresses associated with larger tidal ranges and shallower water depths. However, some features, including those close to the shelf break and in the Malin Deep, would have been situated in water depths exceeding 70 m. Therefore it is probable that these formations were beyond wave base interaction, even at the time of lowstand. As a result, there is potential that this reworking occurred as a result of mobile sediments under a long-standing and relatively strong current regime. Given understanding of shelf currents and sediment distribution, it is therefore possible that contemporary hydrodynamic conditions are generating sufficient bed stress to currently

mobilise many of these formations (Bassetti et al., 2006, Lynch et al., 2004, Van Landeghem et al., 2009a)

Chapters 3 and 4 utilise repeat multibeam surveys, collection or simulation of bottom currents and further ground truthing of sediments to provide further understanding of active and relict sediment transport on the shelf. Collectively this research has implications for the management of shelf resources such as aggregates and substrates important for spawning of commercially important fish species. It can also inform the siting of marine engineering projects (Rourke et al., 2010) and associated cabling.

2.6. Map Design

The area chosen for this map (Fig. 2.11) was selected based on quality of data and the extensive mapping of glacial formations already undertaken in the area. These factors provide an excellent platform upon which to further examine shelf through mapping of modern sediments and examine possible interactions with older sediments. Bathymetry data was not included on the main chart for the sake of clarity given the large number and wide distribution of elements mapped. It is felt that the inclusion of isobaths compensates well for this exclusion. Moraines identified as part of previous research were included to reinforce the hypothesis that modern bedforms are overlapping or traversing these relict features. The moraines are placed below modern formations in order to visualise actual shelf stratigraphy. Bathymetry, backscatter and slope map are included as these are the three components from which all data for this study were derived. By splitting this data into smaller panels it allows the data to be presented in a clear and non-cluttered manner.

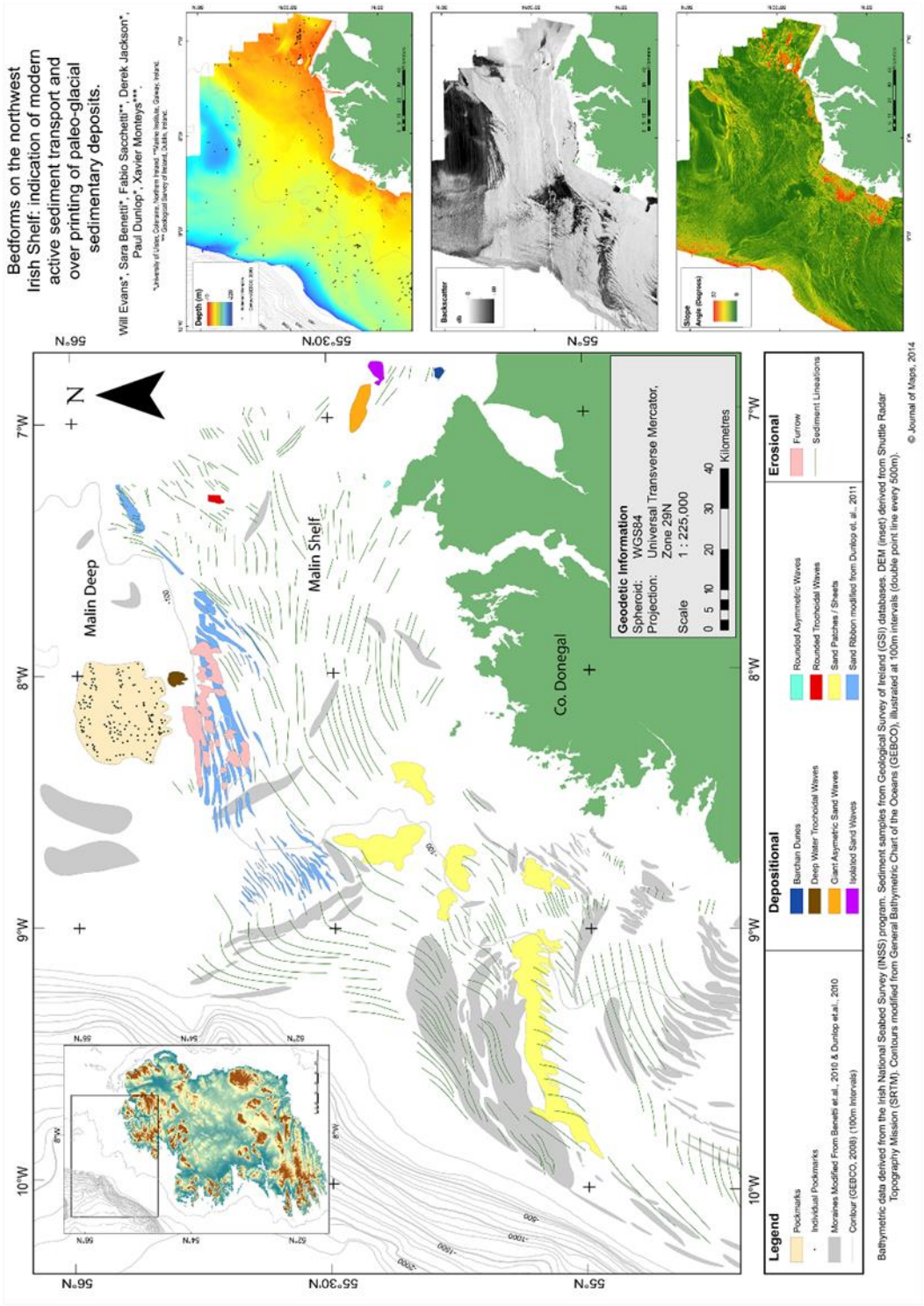

Fig. 2.11. Overview map published in Journal of Maps (2015) indicating locations of previously mapped glacial features overprinted by modern sediments. White spaces indicate areas where no modern bedforms have been mapped.

Chapter 3 – Bedform migration on a high-energy shelf: examples from the north Irish shelf

Evans, W., Benetti, S., Sachetti, F., Jackson, D., Lyons, K. *Bedform migration on a high-energy coast: examples from the north Irish shelf* (Submitted to Earth Surface Processes and Landforms (special edition)).

3.1 Introduction

It is widely accepted that understanding the movement of sediments on a shelf scale is of significant importance to our continued interaction with the marine environment (Barnard et al., 2013). Shelf wide surveys focusing on seafloor sediments increased in prevalence during the 1970's through the introduction of novel equipment and increased computing power (Belderson et al., 1982, Kenyon and Stride, 1970, King and MacLean, 1970). As technology and methodologies have been further refined, shelf scale analysis of sediment movement has proved useful in a number of applications. Knowledge of sediment volume and type is important for managing economic resources such as aggregates for extraction (Alder et al., 2010, Singleton, 2001). Rate and direction of movement can be key to maintaining shipping waterways or sediment supply to coastal islands and beaches (Staneva et al., 2009, Rosati, 2005). Longstanding oceanographic currents can be identified through sediment transport trends and the bedforms these flows create (Hanquiez et al., 2007b, Masson et al., 2004). Sediment transport research can also have biological applications through shelf scale mapping of substrates, which can be

used to apply habitat suitability for species or other classifications, including those susceptible to smothering by mobile substrates (McBreen et al., 2011, Brown and Blondel, 2009).

Early attempts in the 1970s and 1980s to describe sediment movement on the north Irish shelf relied largely on interpreted side-scan sonar data (Kenyon and Stride, 1970) and the analysis of bedform asymmetry to determine transport potential and direction (Belderson et al., 1982). While subsequent sediment specific surveys have not occurred on the north Irish shelf to the same scale as Kenyon & Stride (1970), many similar sediment transport investigations utilising modern techniques have been conducted on shelfs globally (Denny et al., 2013, Feldens et al., 2012, de Juan et al., 2013).

Anthropogenic interactions with the marine environment have become more frequent and widespread, and as a result, the analysis of sediment transport for specific applications in smaller sections of shelf has also increased (Barnard et al., 2013, Holt et al., 2009). It is the analysis on these smaller spatial scales which has been key to understanding sediment wave migration, bedform formation and distribution. Early examination of the interaction between current flow and grain size has become the foundation of understanding sediment transport, supported by analysis of bedform characteristics such as geometry (Allen, 1980, Belderson and Stride, 1966, Miller et al., 1977). Extensive work has been carried out to classify bedforms based on morphology, this classification often indicating the typical grain size and current flows associated with their formation (Belderson et al., 1982, Van Landeghem et al., 2009b). In addition to this, a key indicator of mobility in sedimentary bedforms is the asymmetry of profile. Asymmetry of sediment waves in the marine environment

(i.e. the variation in ratio of lee and stoss slopes) has typically been used as a proxy for sediment transport rate and direction. Migration is assumed where a gently sloping, longer stoss slope is followed by a steeper and shorter, lee slope. Transport is then interpreted as a movement in the direction of the lee slope; with a steeper slope angle suggesting increased mobility (Belderson et al., 1982, Ferret et al., 2010, Knaapen et al., 2005, Lobo et al., 2000, Van Landeghem et al., 2012). The validity of these assumptions is, however, fraught with complications. Variations in sediment grain size and bedform height can affect the rate at which the morphology of the bedforms is altered in response to forcing conditions (Van Landeghem et al., 2012). The influence of multiple tidal constituents over a bedform can result in variation in morphology over time due to varying current speed and direction associated with differing tidal amplitudes (Bartholdy et al., 2010c). Localised hydrodynamic interactions between larger and smaller bedforms formations and indeed, between individual sediment waves, may also influence sediment transport potential through downstream shadowing and associated deceleration of flow rates (Belderson et al., 1982, Besio, 2004, Van Landeghem et al., 2012). To investigate these variations and verify asymmetry-based assumptions on transport, marine geophysical surveys repeated over the same area at different times have been used to measure sediment movement from kilometre to centimetre scales (Knaapen et al., 2005, Ma et al., 2014, Németh et al., 2002). While data resolution, direction of insonification and tidal variations must be considered (McGonigle et al., 2010a), repeat multibeam echosounder (MBES) bathymetric surveys do reveal differences in morphology, direction and rate of migration of bedforms at the seafloor. Accompanying MBES acoustic backscatter data can also be used to

infer changes in surficial sediment composition (Ma et al., 2014). Further datasets such as flow velocity data may be used to compliment the repeat MBES survey, providing increased certainty of sediment transport patterns observed (Bøe et al., 2009). Water flow velocity near the seabed is accepted as key to the formation of bedforms and the driver behind their movement (Allen, 1980, Belderson et al., 1982, Besio et al., 2008c, Feldens et al., 2015). Knowledge of these flow rates allows comparison to both grain size and migration rate and direction to insure that realistic observations can be made and to provide rationale for any anomalies such as reverse asymmetry migration (Van Landeghem et al., 2012). The use of moored current meters such as Acoustic Doppler Current Profilers (ADCP) can be impractical over large areas of shelf (Gunn and Stock-Williams, 2013, Holt et al., 2009). As a result, hydrodynamic simulations of water movement are often utilised to provide a near seafloor value for flow velocity (Sheng and Yang, 2010, Young et al., 2011). In addition, shallow seismic profiling over sediment waves can reveal internal structures or layers, which in turn are interpreted as differing depositional or erosional events. Their orientation and angle can be used to validate inferences on sediment wave migration direction and rate derived from profile asymmetry or time lapse MBES surveys (Ferret et al., 2010, Lobo et al., 2000, Ma et al., 2014, Van Landeghem et al., 2009a). This multidisciplinary approach can therefore provide a robust approach to the analysis of shelf sediment transport at a range of scales.

Sites on the north Irish coast were selected to investigate sediment transport not only to further understand the movement of individual bedforms, but to understand the implications of this transport for a range of applications.

Baseline MBES data acquired as part of the Irish National Seabed Survey (INSS; http://www.gsiseabed.ie) and the Joint Irish Bathymetric Survey (JIBS; http://infomar.ie/associated_projects/index.php#JIBS) programmes, are compared with MBES from University of Ulster's student training cruises and R.V. Celtic Voyager Cruise CV13030 to form repeat marine geophysical surveys (i.e. time-lapse surveys). Sediment samples and seismic data were also collected to support the investigation sediment mobility in this region (Fig. 3.1).

The aims of this study are two-fold. (1) To assess and quantify seafloor bathymetric changes over the course of several years using time-lapse survey data, specifically focussing on the migration of sediment waves in relation to the modelled hydrological conditions for this region. A novel method for measurement of sediment wave migration has been developed as part of this study and it is also presented. (2) To examine the links between bathymetric change, modelled hydrological conditions and sediment type, using ground-truthing and backscatter data to define grain size across selected sediment waves.

3.2 Regional Setting and hydrological regime

The north Irish epicontinental shelf, between the north Irish coast and Scotland, has a widely ranging water depths from shallow platforms near the coastline in ~20 m water depths to deep troughs up to ~200 m (Figs. 1.10 and 3.1). The study area extends in the Irish portion of the continental shelf from the coastline to water depths around 150 m, ca. 55°30'N and between 7°10'W and 6°30'W and this investigation focuses on two particular areas, A and B (Fig. 3.1). Sediments, up to 6 m deep, cover bedrock at the centre of the general study area adjacent to Lough Foyle (Cooper et al., 2002, McDowell et al., 2005). Gradual slope, and planar morphology have been attributed to the depth of these sediment deposits in the area between Lough Foyle and the River Bann estuary (McDowell et al., 2005, Plets et al., 2011). The westernmost portion of the study area between 7º20'W and 6º56'W, however, is dominated by exposed bedrock and gravels with only a few pockets of softer sediment (Evans et al., 2015, Plets et al., 2011). As a result, near-bed currents greater than 1 ms^{-1} occur on the north Irish coast, with peaks concentrated in the narrow 6 km wide channel separating the Inishtrahull Island complex from Ireland (Fig. 3.1) (Muir et al., 1994, Rourke et al., 2010).

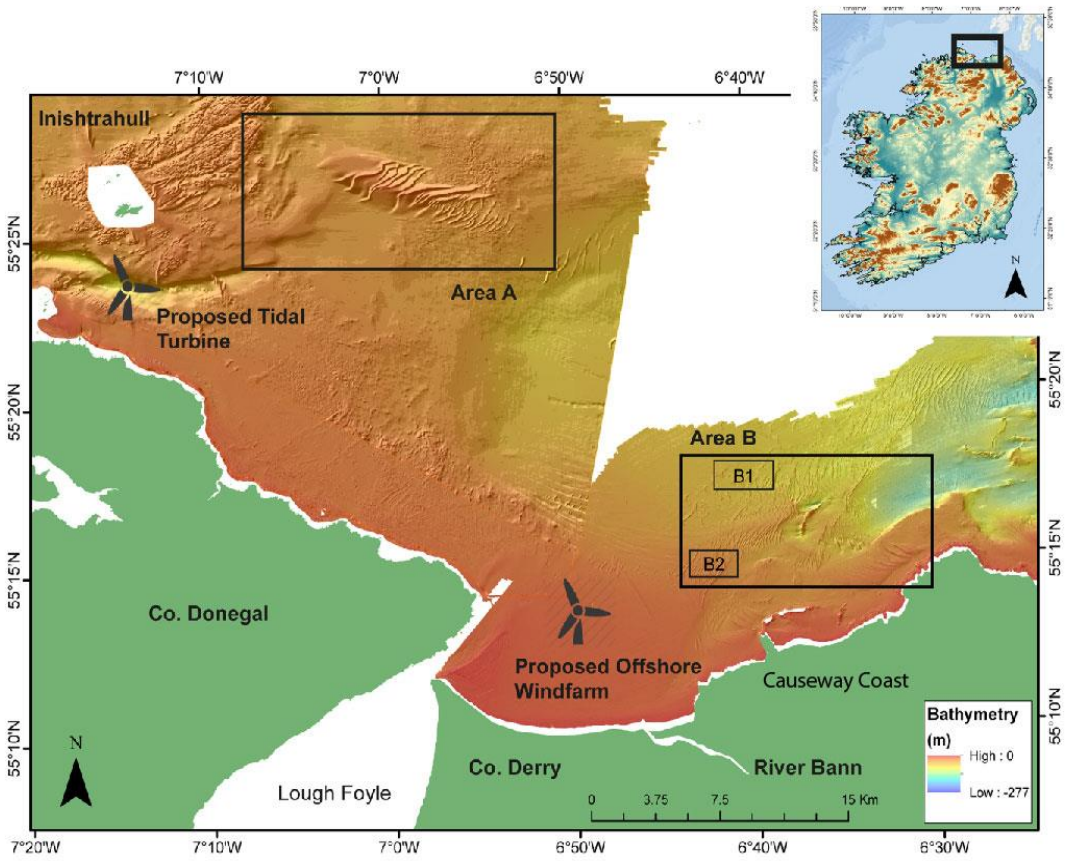

Fig. 3.1 Overview of study area and specific areas selected for repeat geophysical surveys and sediment sampling. Area A contains isolated soft sediments forming large sand waves. To the west of this location, current energies south of Inishtrahull are some of the highest in Irish waters (up to 514 GWh/y, >2 m/s (Rourke et al., 2010). Area B includes a distinctive rock outcrop named the Ridges. Subsets are also labelled. Due to favourable wind and tidal conditions, two marine renewable sites for this section of shelf are proposed by independent stakeholders. Some linear artefacts are present ~55º18'N 6º50'W.

This section of the north Irish shelf also experiences significant freshwater influences. The estuary of Lough Foyle has a tidal basin spanning 186 km^2, with one of the largest catchment areas of all Irish sea loughs (Fig. 3.1). Several rivers also enter the study area providing freshwater and sediment input, the largest of which is the River Bann with a fluvial discharge of between 250 and 2000 m^3s^{-1} (McDowell et al., 2005).

3.3 Study area

The energetic hydrodynamic conditions of the north Irish coast and presence of potentially mobile sediments make this a suitable section of shelf to examine sediment transport. Existing high-resolution MBES data also allow time-lapse geophysical surveys to be utilised to quantify this mobility. Two areas were specifically selected for sediment transport assessment based on variance in bedform types, the high likelihood of mobility dictated by significant wave asymmetry and the availability of MBES data from previous surveys (Fig. 3.1). The presence of fixed depth objects, in this case rock outcrops, was considered to provide a vertical datum control on bathymetric data. The proximity to proposed sites for marine renewable energy sites makes this work also of relevance to offshore installations planning but was not a deciding factor in the selection of the study areas.

Area A is located14 km from the coastline between 7º19'W and 6º51'W, with water depths ranging from 20 m to 50 m (Fig. 3.2). A MBES survey of this area was carried out in 2004 as part of the INSS programme and provides the baseline data for this study. The seafloor is dominated by large asymmetric sandwaves, with amplitudes up of 20 m decreasing in size towards the south-east (Evans et al., 2015).

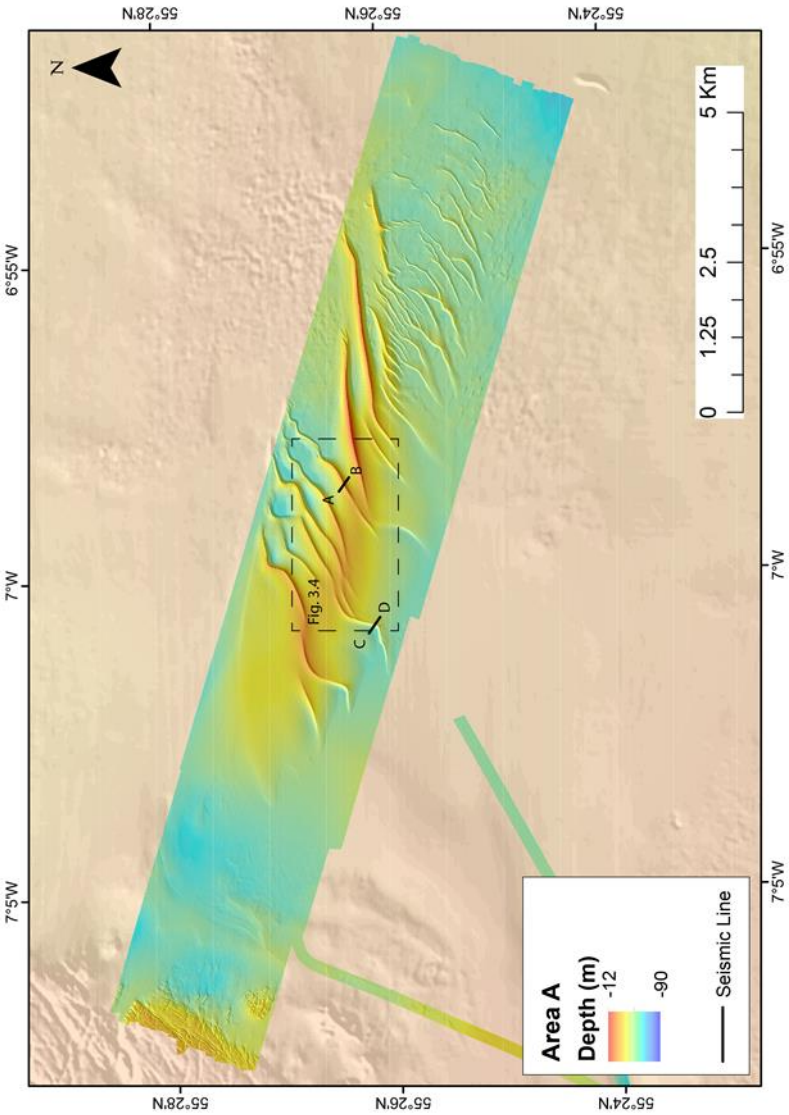

Fig. 3.2 Bathymetry of Area A, characterised by large asymmetric sediment waves and a field of smaller amplitude waves to the southeast. These waves are a stark contrast to the surrounding shelf. Bedrock from the Inishtrahull rock complex is apparent in the northwest. Locations of example crest measurements – dashed box (Fig.3.4) and seismic lines (Fig.3.8) are indicated. Background data from INSS (2004).

These sandwaves are superimposed upon a single feature which can be classified as a tidal sandbank or ridge (Caston, 1972, Williams et al., 2000). Exposed bedrock, known to be Paleoproterozoic granitic gneiss, is present in the north east of the area and forms part of the Inishtrahull Island rock complex (Muir et al., 1994).

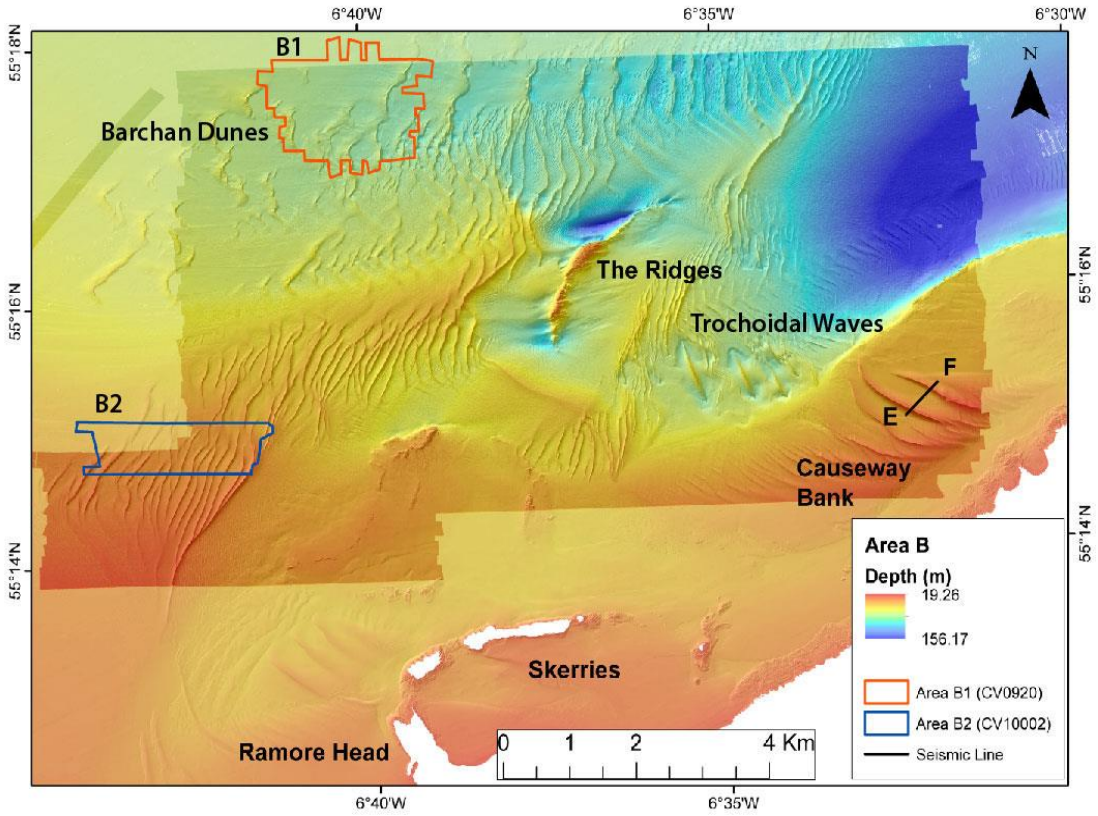

Fig. 3.3 Overview of bathymetry of Area B and subset areas B1 and B2. The Ridges and the Causeway Bank are evident in the data. Diversity of wave-form is displayed across water depths, for example >5 m waves in 35 m water depth atop the Causeway Bank and 2-3 m barchan dunes offshore in 70 m water depth. Underlying (translucent) data taken from JIBS survey (Oct, 2007) resurvey extent is defined by full colour scale.

Area B (Fig. 3.3) extends from the Causeway coast, northwards and westwards, up to 9 km from shore. Original MBES surveys were undertaken here in 2007 as part of the JIBS project. The centre of this area is dominated by a rocky reef outcrop known as 'The Ridges' (Plets et al., 2012) which provides a fixed depth object for surveying purposes. This site presents a variety of bedform sizes and morphologies. Notable bedform features include a barchan dune field in the northwest, three >20 m amplitude trochoidal waves in the southeast and the Causeway Bank which is a shallow linear shoal inshore (Fig. 3.3).

Both areas A and B were resurveyed in their entirely during cruise CV13031 (Sept 2013) as detailed in the following section. In addition, the two subset

areas of site B (B1 and B2, Fig. 3.3) were surveyed as part of other research cruises. Subset area B1 has undergone three separate MBES surveys. This 3.7 km^2 area was used as an open sea disposal site for dredge material from Lough Foyle (Bates, 1996). Characterised by crescentic barchan dunes, the area was first surveyed in 2007 as part of the JIBS program, then in 2009 as part of a University of Ulster's student survey with the most recent survey CV13030 carried out in 2013 as part of this research (time-lapses of two and four years respectively). Subset area B2, a 2.2 km^2 area, is 4.3 km to the northwest of Ramore Head (Fig. 3.3). Initial MBES data were collected as part of the JIBS survey in 2007, followed in 2010 by a University of Ulster's student training cruise (three-year time lapse period). A subsequent survey was carried out three years later as part of CV13030. This area is characterised by 5 m amplitude, sharp, crested sand waves.

3.4 Data Acquisition and Processing

This study will build upon the methodology adopted by others (Knaapen et al., 2005, Ma et al., 2014, Van Landeghem et al., 2012) by analysing changes in MBES data at two sites (Figs. 3.2 and 3.3). High resolution MBES data were collected off the north Irish coast in the two study areas A and B with a SIMRAD EM3002D system as part of research cruise CV13030 aboard the R.V. Celtic Voyager in late 2013 resulting in 48.8 km^2 of seafloor at Area A resurveyed in depths ranging from 19 m to 54 m (Fig. 3.2) and 83 km^2 coverage in depths ranging from 24 m to 155 m at Area B (Fig. 3.3). Differential Global Positioning Systems (DGPS) were used to provide decimetric horizontal and vertical

accuracies. Bathymetric and backscatter data were processed in Caris Hips & Sips v7.1 to 2 m resolution and converted to ASCII format for ease of integration with ESRI ArcGIS 10.1. (Evans et al., 2015).

Area	Survey ID	Survey Year	Program
A	INSS Combined Surveys	2004	INSS
A	CV13030	2013	MI Ship Time Grant
B	JIBS Combined Surveys	2007	JIBS
B	CV13030	2013	MI Ship Time Grant
B1	CE0920	2009	University of Ulster Student Training
B2	CV10002	2010	University of Ulster Student Training

Table 3.1 Table identifying each survey identification, year and the corresponding area identified in Fig. 3.1. Each survey formed part of a larger grant or mapping program which are also included for reference.

Existing raw data collected as part of the INSS in 2004, JIBS programs in 2007, student training cruises CE0920 (2009) and CV10002 (2010) were acquired with a SIMRAD EM3002D and were also processed, tidally corrected and vertically adjusted as part of this study to reflect CV13030 vertical datum. The alignment of each dataset to a common vertical datum allow for accurate interrogation of seabed changes using the Caris Hips & Sips surface difference module. The resulting data were then imported in ESRI ArcGIS 10.1 for further analysis.

3.4.1 Analysis of bathymetric data

Bathymetry data were examined using the ESRI ArcGIS hydrology toolbox. Research has proven bedforms differ in appearance when they have different solar illumination directions, known as azimuth bias, this coupled with user skill in interpreting 3d visual representation of bedform data necessitates an more quantitative approach to wave crest mapping (Smith and Clark, 2005, Smith and Wise, 2007). As a result, changes in bathymetry were scrutinised using the 'Flow Direction' script to provide a directional input for 'Flow Accumulation' analysis (Fig. 3.4). Flow accumulation is based on the number of inflow cells from the 'Flow Direction' script and identifies areas of bathymetric highs as zero values, with channels represented by high positive values. These high values are typically used by terrestrial hydrographers to map runoff channels and water pathways (Drake et al., 1985, López-Vicente et al., 2014, Neill et al., 2009) and have been applied in the marine environment to define the base of sumbmarine canyons (Sacchetti et al., 2011). In this instance, the inverse approach is applied, with focus on the zero values of the 'Flow Accumulation' script. These points identify slope peaks and were manually digitised as sediment wave crests.

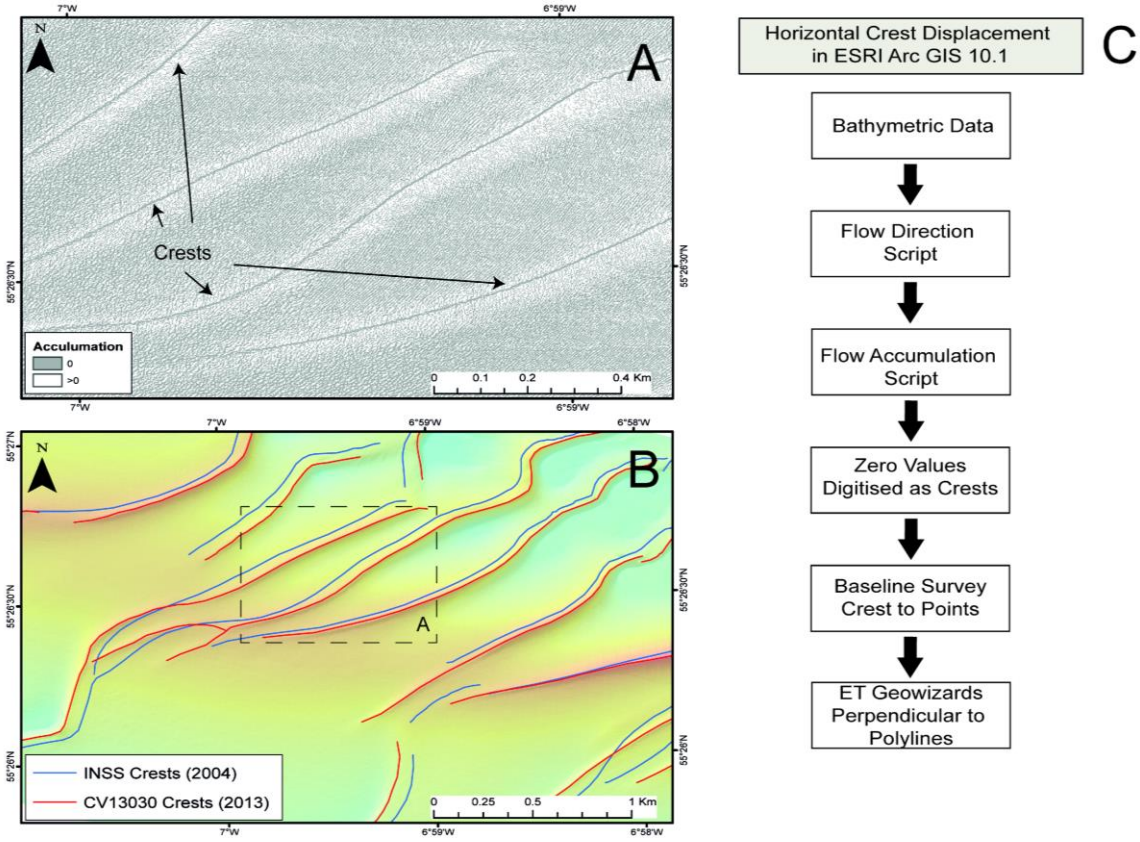

Fig. 3.4 Example of 'Flow Accumulation' data generated in ESRI ArcGis10.1 (A) where zero values represent crests (location Fig. 3.2). Digitised crests from 2004 (blue) and 2013 (red) show the displacement of sediment wave crests in this 9-year time lapse (B). Methodology workflow for derivation of crest position and measurement of migration between surveys (C).

This method removes the possibility of azimuth bias when interpreting crest ridge position manually (Fig. 3.4). Crestlines between successive surveys were then mapped to allow measurement of horizontal change. The ET Geowizards script 'Perpendiculars to Polylines' was used to create multiple perpendicular measurements between crests without the need to generate profiles. Vertical bathymetric change was calculated using Caris Hip & Sips v7.1 and presented as a surface difference model. Measurement inaccuracies were calculated by comparison of readings over the fixed depth objects in each survey area. As a result, allowance was given in each area to account for change in depth due to sampling inaccuracy, +/- 50 cm (area A) and +/-30 cm (area B). Changes

smaller than these calculated margins were classified as ‘Stable’ due to lack of confidence in the accuracy of the measurement.

3.4.2 Sediment sampling and grain size analysis

Sediment sampling was carried out at 63 stations across Area A and Area B using a Day grab during cruise CV13030 (locations illustrated in Fig. 3.5 B and 3.9 B). Sampling locations were selected using concurrent backscatter data in order to ensure a wide range of acoustic responses were ground-truthed. Samples were weighed, washed and wet-sieved at 63 microns to calculate the mud fraction. The remaining sediment was dried, weighed and sieved (at 4000, 2000, 1400, 710, 500, 355, 250, 180, 125, 90, 63 µm) (Goff et al., 2000). Grain size distribution was assessed using Gradistat v4.0 (Blott and Pye, 2001).

3.4.3 Backscatter classification

Backscatter and ground-truth data were collated in ESRI ArcGIS 10.1 to enable further analysis of sediment distribution across the two areas. Classification of backscatter using ground-truthing samples as verification is a commonly used method to infer sediment coverage in the marine environment (Goff et al., 2000, Lamarche et al., 2011, McGonigle and Collier, 2014). ‘Isocluster Unsupervised Classification’ routines were used to create a signature file, which then informed a ‘Maximum Likelihood’ multivariate classification of the backscatter response. The resultant clusters were then assigned a sediment type based on the analysed ground truth samples collected (Evans et al., 2015, Plets et al., 2012). It should be noted that some areas exhibit ‘striping’ in backscatter in areas of rapidly varying water depth; this is particularly obvious in Area B data (Fig. 3.9).

This striping could have been avoided by repositioning the survey track to insonify the seafloor alongslope rather than upslope/downslope (McGonigle et al., 2010a, Lamarche et al., 2011). Unfortunately a resurvey of this area had not been scheduled into the survey planning and alterations were not feasible while afloat. Through post-processing of the data, it may be possible to remove the erroneous beam signatures individually, removing the striping effect at the expense of data density (McGonigle et al., 2010b). The extent of correction required in this instance the resulting acoustic signatures would have required significant interpolation to present a complete backscatter mosaic, therefore it was decided to leave the artefacts rather than replace them data which may not truly reflect the sediments in that area.

3.4.4 Seismic profiling

Sub-bottom seismic profiling was also carried out during CV13030 using the hull-mounted SES Probe 5000 pinger system to examine internal structures within sedimentary bedforms. The seismic reflectors identified within the bedforms are interpreted as changes in sediment acoustic properties and therefore as variations in sediment grain size, composition and/or compaction (Bastos et al., 2003). Raw data were processed using IHS Kingdom Suite v7.1 and exported to Adobe Illustrator v5.0 for annotation.

3.4.5 Hydrodynamic model

Existing modelled hydrodynamic data were used to investigate the possible drivers of bedform mobility (or lack of it). Hydrodynamic data presented here were extracted from the Irish Marine Institute’s annually validated Regional

Ocean Modelling System (ROMS, www.myroms.org) and illustrated in ESRI ArcGIS 10.1. Outputs from the deepest depth averaged layer for the years 2011 - 2014 are shown in an attempt to examine long-term processes (Xing and Davies, 1996) and to illustrate flows at time of the most recent survey. These include residual flow and maximum flow, which are presented due to their particular relevance to sediment transport processes (Besio, 2004, Bøe et al., 2009, Lefebvre et al., 2014, Lobo et al., 2000). The tidal rule of 12ths suggests that in areas such as the Irish north coast, peak flow typically occurs 3 to 4 hours after high or low water. In a sediment transport context, these maximum flows may represent the only point at which grain sizes of a particular size are mobile (Martin-Short et al., 2015). As a result, some sediments may only be mobilised during certain elevated flow conditions (Barnard et al., 2013, Drake et al., 1985, Thiébot et al., 2015). The directionality of these peaks in flow velocity are also important as they may represent the more dominant flow orientation of a bi directional current (Sanay et al., 2007). It may also relate to an unusually high flow related to an extreme storm. The residual current (daily vector mean) can often vary in direction to the peak flow. It presents an overview of the averaged flows at a location throughout the measured or simulated time (Herman, 1983). In a sediment transport context this has a number of applications. Firstly if the mean flow is capable of mobilising sediments, it can give insight into the mean rate and direction of sediment transport (Masson et al., 2004, Wynn and Stow, 2002). When compared to matrixes such as that of (Stow et al., 2009) and (Belderson et al., 1982), the type of bedform expected to occur in that area can be identified. Residual current can be key to identifying longstanding currents such as European Shelf Current and Mediterranean

Outflow Water, but may also suggest more localised persistent effects these flows on sediments (Hanquiez et al., 2007b, White and Bowyer, 1997). A residual current which direction is opposed to other flows (either seasonal, maximum or certain states of the tide) may account for reduced migration or the displacement of sediment waves around a central point (Sanay et al., 2007).

The 2.1 km by 2.1k m model resolution for the study area, results in a paucity of hydrodynamic data within the specific study areas. While this model is useful in providing an overview of hydrodynamic conditions across the shelf, it cannot be used to discuss specific flow conditions at a bedform scale as they are smaller than the model grid resolution of 2.1km. It should also be noted that due to the scale of the model, it does not include small outlying islands such as Inishtrahull Island, which may have localised effects on hydrodynamics.

3.5 Results

3.5.1 Area A

The backscatter data for this area (Fig. 3.5A) show a large dark coloured area of soft sediments, clearly identified by the lowest dB values in the centre of the site. Backscatter response increases with distance from this centre point with harder substrates illustrated by lighter colours. This outward coarsening trend identifies the bedform at the centre to be composed of different grain sizes to the surrounding shelf. Sediment sampling and classification (Folk, 1954) at the site revealed four main substrate types (sandy gravel 35%, gravelly sand 27%, pebbles / gravel 27%, coarse sand with shell 11%) with the large asymmetric sediment waves in the centre of the area comprised almost entirely of coarse sand with shells (Fig. 3.5B, Sample 4).

Sediment generally becomes increasingly coarse with distance from the mid crest of these sand waves (Fig. 3.5B). Gravelly sand (Fig. 3.5B, Sample 2) and sandy gravel (Fig. 3.5B, Sample 11) surround the large asymmetric sand waves while pebbles and cobbles dominate the southeast extreme of the study area (Fig. 3.5B, Sample 1). High concentrations of the bivalve *Glycymeris glycymeris* were found within this pebbly material.

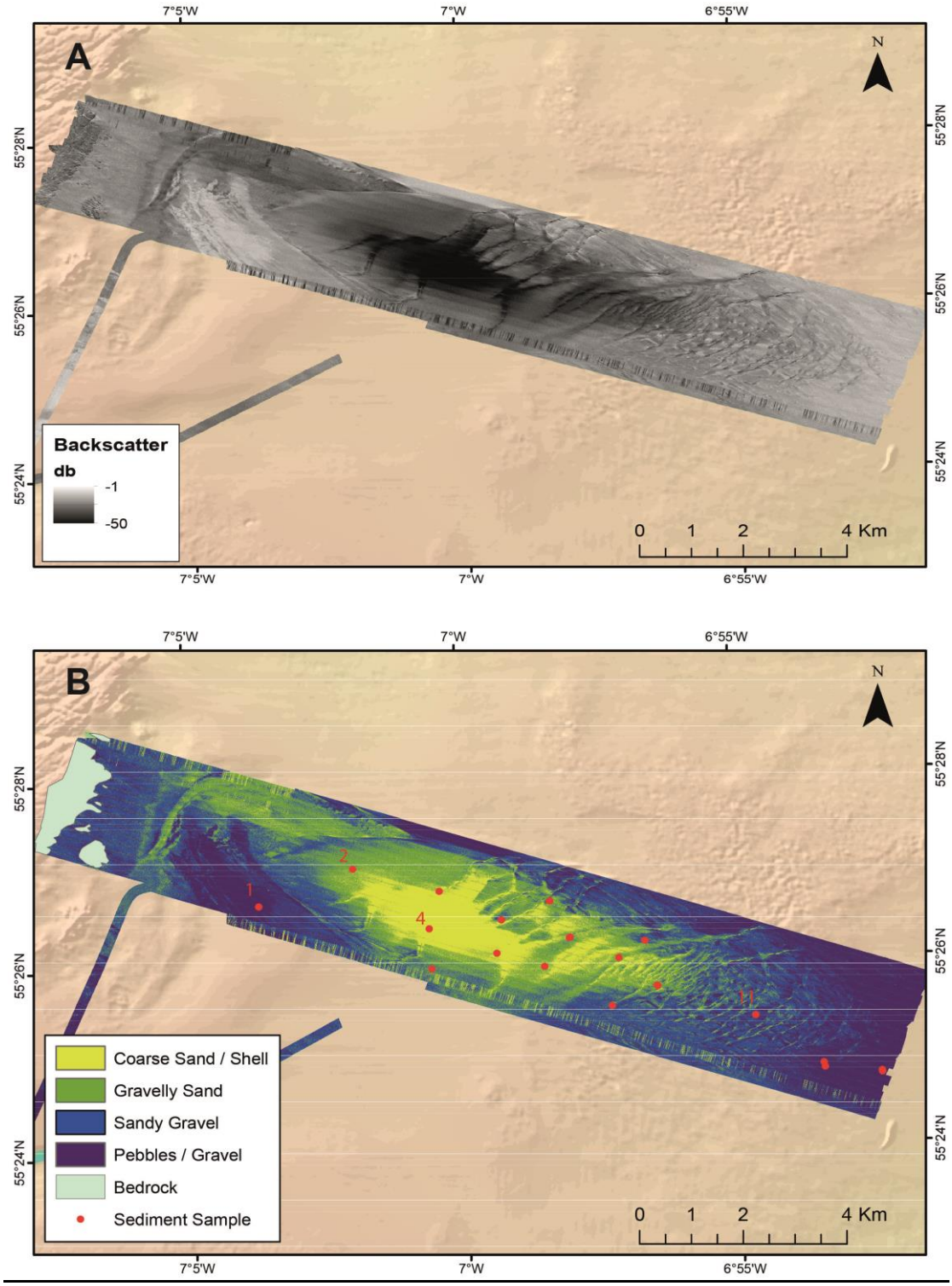

Fig. 3.5 Backscatter response recorded during CV13030 survey of Area A. (A) A large area of soft sediment is indicated by the lowest dB values (darkest colour) in the centre of the image. (B) Classification of backscatter using ground truth samples (red) reveal coarse sand in the area of the sediment waves surrounded by sediments of distally increasing grain size. Background imagery is 20 m resolution INSS data.

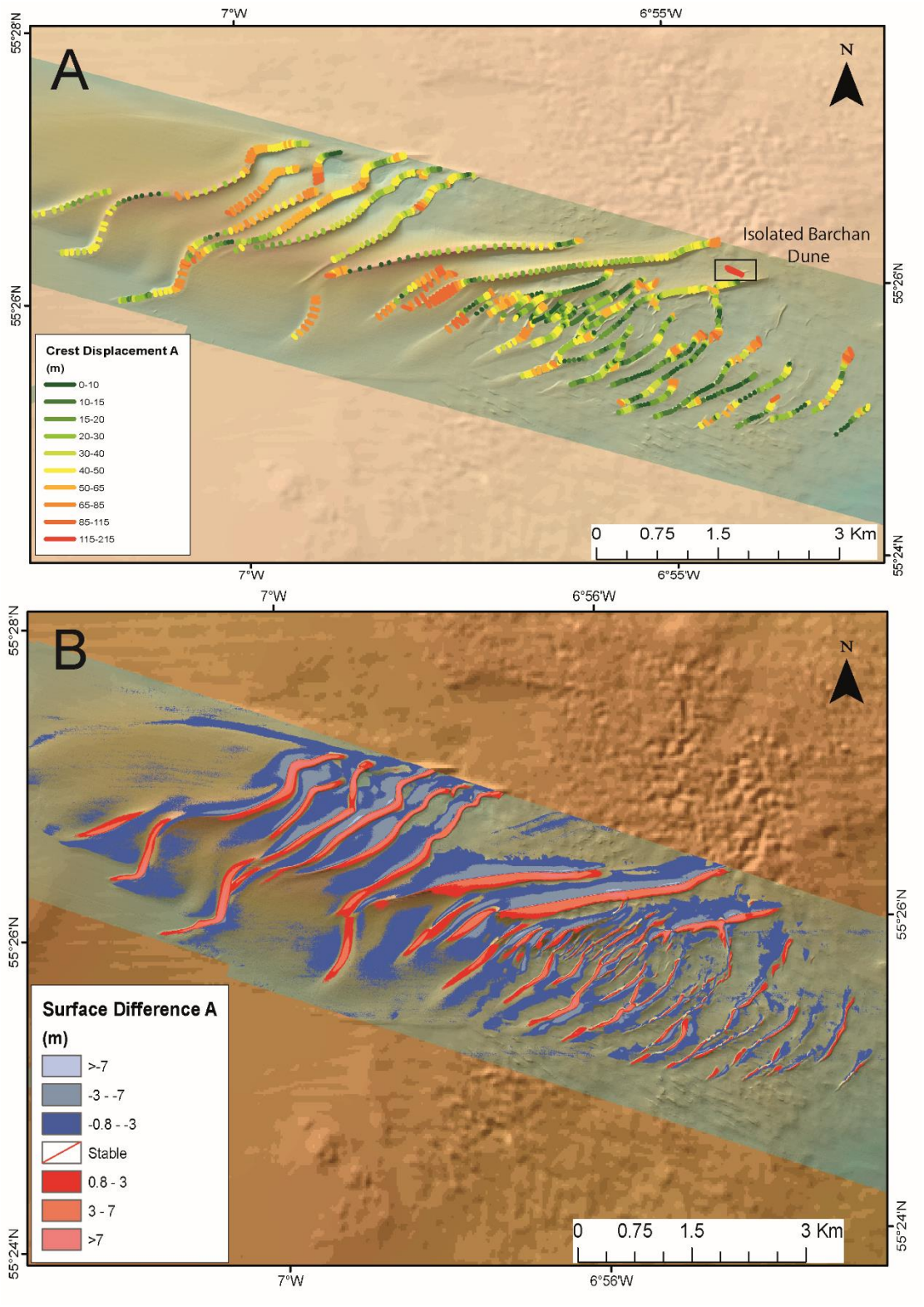

Fig. 3.6 (A) Crest displacement in metres across area A following 9-year interval. Highest migration rates are observed towards the northwest and centre sections of this site. Largest single wave migration measured at 211 m for an isolated barchan dune (black rectangle). (B) Surface difference model for area A. Changes of +- 30 cms are considered stable given the resolution of data acquired. Background imagery is 20 m resolution INSS data.

The crestlines of the sand waves range in length between 3.8 km and 0.8 km. Giant asymmetric waves present the longer sinuous crests (~3 km) whereas smaller amplitude waves in the southeast have shorter crest lengths (~0.9 km). In the time-lapse period of nine years, a clear migration of crests occurred across the entire bedform field (Fig. 3.6A). Maximum displacement was measured at 211 m and affected an isolated barchan dune on the fringes of the main bedform (approx. 23 m yr^{-1})(Fig. 3.6A). The giant asymmetric waves presented an average migration of 70 m at the mid-crest point over this time period (rate of 7.7 m yr^{-1}); however, this value decreases towards the crest ends. Crest movement is lower (<3 m yr^{-1}) towards the southeast of the site, where smaller amplitude waves are found. In contrast, these waves display larger (~5 m yr^{-1}) migration rates at the crest ends than at the mid-point (Fig. 3.6A). Highest migration rates (31% of total distance at the site) occurred in areas classified as gravelly sand and in water depths ranging 35-40m. Pebbly substrates underwent shortest migration rates when compared to other substrates, accounting for only 10% of the total migration across the area.

By examining the hydrodynamic forces across the area using the published ROMS model, it is possible to compare migration pathways with direction and intensity of bottom water flows over the site (Fig. 3.7) . Residual flow direction varies across Area A with a clockwise flow pattern (Fig. 3.7A), where higher residual flow velocities occur to the northwest and southeast of the large sand waves. This pattern is similar to that of the rate of crest displacement over the site (cf. Fig. 3.6A).

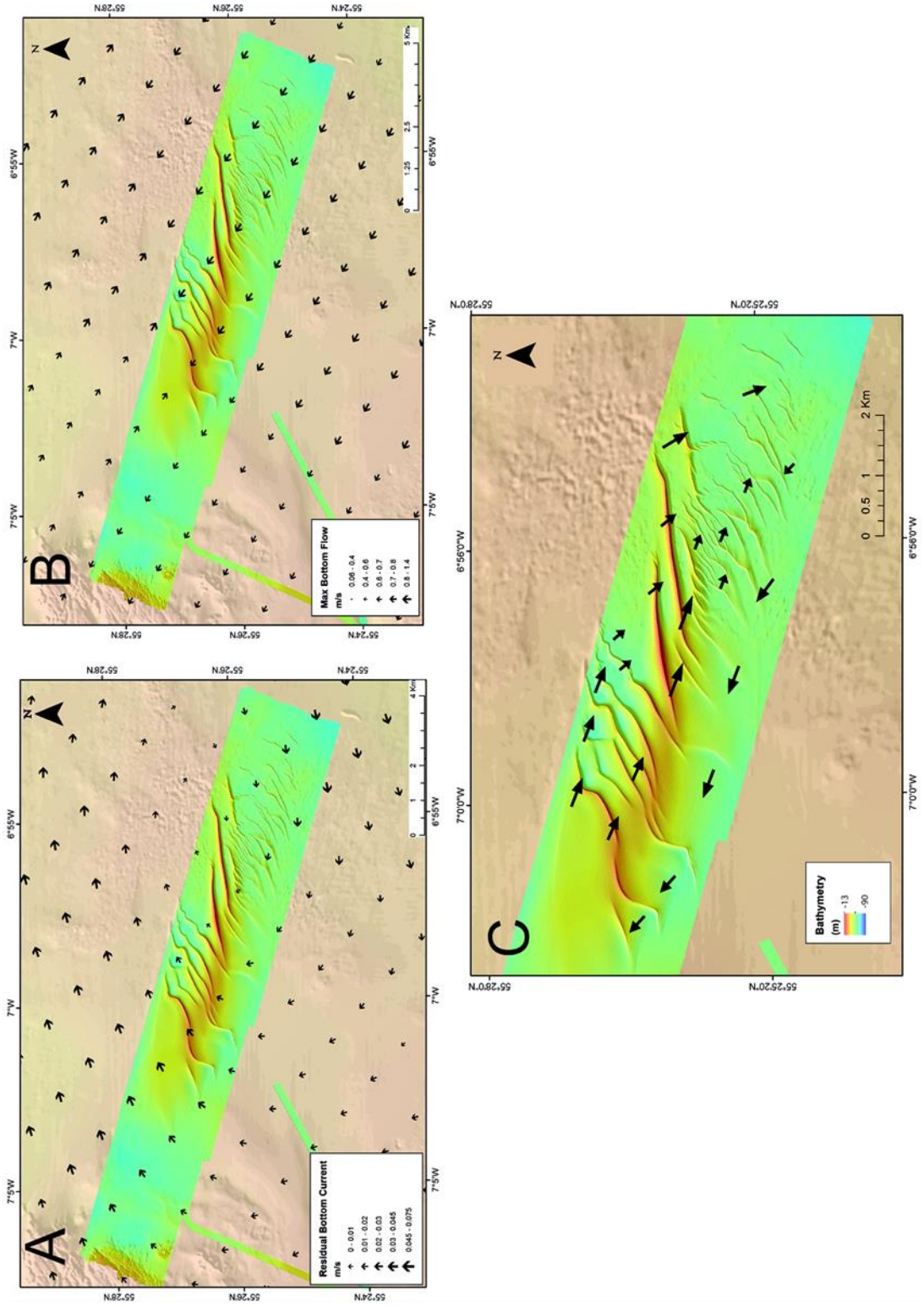

Fig. 3.7 Residual (A) and maximum flows (B) from the ROMS model (m/s). Note the similarities between residual flows and migration patterns (C) derived from time-lapse data. Arrows were created in ESRI ArcGIS using measurements from the 'Perpendiculars to Polylines' script and scaled according to migration distance.

Model data simulates maximum bottom current (Fig. 3.7B) velocities of 0.6 m–0.8 m/s, typically in a northwest direction. In all cases, direction of crest migration is in agreement with wave asymmetry and correlates with the direction of simulated bottom currents. The direction of migration, however, is not uniform across the entire bedform with crests presenting a clockwise, rotary migration pattern (Fig. 3.7C). This is consistent with hydrodynamic assessment of morphologically similar sandbanks in UK (Caston, 1972, Williams et al., 2000) and global shelf seas(Swift et al., 1978). The mid and northerly portions of the bedform appear to migrate in a southeast direction, whereas the southern crests and crest edges present movement in a northwest direction (Fig. 3.7C). In terms of their sub-bottom acoustic response, the large sediment waves are defined by a contact between acoustic unit 1 (AU1 in Fig. 3.8) and acoustic unit 2 (AU2 in Fig. 3.8). The clearly defined nature of this contact suggests a significant difference between the composition and/or compaction of the sediment that comprise these units. AU1 makes up the body of the sediment wave and is likely composed of coarse sand based on ground-truthing, whilst AU2 represents the underlying substrate. In some of the seismic profiles, an additional acoustic unit (AU3) is identified below AU2. This unit may possibly represent the underlying bedrock (Cooper et al., 2002, Plets et al., 2012).

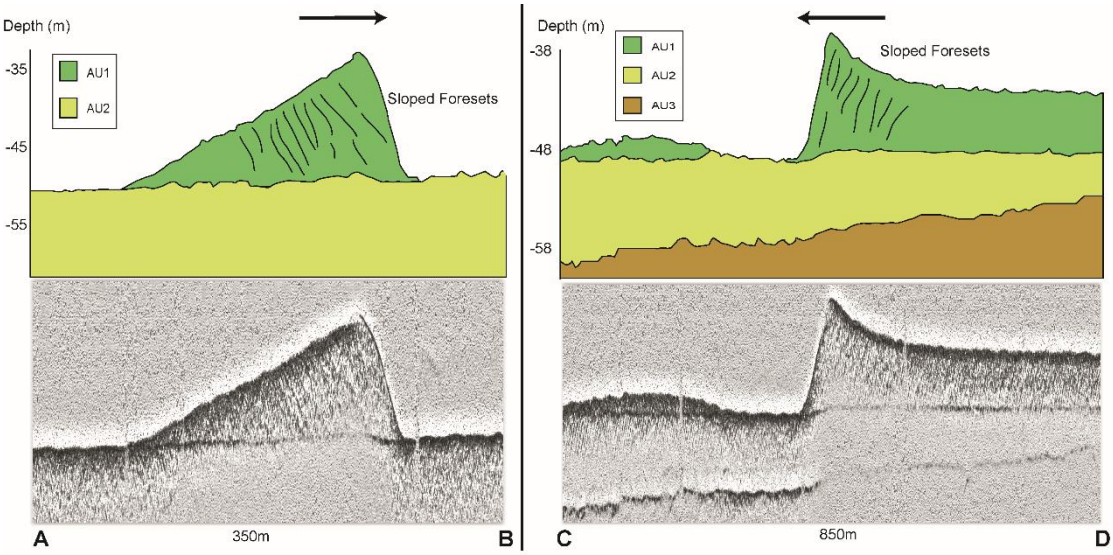

Fig. 3.8 Interpreted seismic lines and raw data from Area A (location indicated on Fig. 3.2). Sand waves (AU1) can be clearly identified and display a sharp contact with AU2. Inner sand wave stratigraphy reveals sloping reflectors interpreted as forests. Arrows indicate inferred migration direction.

The seismic data, acquired in lines typically perpendicular to wave crests, also revealed some of the internal structures within sediment waves (Ferret et al., 2010, Lobo et al., 2000). Steeply dipping foresets are revealed within the large asymmetric waves with an absence of opposing slip faces (Fig. 3.8). Investigation of cores taken over the site would confirm the composition of the acoustic units identified, the location of bedrock and potentially the foreset features present in the seismic data. The bedrock has however been identified as mudstone, formed from depositional processes and presents s stark contrast to the granites of Inishtrahull Island. The hard acoustic signal presented by AU2 suggests a glacial diamict possibly morainic in nature (Benetti et al., 2010b, www.gsiseabed.ie).

3.5.2 Area B

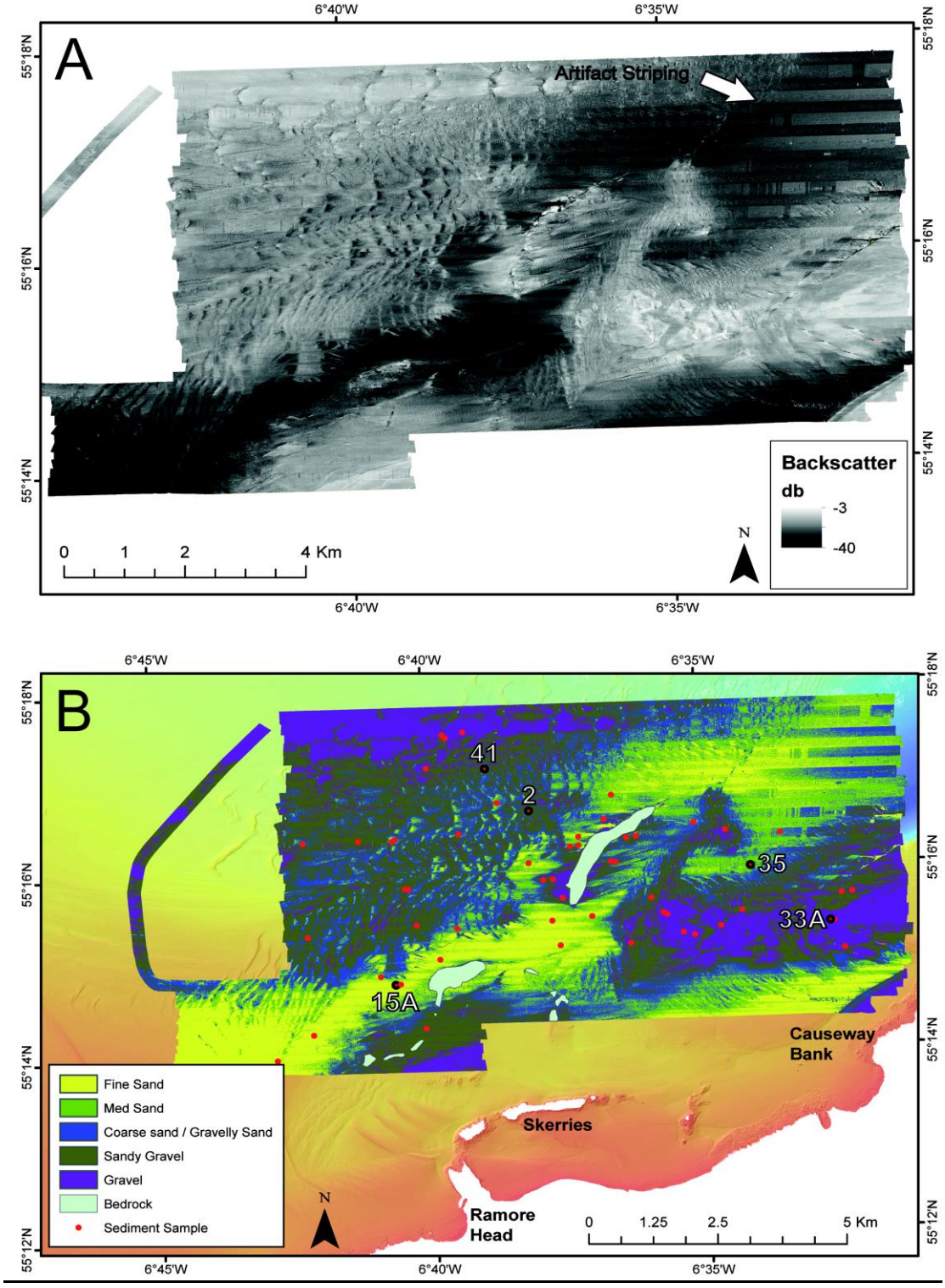

Fig. 3.9 Processed backscatter data (A) and classification (B) within Area B. (A) Some artefacts are present due to the difficulties in processing backscatter data in areas of rapidly varying bathymetry. (B) Five main sediment types have been identified with clear zonation of finer and coarser sediments across the site.

Sediment distribution in this region is more complex than that of Area A. This is illustrated by the pattern of backscatter response (Fig. 3.9A). Five main sediment types have been defined by sediment samples and backscatter classification (as percentage of total distribution - sandy gravel 27%, gravelly sand 21%, medium sand, 20%, gravel 17%, fine sand 15%) (Folk, 1954). Fine sand (Fig. 3.9B, Sample15A) forms three distinct zones: northwest of the Skerries, on the Causeway Bank and to the northeast of the Ridges. These fine sands are typically fringed by bands of medium (Fig. 3.9B, Sample 35) and coarse sand (Fig. 3.9B, Sample 41). Gravel (Fig. 3.9B, Sample 33A) and sandy gravel (Fig. 3.9B, Sample 2) dominate the northwest of the site and immediately north of the Causeway Bank. Some sediment samples in these areas were comprised entirely of very coarse shell hash and whole shell material. Classification of this shell hash as a single backscatter response grouping is difficult due to the similarity of signal return to that of other sediment types (Goff et al., 2000). Digitized crestlines at this site range from 7 m to 2.3 km in length and the form of the sediment waves varies from sinuous/crescentic to straight (Fig. 3.10A). An average migration of 14 m (2.3 m yr^{-1}) has been calculated over the 6-year time-lapse period. The largest displacements of >70 m are recorded to the east of ‘The Ridges’ (65m water depth) in an area of gently sloping bathymetry, with similar distances also measured on the ‘Causeway Bank’ (Fig. 3.10A).

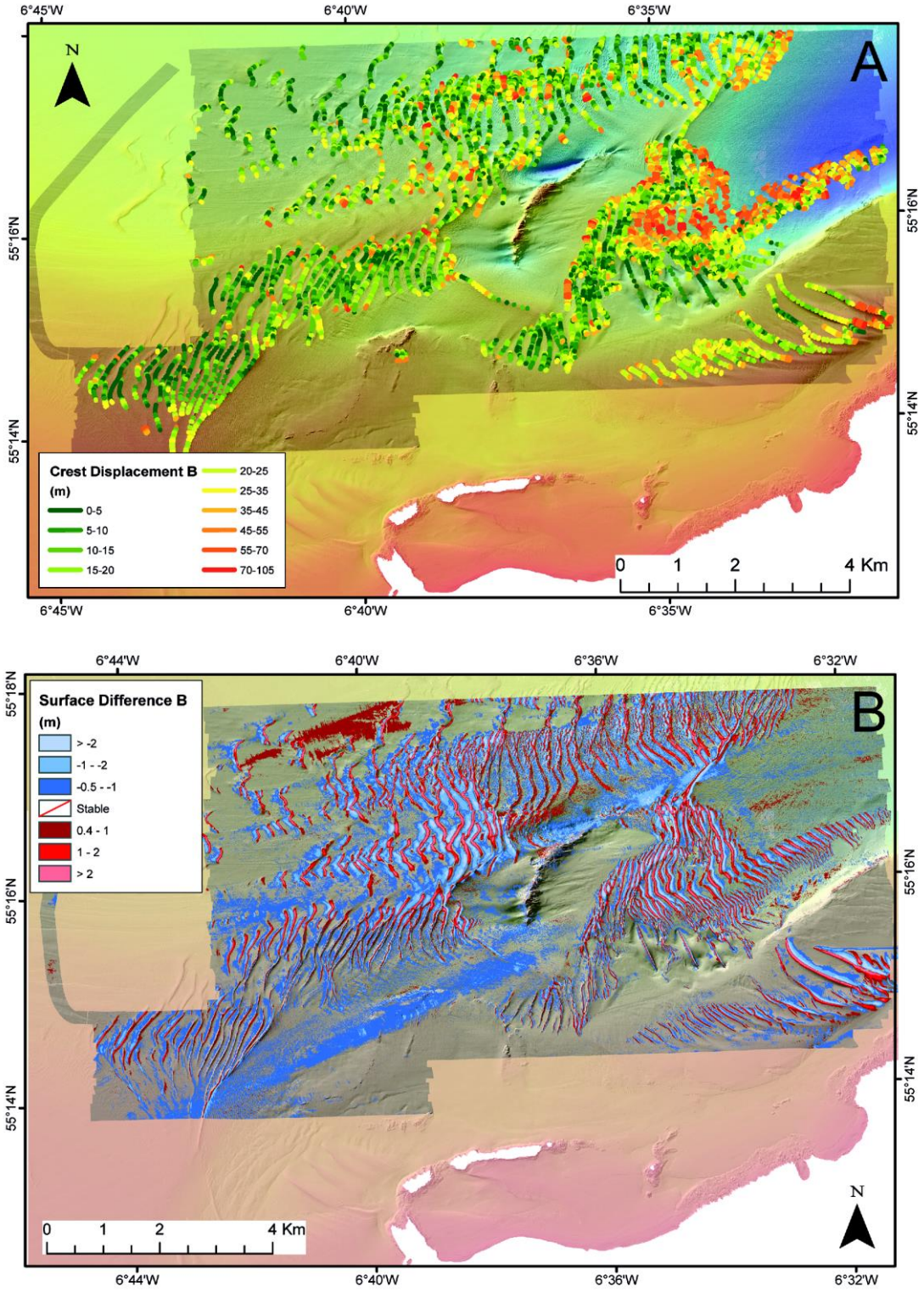

Fig. 3.10 (A) Crest displacement across Area B in metres displays the highest migration rates (over 70 m in 6 years) in the east and at closer distance to the shore. Colour palette has been adjusted to allow for easier identification of varying mobility rates. (B) Surface difference model for Area B has revealed distinct stripes of erosion and accumulation with a net loss of sediments across the area. JIBS MBES data is provided in background for context.

Migration distances between 14 m and 40 m, with rates between 2.5 m yr^{-1} and 5.2 m $yr^{-1}$the most common throughout Area B. Highest rates are observed in the shallower waters on the 'Causeway Bank' and in areas of sloping bathymetry. Crests displaying the lowest of migration distances of 1-5 m are located in the barchan dune fields to the northeast of the resurveyed area in ca. 70 m water depth (Fig. 3.10A). The distinctive, three large trochoidal waves (see. Fig. 3.3) also display movement of less than 5 m over this 6-year period. Migration was most prevalent in areas classified as gravelly sand, accounting for 31% of measured migration. Lowest migration rates were recorded in areas of fine sand (10%).

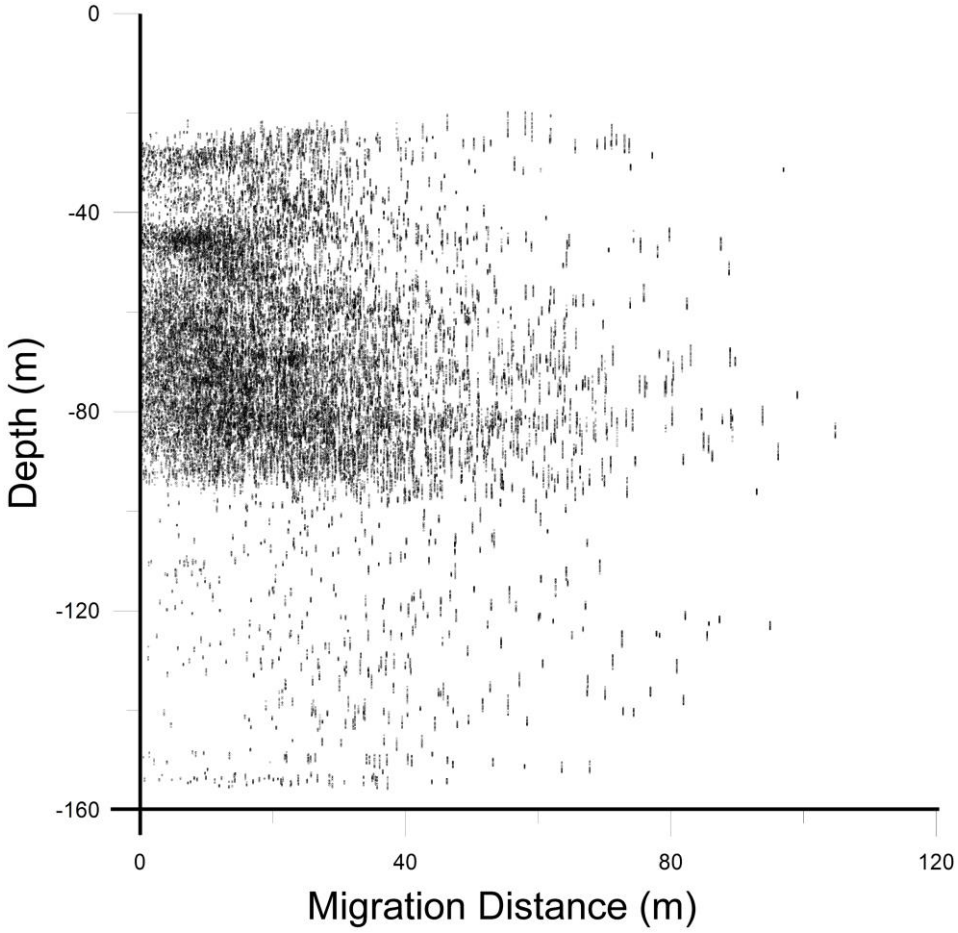

Fig. 3.11 Scatterplot illustrating variance of crest migration rate (m) with depth (m) at Area B. sediment waves are concentrated between 20 m and 85 m water depths.

Highest concentrations of sediment waves occur in 20-80 m water depth, with a slight increase in migration with depth across this range. Beyond 80 m depth, occurrence of sediment waves decreases (Fig. 3.11). This is in agreement with the findings of (Van Landeghem et al., 2009b) in the Irish Sea where sediment waves were found to be most prevalent up to 90 m water depth at which point there was a significant reduction. (Van Landeghem et al., 2009b) did however notice a reduction in sediment waves between 50 m and 80 m water depth which has not been evidenced on the north Irish Coast.

Hydrodynamic plots across the area give insight into flow / migration relationships. Residual flows suggest east and southeasterly flows across the area (Fig. 3.12A). ROMS model data reveals maximum flow velocities between 0.06 and 0.65 ms^{-1} (Fig. 3.12B). Results from this study present an overall trend for migration with movement from east to west in the offshore portion of the site with a counter, east to west, movement recorded inshore (Fig. 3.12C). Sediment wave crests in the northwest, including the barchan dune field, display movement in an easterly direction. This migration direction continues until an absence of sedimentary bedforms at the base of ‘The Ridges’. East of this rocky outcrop, bedforms display a south-westerly migration pattern including in the shallower waters of the ‘Causeway Bank’. 3 km to the west of the Skerries this westerly migration trend continues inshore, with a rotation in direction to the north-west (Fig. 3.12C). This pattern of migration can be linked to dominance of westerly flow in modelled currents for the inshore sections of Area B.

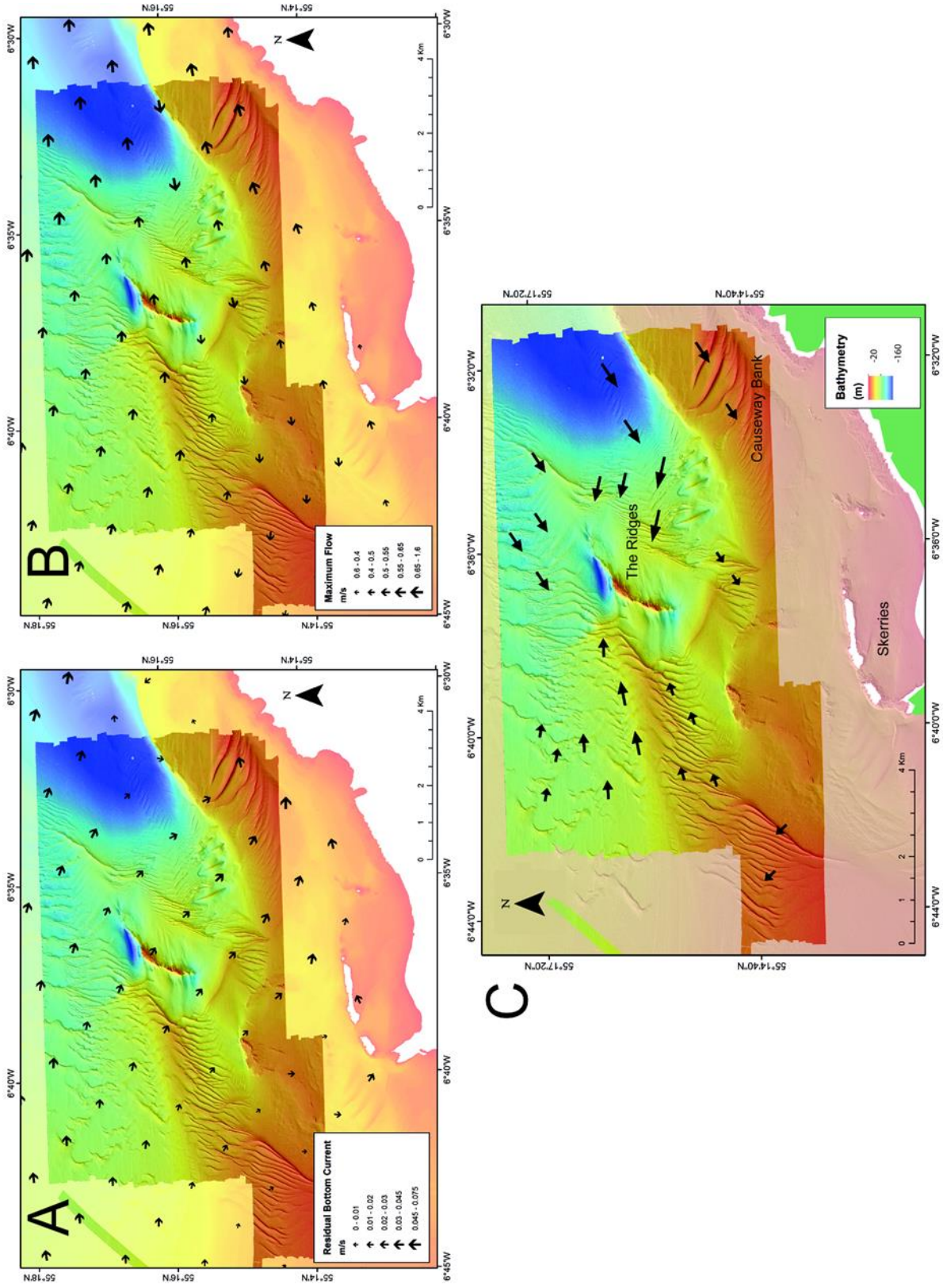

Fig. 3.12 Residual (A) and maximum (B) currents in Area B reveal significant differences in flow direction. (C) Observed crest migration appears to converge on The Ridges rock outcrop. Arrows were created in ESRI ArcGIS using measurements from the 'Perpendiculars to Polylines' script and scaled according to migration distance.

As in area A, seismic data collected over selected bedforms at site B show some of the internal structures within sediment waves (Fig. 3.13). Three acoustic units are clearly identified. AU1 comprises asymmetric waves, which are composed of medium and coarse sands. Sloping foresets of varying angle are present throughout this unit, though not always aligned with the orientation of the waves (Fig. 3.13). These waves are superimposed upon acoustic unit AU2, which is between 2 m and 5 m thick. The boundary between these units is not as clearly defined as in area A. This may be a product of data quality or mixing of sediments between these two units.

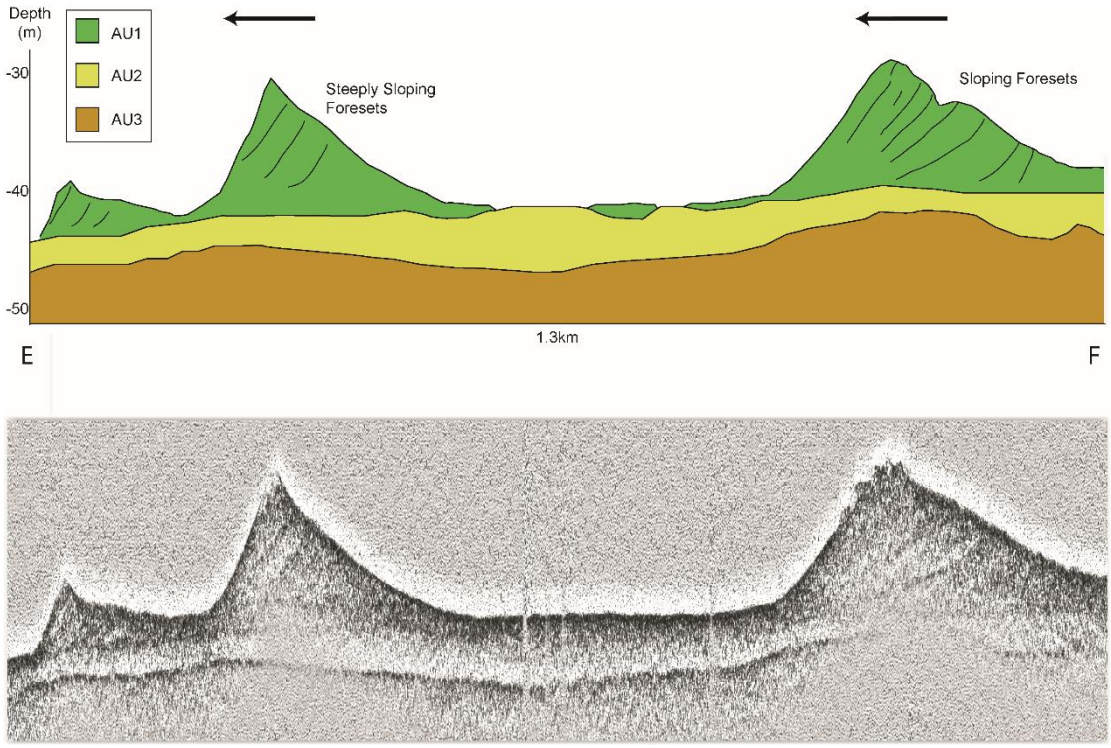

Fig. 3.13 Seismic line from the Causeway Bank identifying 3 acoustic units. Sand waves on the bank (AU1) overlay and infill AU2. AU2 and AU3 display a sharp contact, suggesting AU3 may be underlying bedrock. Sloping foresets within the sediment waves suggest these bedforms may be mobile. Arrows indicate inferred migration direction.

The top of the third acoustic unit AU3 is clearly defined by a sharp reflector and the unit itself does not present any internal acoustic response suggesting this may be the underlying bedrock. As with Area A, sediment composition, acoustic unit thickness and the nature of foresets could be identified by sediment coring across the site. It is however known that the underlying bedrock is igneous in nature and like much of the Causeway Coast, this shelf is composed of Tertiary basalt. Based on seismic studies in the area, AU2 is interpreted as glacio-marine sediment (Cooper et al., 2002, Kelley et al., 2006).

3.5.3 Subset B1

Sediment samples in this area comprise mostly gravel (Fig.3.9B, Sample 33A) and sandy gravel (Fig. 3.9B, Sample 2). Simulated currents suggest residual and maximum flows in an easterly direction with peak flows of 0.5 – 0.65 ms^{-1} (Fig. 3.12B). During the first 2-year time lapse a mean crest movement of 6 m was observed across the site (3 m yr^{-1}). While many of the barchan dunes to the north and east present little displacement, to the south and southwest, dune crests have migrated between 10 m and 15 m (5-7 m yr^{-1}). Movement is typically in an easterly direction with dunes of larger amplitude displaying higher migration rates. For the second time-lapse period of 4 years the data reveals a 10 m mean migration distance (rate of 2.5 m yr^{-1}). Almost all crests display movement in an easterly direction, up to a maximum of 35 m. Northern barchan dunes show little displacement during the first time-lapse, with measured migrations of up to 20m (5 m yr^{-1}), also in an easterly direction.

3.5.4 Subset B2

Sediment samples show that this area is covered mostly by fine sand (Fig.3.9B, Sample 15A), fringed by medium (Fig. 3.9B, Sample 35) and coarse sand (Fig.3.9B, Sample 41). Maximum simulated flows in the area range from 0.5 to 0.55 ms^{-1} in a westerly direction. Residual flow direction is counter to this with south and southeast orientations modelled (Fig. 3.12A). During the first time-lapse period of 3 years, average rate of crest migration was 4 m yr^{-1}, with maximum crest movements (up to 27 m) occurring in the south and east. Crest displacement in a southwest direction is typical across the site, with lowest migration rate values towards the centre of the surveyed area. The subsequent time-lapse (3 years) shows average rate of crest migrations of 3 m yr^{-1}. Wave crests appear to have oscillated back in an easterly direction, towards their position at the time of the original JIBS survey. No notable change in bedform asymmetry is apparent between the three surveys at this site.

3.6 Discussion

Repeat surveys of two selected areas of the north Irish shelf has revealed complex patterns of sedimentary migration. It is accepted that irregular intervals of resurvey data, variances in equipment, and vessels used may constrain the accuracy and interpretation of the data, however in investigations of this type some of these issues cannot be avoided and the only mitigation is to factor possible errors into analysis of data (Schmitt et al., 2008). While net fluxes of sediment over each area are suggested and average migration rates are defined for crest displacements, it is also accepted these are open to challenge

due to the nature of time-lapse survey at this temporal resolution. For example, the migration of sediment waves in two opposing directions, such as those identified in Subset B2, can be difficult to interpret without the increased temporal resolution of data. In the case of crest flexing shown by the trochoidal waves, repeat surveys through a daily tidal cycle may be required to capture the extent of this movement (Smith et al., 2007, Xu et al., 2008). Nevertheless, careful site selection and post-processing have given insight into sediment mobility rates and their correlation with bedform asymmetry, sediment type and modelled hydrodynamic conditions across the shelf.

3.6.1 Area A

The sandwaves which dominate the section of seafloor surveyed at Area A appear to be superimposed upon a single feature with dimensions and geometry consistent with features classified as offshore tidal sandbanks or ridges (Caston, 1972, Swift et al., 1978). Sandbanks are found globally in shelf environments where sand is abundant and flow rates are < 0.5 m/s. As a result, the local distribution of coarse sands (Evans et al., 2015) and flow rates calculated by the Marine Institute ROMS model (Fig. 3.7) can account for the formation of the sandbank at Area A.

While documentation of sandwaves reaching heights of 10 m is prevalent (Field et al., 1981, Li and King, 2007, Németh et al., 2007), examples of heights reaching 20 m are not common in shelf environments and published literature on their properties is sparse (Van Landeghem et al., 2009b). At these water depths (40 m max) these sand waves do not agree well with the equations of

(Francken et al., 2004, Terwindt, 1971)) which state that an upper limit for bedform height is 0.25 times the water depth. In this instance the sandwaves reach more than twice this upper limit of ~ 10 m. These calculations were devised within riverine systems however, and increasing examples of deviations from their values are observed in coastal environments (Bartholdy et al., 2002). An average displacement rate of 7.7 m yr^{-1} for large waves of this height is consistent with annual migration displayed by similar sandwaves in other tidal seas (Németh et al., 2007, Li and King, 2007, Van Landeghem et al., 2012). Crest displacement across this area displays a correlation between bedform height and transport rates, with larger amplitude sand waves achieving greater mean migration rates. The lower amplitude, more rounded sediment waves to the south-east represent an area with smaller volumes of sediment, which is coarser. This coupled with possible shadowing from the larger sandwaves to the north east may account for their reduced migration rates (Van Landeghem et al., 2012).

Sediment transport is not linear across the site with crest displacement indicating a clockwise, rotational movement. This rotational current is described on sandbanks globally, evidenced through in situ measurement (Huthnance, 1973, Williams et al., 2000) and modelled calculations (Sanay et al., 2007). These banks are therefore proven to have a profound effect on local hydrodynamics (Sanay et al., 2007). This rotary current best evidenced at Area A by the residual flow outputs from the ROMS model (Fig. 3.7). Residual flow has been identified as the most important mechanism for sediment transport in offshore tidal sandbanks and can drive movement even when flow velocities are low (Warner et al., 2005). This is evidenced by the migration patterns of the

sandwaves at this location which closely follow the modelled residual flow (Fig. 3.7).

Surface difference models also suggest that there has not been considerable loss of sediment from the bedform over the 9-year lapse, adding weight to the assumption that while a bidirectional current is in effect across the bedform with hydrodynamics reworking the sediment within the confines of the bedform boundaries. With high-energy tidal currents in the region contributed to by the constriction of water flow at Inishtrahull Sound to the west, it is likely that the sandbank upon which the waves are superimposed, is experiencing complex hydrodynamic forcing. This creates rotary currents generated by the morphology of this sandbank and its orientation to tidal flows (Huthnance, 1973, Williams et al., 2000). As a result, the scale of these sand waves may be accounted for by localised reworking of sediments within this rotary current system (Hill et al., 1996, Zhu and Chang, 2000, Ferentinos and Collins, 1979). Further analysis using Acoustic Doppler Current Profiler (ADCP) or hydrodynamic modelling at an appropriate scale is required to confirm this.

Area A surface difference models also identify migration through accretion and erosion in patterns matching the geometry of the sediment wave's crests and troughs. There is a net loss of sediment from the area resurveyed. This is in agreement with pre-existing oceanographic modelling of the Irish shelf, where an off-shelf suspended sediment transport pattern had been identified (Davies and Xing, 2002). As a result, while an eddy system may account for the scale of these sand waves trapping sediments in a localised area, storm processes and periods of upwelling inducing winds could result in a removal of sediment from the site through suspension (Davies and Xing, 2002). The steeply angled

foresets revealed within acoustic unit 1 (Fig. 3.8A) of these sand waves agrees with bedform migration and asymmetry direction. Their acute angle on the stoss slope indicate high sediment mobility (Lobo et al., 2000, Ma et al., 2014). The lack of opposing slip faces suggests that these waves are little influenced by oscillating currents (Bastos et al., 2003, Van Landeghem et al., 2009a).

3.6.2 Area B

The majority of sediment waves occur between depths of 30 m and 90 m in Area B (Fig. 11). This is consistent with the findings of (Van Landeghem et al., 2009b) in the Irish Sea, where concentrations of sedimentary waves were measured between 30 m – 40 m and 85 – 95 m. Horizontal migration rates display significant variance across Average rates of crest displacement of 2.3 m yr^{-1} may not suggest an area of high mobility. However, localised patches of highly mobile sediment waves have been identified. The highest rates of crest displacement ~10 m yr^{-1}, are found in a 700 m-wide band on a slope ranging from 85 m to 130 m water depth. This suggests that this area is undergoing enhanced migration due to temporally changing bathymetry (Van Landeghem et al., 2012). The Causeway Bank, at a 25 m water depth, experiences higher than average migration rates for the site, between 5 m and 6 m yr^{-1}. This is likely due to increased effects from tidal flows due to reduced water depths. Lowest migration rates occurring offshore are not surprising given the increased water depths at these locations (Berelson, 2001). Migration direction is complex with two main opposing directions of movement, which appear to be divided by a rocky outcrop (Fig. 3.12). This outcrop displays significant scouring on the

western side and lack of bedforms (capable of being resolved by this data resolution) for 0.9 km either side of its peak. This can likely be attributed to turbulence caused from the outcrop under bi-directional flow conditions (Lefebvre et al., 2014, Quinn et al., 2007). A net migration towards this rock from the west is typical in this area, with the exception being sediment waves on the seafloor to the south, which display movement in the opposite direction. To the east of the survey area, crest migration also seems to converge on the rock outcrop, thus supporting the argument that this 20 m - 30 m obstruction into the water column is having a significant effect on a bidirectional current in the area. Migration of sediments in an upslope direction is also prevalent in this eastern portion of area B. This suggests a forcing factor beyond the boundaries of the survey area that is creating a westerly residual current in the near-bed even at depths >100 m. Three distinctive large trochoidal waves in the area have undergone little change in the 6-year time-period. This is consistent with the development and maintenance of bedforms of this size and symmetry (Barrie et al., 2009, Cataño-Lopera and García, 2006, Masson et al., 2004, Wynn and Stow, 2002). Bedforms such as these typically occur due to internal tides where a bidirectional flow interacts with a sharp change in bathymetry (Hand, 1988), in this case, the Causeway Bank. Surface difference models for Area B, like Area A, display accretion and erosion associated with the movement of a sediment wave through its wavelength. A net decrease in surface height between surveys suggests a negative sediment budget (i.e out of this area). Highest levels of erosion (without subsequent accretion) occur to the south west and in a narrow band immediately north of The Ridges (Fig. 3.10B). These strips are in the base of bathymetric depressions with no discernible bedforms in MBES data and are

adjacent to rock outcrops. As a result, these areas may be undergoing erosion of between 10 cm yr^{-1} and 30 cm yr^{-1} due to tidal interaction with these outcrops. It is unclear however where this eroded substrate is being deposited. It is likely that this is a long standing process and it is hypothesised that due to the turbulence associated with rock outcrops, any finer sediments have been carried away in suspension (Quinn et al., 2007). Seismic data from the Causeway Bank (Fig. 3.13) have revealed sediment waves (AU1) with sloping, curved foresets. Curved foresets are normally the result of sediment movement down the lee slope of the bedform (Bastos et al., 2003, Van Landeghem et al., 2009a) and can be attributed to lower energy environments than those observed in Area A. These waves appear to migrate over an underlying surface (AU2), interpreted as coarser material that has not been mobilised by currents. While the use of three surveys over area B1 suggested a constant migration trends, area B2 showed more variation. Over the 6-year period, wave crests have displaced and average of 4 m yr^{-1} to the west (3 years) then 3 m yr^{-1} back to the east in the following 3 years. Crest flexing, the movement of a crest under bidirectional flow about a centre point in of the sediment wave, may be ruled out due to the geometry of the sediment waves in question but may be accounted for by the opposing directions of modelled peak and residual flows over these bedforms. Higher temporal resolution of survey is therefore required to better understand the oscillatory movement of these sediment waves (Smith et al., 2007, Xu et al., 2008).

3.6.3 Comparison between Area A & Area B

The areas selected for repeat surveys encompass a range of water depths, differing hydrodynamic regimes and are characterised by different bedform types. It is therefore unsurprising that the rate of bathymetric change varies throughout the period of data acquisition. Due to the narrow range of water depths at Area A, comparison of migration rates with Area B is difficult. However, bedforms on the Causeway Bank, in water depths comparable with the giant asymmetric sand waves of Area B, appear to migrate at similar rates of between 6m yr^{-1} and 7m yr^{-1}. The direction of migration at both sites seems to be controlled by a dominant feature, a counter clockwise current in the case of Area A, and outcropping bedrock in Area B. While the ROMS model outputs are not of high enough resolution to allow accurate comparison between simulated flow and migration patterns, modelled residual currents present some agreement in both areas. Calculations of net sediment movement reveals that both areas to have lost sediment between surveys. This overall erosion appears to be more uniform in Area A and more localised in Area B. The relatively small scale of these repeat surveys in a shelf context makes it difficult to identify where this sediment has been deposited or to identify all the erosive processes that contributed to this process.

3.6.4 Limitations

The lack of definitive data on oceanographic conditions across these two sites represents a significant data gap when assessing sediment transport at these two sites. Deployment of current meters, such as Acoustic Doppler Current

Profilers (ADCPs), presents challenges in such a dynamic environment due to the possibility of burying through accretion of sediments. Additionally, the shiptime grant associated with this research could not allow for the deployment and recovery of moored equipment over the time periods required to acquire meaningful current data. Not only would this accurate flow data be invaluable to understanding localised flow regime, it would further validate the hydrodynamic model upon which many hypotheses included in this chapter are based. It can be argued that the Marine Institute's ROMS model is limited in application for these two sites. Horizontal resolution is too low to allow proper interrogation of flow rates across differing zones of sediment type, bedform or migration rate. A depth averaged vertical resolution also means that the distance of output data from the seafloor can vary greatly. This also calls into question the accuracy of the flow velocities which the model calculates at this scale. This lower resolution mesh is unable to account for localised flows around islands and headlands, and by design, must smooth coastline to compliment cell size. It does however present the most comprehensive of all existing models considered as part of this research, including data spanning the required time and area (including depth), regular validation and outputs which can be easily accessed. It is clear that further studies into the drivers of formation and migration of these bedforms would benefit greatly from a hydrodynamic model designed with sediment transport processes in mind, including an increased horizontal and vertical resolution over bedforms and the ability to create outputs specific to seabed processes such as bed stresses (Cacchione et al., 2008, Kheiashy et al., 2010, Staneva et al., 2009, Thiébot et al., 2015). It may be possible, through the description of cores aligned with seismic lines, to better define the nature of the

acoustic units identified in Fig 3.9 and 3.13. An understanding of the composition of these units would allow inferences to be made as to the volume of sediment which is moving the foresets within the seismic data to be identified,

3.6.5 Significance of Sediment Migration

Analysis of data from Area A, characterised by large asymmetric sand waves, has revealed highly mobile sandy sediments. These sandy sediments appear to be reworked in a rotational current generated by the morphology of an offshore tidal sandbank isolated on a largely planar, gravel-covered portion of the Irish shelf (Evans et al., 2015, Huthnance, 1973, Plets et al., 2011, Williams et al., 2000). The retention of these sediments may be dependent on the unique hydrodynamic conditions in the area (Bartlett and Celliers, 2016). This is significant for several reasons. Proposals are in place to install an offshore tidal turbine at Inishtrahull Sound ~15 km to the southwest (Fig.3.1) (Rourke et al., 2010). While research concerning the downstream effects of these installations is ongoing, an alteration to the hydrodynamic regime that creates and maintains these giant sandwaves is possible (Barrie and Conway, 2014, Thiébot et al., 2015). Modelled data of proposed sites around the globe suggest that turbine effect on sediment transport can be far reaching and typically reduces flow energy downstream (Ahmadian et al., 2012, Neill et al., 2009). This reduction in downstream flow could result in a potential break down in these sandwaves (Nash and Phoenix, 2017). This would result in the release of large volumes of soft sediment across an otherwise rock and gravel-dominated shelf area. This not only could have an effect on benthic organisms in the area (Hendrick et al.,

2016), but may also have implications for marine installations themselves (Morelissen et al., 2003). Given that the feasibility of marine engineering sites and routing of associated cabling is often governed by the stability and composition of the seafloor (Morelissen et al., 2003, Thiébot et al., 2015), the high mobility rates and large volumes of sediment contained within the bedforms at Area A should be taken into account (Martin-Short et al., 2015). Erosion and accretion of sediment on the shelf can also impinge onto processes further inshore. Sediment budget, affected by shelf sedimentary transport processes, is an important factor in determining appropriate management of marine resources such as aggregates and the location of dredge disposal sites, especially in areas of coastline vulnerable to erosion by wave action (Rosati, 2005). Habitat classification has become increasingly important in the marine environment to enable adequate management of our waters. Further understanding of the rate at which the seafloor moves in this area has implications for this, with sediment type and mobility forming the basis of Joint Nature Conservation Committee (JNCC) / EUropean Nature Information System (EUNIS) biotope selection. Current flow and sediment mobility are difficult to interpret via conventional methods used in habitat mapping such as video tows, yet both are important factors in determining area suitability for a given species (Reise, 2002). This knowledge of bathymetric change may then be used to identify areas which undergo periods of erosion and inundation, which is important to sessile organisms and may have implications for fishery breeding grounds (Levin and Dibacco, 1995). Lastly the evaluation of erosion and accretion processes has also been highlighted as key to the management of historically significant wreck sites, of which there are many adjacent to the

study area (Brennan et al., 2013, Quinn and Boland, 2010). The rates of sediment migration and net flux of sediment are clearly of significance on the north Irish shelf, however the methodologies to assess them and the implications discussed here are applicable other shelf environments globally.

3.7 Conclusions

- A multi-method approach for the assessment of sediment transport has been utilized effectively in a high energy, continental shelf environment. The use of ArcGIS hydrology tools in the application of wave crest determination and ET Geowizards scripts for measuring crest displacement has proved to be a time effective and quantitative way to quickly generate information on bedform migration. Backscatter classification has allowed a complete picture of the nature of the surface sediments characterizing the bedforms and surrounding areas, while seismic profiles can reveal information about sediment dynamics over time.
- A combination of MBES, seismic profiling and sediment ground truthing have provided a more complete picture of the sediment transport processes occurring on the north Irish shelf. Both areas surveyed revealed mobile sediments with distinct migration directions controlled by a primary factor, a rotational current at Area A, and ‘The Ridges’ rock outcrop at Area B. The use of multiple repeat surveys has also highlighted oscillation of sandwaves at a spatial scale longer than their wavelengths. The utilisation of MBES in analysing both horizontal and vertical change across these two sites has

been effective on a decimetre scale and is corroborated by existing hydrodynamic models of the area.

- This work suggests that shorter time intervals between successive surveys and improved spatial data resolution for both hydrodynamic conditions and sediment distribution are required to improve the validity of these inferences made regarding sediment transport.

Chapter 4 – Hydrodynamic modelling of bedform formation and sediment transport: insights into modern and relict bedforms

Evans, W., Benetti, S., Jackson, D., Lyons, K., Dabrowski, T. *Hydrodynamic modelling of bedform formation and sediment transport: insights into modern and relict bedforms*.

4.1 Introduction

Understanding of shelf sediments, bedforms and their mobility is becoming increasingly important as anthropogenic interactions with our coastal environments rise (Barnard et al., 2013, Daniell, 2015, Rosati, 2005). Early investigations into shelf sediments were conducted by the Victorians, using wax plugs to capture a seafloor sample when measuring water depths (Mayer, 2006). Since then, marine surveys have become increasingly sophisticated over time, with modern equipment presenting 3D imagery of the seafloor, surface sediment composition through backscatter data and sub-seafloor imagery through seismic data analysis (Davies and Thorne, 2008, Li et al., 2012). A range of deployable equipment has also been developed such as Acoustic Doppler Current Profilers (ADCPs) which can measure current velocity and suspended sediment through water column noise (Hoitink and Hoekstra, 2005, Holdaway et al., 1999), or sediment transport specific landers such as Sediment

Transport And Boundary Layer Equipment (STABLE) (Huthnance et al., 2002). These devices are left in situ to record data for defined periods to be retrieved at a later date thus removing the requirement for constant monitoring over extended time periods. An alternative means to investigate sediment transport is the use of scale models to represent real world environments (Curran et al., 2015, Xu et al., 2010). Much of the knowledge on the formation of bedforms and their migration has been developed in these controlled flume tank / wave tank experiments (Messaros and Bruno, 2010, Rubin and Ikeda, 1990).

While in situ measurements are an important element to any marine investigation they often come at high cost. Marine research vessels and associated equipment are expensive to deploy even for short periods of time (Huthnance et al., 2002, Thorne and Hanes, 2002). It may also be the case that the area of research interest is simply too large for in situ measurements or deployable equipment to generate a scientifically robust data set from which conclusions can be drawn (Brown and Blondel, 2009, McBreen et al., 2011). Increasingly, hydrodynamic models have been incorporated into sediment transport investigations to provide water column data at a range of scales. They can be used to calculate bed stress and turbulence, important drivers in sediment transport (Davies and Xing, 2002, Liu and Huang, 2009). Models can also support or disprove assumptions made based on asymmetry, sediment grain size or time-lapse survey measurements (Bellec et al., 2008, Bøe et al., 2009). Hydrodynamic models range in size with Global ocean models providing an excellent overview of large-scale phenomena such as El Niño or the North Atlantic Oscillation However it has long been recognised that it is the shelf and coastal regions that are the centres of biological productivity, chemical cycling

and socio-economic importance (Barnard et al., 2013, Crowder and Diplas, 2000, Holt et al., 2009, Shan et al., 2011). It is also in these coastal regions that an understanding of sediment transport is critical to maintaining shipping lanes, managing sediment budgets and siting of marine engineering projects (Staneva et al., 2009, Rodríguez and Dean, 2009), As a result of this need for coastal modelling, there has been an increase in resolution from global models at a cell size resolution of ~200 km, to cell sizes of less than 1 km resolving complex coastlines within confined bays and inlets (Brière et al., 2007, Shan et al., 2011, Sheng and Yang, 2010, Staneva et al., 2009, Wu et al., 2011). These coastal models, however, are not entirely removed from the larger global scale models. Each boundary for a hydrodynamic simulation requires a time series of inputs to drive the numerical calculations. These are typically wind, tide, atmospheric pressure, runoff or some anthropological input to a system (Béranger et al., 2004, Wakelin et al., 2008, Zanuttigh, 2007). As a result, coastal or regional ocean models typically use inputs from a global model as forcing boundary conditions (Holt et al., 2009, Shan et al., 2011, Sheng and Yang, 2010, Staneva et al., 2009).

Several areas in Irish territorial waters have proved both challenging and of great interest to modellers, in particular, the Irish Sea, the Malin Sea, and the North Channel with the ebb and flow of its tidal streams (Fig. 4.1). The latter areas were selected for investigation due to varied seafloor morphology including submarine canyons, shallow banks and ridges, which not only made simulating real world conditions a challenge, but also ensured that the research could be applicable to many shelf environments around the globe (Davies and Xing, 2002). The natural constriction of the North Channel (Fig. 4.1) also

provides an excellent location to examine water exchange processes between the Irish Sea and waters of the Atlantic (Knight and Howarth, 1999, Young et al., 2000). Early attempts to model oceanographic processes in these regions were 2D and coarse (>1 km) in resolution. While allowing numerical analysis of flows at a particular height in the water column, elements such as turbulence, bed stress and vertical currents could not be examined (Davies and Gerritsen, 1994, Xing and Davies, 1996).

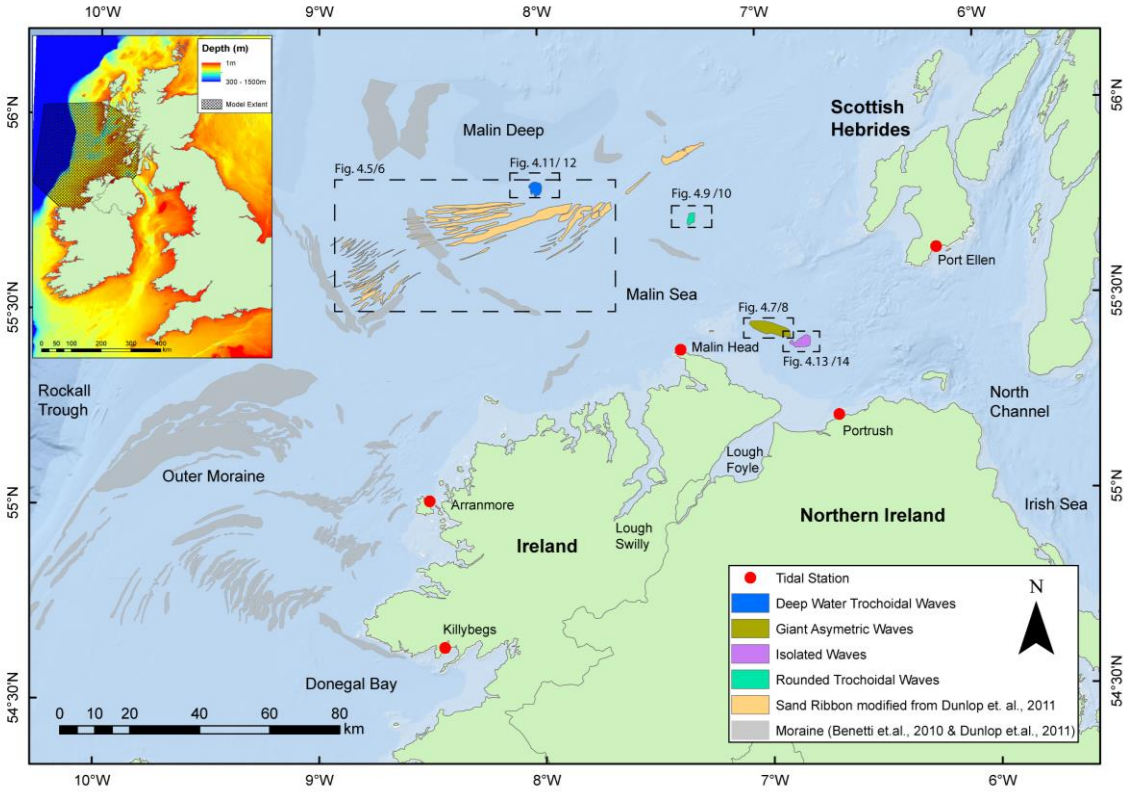

Fig. 4.1 Study area with distribution of bedforms of interest. Tidal station locations are shown spanning the model domain. Model extent with bathymetric data is also indicated (Inset).

These early models, however, illustrated the importance of tidal phases within coastal waters, in particular the influence of the M_2 and M_4 tidal harmonics around Ireland (Sinha and Pingree, 1997). When the complex hydrodynamics of the North Channel were successfully simulated using a 3D model, numerical

analysis of water flows began to show their full potential (Young et al., 2000). (Xing and Davies, 2001) utilised a similar 3D model to fully examine complex, shelf edge flows, mixing and internal waves in the Malin Sea. In a similar study (Lynch et al., 2004) utilised models (FUNDY, THURXTON and QUODDY) to identify a seasonal current circulation on the Irish west coast, which has since been linked to the transit of anadromous fish, spawning cycles of commercially important species and the appearances of harmful algal blooms during the summer months (Goodwin et al., 2013, Raine, 2014).

While simulation accuracy is governed by the resolution of the model mesh used, computational capability may also be a limit on model resolution (Callaway et al., 2011b, Crowder and Diplas, 2000, Knight and Howarth, 1999, Legrand et al., 2006, Young et al., 2000). As a result, model meshes of varying resolution can be utilised to downscale grid size over areas or objects of interest (Legrand et al., 2006, Staneva et al., 2009). These nested mesh models are typically used in areas with complex coastline or tidal harmonics and have been used to great effect on Canadian macrotidal inlets (Sheng and Yang, 2010), for Atlantic hurricane storm surge prediction (Shan et al., 2011) and sediment accretion assessment of shipping channels in the German Bight (Staneva et al., 2009). Applications for these hydrodynamic models are ever expanding. In an Irish shelf context, these numerical simulations have been utilised to examine biological properties such as chlorophyll content (Dabrowski et al., 2014, Siddorn et al., 2007), nutrient fluxes at depth (Moll and Radach, 2003, Proctor et al., 2003) distribution of pollutants (Callaway et al., 2011a, Raine, 2014) and defining sites with greatest marine renewable energy potential (Rourke et al., 2010).

While previous investigations into modelled shelf currents and possible interactions with shelf sediments have been investigated at a coarse >2 km resolution, they did not have access to wealth of high-resolution bathymetric and sedimentary data that have become available for the Irish continental shelf in the last 10 years. This research aims to utilise this high-resolution bathymetric data (ranging from 20 m to 2 m) and recent studies of sediment distribution on the shelf to generate a higher resolution, sediment transport specific hydrodynamic model for the north Irish shelf. To this end, a nested mesh model encompassing an offshore area of 103,000 km^2 (Fig. 4.1, inset) has been generated with the capability to resolve hydrodynamic conditions at a scale more relevant to bathymetric data. This nested mesh approach allows shelf-wide measurements of current speed to be calculated at <1 km resolution while in areas of special interest identified from MBES data, maximum resolutions of 5 – 10 m have been achieved. This flow data can then be analysed alongside sediment grain size to make robust predictions of sediment transport (Hjulstrom, 1935, Miller et al., 1977). Further to this, bed stress simulation accuracy has been improved by including sediment grain size distribution as a model input. Bed stress is a key factor in measuring the likelihood of a specific sediment type to become mobile and significant effort has been made to ensure this output is as realistic as possible (Huthnance et al., 2002, Miller et al., 1977, Wu et al., 2011).

This newly developed hydrodynamic model is utilised here to:

- Investigate the formative processes influencing selected bedforms mapped on the north Irish shelf by (Benetti et al., 2010a) and (Evans et al., 2015)
- Validate assumptions based on asymmetry and time lapse MBES measurements made in Chapter 3 relating to bedform mobility.
- Identify if classification of these bedforms as actively mobile is substantiated by model data

4.2 Regional Setting and rationale for selection of seabed features

The study area encompasses the north Irish Shelf and includes sections of the Rockall Trough and approaches to North Channel between Scotland and Northern Ireland (Fig. 4.1). As a result, depth ranges from ~2000 m at the bottom of the continental slope to 180 m at the shelf edge, from which depths vary more gradually to shore. Recent mapping programmes have significantly increased knowledge of bathymetry in this region and have resulted in identification on the seafloor of glacial bedforms such as moraines, drumlin fields and iceberg scour marks (Benetti et al., 2010b, Dunlop et al., 2011, O'Cofaigh et al., 2012), and contemporary bedforms such as sand sheets and ribbons, as well as mapped surface sediment distribution (Evans et al., 2015, Plets et al., 2012). Much of the shelf is composed of gravelly, coarse sand and

gravels with coarse sediments and bedrock dominating the inshore waters <50 m. Mud and silt distribution is confined to bathymetric depressions considered to be low energy environments. Fine to medium sand distribution is localised and relates to the contemporary bedforms identified by (Evans et al., 2015), some of which have been selected for further investigation as part of this research (Fig. 4.1). They include sand ribbons, giant sandwaves, rounded trochoidal waves and isolated waves, which were selected to enable analysis of hydrodynamic conditions across varying bedform morphology, water depth, sedimentary composition as well as assumed transport potential. Sand ribbons in the area form elongated ridges up to 16 km long and 1.2 km wide (Evans et al., 2015). The orientation of these crests give indication of dominant flow direction across a large section of the shelf (Belderson et al., 1982, Hanquiez et al., 2007a). Giant sand waves composed of coarse sand are up to 20 m high and have crests reaching 5 km long. Located in 35 m water depth, these waves were selected due to the high degree of asymmetry they display. This is an indicator of bedform mobility (Belderson et al., 1982, Besio et al., 2008c, Kenyon and Stride, 1970, Van Landeghem et al., 2009b, Van Landeghem et al., 2012). Chapter 3 utilises MBES data collected several times at the same location to confirm this interpretation, measuring an annual migration of 7.7 m yr^{-1}. Rounded deep water trochoidal waves were chosen to examine the hydrodynamic energy in proximity to bedforms which display indicators of low mobility, in this case rounded crests and low asymmetry (Terwindt and Brouwer, 1986). The high energy of this environment has led to difficulty in collecting annual in situ data and has resulted in a seasonality bias with higher resolution data collected in calmer months (McMahon, 1995). The result has been reliance

upon remote sensing methods, langrangian and eularian floats to study much of the oceanographic conditions on the north and west Irish shelf (Fernand et al., 2006, Inall et al., 2009, Pingree et al., 1999). A number of studies described common oceanographic patterns (Fernand et al., 2006, Inall et al., 2009, Lynch et al., 2004, Pingree et al., 1999, Raine, 2014, White and Bowyer, 1997). The most prominent is the northward flowing European Slope Current (ESC), which closely follows the shelf edge offshore Ireland for some 1600 km (Inall et al., 2009). Described as a barotrophic, geostrophic flow with velocities controlled by bathymetry (Pingree et al., 1999), flows from the ESC in excess of 0.66 m/s have been recorded in portions of the northwest Irish Shelf, with peak flows typically occurring during winter months. The ESC makes intrusions onto the shelf, between 55^{o}N and 56^{o}N, resulting in a split in the current. These intrusions appear to relate to winter conditions (Souza et al., 2001). The ESC has remained the defining feature of multiple studies, using a variety of instruments, across a 15-year period and illustrates its persistence as the dominant oceanographic characteristic of the Irish shelf. It is therefore feasible to envisage that this current has influenced sediment transport and bedform formation in the path of its flow (Masson et al., 2004). Understanding the potential mobility of these features and the forces driving sediment transport are of relevance in both an Irish and global context. Habitat mapping relies heavily upon sediment type and flow velocity as part of biotope classification processes (Reise, 2002). Further to this, sediment movement is particularly important for fishery breeding grounds and sessile organisms where inundation by new sediments can lead to unsuitability for spawning or attachment (Levin and Dibacco, 1995). This shelf region experiences high wind and wave energy from

Atlantic Ocean weather systems (Fernand et al., 2006). Forecast models suggest this wave energy is set to increase due to alterations in wind fields as a result of global warming predictions (Dodet et al., 2010, Zacharioudaki et al., 2011).

4.3 Methods

4.3.1 Model

The hydrodynamic model selected to simulate currents on the north Irish shelf, Mike 3 by DHI, is capable of simulating flows in estuaries, bays and coastal areas. Three-dimensional models in marine environments require mass conservation, momentum conservation, conservation of salinity and temperature and also equations relating local density to salinity, temperature and pressure (Ferziger, 1987). For this reason, Mike 3 by DHI utilised the mass conservation equation, The Reynolds-averaged Navier-Stokes equations which describe how the velocity, pressure, temperature and density of a moving fluid are related (Chorin, 1997, Lewis, 1980). The Reynolds component of the equation expresses the ratio of inertia forces to viscous forces. Lastly Boussinesq assumptions are included to better calculate propagation of flow from deep to shallow water (Madsen et al., 1991), particularly important given the range of depths within the model domain here (https://www.mikepoweredbydhi.com/products/mike-3) . Inputs into the model include: MBES bathymetry, atmospheric pressure data, variable bed roughness data and tidal elevation data for boundaries.

Land boundaries were converted from Geological Survey of Ireland (GSI) coastal shape files with non-wet/dry offshore islands digitised as polygons to exclude them from the computational mesh. Five open model boundaries were selected to avoid areas of rapidly varying bathymetry and to promote perpendicular intersections with land boundaries in an effort to mitigate erroneous results (Fig. 4.3A). Due to their open-ocean, deep-water location which can often cause issues with wave build up in the model, a boundary in the northwest has been designated a 'Flather' boundary to improve model stability, with the validated Marine Institute ROMS model providing additional inputs (Flather, 1976, Oddo and Pinardi, 2008, Sleigh et al., 1998). This allows waves to propagate out beyond the model boundary and ensures tidal elevation input at the model extents remains realistic.

To provide an overview of shelf conditions, a flexible triangular mesh with a maximum element size of $3x10^5$ m^2 was generated, resulting in 113,963 nodes. MBES data collected as part of Joint Irish Bathymetric Survey (2 m resolution, JIBS), of the Irish Nation Seabed Survey (20 m resolution, INSS) and of the Integrated Mapping For the Sustainable Development of Ireland's Marine Resources programme (20 m resolution, INFOMAR) form the baseline bathymetry for the model. In offshore areas where this high-resolution data (<20 m) is not available, General Bathymetric Chart of the Oceans (GEBCO) data at 1 km resolution was used to complete depth interpolation across the entire mesh (IOC et al., 2003). None of the features discussed in this research are sited within a 10 km radius of this lower resolution data, in order to maintain accuracy of bathymetric influence. This bathymetric data was interpolated into the mesh using a natural neighbour algorithm and then smoothed through 100

iterations to improve simulation performance. Vertical resolution was defined by a combination of 6 sigma and 5 z-layers (Song and Haidvogel, 1994). Sigma layers allow a more accurate representation of seabed contours but require more computational effort to simulate. Sigma layer distribution was varied to increase resolution in the boundary zone as illustrated in Fig. 4.2A and 4.2B (c=0.1, θ=4, β=1). Z layers are useful to resolve deep section of the model where high-resolution outputs for the water column are not required. As Fig. 4.2C shows, the reduction in computation requirement comes at the cost of seafloor resolution, creating the blocky appearance. As a result z layers have only been used to resolve areas beyond the shelf break and a suitable distance from areas of specific interest (Song and Haidvogel, 1994).

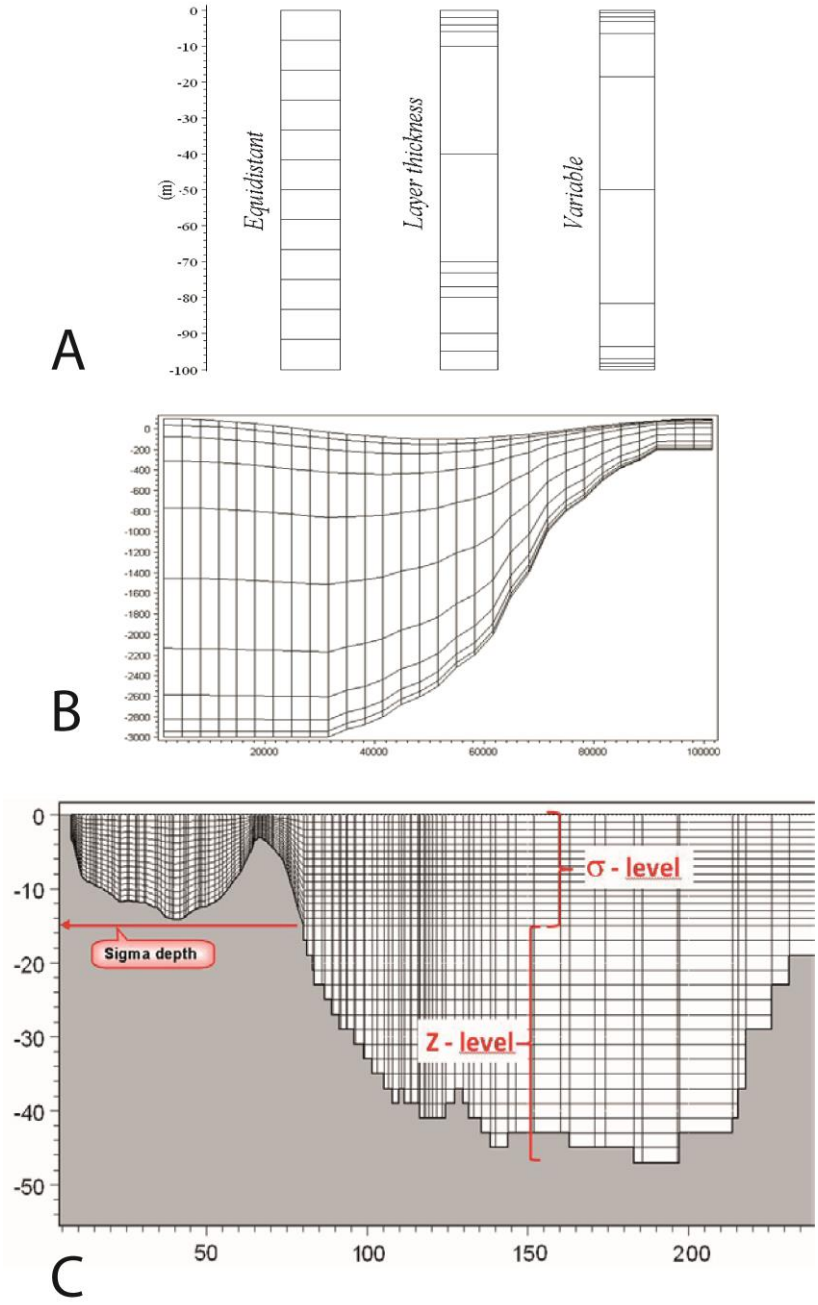

Fig 4.2 Diagram illustrating vertical mesh setup in Mike by DHI. A and B illustrate the use of a variable approach to model layers when higher resolution close to the seafloor is required. C demonstrates the effect of sigma and z layers on resolution of bathymetry.

This mesh was then adapted to increase resolution over areas of interest, with element sizes of 300 m^2 achieved resulting <22 m between data points. The time-period modelled spans 365 days between 2003 and 2004 with data binned in 20-minute intervals to maintain accuracy across the tidal curve. This period

was selected to coincide with the dates of multibeam acquisition, the data from which forms the basis of bedform classifications. It also represents a length of time relevant to seasonal variation and tidal harmonics.

Tidal elevations at boundaries are derived from the Technical University of Denmark (DTU), Global Ocean Tide model with a resolution of 0.125º x 0.125º and including 12 major tidal constituents. Atmospheric forcing is derived from European Centre for Medium-range Weather Forecasts (ECMWF) data, which provides mean sea level pressure with u and v wind velocities every 6 hours at a 0.1º x 0.1º resolution. This atmospheric model data was provided by DHI's hindcast modelling department and was optimised for use with the mesh designed for this research.

To more accurately simulate bed stresses across the area, a variable bed roughness is included. Sediment grain size derived from backscatter classification carried out by (Evans et al., 2015) between 2 m and 12 m resolutions is used to calculate a Nikuradse roughness value (typically 2.5 x grain size) with the exception being areas of <63 μ, where morphology typically becomes the governing factor on bed stress (Nielsen and Guard, 2011). In non-surveyed areas where backscatter classification data is unavailable, values were chosen based on United Kingdom Seamap data (McBreen et al., 2011).

Model validation was carried out by comparing simulated elevation data to Global Ocean Tide model elevations and measurements at 5 coastal tidal gauges (Arranmore, Killybegs, Malin Head, Port Ellen and Portrush) (Fig. 4.1). Root mean square errors between simulated and measured tidal elevations were calculated and a percentage agreeance value generated (Gunn and Stock-Williams, 2013). This method of validation has been selected due to the

size of the model area, lack of current data and the associated difficulties with using current data to validate complex flow regimes across a large area (Gunn and Stock-Williams, 2013).

The model outputs include: maximum and mean current velocities and bed stresses. These are the data that can provide the key hydrodynamic information to interpret the formation of seafloor bedforms (Wu et al., 2011).

4.4 Results

4.4.1 Current Data

Modelled current velocities at the near-bed zone across the shelf range from negligible to 3.8 m/s with an average flow rate of 1.2 m/s. Peak flow (Fig. 4.3A) rates display considerable variation in current speeds. The nature of maximum velocity calculations means they may be accounted for by a single snapshot in time or a short-term process such as a storm. As a result, many of the bays in the model mesh exhibit peak velocities exceeding 1 m/s. These high velocities are also apparent in the North Channel and to the north of Malin Head. The Rockall Trough, Malin Deep and a shelf region between 8º58W and 9º35W are the few areas to maintain consistently low flow velocities of less than 0.2 m/s. Lowest flow rates <0.1 m/s occur in the Rockall Trough and Donegal Bay areas of the model domain. The majority of the remaining shelf area experiences average flow rates of between 0.1 and 0.3 m/s (Fig. 4.3B). Localised increases in these rates occur proximal to sea loughs (Loughs Swilly and Foyle) and around areas of constricted flow (offshore islands and the North Channel). In these areas mean flow rate can exceed 0.8 m/s.

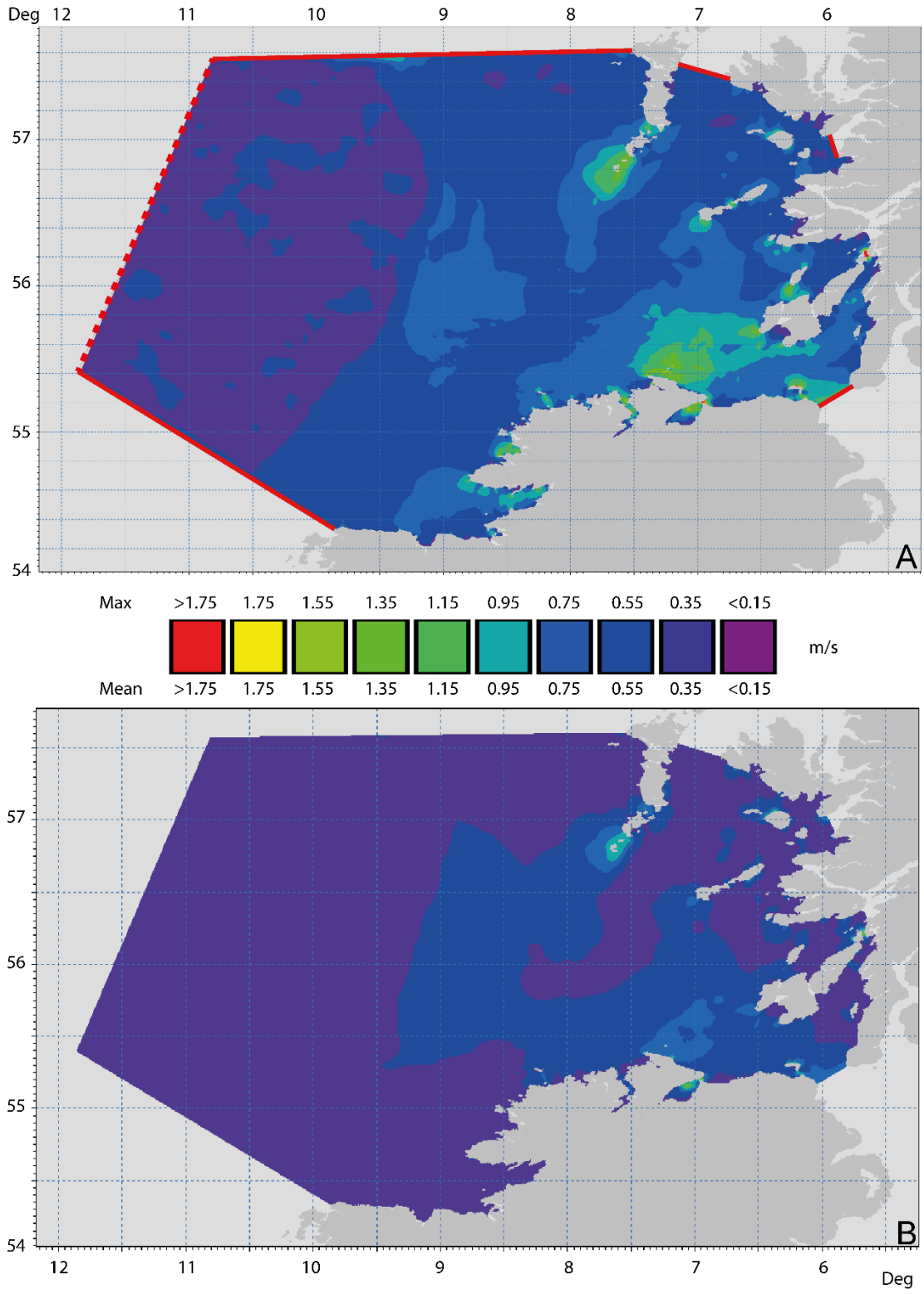

Fig. 4.3 Analysis of hydrodynamic flow velocities in the boundary layer across the model domain, A, maximum flow (m/s) and B, mean flow (m/s). The shelf is clearly defined by a drop in maximum flow west of -9ºW. Mean and maximum flows are noticeably higher in the approaches to the North Channel. Solid red lines (A) indicate 5 model boundaries, dashed red line indicates the location of the single Flather boundary.

4.4.2 Bed stress Data

Bed stresses were calculated across the shelf using high-resolution bathymetry, sediment grain size distribution and hydrodynamic forcing as inputs

$$\tau_c = \frac{1}{2} \rho f_c V^2$$ (Equation 1) where:

τ_c = bed shear stress (N/m2)

ρ = density of fluid (kg/m3)

V = mean current velocity (m/s)

f_c= current friction factor (composed of water depth and bed roughness)

Bed stresses across the north Irish shelf region vary greatly (Fig. 4.3A&B). Mean bed stresses throughout the simulation revealed zonation of energies (Fig. 4.4B). Low bed stresses, incapable of mobilising even muds <0.03 N/m^2; (Miller et al., 1977, Wilcock, 1993), are located in the Rockall Trough, Malin Deep and in the Donegal Bay area. Bed stresses >0.03 N/m^2 are confined to coastlines and embayments. The majority of the shelf-mean bed stresses are composed of forces capable of mobilising muds (0.03 – 0.14 N/m^2)(Fig. 4.4B). Model calculations indicate that elevated bed stresses with enough energy to initiate the movement of sand (>0.15 N/m^2) (Miller et al., 1977, Wilcock, 1993) typically occur in bays and inlets and increase in prevalence towards the entrance to the North Channel. As a result the simulations show that all sands, east of 7º44W have the potential to be mobile under mean bed stress

conditions excluding localised pockets of lower energy like those apparent around 6º38W. Forces capable of mobilising gravels (>1.3 N/m^2) (Miller et al., 1977, Wilcock, 1993), are present only in close proximity to shore and in the narrowing North Channel. Maximum bed stresses (Fig. 4.4A) represent the peak forces acting on the seafloor over the one-year duration of the simulation. While it is accepted that mean bed stresses present a better overview of long term processes (Wu et al., 2011), maximum values that may be the result of a solitary event (e.g. storm) provide insight into the upper range of energies acting across the simulation domain (Wu et al., 2011). Model results indicate that maximum stresses are capable of transporting sands across the majority of the shelf region. Areas of lower energy are confined to the Malin Deep, shelf and Rockall Trough. Three distinct bands of these lower energies occur at 55º12N 9º35W, 55º15N 8º46W and 55º52N 8º08W. The first, which spans a larger outer glacial moraine is 32 km wide and 44 km long (Fig. 4.1) and can be distinguished from the low energy Rockall Trough environment by a narrow band of increased bed stress running parallel to the shelf break in a north-south orientation. The second, occurring at 8º46W is 22 km wide and 56 km long. This location coincides with an area of bathymetric depression some 10 m lower that the surrounding seafloor. The final area is 65 km by 30 km and is another area of increased water depth known as the Malin Deep. Highest stresses (>1.3 N/m^2) occur in embayments and the North Channel entrance and in a band between 7º28W and 6º46W.

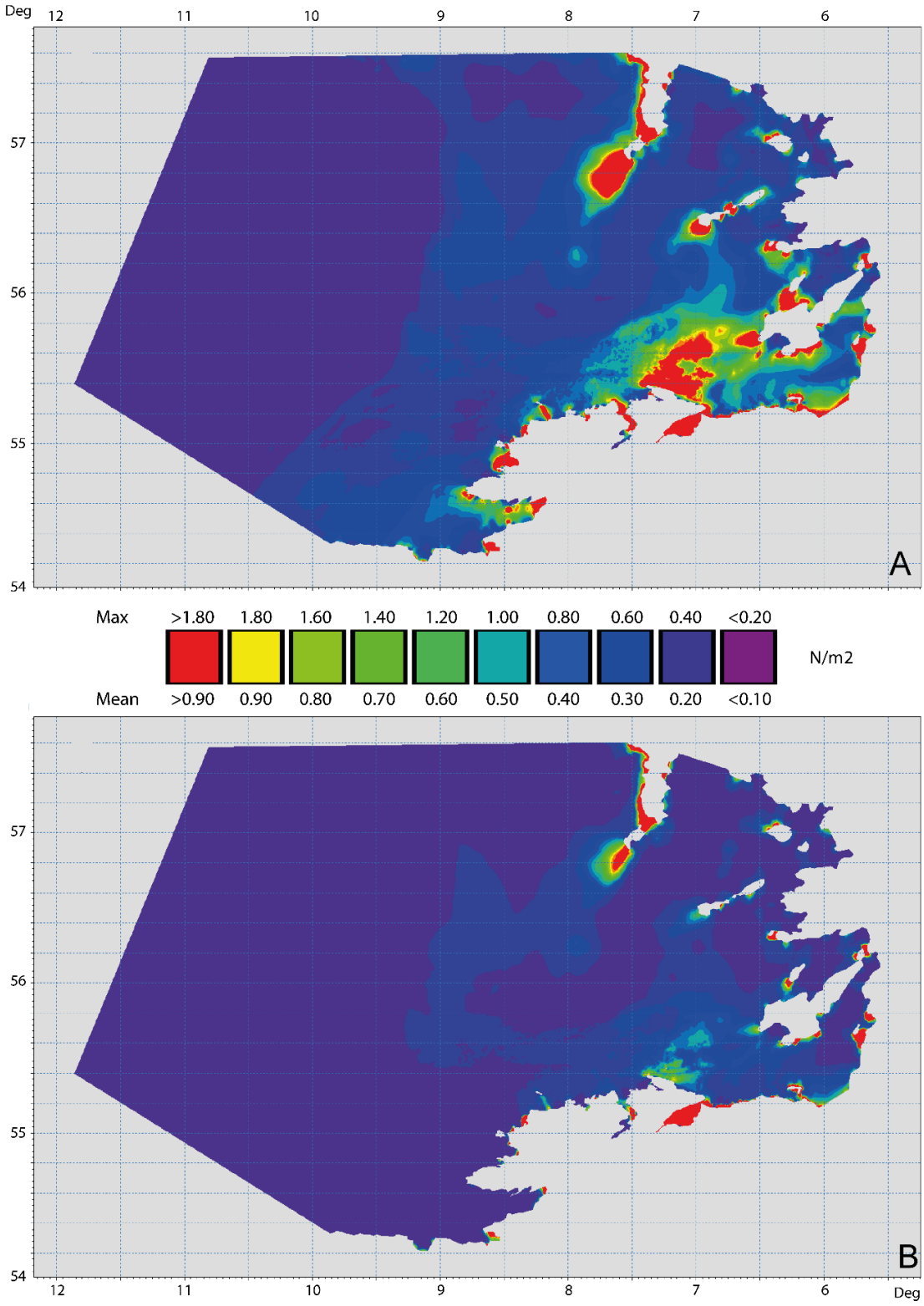

Fig. 4.4 Statistical analysis of bed stresses across the model domain (N/m^2). A indicates maximum stresses while B illustrates the mean bed stresses for the simulation period. Elevated mean and maximum bed stresses typically occur in shallows, sea loughs and constricted channels around islands.

4.4.3 Validation

Across the five tidal gauge stations used (locations in Fig. 4.1), agreement was achieved within the 95% range (Table 4.1). Given the large size of the modelled area, this agreement indicates that the model is accurately simulating magnitude and velocity of water body movement in the area.

Table 4.1

Tidal Station	**Root Mean Square Error**
Killybegs	4.2%
Arranmore	3.6%
Malin Head	2.2%
Portrush	4.1%
Port Ellen	3.9%

4.5 Discussion

The north Irish shelf displays varied hydrodynamic flow and bed stress patterns that could be expected on an energetic shelf, encompassing a wide range of water depths, complex coastline and exposure to north Atlantic weather systems. By examining near-bed current velocity, bed stress and sediment grain size distribution, the potential mobility of the seafloor can be assessed (Miller et al., 1977, Wilcock, 1993). Areas of low bed stress correlate well with bathymetric depressions, most notably the muddy Malin Deep at 55º52N, where even peak stresses are incapable of initiating movement of these cohesive sediments (Fig. 4.4). Elsewhere, fine and medium sand distribution correlates well with stresses of <0.14 N/m^2. This is particularly evident with sand patch distribution described in Evans et al (2014) between 9º50 and 8º57W (Chapter 2 Fig. 2.8) and in bathymetric depressions further north at 55º27N. Shelf sediment distribution analysis has revealed that surface sediments comprise mostly sandy gravels. Model outputs therefore suggest that while the energies required to initiate movement of the sand component of this sediment group are widespread, elevated energy capable of transporting gravel is rare (Hjulstrom, 1935). This may account for the subtle nature of 1 m amplitude, sandy gravel lineations identified in (Evans et al., 2015) which occur at 55º30N. The following analysis of small-scale variation in bed stress and current velocity reveals further relationships between sediment distribution, bedform formation and bathymetry. The selected seabed features were investigated using a higher resolution mesh (in the order of 10's of metres) to better understand localised hydrological processes contributing to the formation, evolution and potential

mobility of sedimentological features. This increased knowledge also better informs classification of bedforms as modern active features, or relict formations created during a period of differing hydrodynamic conditions.

4.5.1 Sand Ribbons

Elongate, 4 m amplitude ridges, previously identified as sand ribbons (Dunlop et al., 2011, Evans et al., 2015) correspond with areas of higher (0.16 N/m^2) and lower (0.01 N/m^2) bed stresses in the area between 8ºW and 7º58W (Fig. 4.5). The levels of these forces indicate that there is sufficient energy acting upon these fine sands to initiate sediment transport (Hjulstrom, 1935, Wilcock, 1993). This correlation suggests that transport is in an along-ribbon direction, confirming the bedform classification of (Evans et al., 2015) and identification of superimposed sand waves by (Dunlop et al., 2011).

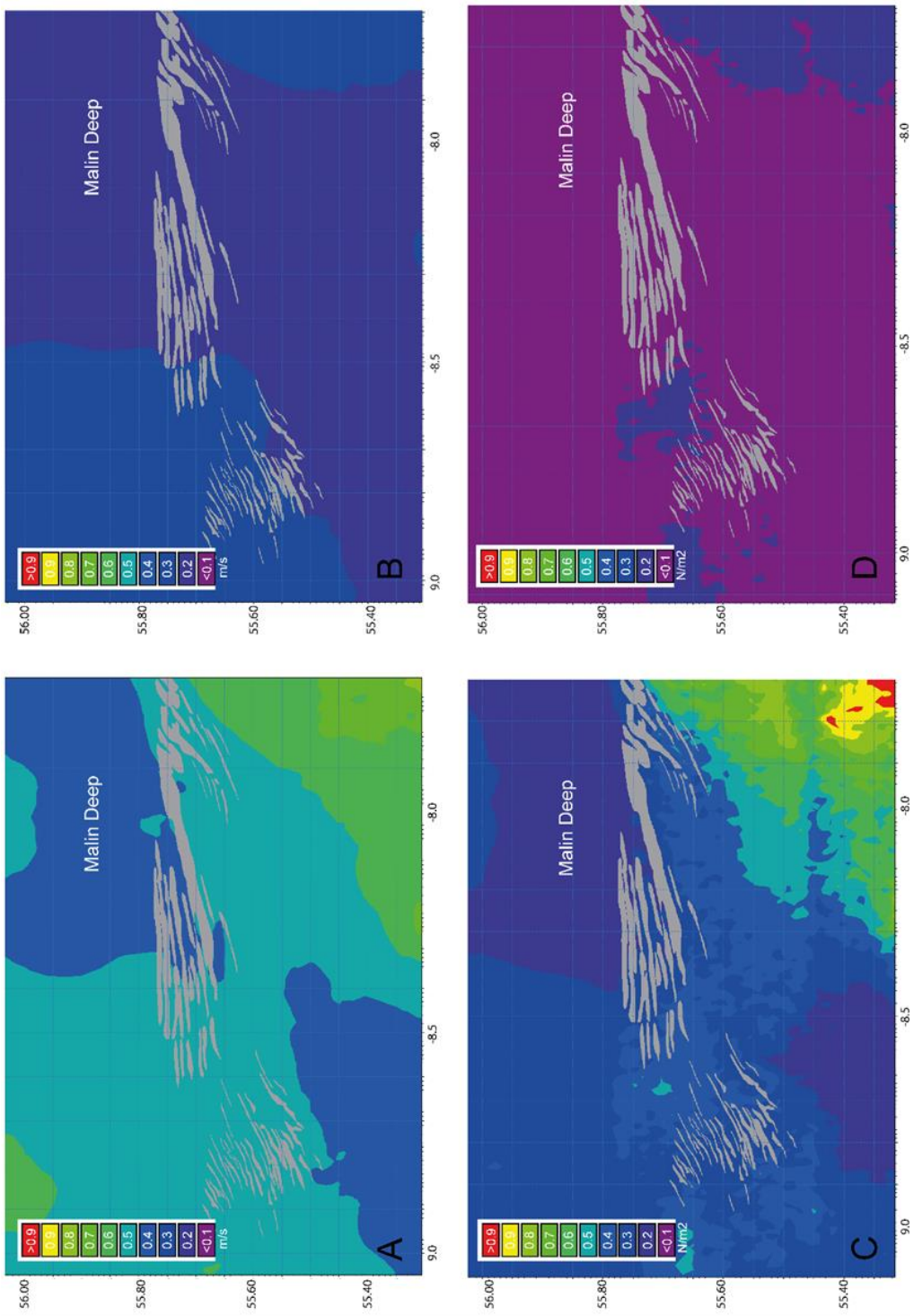

Fig. 4.5 Model outputs for hydrodynamic forces over sand ribbon bedforms. A, maximum flow velocities and B, mean flow velocities (m/s) are indicated. C & D represent maximum and mean bed stresses respectively (N/m^2). Note that scales are not standardized to better enable visualisation of variance in forces. Grey outlines show the distribution of the sand ribbons (Evans et al., 2015) in this area. Location illustrated in Fig. 4.1.

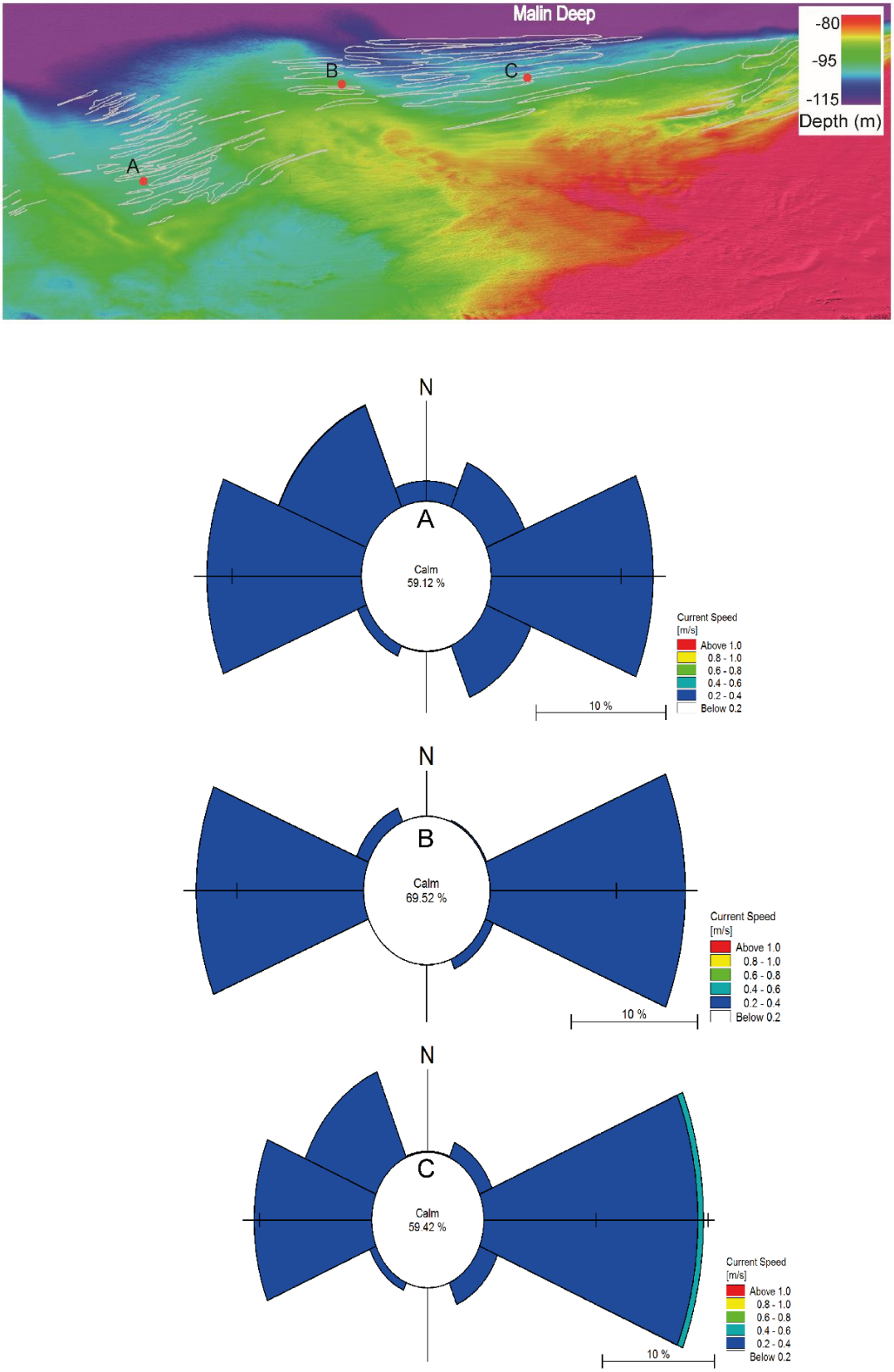

Fig. 4.6 MBES data illustrating sand ribbons and surrounding seafloor. Locations of current roses are also shown. Note the agreement between flow direction and bedform orientation with a dominant easterly flow.

Average current speeds in this area (Fig. 4.5B) of 0.2 m/s correlate well with this bedform morphology (Stow et al., 2009). Dominant flow direction agrees with the west-east orientation of these ribbons (Fig. 4.6).

This orientation evident around 55º30N correlates with the suggested location of ESC intrusion onto the shelf (Inall et al., 2009, Souza et al., 2001), further corroborated by the southwest-northeast alignment of bedforms south of this latitude (Evans et al., 2015).

4.5.2 Giant Sand Waves

Giant sand waves ~20 m in amplitude and up to 5 km in length (Fig. 4.7) are a contrast to the gravel covered shelf which surrounds them.

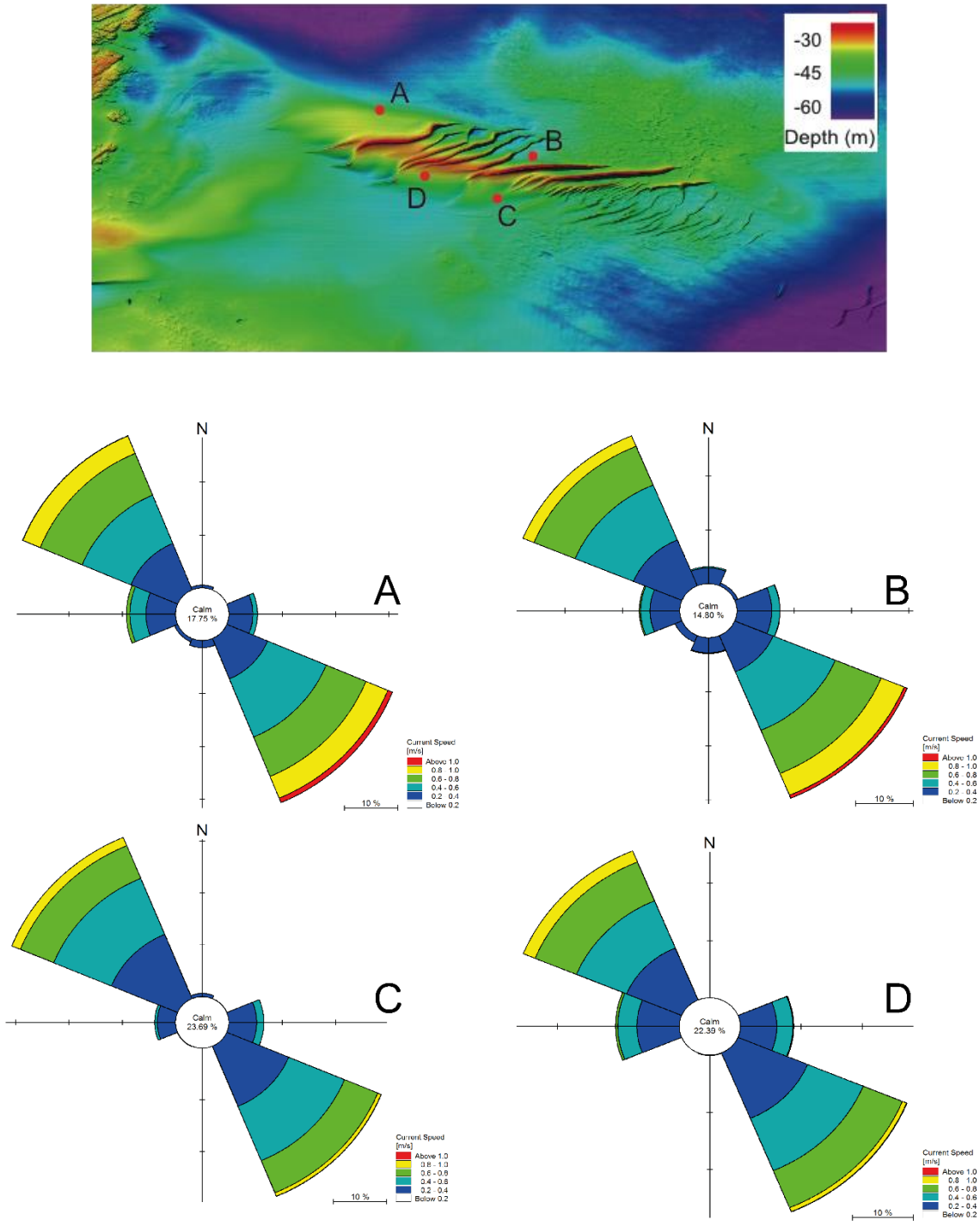

Fig. 4.7 MBES data of giant sand waves and surrounding seafloor. Current roses A & B display a dominant south easterly current while C + D a stronger north westerly current. This correlates well with bedform orientation and asymmetry.

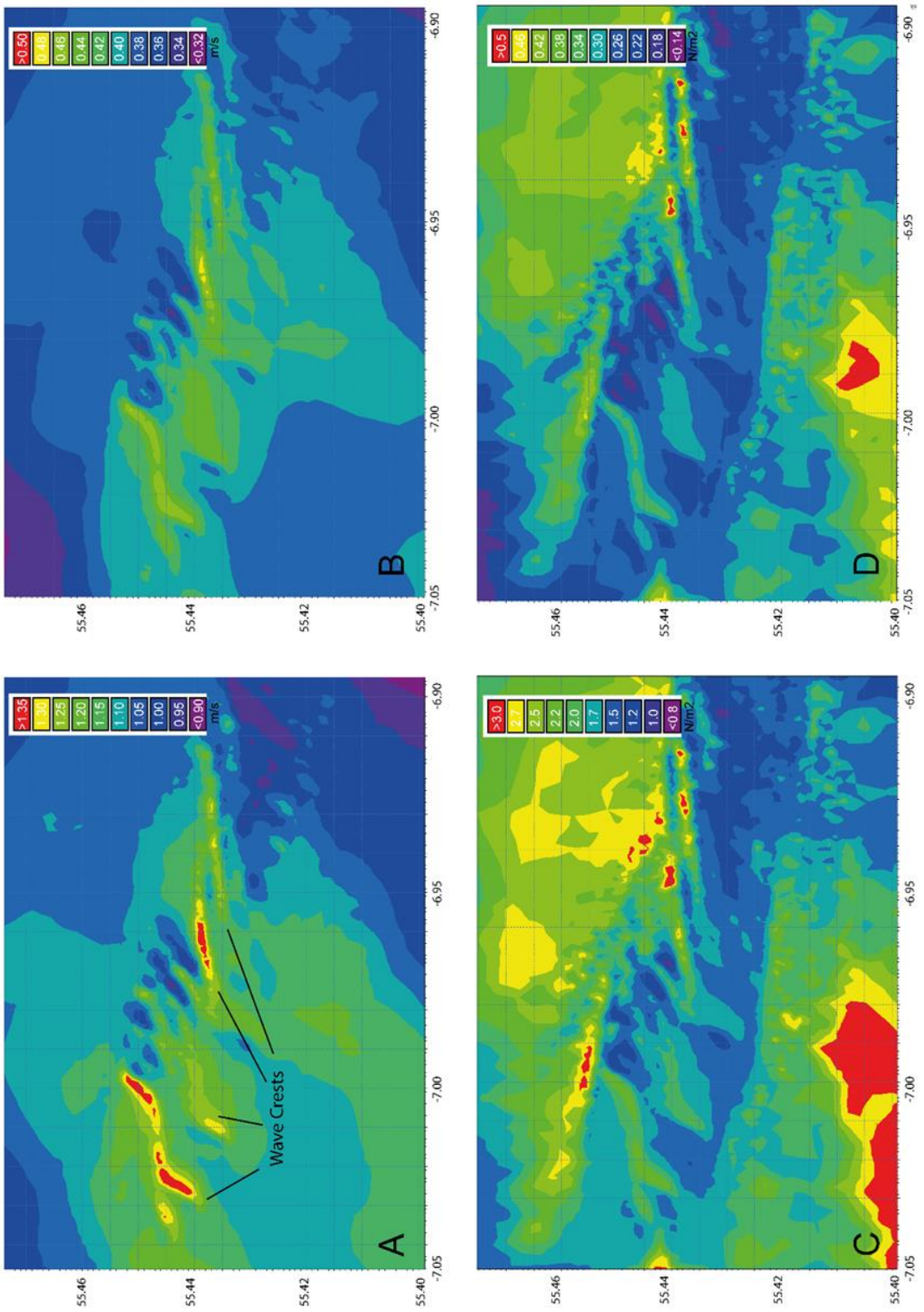

Fig. 4.8 Model outputs for hydrodynamic forces over giant sand waves shown in Fig. 4.6. Wave crests can be identified as areas of peak maximum flow (m/s) (A), and maximum bed stress (N/m^2) (B). While less evident in mean flow (B) and bed stress (D), waves can be distinguished by corresponding areas of high and low energies. Scales are not standardised to aid visualisation.

Bed stresses acting upon this bedform (Fig. 4.8) have been calculated to range between 0.2 and 1.6 N/m^2, energy levels more than capable of mobilising the coarse sands of which these waves are comprised (Hjulstrom, 1935, Wilcock, 1993). Modelled currents in the area average 0.4 m/s increasing to 1 m/s at times of peak flow (Fig. 4.8). These flow rates are typical in the formation of sand waves of this grain size (Belderson et al., 1982, Stow et al., 2009). These waves display a high degree of asymmetry (Evans et al., 2015), often used as an indicator of substrate mobility (Németh et al., 2007, Van Landeghem et al., 2012), which may be accounted for by these flow rates and the aforementioned bed stresses initiating and sustaining wave migration. Directionality of flow is affected heavily by the ebb and flow of tide in this area (Fig. 4.7), and flow plots C and D (Fig. 4.7) corroborate the identification of a rotary current in the area in Chapter 3.

4.5.3 Rounded Troichoidal Waves

Rounded troichoidal waves (Fig. 4.1, 4.9) comprised of coarse sand (Evans et al., 2015) are situated to the SE of the Malin Deep. They are located in a pocket of lower bed stress than the surrounding shelf area (Fig. 4.10). Mean stresses of 0.1 N/m^2 are not typically capable of mobilising coarse sands, however, the bedform does undergo periodic increases of energy to a maximum of 0.6 N/m^2 (Fig. 4.10). As with bed stress, average flow velocities in the area of 0.2 m/s (Fig. 4.10) do not typically generate bedforms of this type, during periods of increased flow (0.6 m/s) however, coarse sand grain transport is possible(Fig. 4.10) (Hjulstrom, 1935, Miller et al., 1977).

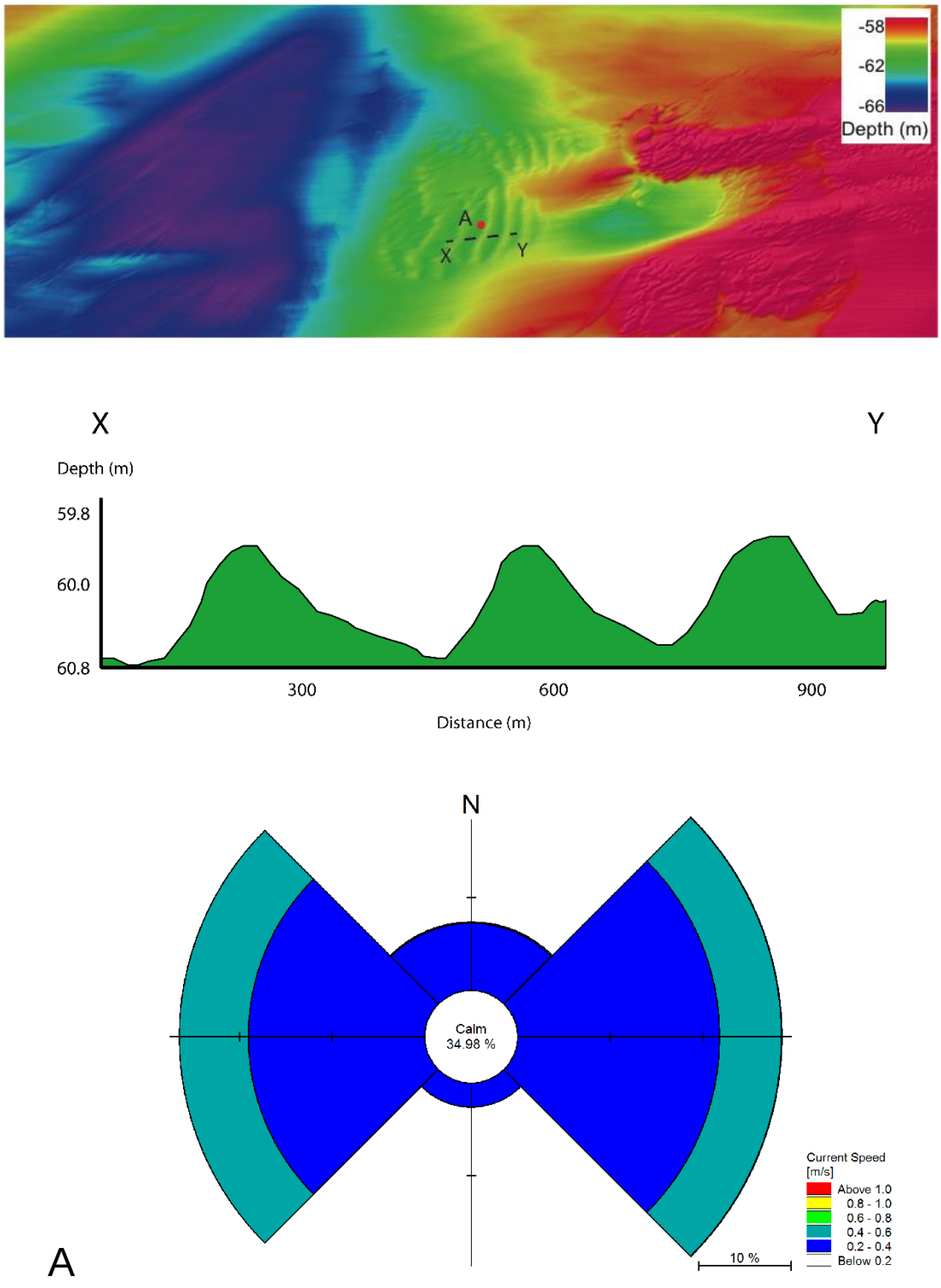

Fig. 4.9 Rounded trochoidal waves. The bathymetric profile XY shows well their shape and rounded crests. Current rose (A) agrees with the orientation of these waves and extended periods of calm, even bi-directional flow and low velocities account for the bedforms morphology.

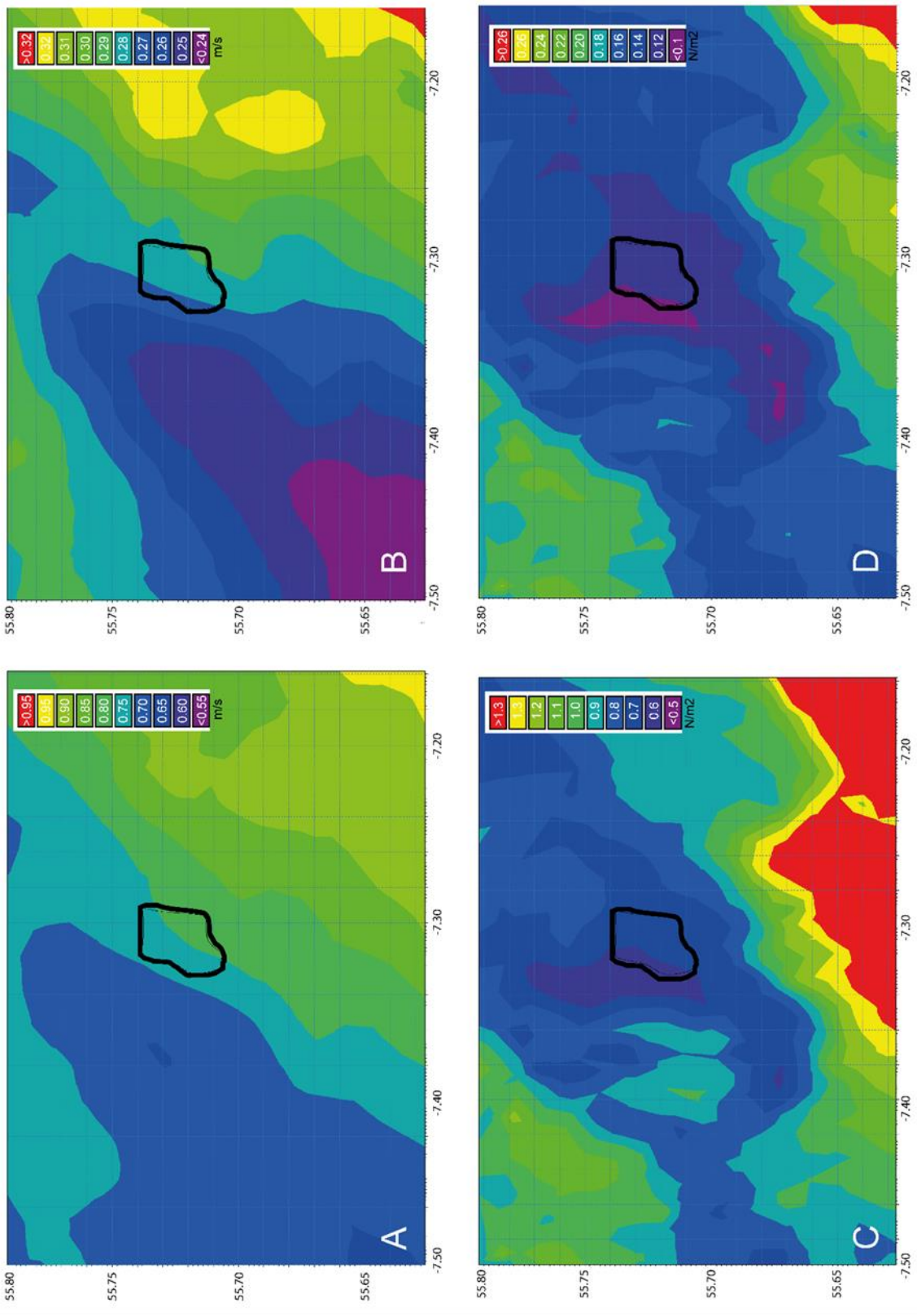

Fig. 4.10 Rounded trochoidal waves shown in Fig. 4.9 (black outline) are situated in areas of lower maximum (A) and mean (B) flow velocities (m/s). They also coincide with the lowest values of maximum (C) and mean (D) bed stresses (N/m^2) on this section of the shelf.

Waves typically adopt a symmetrical profile due to an equal bi-directional, transverse crest flow, while rounded crests indicate low mobility or periods of dormancy (Bartholdy et al., 2010b, Lefebvre et al., 2014). The mean bed stress (0.1 N/m^2) and flow levels (0.2 m/s) are not capable of initiating transport of coarse sand in this area (Hjulstrom, 1935, Miller et al., 1977). This may account for rounded wave morphology and supports the hypothesis that this formation undergoes periods of inactivity. The energy levels capable of mobilising these coarse sands (e.g. teal coloured band Fig. 4.9A) are both short in duration and bi-directional, which suggests that while modern hydrodynamics did not cause these waves to form, they are capable of preventing complete wave degradation through processes such as bioturbation (Borsje et al., 2008). It is suggested that the formation of these waves occurred at a time of increased average hydrodynamic energies. These energies are typically associated with periods of lower sea level on the north Irish shelf (Neill et al., 2010, Terwindt and Brouwer, 1986, Uehara et al., 2006). It is therefore proposed that these waves formed in an environment with higher hydrodynamic energy and as this water levels rose, hydrodynamic forcing and sediment migration declined resulting in degradation of wave crest definition (Feldens et al., 2015, Terwindt and Brouwer, 1986).

4.5.4 Deep Water Trochoidal

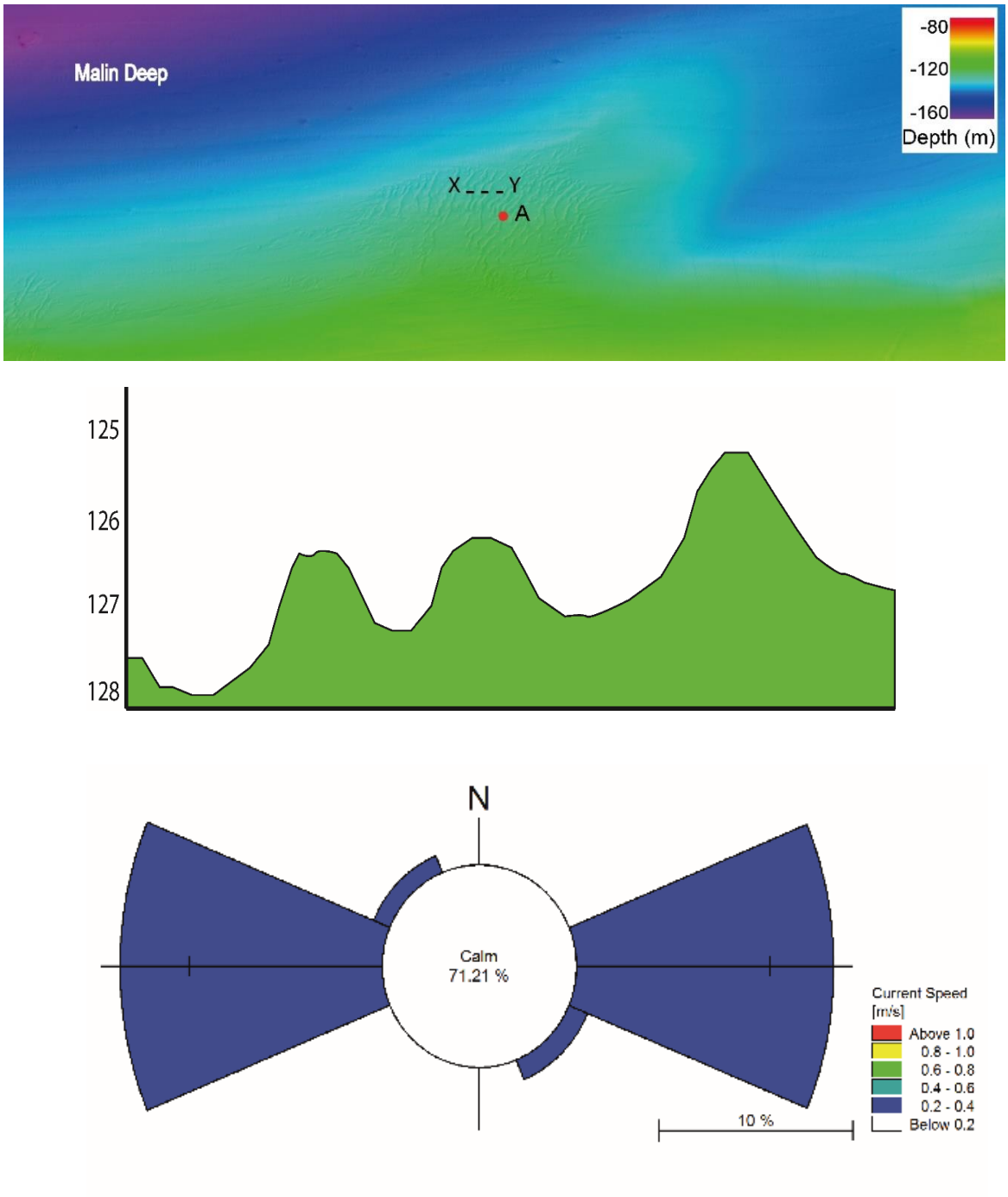

Fig. 4.11 Deep water trochoidal waves situated on the fringes of the Malin Deep. The bathymetric profile XY shows well their symmetric shape and rounded crests. Significant periods of calm and low flow velocities (current rose in A) support the hypothesis that these bedforms are relict.

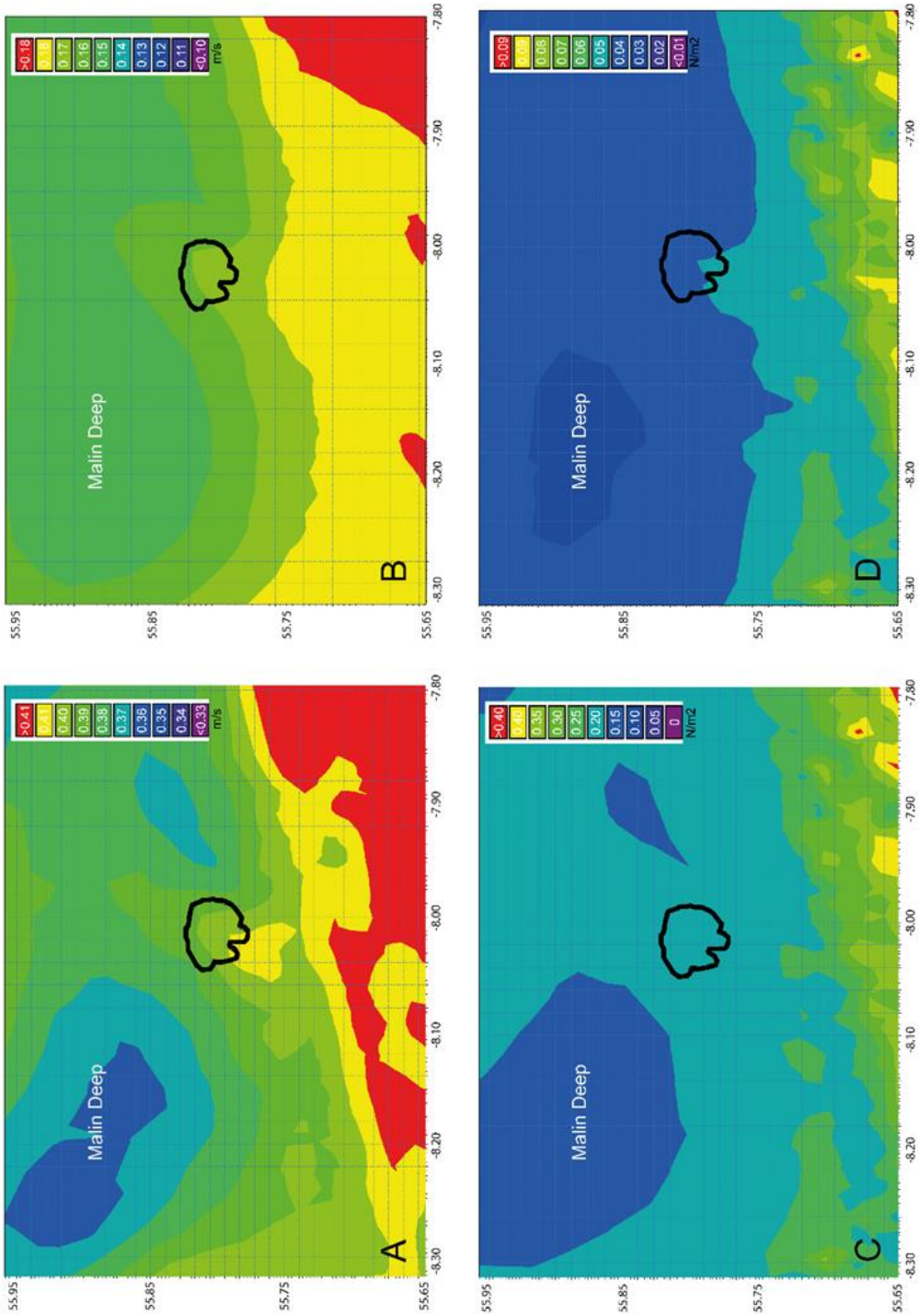

Fig. 4.12 Hydrodynamic forces surrounding deep water trochoidal waves shown in Fig. 4.10 (black outline). Maximum (A) and mean (B) velocity outputs (m/s) indicate that the bedform occurs in an area of marginally higher energy extending north into the Malin Deep. This trend is also evident in mean bed stress (N/m^2) outputs (D) but not in maximum bed stresses (C).

These waves occur on the fringes of the Malin Sea (Fig. 4.1, 4.11), identifiable as a coarse sand patch surrounded by the muds which typify this region (Evans et al., 2015). Average bed stresses are low, 0.03 N/m^2 with a peak of 0.16 N/m^2 and lack the energies required to mobilise sediment of this grain size (Fig. 4.12) (Hjulstrom, 1935, Miller et al., 1977). Furthermore, average current speed (Fig. 4.12) of 0.17 m/s struggles to form bedforms larger than ripples (Belderson et al., 1982, Stow et al., 2009). The rounded, symmetrical profile of these waves suggests that they are no longer actively mobile (Bastos et al., 2003, Knaapen et al., 2005), an interpretation substantiated by the consistently low hydrodynamic forces in the area. As with the rounded trochoidal waves in section 4.5.3 it is probable that these waves formed at a time of increased bed stress and flow velocity (Terwindt and Brouwer, 1986).

4.5.5 Isolated Waves

Fine to medium sand waves occur in isolation SE of the giant sand waves and close to the north Irish coastline (Fig. 4.1, 4.13). These waves undergo average bed stresses of 0.1 N/m^2 with peaks of 0.5 N/m^2, sufficient energies to mobilise these sands for the majority of the simulation (Fig. 4.14) (Hjulstrom, 1935, Miller et al., 1977). Flow velocities (Fig. 4.14) ranging from 0.2 m/s to 0.6 m/s are consistent with the formation of bedforms of this type (Stow et al., 2009).

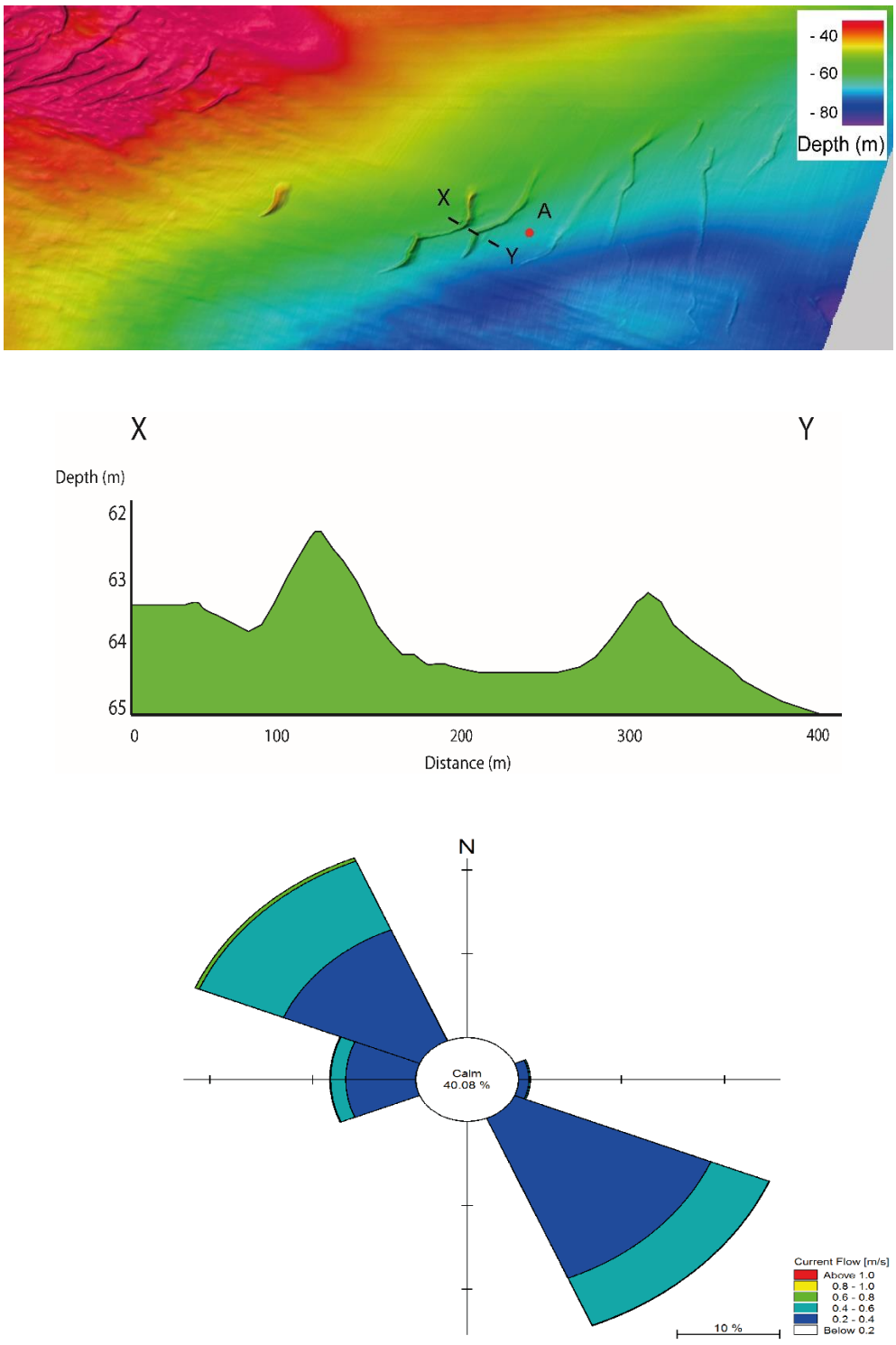

Fig. 4.13 MBES visualisation of isolated waves with giant sand waves present in the NW of the image. Dominant flow (at higher velocity) to the NW indicated by current rose A corroborates with bedform asymmetry. The westerly element of the flow regime may account for variation in wave crest orientation. Profile asymmetry indicates marginal transport to the northwest.

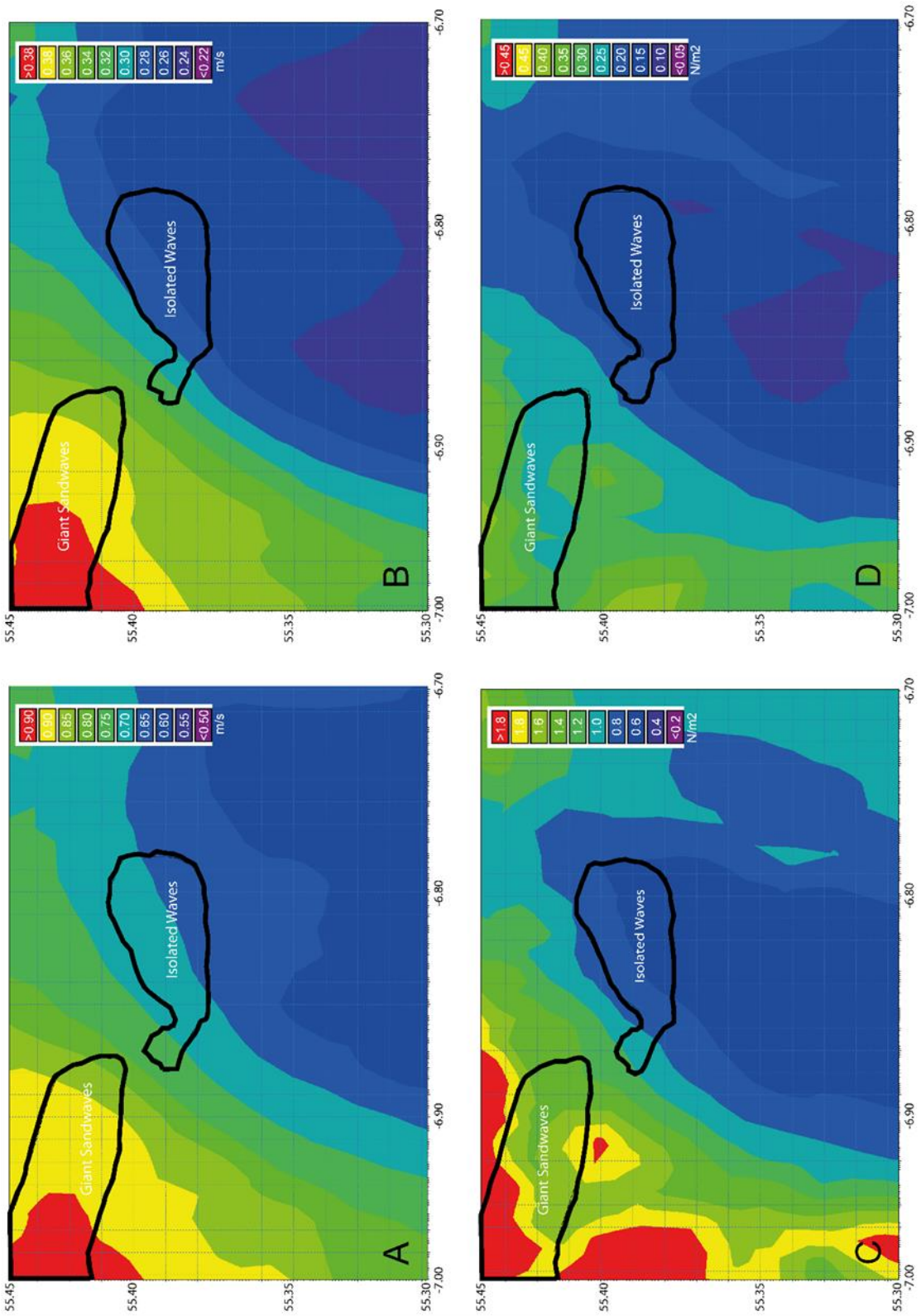

Fig. 4.14 Isolated waves located to the SW of giant sandwaves (black outline) are located in an area of reduced maximum (A) and mean (B) hydrodynamic flow velocity (m/s). Maximum (C) and mean (D) bed stresses (N/m^2) indicated these waves are flanked to the north, west and east by areas of higher energy.

The fine and medium sands of which these waves are composed are enveloped by gravels and bedrock (Evans et al., 2015). The location 3 km downslope of the large concentrations of sediments, which form the GSW, and in an area of lower hydrodynamic forcing than in the west, north and east (Fig. 4.14), it is probable that this area of reduced energy allows sediments to drop out of suspension and therefore represents a depositional zone (Berelson, 2001, Hjulstrom, 1935). This would account for the existence of these soft sediments in this section of gravel dominated shelf. The migration of these isolated waves appears to be driven by the dominant current (Fig. 4.13) and is consistent with the findings of (Ediger et al., 2002) who also noted upslope movement of sediment waves in Italian waters.

4.5.6 Outer Moraine

The Irish Shelf has undergone multiple periods of glaciation and as a result many glacial features are identifiable in MBES data (Benetti et al., 2010b, Dunlop et al., 2011, O'Cofaigh et al., 2012). One these features, a moraine on outer shelf displays an atypical geometry and is not consistent with similarly classified features in the area. This moraine can be identified by gently sloping crests, wider dimensions and a segmented arrangement (Benetti et al., 2010b). A sediment drape of gravelly sands has been identified in (Evans et al., 2015) and while this may alter morphology via infilling, it does not account for unusual arrangement and increased proportions of the formation with respect to terrestrial moraines or those found further inshore on the Irish shelf. Despite

being located in an area of known ESC intrusions (Inall et al., 2009, White and Bowyer, 1997), modern bed stresses over the moraine average 0.05 N/m^2 with peaks of 0.18 N/m^2 (Fig. 4.4) with boundary layer flows ranging between 0.15 m/s and 0.3 m/s (Fig. 4.3). While these energies may be capable of mobilising muds, they lack the necessary force to initiate transport of coarse sands and gravels that overprint this feature, likely composed of highly compacted glacial diamicton (Freiwald et al., 2002, King, 1969). As a result, it is proposed that changes in the morphology of this moraine occurred via an alternative process to modern seabed currents or at a time of increased seabed energy e.g. during sea level transgression (Nio, 1976).

4.5.7 Relative Sea Level and Paleotidal Conditions

The north Irish shelf has undergone changes in water depth, tidal range and bedstress since the Malin Shelf flooded somewhere between 21 ka BP., (Ward et al., 2016). Paleotidal models incorporating isostatic release have predicted a lowstand of -41m ~ 14,500 ka BP., (Bradley et al., 2011, Brooks et al., 2008, Kuchar et al., 2012) however this value varies across the Malin Shelf. Tides and tidal currents in the area up to 10 ka BP were driven by enhanced ocean tides and were significantly larger than present leading to increased flow and bed stresses (Uehara et al., 2006).

By examining paleotidal models it is possible to better constrain the points at which specific sediments may have become mobile within our study area. Several bedforms have been identified as either relict, or having formed during

elevated hydrodynamic conditions and merely being maintained by modern conditions. (Neill et al., 2010) have shown that 10 ka BP. the location of this moraine underwent elevated bed stresses of 1 N/m^2 for 40% of annual readings, rising to 100% approximately 12 ka BP (Neill et al., 2010). These energies are capable of transporting gravel-sized sediments which suggests some of the glacial sediment might have been mobile during both these periods (Wilcock, 1993). By 8 ka BP., these forces had reduced significantly enough to fall below the threshold capable of transporting gravels (Hjulstrom, 1935, Neill et al., 2010).

Other bedforms identified as having paleo origins are comprised of sediments finer than gravel, the rounded trochoidal waves (Fig. 4.9) and deep water trochoidal waves (Fig. 4.11). (Neill et al., 2010) model suggests that the coarse sands in these bedforms were mobilised by minimum bed stresses 12 ka BP, and by mean conditions by 8 ka BP. During this period ~ 10 ka BP, (Ward et al., 2016) modelled a reduction in water depths for both bedforms. Rounded trochoidal waves, currently found in 62 m water depth were predicted to have been situated in ~ 40 m at that time. Likewise the deep water trochoidal waves, found in 130 m water depth present day, were located in 70 m at 10 ka BP (Ward et al., 2016). Due to the large timeframes and low temporal resolution of these models, it is difficult to more accurately define at which point mean hydrodynamic conditions failed to reach the thresholds required to mobilise coarse sands. It is clear however that mobilisation of coarse sands and the cessation of gravel transport during mean conditions happened many thousands of years before present conditions.

While there is scope to adapt the model developed for this research for paleo-oceanographic applications, such simulations are complicated by the increased variables to create accurate reconstructions such as sea-ice cover, shoreline change, isostatic release and paleotidal elevation (Neill et al., 2010). Much of the research into changes in relative sea level and paleotidal condition works to compare various models in an effort to further define accepted timelines and values (Ward et al., 2016). As a result, it must be accepted that the values presented in this chapter represent the most recent work in an evolving field. Development of a paleomodel focussed on bedform formation and sediment distribution for the north Irish shelf, such as that by (Ward et al., 2015) presents an opportunity to further investigate the provenance of these bedfoms.

4.6 Conclusions

- A high-resolution hydrodynamic model was generated which enables the investigation of relationships between flow regime, bedform formation and morphology due to development of a flexible mesh at an appropriate scale.
- Building on the shelf sediment composition and bedform classification work of (Evans et al., 2015), a close link between sediment distribution and hydrodynamic forcing has been revealed.
- These links identify many oceanographic current pathways suggested by previous investigations in the region, including sedimentary record of possible ESC ingress onto the shelf.

- The integration of hydrodynamic models, high-resolution bathymetry and sediment distribution data is revealed as a robust method for analysing bedform formation and transport, including classification of relict and active features. Where potentially relict features have been identified, the use of paleo-oceanographic models to identify a time where hydrodynamic forces were capable of creating these formations has been highlighted.
- This work has provided new insights into sediment transport and the formative forces creating key modern bedforms across the north Irish shelf.
- The result is an approach to sediment transport investigation that is applicable to many global shelf seas, particularly those that have undergone periods of marine transgression. Further work is required to develop forecasting potential of this model informing predictions about pathways and migration rates of sediments, which are of particular significance to offshore engineering and habitat mapping.

Chapter 5 – An integration of high-resolution hydrodynamic modelling with time-lapse bedform migration on the north Irish shelf.

Evans, W., Benetti, S., Jackson, D., Clarke, S., Sacchetti, F, Lyons, K. *Integration of high-resolution hydrodynamic modelling and time-lapse bedform migration on the north Irish shelf*. (To be submitted (Continental Shelf Research).

5.1 Introduction

Increased mapping efforts in Irish and UK waters have revealed an abundance of sediments waves and other seafloor bedforms varying in size and morphology distributed across inshore and shelf environments. Understanding of the formative processes creating these bedforms, their evolution and mobility are becoming of increasing importance due to the intensification of anthropogenic interaction with the marine environment (Barnard et al., 2013, Brennan et al., 2013, Holt et al., 2009); in particular when these, often mobile, bedforms are found around marine installations such as pipelines or tidal turbines (Knaapen and Hulscher, 2002, Morelissen et al., 2003, Thiébot et al., 2015). In the investigation of sediment waves and other seafloor bedforms, common baseline data often take the form of a high-resolution bathymetry, typically collected by multibeam echosounders (Besio et al., 2008c, Knaapen et al., 2005, Li and King, 2007, Shaw et al., 2014, Van Landeghem et al., 2009b, Van Landeghem et al., 2012). By enabling accurate measurement of bedform

geometries, MBES data assists in the classification of these features. This is not limited to applying nomenclature (Allen, 1980, Field et al., 1981, Wynn and Stow, 2002), but also enables the application of bedform matrix principles such as those in (Belderson et al., 1982, Stow et al., 2009). These classifications then allow inferences to be made about the oceanographic flow velocities around the bedform, its grain sizes and its potential mobility (Belderson et al., 1982, Hjulstrom, 1935, Miller et al., 1977). A key measurement in both classifying and assessing the mobility of a sediment wave is asymmetry of wave profile. Asymmetry is calculated as the variation in length ratio between a gently sloping, longer stoss slope and a shorter, steeper lee slope. Transport is assumed to occur towards the lee slope, with a more varied ratio suggesting higher mobility rates (Belderson et al., 1982, Caston, 1972, Lobo et al., 2000). A symmetrical waveform, with equal length lee and stoss slopes, indicates low mobility rates (Ferret et al., 2010, Van Landeghem et al., 2012). The validity of geometry-based interpretations of sediment movement rate and directionality are coming under increasing scrutiny and also fail to provide insight as to the forces facilitating this transport (Besio, 2004, Van Landeghem et al., 2012). As a result, the need for further methods of measurement and validation has been highlighted. As with other types of field measurement in the marine environment, quantification of sediment mobility can be difficult, in particular with in situ measurements of sediment movement being expensive and unsuitable when considering mobility over a large area (Huthnance et al., 2002). The use of sequential bathymetric surveys is proving increasingly beneficial as a means to measure horizontal and vertical change in the sedimentary bedforms due to the instrumental capability to cover a large area,

at up to centimetric, resolution, in a relative short period of time (Knaapen and Hulscher, 2002, Knaapen et al., 2005, Ma et al., 2014). For example, it has been shown that repeat multibeam surveys can be utilized effectively to document sandwave migration (Barnard et al., 2013, Knaapen et al., 2005, Van Landeghem et al., 2012). However, these time lapses are limited by the temporal resolution of subsequent surveys which can become particularly problematic when monitoring areas of high mobility (Barrie and Conway, 2014) (Smith et al., 2007). As a result, the forces that drive this mobility, typically hydrodynamics, can be the key to understanding the direction and rate of migration (Liu and Huang, 2009, Wu et al., 2011). The hydrodynamic forces that induce sediment transport are difficult to measure at the appropriate resolution, often requiring mooring of specialist equipment, such as Acoustic Doppler Current Profilers (ADCPs), offshore for extended periods of time (Thiébot et al., 2015, Zanuttigh, 2007). Advances in numerical modelling and computational power have enabled the construction of hydrodynamic simulations capable of recreating real-world oceanographic conditions, based on a series of governing equations, thus reducing the need for extensive field measurements (Feldens et al., 2015, Zanuttigh, 2007). Obtaining outputs from these models at an appropriate scale is necessary, but simulation accuracy is often governed by the resolution of its computational mesh (Crowder and Diplas, 2000, Legrand et al., 2006). As the number of cells in a model mesh increases, computational effort required also increases, resulting in the need to compromise between data density, area of coverage and computational run time (Callaway et al., 2011a, Young et al., 2000). More sophisticated models utilise computational meshes that allow variance in spatial resolution across a study area, resulting in

reduced simulation effort without compromising on data density. These nested meshes are useful where increased resolution is required to resolve flows in areas of complex coastline, narrow channels or harbours, intricate tidal harmonics or particular areas of interest, such as specific seafloor bedforms. (Legrand et al., 2006, Staneva et al., 2009, Sheng and Yang, 2010). From these models, it is possible to extract the forces that drive sediment transport, such as bed stress, turbulent kinetic energy, and flow velocity (Davies and Xing, 2002, Liu and Huang, 2009, Wu et al., 2011). These outputs can then be used to validate interpretations based on other interpretations of sediment wave asymmetry or time lapse measurements. For the outputs of hydrodynamic models to accurately represent sediment mobility, model configuration should be optimised for simulating conditions at, or near to seabed. This is typically achieved by increasing vertical resolution close to seafloor, utilizing high-resolution bathymetry and introducing a bed roughness distribution to enable accurate calculation of bed stress (Davies and Xing, 2002, Hall and Davies, 2004, Wu et al., 2011).

The aim of this study is to examine the relationships between bathymetric changes measured by repeat multibeam surveys carried out on the Irish shelf and a hydrodynamic model of appropriate scale. This will further understanding of the relationship between bed stresses, flow regime and sediment transport on the north Irish shelf in selected areas where mobile sediment waves of mixed geometry had been mapped (Chapter 3 & Fig. 5.1). To this end, the sediment mobility data from successive surveys described in Chapter 3 have been compared to outputs (bed stress and bottom flow velocity) from a modified version of the model described in Chapter 4. The model was modified to

increase resolution of specific areas A & B to allow for detailed analysis of the hydrodynamic effects on migration down to an individual wave scale. Lastly the relationship between simulated forces and variances in morphological change are examined.

5. 2 Study Area

This study examines a narrow stretch of Malin shelf (<15 km) between the Scottish Hebrides and Northern Ireland, within Irish waters where high-resolution bathymetric data exist (Fig. 5.1). Surveys conducted here have revealed a wide range of water depths, averaging 80 m, and reaching over 250 m close to the North Channel (Cooper et al., 2002). The seafloor north of Malin Head is dominated by gravels and exposed bedrock (Evans et al., 2015, Plets et al., 2011), but the thickness of the sediment cover increases moving eastwards, forming thick planar deposits offshore of Lough Foyle (Cooper et al., 2002, Plets et al., 2011). To the east of Lough Foyle, sediment cover remains varied with a combination of soft coastal sediments amongst outcropping bedrock (Westley et al., 2011).

Waters off the north Irish coast experience seasonal temperature changes, prevailing westerly winds and exposure to Atlantic storm processes (Cooper et al., 2004, Fernand et al., 2006). The result is a highly dynamic environment with energetic wave climate (Jackson et al., 2005, Plets et al., 2011) which have been forecasted to increase in future years (Zacharioudaki et al., 2011). Tidal flows also have a prominent influence on the shelf oceanographic conditions. Bi-directional tidal flows experience elevated flows in the natural constrictions of

Inishtrahull sound. As a result, measured near bed velocities on the shelf at this point can exceed 1 m/s (Giorgi and Ringwood, 2013, Rourke et al., 2010). Two specific areas off the north Irish coast were selected for this study (Fig. 5.1). The selection was based on the existence of MBES data acquired at different times over the same area (Chapter 3), high likelihood of mobility (based on asymmetry assumptions), and variation in bedform type. The extent of each area was designed to include a fixed depth object, such as exposed bedrock, in order to enable accurate correction of the MBES datasets from different surveys to a common datum (Knaapen et al., 2005, Schimel et al., 2015). The proximity to proposed sites for marine renewable installation makes this work of relevance to proposed offshore installations on this section of shelf, but was not a deciding factor in the selection of the study areas (Giorgi and Ringwood, 2013, Rourke et al., 2010).

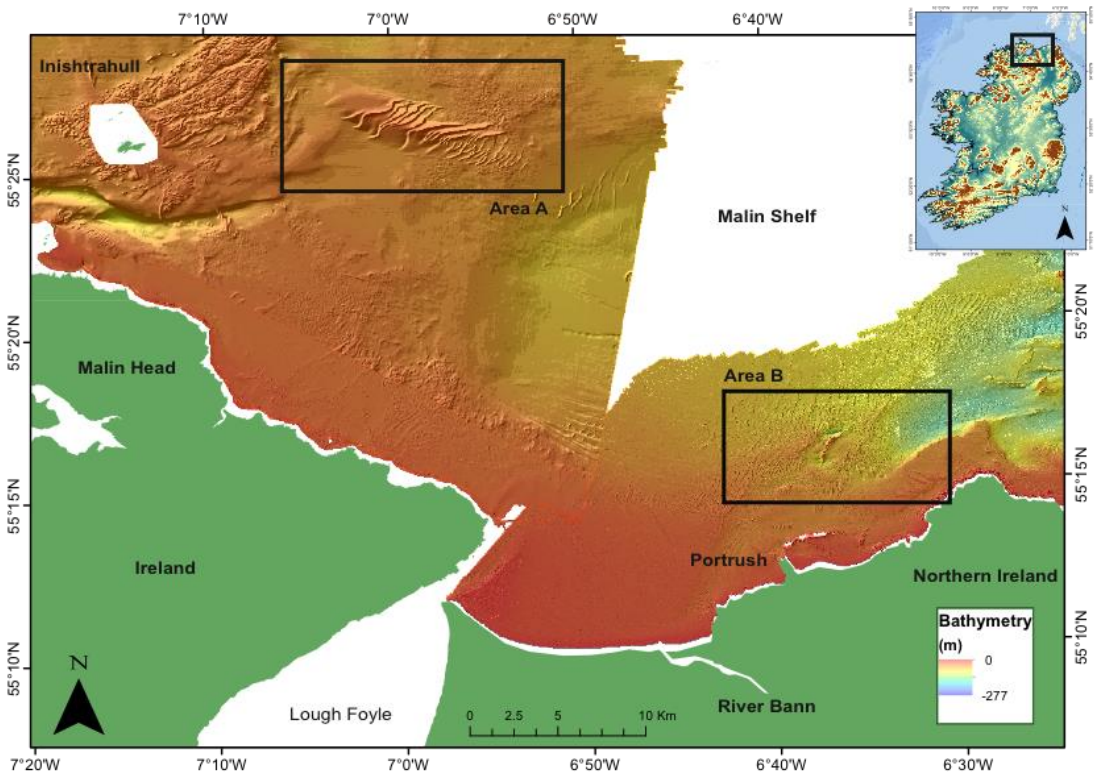

Fig. 5.1 Overview of areas selected for repeat survey and high-resolution hydrodynamic modelling. Areas A and B are the sites where time-lapse surveys where used to investigate sediment mobility and rates of crest displacement. For detail view of sites see Figs. 5.2 and 5,3. In Area A, isolated soft sediments forming giant asymmetric waves are a striking contrast to the surrounding shelf. Scouring evident in the sound south of Inishtrahull confirms measured high flow rates at this site. White colour denotes sections of seafloor with no MBES coverage. Inset shows the location of the study area on the Malin – Hebrides shelf.

5.2.1 Area A

Area A (48.8 km^2) is situated 14 km from the coast in the western portion of the general study area between 7º19'W and 6º51'W and 55 º25' N and 55 º27' N, in waters ranging from 20 m to 50 m deep (Fig. 5.1 & 5.2A). This section of the seafloor contains an isolated pocket of coarse sand with shells, where large asymmetric sediment waves are found, surrounded by exposed bedrock, gravels and boulders (Evans et al., 2015, Plets et al., 2011). These striking

asymmetric sand waves have maximum heights of 20 m with waves decreasing in size as the bedform extends to the south-east. Average heights of 13 m and wavelengths of 326 m have been calculated for these waves with steep, lee slope angles up to 7.6º and clear asymmetry (Evans et al., 2015). Exposed bedrock in the form of Paleoproterozoic granitic gneiss is evident to the northwest and comprises part of the Inishtrahull Island complex, which exerts a significant influence on hydrodynamic flows in the area (Muir et al., 1994). The constricted flow between Inishtrahull and the north Irish coast generates some of the highest flow velocities in Irish waters and as such has been identified as a potential site for renewable tidal energy (Giorgi and Ringwood, 2013, Rourke et al., 2010).

The investigation into sediment mobility using repeat geophysical surveys showed a migration in all sediment waves between the initial INSS survey in 2004 and CV13030 in 2013 (Fig 5.2B). In this 9-year period, all waves migrated from ~10 m to 211 m with the large asymmetric waves showing a displacement of up to 70 m. Smaller amplitudes waves to the southeast display significantly lower migration rates of ~18 m on average, with slightly larger movements of up to ~30 m at crest ends. The north and central sections of the sand wave assemblage show movement in a south-easterly direction. In contrast, the crests in the south and west illustrate movement in a counter, north-westerly direction (Fig. 3.7, Chapter 3). The direction of migration is in agreement with wave asymmetry.

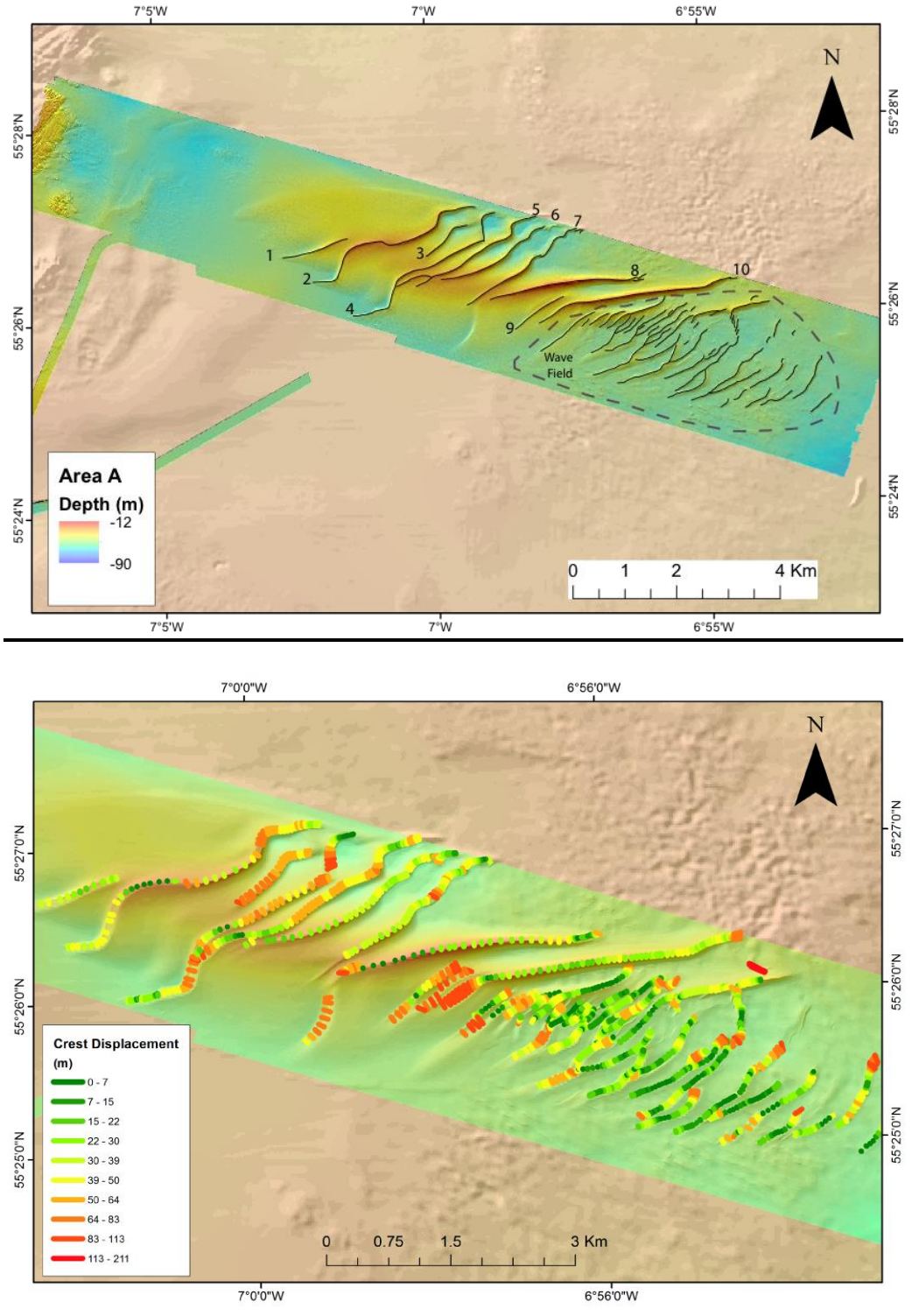

Fig. 5.2. (A) Extent of Area A. Large asymmetric waves are numbered 1-10 to aid in text description. A field of smaller sediment waves is delineated in the southeast (dashed line). Background bathymetry is from INSS survey (2004). (B) Calculated displacement of wave crests in 9 years between INSS survey (2004) and CV13030 survey (2013). Highest migrations (reds) occur in larger waves to the northwest. Lower displacements (green) typically occur in the wave field to the southeast.

5.2.2 Area B

Area B (83 km^2) is located between 6º30'W and 6º45'W and 55º14'N and 55º18'N. It extends from the Causeway coastline in Northern Ireland up to 9 km offshore, in water depths ranging from 20 m to 155 m (Fig. 5.3). A rocky reef known as 'The Ridges' represents the largest exposed bedrock outcrop in the area, with a 1.6 km long crest extending up 40 m above the surrounding seafloor. Sediments in the area range from fine sands to gravelly deposits in deeper waters to the north and northeast. The deeper portions of Area B historically have been used for disposal of dredge material from nearby Lough Foyle (Bates, 1996).

Area B displays variance of sediment wave morphology and classification. Notable features include three >20 m amplitude trochoidal waves, just south of the East Ridges, and an inshore linear shoal known as the Causeway Bank (Fig. 5.3A). Due to the number and variation in the shape of the sediment waves, the description of the results has been split into zones (shown in Fig. 5.3A) to aid discussion, with specific values of bedform migration included in the results section. An average bedform migration of 14 m was calculated for the 6-year time-lapse period, with the largest displacements of >70 m in the area of the East Ridges and the nearshore portion of the Causeway Bank (see Fig. 5.3A). The lowest levels of migration are observed in the barchan dune field and in the trochoidal waves in the East Ridges area (1-5 m over 6 years). Migration was most prominent in gravelly sand, whilst lowest migrations rates were found in areas of fine sand (Figs. 3.9B and 5.3B).

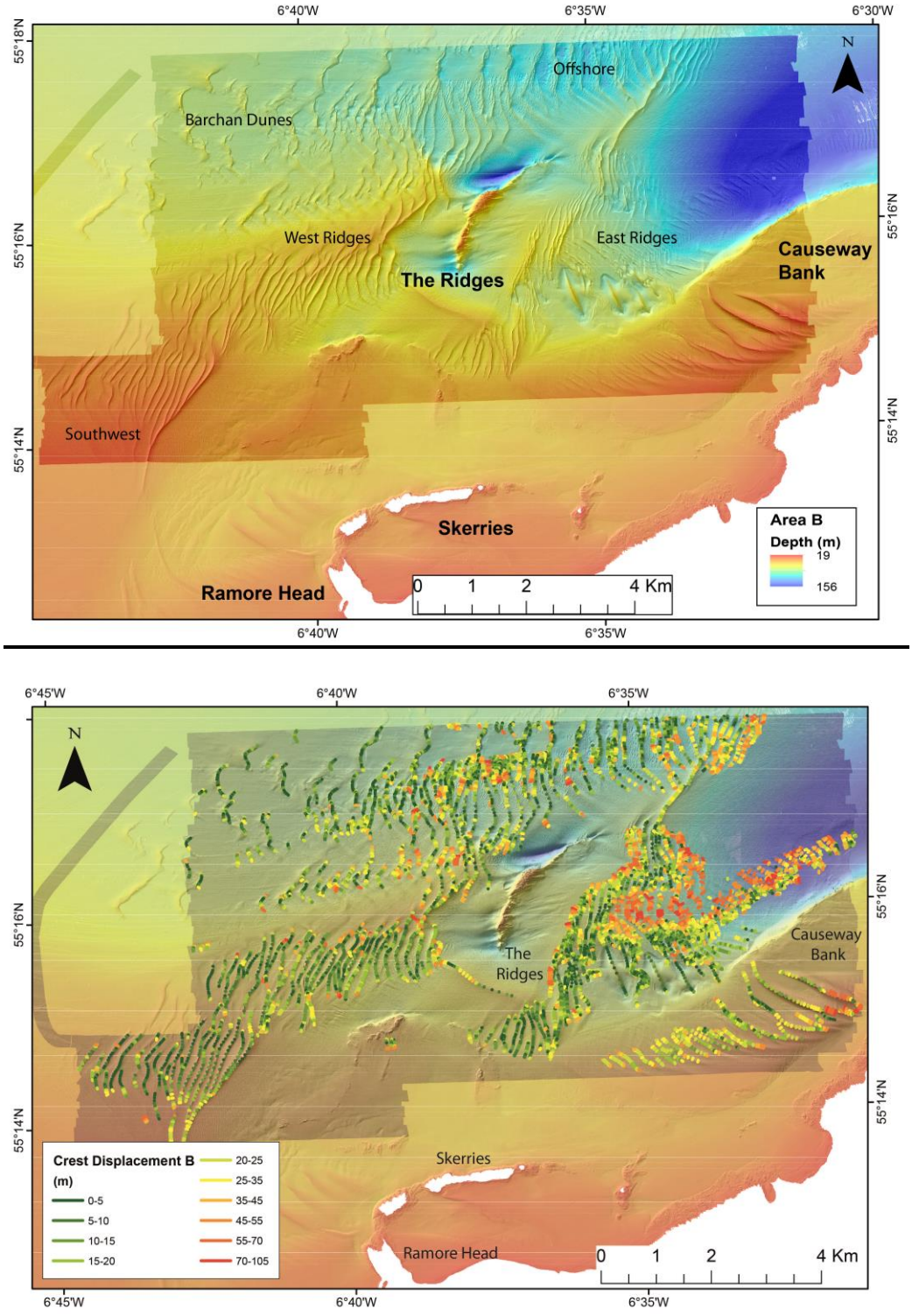

Fig. 5.3. (A) Extent of Area B with the Ridges rock outcrop in its centre. Distribution of zone names created by author are defined in lower font size, place names in bold. Bathymetric data in a darker shade are from the CV13030 survey, whilst the background bathymetric data in paler colours is taken from the JIBS 2007 survey. (B) Calculated displacement of wave crests in 6 years between JIBS survey (2007) and CV13030 survey (2013). High crest displacements are coloured red with lower measurements coloured green

5.3 Methods

To model hydrodynamic forces on the north Irish shelf the software package Mike3 by DHI (https://www.mikepoweredbydhi.com/products/mike-3) was utilised. Three-dimensional models in marine environments require, mass conservation, momentum conservation, conservation of salinity and temperature and also equations relating local density to salinity, temperature and pressure (Ferziger, 1987). For this reason, Mike 3 by DHI utilised the mass conservation equation, The Reynolds-averaged Navier-Stokes equations which describe how the velocity, pressure, temperature and density of a moving fluid are related (Chorin, 1997, Lewis, 1980). The Reynolds component of the equation expresses the ratio of inertia forces to viscous forces. Lastly Boussinesq assumptions are included to better calculate propagation of flow from deep to shallow water (Madsen et al., 1991), particularly important given the range of depths within the model domain here (https://www.mikepoweredbydhi.com/products/mike-3). Land boundaries were derived from GSI coastal shape files, including offshore islands, which were removed from the computational mesh. Five open model boundaries were selected to avoid areas of rapidly varying bathymetry and to promote perpendicular intersections with land boundaries to mitigate erroneous results. Due to an open-ocean, deep-water location which can often cause issues with wave build up in the model, a boundary in the northwest has been designated a ‘Flather’ boundary to improve model stability, with the validated Marine Institute ROMS model providing additional inputs (Flather, 1976, Oddo and Pinardi, 2008, Sleigh et al., 1998). This allows waves to propagate out beyond the model boundary and ensures tidal elevation input at the model extents remains

realistic. As a consequence, the model domain is much larger than the area of interest on the shelf (Fig. 5.4A). A flexible triangular mesh was generated to encompass the entire domain. Unlike in Chapter 4, the areas of interest A and B are relatively small. Thus, a lower model resolution is required at distances further away on the shelf. Reduction of resolution away from the areas of interest also serves to significantly decrease the computational effort for the model. As a result, a nested mesh setup was designed with 16,994 nodes and 32,180 elements. A coarse mesh with node spacing >5 km which reduces to a spacing of <5 m over areas A and B to creates a compromise between simulation time and appropriate data resolution (Fig. 5.4B).

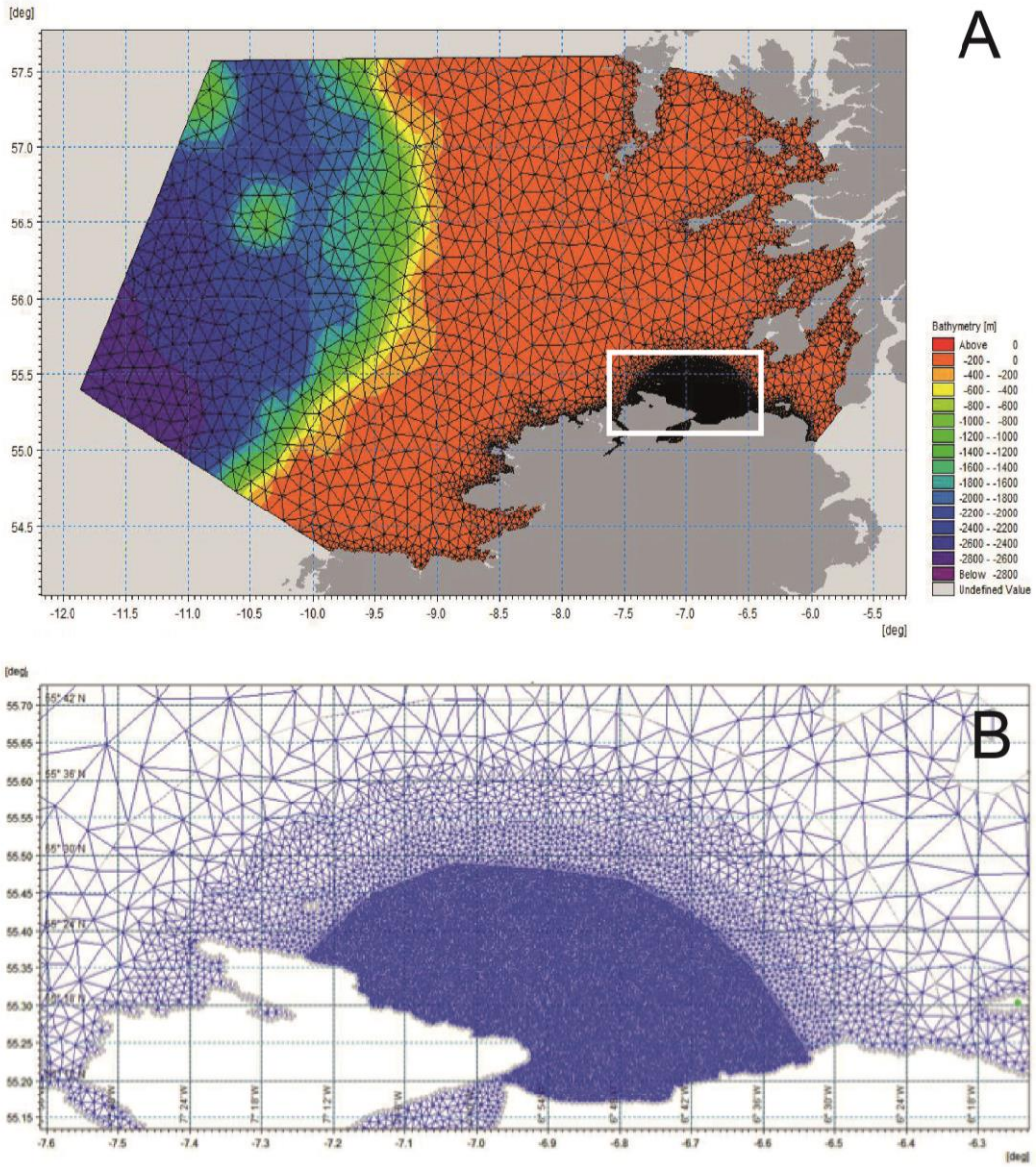

Fig. 5.4. (A)- Chart of model extent. The shelf break is clearly defined by a sharp increase in water depth. Inset – Location of Fig. 5.4B. (B) Zoom on nested mesh. Reduction in mesh size is stepped by a factor of 10 to improve model stability. Final resolution of finest mesh has not been included to provide clear visualization of the nested design.

A range of inputs were required to improve the accuracy of modelled hydrodynamic forces. Several MBES bathymetric datasets were used as input for the model. They include data from the Joint Irish Bathymetric Survey (2 m resolution), the Irish National Seabed Survey (20 m resolution), the INFOMAR

programme (20 m resolution) and cruise CV13030 led by the author (2 m resolution). Where high-resolution MBES data is not available, the General Bathymetric Chart of the Ocean (1 km resolution, GEBCO) was used to complete the interpolation across the mesh (IOC et al., 2003). The effects of this lower resolution data on simulation outputs should be negligible given the distance (over 10 km) from the study areas. Bathymetric point data was interpolated using a nearest neighbour algorithm and then smoothed through 200 iterations to improve model stability and performance. Vertical resolution with an emphasis on the boundary layer was achieved through a combined 6 sigma layer (c=0.1, θ=4, β=1) and 5 z layer combination (Song and Haidvogel, 1994). The time-period of the model spans 2004 – 2013, the longest period between MBES data sets. Data was binned at 20 min intervals at tidal gauge locations. Elsewhere data was exported at 60 min intervals to reduce data volume without compromising on resolution required to accurately interpret outputs.

Mean sea level pressure with u and v velocities at a 0.1º x 0.1º resolution provide atmospheric forcing (European Centre for Medium-Range Forecasts). Tidal elevations containing 12 major tidal constituents were extracted from the Global Ocean Tide Model developed by the Technical University of Denmark (0.125º x 0.125º resolution, DTU)

A variable roughness input is included to enable more accurate simulation of bed stresses (Davies and Xing, 2002). Grain size outputs derived from the backscatter classification for the wider area (Fig. 2.4 and (Evans et al., 2015) were used to create a Nikrudase roughness value (2.5 x grain size) capable of

further informing the simulation. The higher resolution backscatter classifications available for the selected study sites were also included (see Figs 3.5B & 3.9B) While there are known issues with using backscatter values to derive sediment grain size (McGonigle and Collier, 2014, Lamarche et al., 2011), the methodology adopted by Evans et. al, (2015) and in Chapter 3 was also used here to mitigate these. United Kingdom Seamap data (McBreen et al., 2011) was used in the absence of backscatter data to ensure complete model coverage.

From the model surface elevation (for model validation), mean and maximum velocities (m/s) in the boundary layer and mean and maximum bed stresses (Nm/2) were outputted to allow for analysis of sediment transport processes. Due to the large numbers of nodes and high resolution of input data, model simulation times were lengthy despite the use of 256 processing cores in the Ulster University High Powered Computer (HPC).

Five coastal tidal gauges were utilised to act as validation points for model data (Arranmore, Killybegs, Malin Head, Port Ellen and Portrush). Root mean square errors between simulated and measured tidal elevations were calculated and a value of agreeance generated until model validation was reached within 5% tolerance at all tidal stations. Due to the size of the model and lack of current data available on the shelf this method of data was selected as a best means to access validity (Gunn and Stock-Williams, 2013).

5.4 Results

5.4.1 Area A modelled hydrodynamic conditions

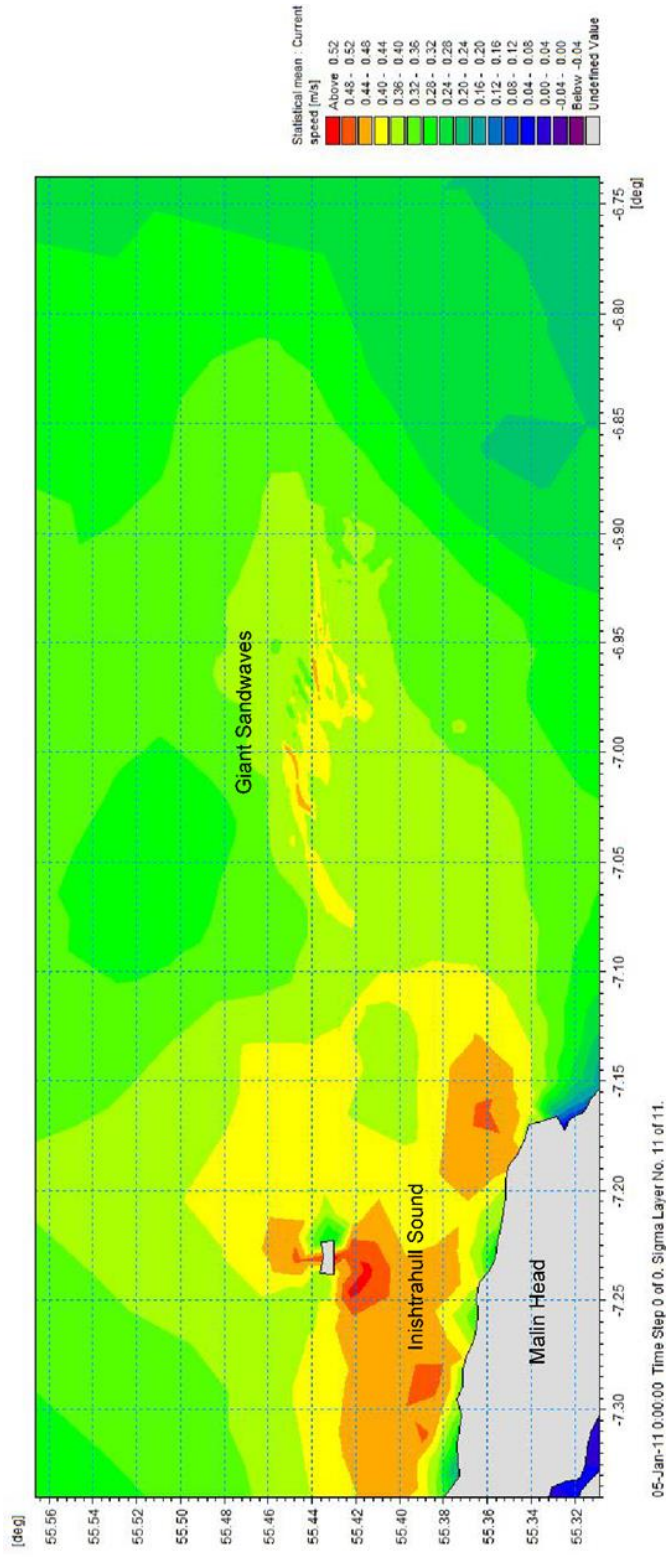

Fig. 5.5. Overview of mean current speed (m/s) across the wider study area provided by the high-resolution hydrodynamic model. A band of increased energy extends from Inishtrahull Sound to the location of the Giant Sandwaves. The grey shape (ca.7ºW23'W longitude) is Inishtrahull Island .

In area A, sediment waves 1, 2 and 8 (see Fig. 5.2A for numbering of bedforms) experience the highest boundary flow velocities across the bedform, with rates exceeding 1.35 m/s (Fig. 5.6A). These flows peak at the highest crest points on these waves, with velocities reducing as wave amplitude decreases. As a result, lower flow velocities typically occur on the outer boundaries of the bedforms, the only notable exception being wave 4, where highest maximum velocities occur at the southwest crest end. Sediment waves 3 to 7 experience lower maximum flow velocities (1 – 1.15 m/s) with prominent reductions of maximum flow velocity in wave troughs (<0.85 m/s). The smaller amplitude waves to the southeast are subjected to maximum flow velocities of 0.85-1 m/s. The lowest velocities in this area coincide with a decrease in amplitude or absence of sediment waves. These trends are repeated for mean flow velocities (Fig. 5.6B) with waves 2 and 8 experiencing highest mean flow velocities 0.45 m/s and 0.5 m/s respectively. Mean flow rates between 0.39 and 0.42 m/s are typical across waves 1 to 10, decreasing to <0.34m/s in wave troughs.

Simulation of maximum bed stresses (N/m2) across Area A (Fig. 5.7) show that the sand wave formation is situated in a section of the seafloor experiencing on average lower boundary layer forcing than the surrounding shelf. The formation is flanked to the northeast by a gravel and cobble bank (Evans et al., 2015) about 10 m shallower than the base of the sand waves. The bank experiences maximum bed stresses of between 2 N/m2 and 3 N/m2. To the south and west of the bedform, another elevated area (approx. 8 m shallower) of gravel material, coincides with higher simulated bed stresses than those over the sand waves, reaching peaks of over 3.6 N/m2. Within the sand wave formation, wave crests 1, 2, 4, 8 and 10 are easily identified by regions of higher bed stress,

similar to the points of increased simulated hydrodynamic flow data (comp. Fig. 5.6B with Fig. 5.7B). Typical maximum bed stresses at crests range from 2 – 2.8 N/m2. Waves 8 and 10 undergo the highest maximum bed stresses of all waves in the formation, with forces between 3 and 3.4 N/m2 on the northeast edges of their crests. In the troughs of waves 1 to 10, maximum stresses average between 1 and 1.8 N/m2. Further to the south east, the smaller amplitude wave field experiences much lower maximum bed stresses ranging from 0.8 to 1.2 N/m2. An area of increased stress is apparent to the north east of the sand wave field. This correlates with the largest, bifurcating wave in this area and a 10 m barchan isolated wave on its northern flank.

Mean bed stresses (Fig. 5.7B) display similar distribution of energy, suggesting the sediment waves are in a less energetic area than the surrounding seafloor. Similar to the maximum stress data, elevated bed stresses of 0.36 to 0.48 N/m2 are calculated for the raised gravel/ cobble patch to the north east, and 0.36 to 0.52 N/m2 simulated for the coarse material to the south and west. In both instances highest mean bed stress values occur at points of bathymetric peaks. Within the formation, wave crests 1 to 10 undergoing mean forces of between 0.24 and 0.36 N/m2. The troughs of these waves and the majority of the smaller wave field experience reduced stresses of between 0.12 and 0.2 N/m2. Waves 8 and 10 display the highest bed stresses for mean conditions, however, the elevation of these stresses on these crests is much more pronounced than in maximum bed stress data. This suggests that these waves undergo higher energy conditions for longer periods of time than any other in the formation.

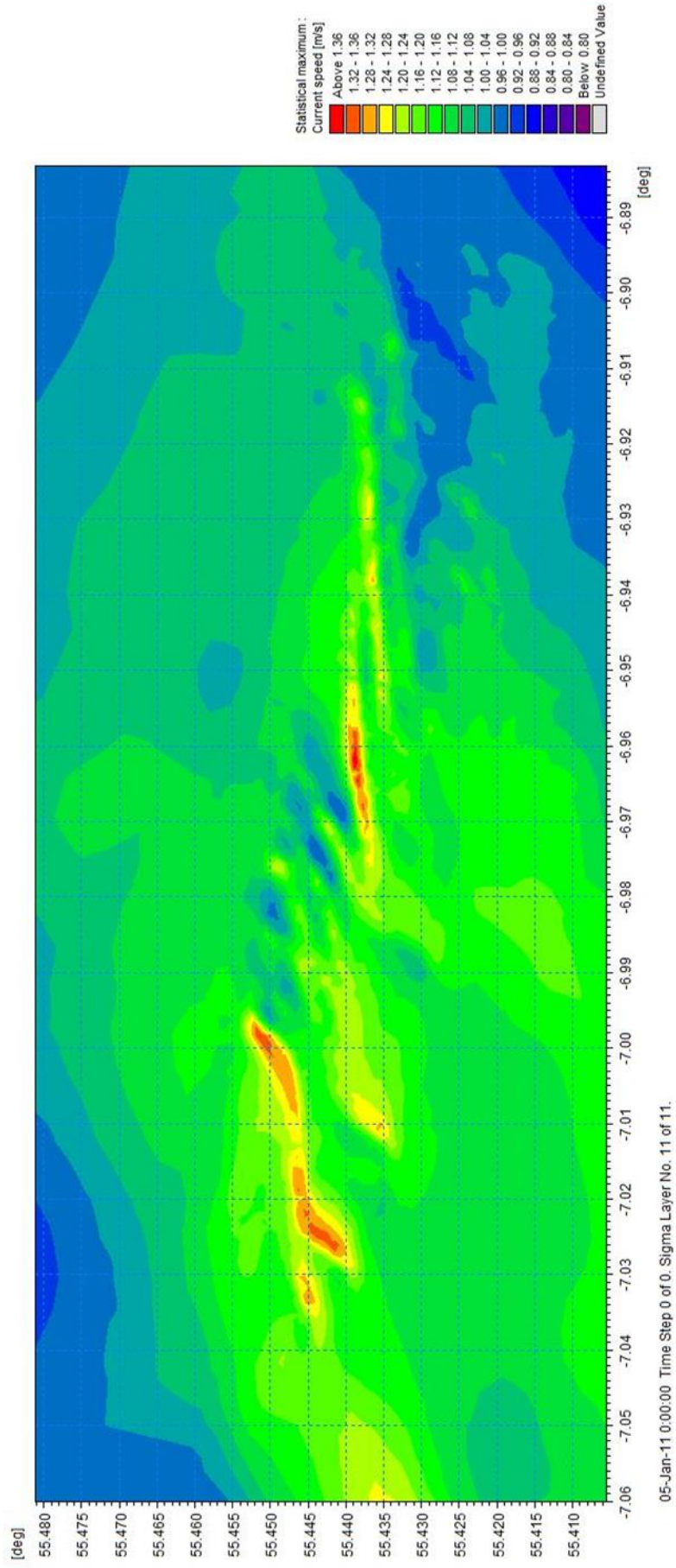

Fig. 5.6. (A) Maximum current speed for area A. Sediment wave crests are easily identified in data as areas of higher velocity flow.

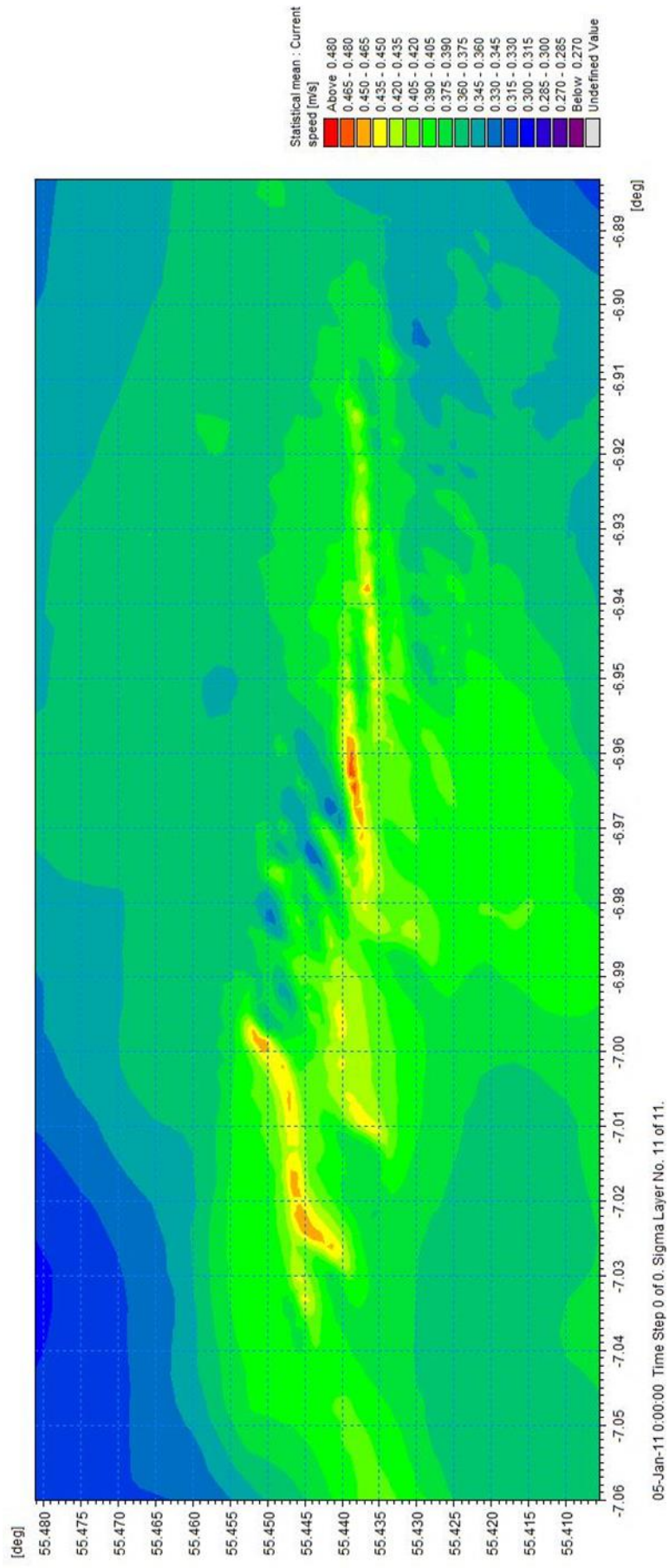

Fig. 5.6 (B) mean current speed for area A. Sediment wave crests are easily identified in data as areas of higher velocity flow.

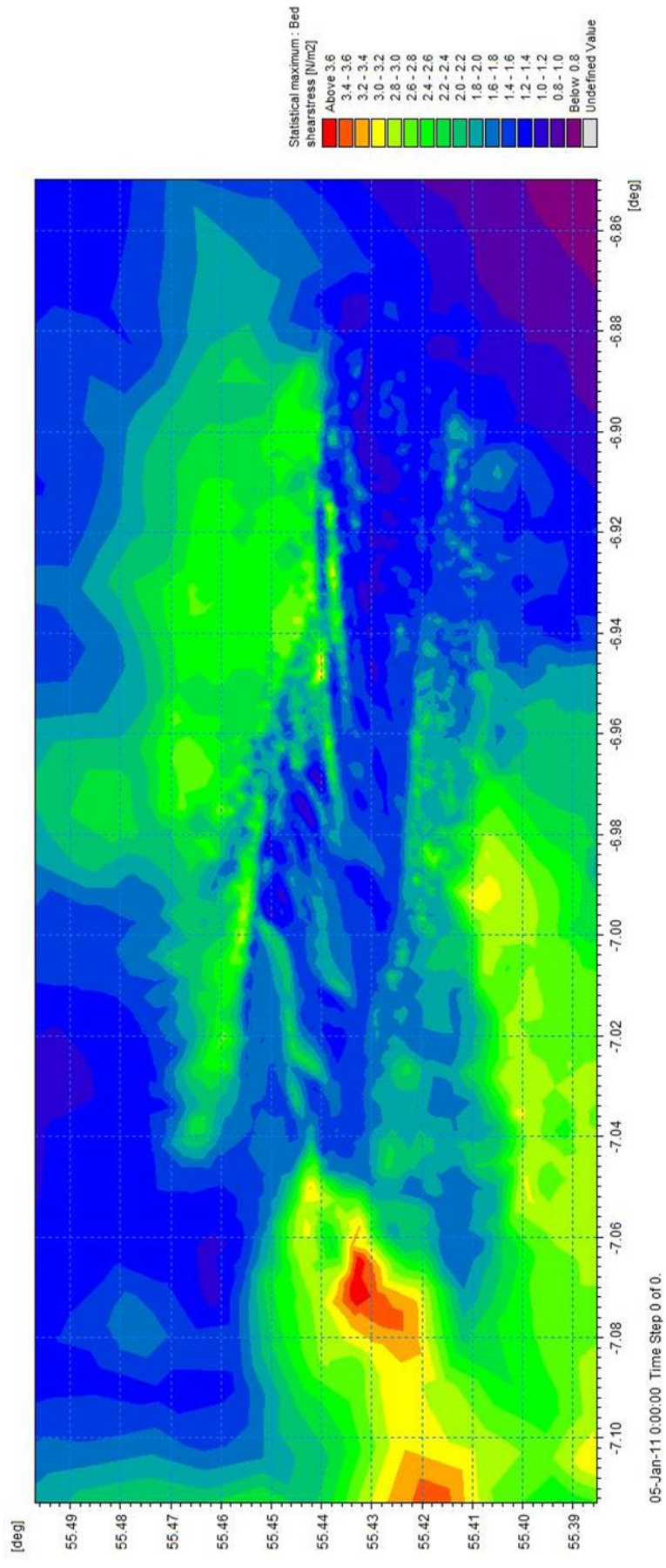

Fig. 5.7. (A) Maximum bed stress for area B. The sediment waves are situated in an area of reduced bed stress between two areas of coarser grained sediment.

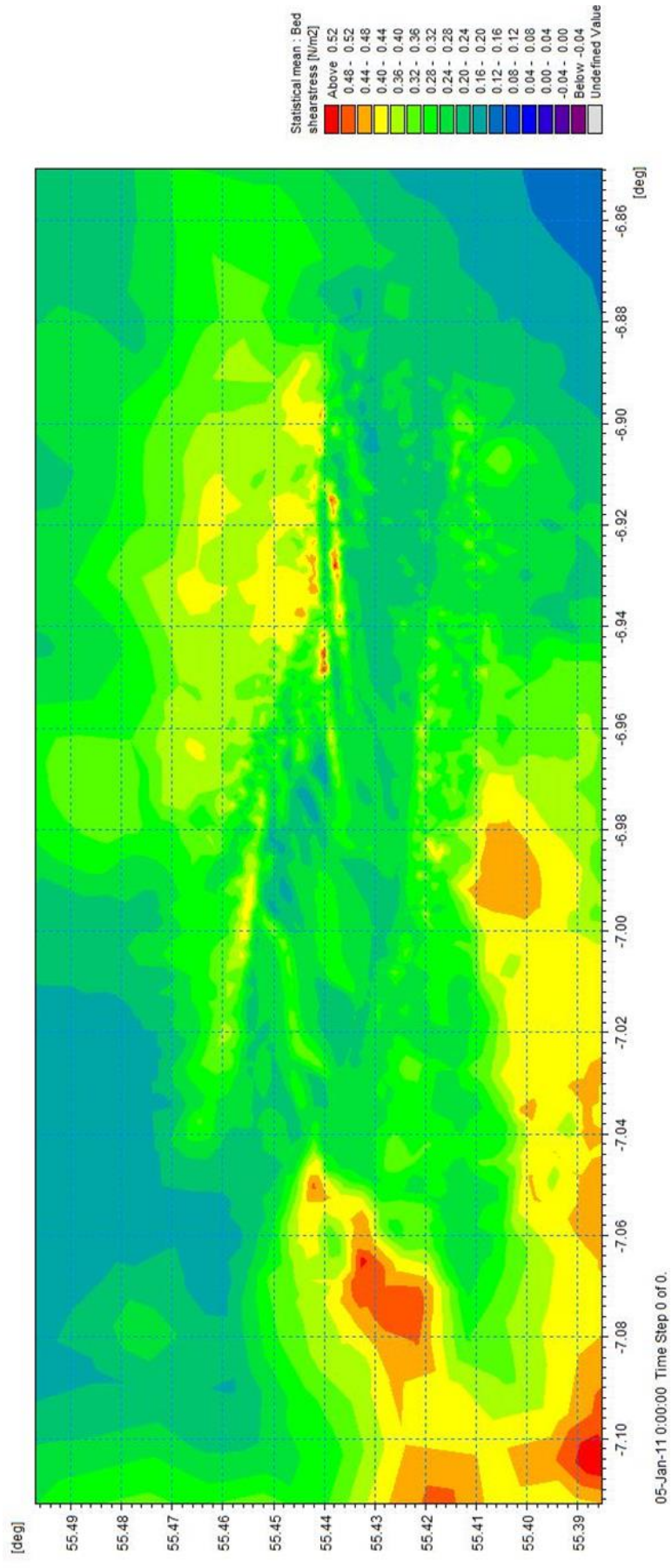

Fig. 5.7. (B) mean bed stress for area B. The sediment waves are situated in an area of reduced bed stress between two areas of coarser grained sediment.

5.4.2 Correlation of sediment wave migration with hydrodynamic flow, Area A

The model resolution allows for a detailed analysis of the flows and bed stresses around each single sediment wave found in Area A and for correlation with the calculated migration distances and rates from Chapter 3.

Between surveys, wave 1 displayed average migration distances of 17 m in a north-westerly direction with maximums measured at 42 m (Chapter 3). Peak flows of 1.3 m/s occur in the southwest extent of the wave. Mean flows across the crest are calculated to be ~0.42 m/s. Maximum stresses range from 2.2 – 2.4 N/m2, with means averaging 0.3 N/m2.

Wave 2 displays variation in migration along the crest with highest movement at crest ends. The northeast end of the wave migrated to the southeast up to 50 m with a similar movement in the southwest end but in a counter, north-westerly direction. Despite these large migrations, the central section of the crest is characterised by a rounding of crest profile that suggests reduced movement. This is thus likely to be the centre point around which the clockwise rotation of the wave occurs (i.e. the pivot point). Highest maximum flow rates (>1.36 m/s) occur at the crest ends, dropping to 1 m/s at the pivot point. The same distribution is apparent in the mean flow plot, with 0.46 m/s velocities at crest ends, reducing to 0.41 m/s at the central point. Highest mean stresses also occur at crest ends (0.32 N/m2), again displaying a reduction over the central pivot point.

Wave 3, 10 m lower in amplitude than wave 2, displays consistent migration distances of ~70 m along the entire crest. Maximum (1.0 m/s) and mean (0.4 m/s) flow velocities are significantly lower than those over surrounding waves.

Maximum (1.1 N/m2) and mean (0.18 N/m2) bed stresses are also the lowest for any wave in the group.

Wave 4 spans the width of the survey area. As with wave 2, a rotary migration is measured with distances of 40 m to the southeast and 25 m to the northwest (Chapter 3). Migration rates are significantly reduced at the pivot point of this rotation. Peak flows occur in the southwest portion of this wave (1.2 m/s) and average 0.4 m/s along the crest. Bed stresses of 2.6 N/m2 (max) and 0.32 N/m2 (mean) follow similar distribution trends to the flow velocities. All model derived outputs for wave 4 do not evidence the presence of a pivot point as clearly as in wave 2, however morphology and migration rates display characteristics similar to pivot points in other sediment waves within this formation.

Waves 4 and 5 are the only sediment waves that come close to intersecting (see Fig. 5.2A). As with waves 2 and 4, wave 5 also displays a clockwise rotation, albeit with only a short section migrating to the northwest by ~40 m. Similar migration distances are recorded for the remainder of the wave towards the southeast. Interestingly, the pivot point occurs in proximity to the centre of rotation in wave 4. Flow rates reach a maximum in the southwest of the crest at 1.2 m/s where the highest mean flows also occur (0.4 m/s). Bed stresses follow a similar pattern with peaks in energy concentrated to the southeast (2.4 N/m2 max, 0.23 N/m2 mean; Fig. 5.7). Typical mean stresses of 0.8 N/m2 occur along the remainder of the crest. The pivot point in wave 5 is not accurately defined by hydrodynamic data.

Wave 6 displays lower migration rates when compared to previous waves. Relatively uniform migration occurs in the southeast crest section with an

average displacement of 15 m, with maximums of 40 m. With typical maximum flows of 1.8 m/s (mean 0.36 m/s) and max stresses of 1.7 N/m2 (mean 0.2 N/m2), wave 6 experiences reduced hydrodynamic energies. An area of significantly reduced hydrodynamic energies clearly defines the 500 m wide trough between waves 6 and 7.

Wave 7 presents higher migration rates (avg. 30 m) than those of wave 6 (avg. 15 m), with a deviation in the trend of decreasing transport rates from the north west to south east across the bedform. Migration of 30 m in a south-easterly direction is typical, with maximum measured movement up to 75 m. Flow rates are higher than those experienced by wave 6, with means of 0.42m/s and peak velocities reaching 1.8 m/s. Similarly, bed stresses are also increased, with a maximum of 1.2 N/m2 and a mean of 0.3 N/m2. In contrast to the other waves, maximum displacement coincides with an area of reduced hydrodynamic forcing. This wave section is characterised by a break in crest continuity.

Wave 8 displays a distinct change in orientation, becoming more north – south aligned when compared to previous waves (Fig. 5.2A). Despite experiencing some of the highest flow velocities (1.3 m/s max, 0.45 m/s mean) and stresses (2.7 N/m2 max, 0.36 N/m2), wave 8 shows relatively low crest displacement averaging 15 m in a south-southeast direction.

Wave 9, positioned between the south east extents of waves 8 and 10, is comparatively short in length at 1.1 km. Like other waves at this site, this wave crest shows migration in two opposing directions, towards the northwest on the southern edge and in a south-easterly direction at the north section of the crest. Migration is highest (65 m) at the southern extent of the crest, with a central pivot point showing minimal migration. There are no discernible change in flow

velocities over the entirety of the crest (1.12 m/s max, 0.4m/s), however peaks in the maximum bed stress to 1.8 N/m2 correlate with the highest migration rates along wave.

Wave 10 represents the longest continuous crest (3.75 km) at this site. Average migration is lowest at the centre of the crest (10 m over 9 years) increasing at crest edges to 40 m in the northeast and 60 m in the southwest. Plots of current direction over this wave reveal flows in opposite directions with a stronger southeast component (Fig. 3.7). Stresses along the crest average 0.4 N/m2 with peaks of 2.4 N/m2. Increased migration to the northeast of the wave correlate with an increase in bed stress. However, this is not the case for the southwest with a migration of 60 m but with reduced hydrodynamic energies.

The wave field to the southeast comprises generally smaller amplitude waves (Fig. 5.2A). Migration distances are typically smaller (~10 m on average, with maximums of 50 m, Fig. 5.2B) than those of waves 1 to 10. Greatest crest displacement typically occurs at crest edges with decreased movement in the centre of the waves, and the field in general. Hydrodynamic energy is significantly reduced across the lower amplitude waves when compared to the larger amplitude waves to the northwest. Lowest mean flows, 0.34 m/s and stresses, 0.18 N/m2 occur through the centre of the wave field, coinciding with lowest migration rates. The outer edges of the wave field display a slight increase in both flow velocity and bed stress, which correlates with increased migration at these locations.

5.4.3 Area B modelled hydrodynamic conditions and bedform migration

Area B is located in a section of shelf which experiences much lower hydrodynamic forcing than Area A. Flow velocities across the area reach only a maximum of 0.5 m/s (Fig. 5.8A). These occur around the Causeway Bank, 'The Ridges' outcrop and an isolated sediment wave to the northeast of this feature. Mean velocities of 0.13 m/s are most prevalent across the area increasing to 0.2 m/s at isolated points (Fig. 5.8B). Bed stresses across the site peak at 1.2 N/m2 (Fig. 5.9A). Like maximum flow velocities, the largest bed stresses occur around 'The Ridges' outcrop and the Causeway Bank. The majority of Area B experiences mean bed stresses between 0.06 N/m2 and 0.17 N/m2 (Fig.5.9B). The following sections describe the results of the hydrodynamic model in relation to the specific bedforms mapped at this site.

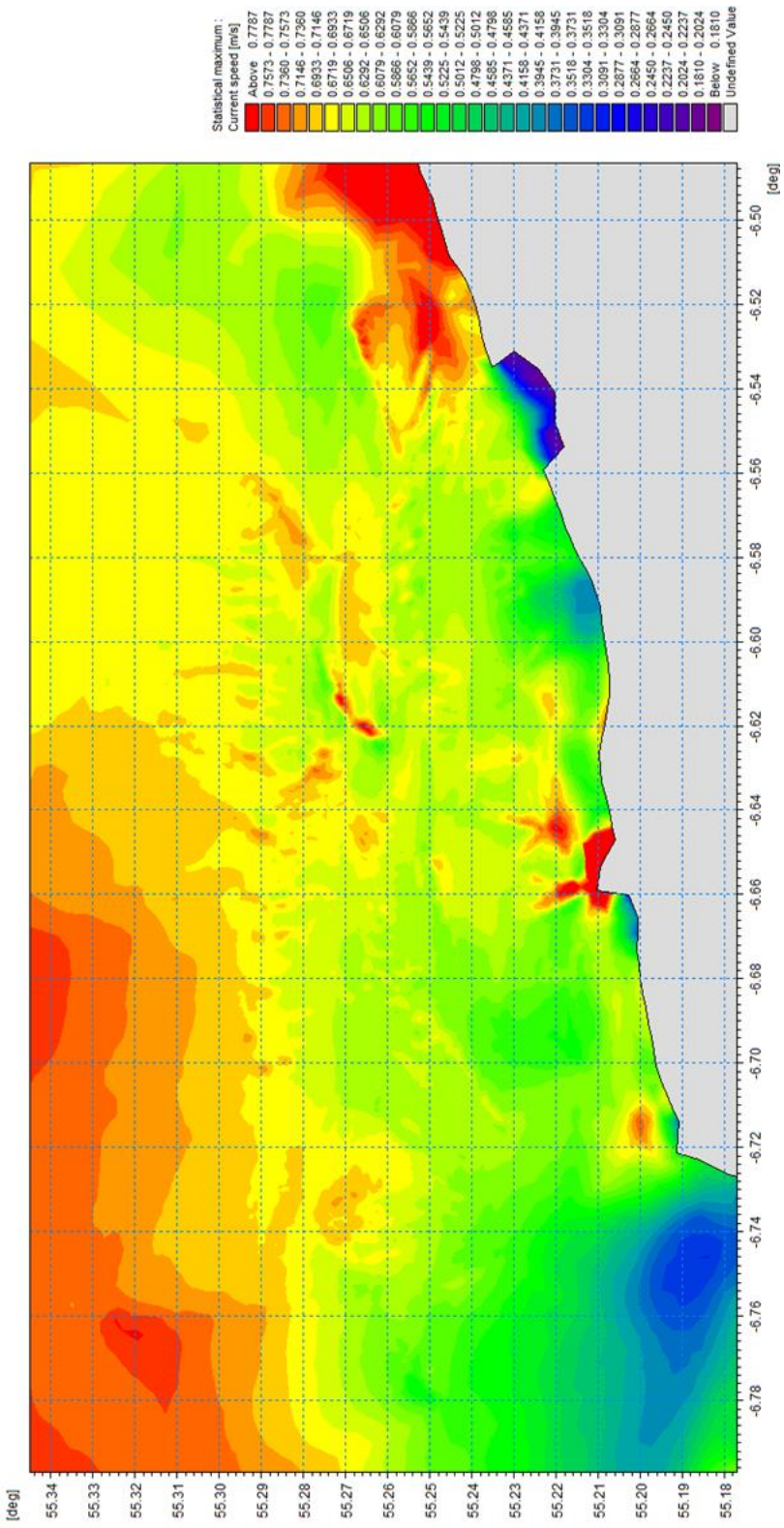

Fig. 5.8. (A) Maximum current speed for area B. 'The Ridges' can be identified within data sets offshore by isolated increase in flow velocity. Highest peak velocities occur in the inshore.

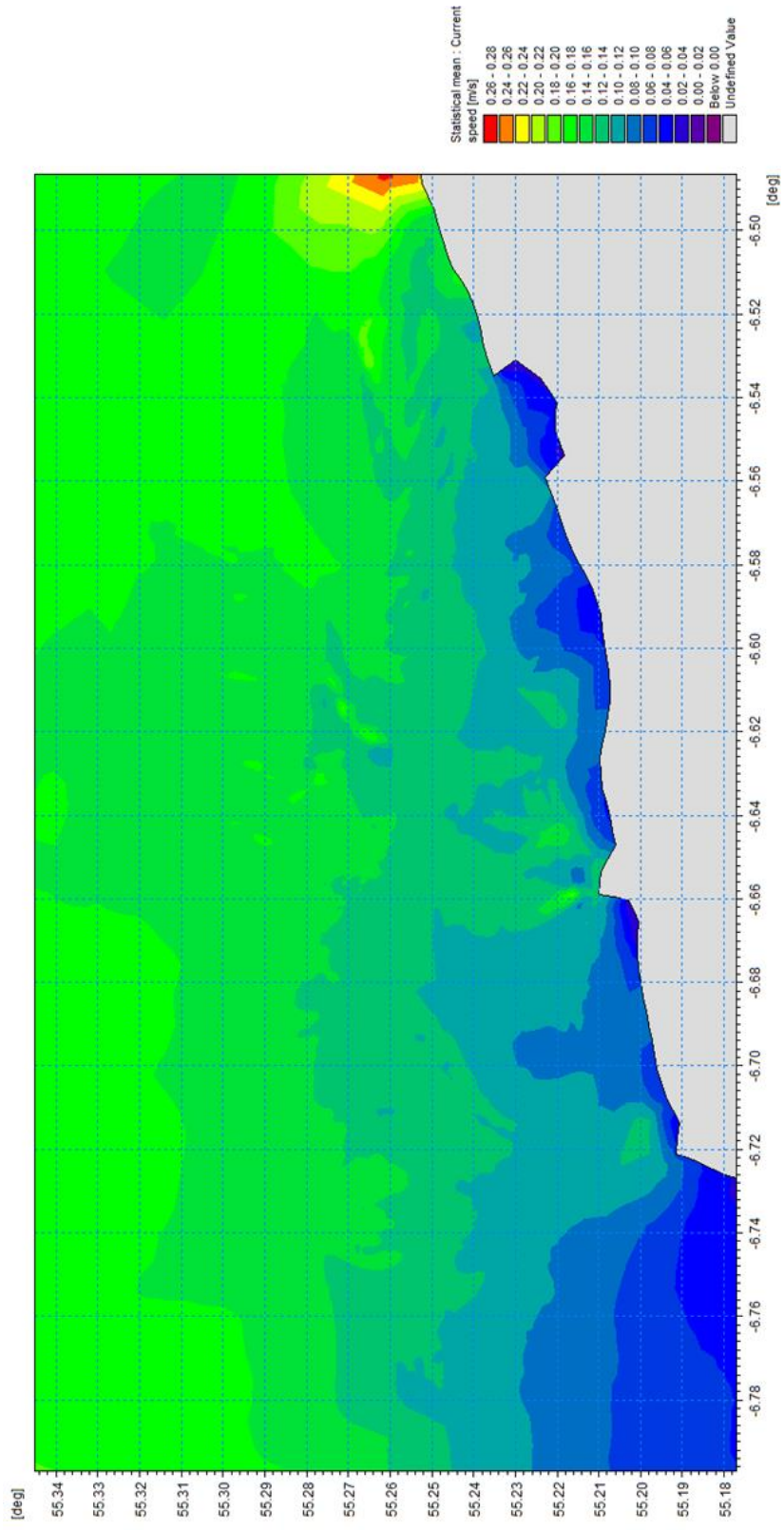

Fig. 5.8. (B) mean current speed for area B. 'The Ridges' can be identified within data sets offshore by isolated increase in flow velocity. Highest peak velocities occur in the inshore.

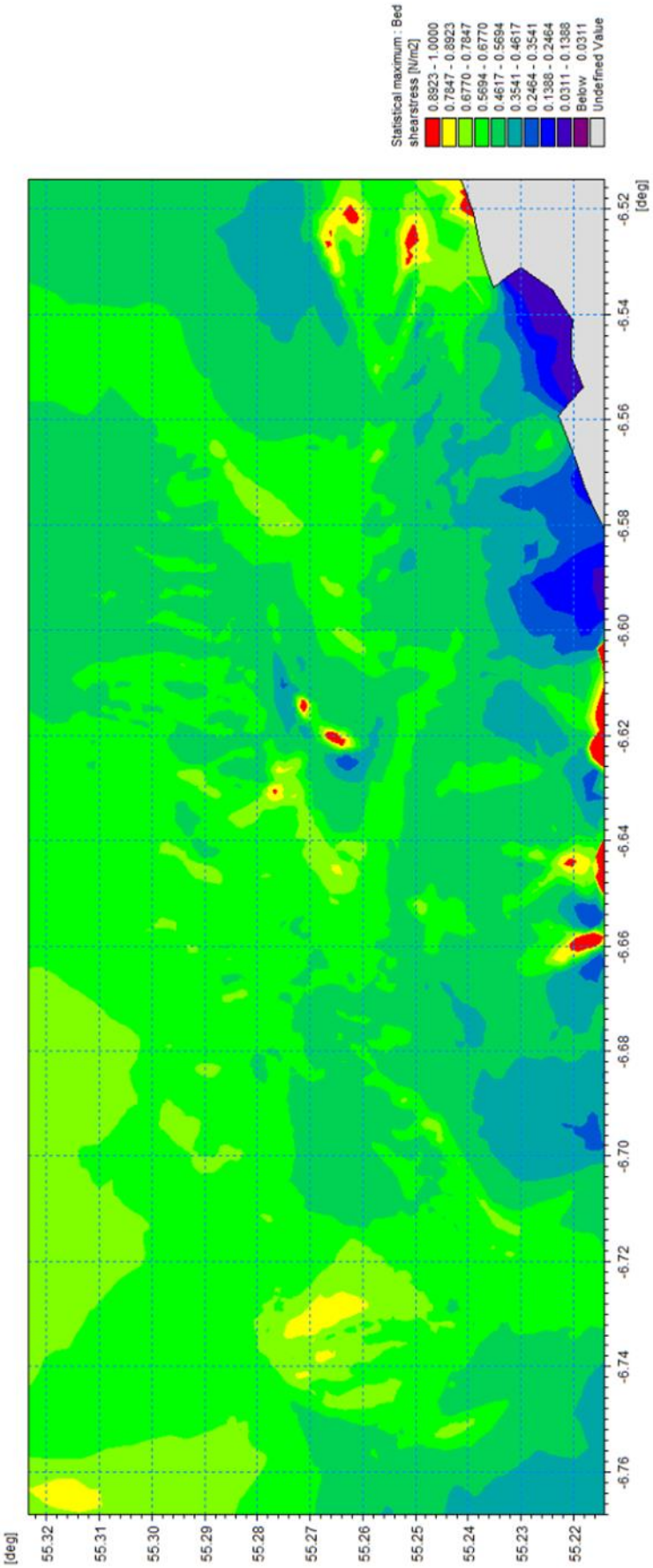

Fig. 5.9. (A) Maximum bed stress for area B. As with flow velocities, 'The Ridges can be identified offshore by isolated peak stresses.

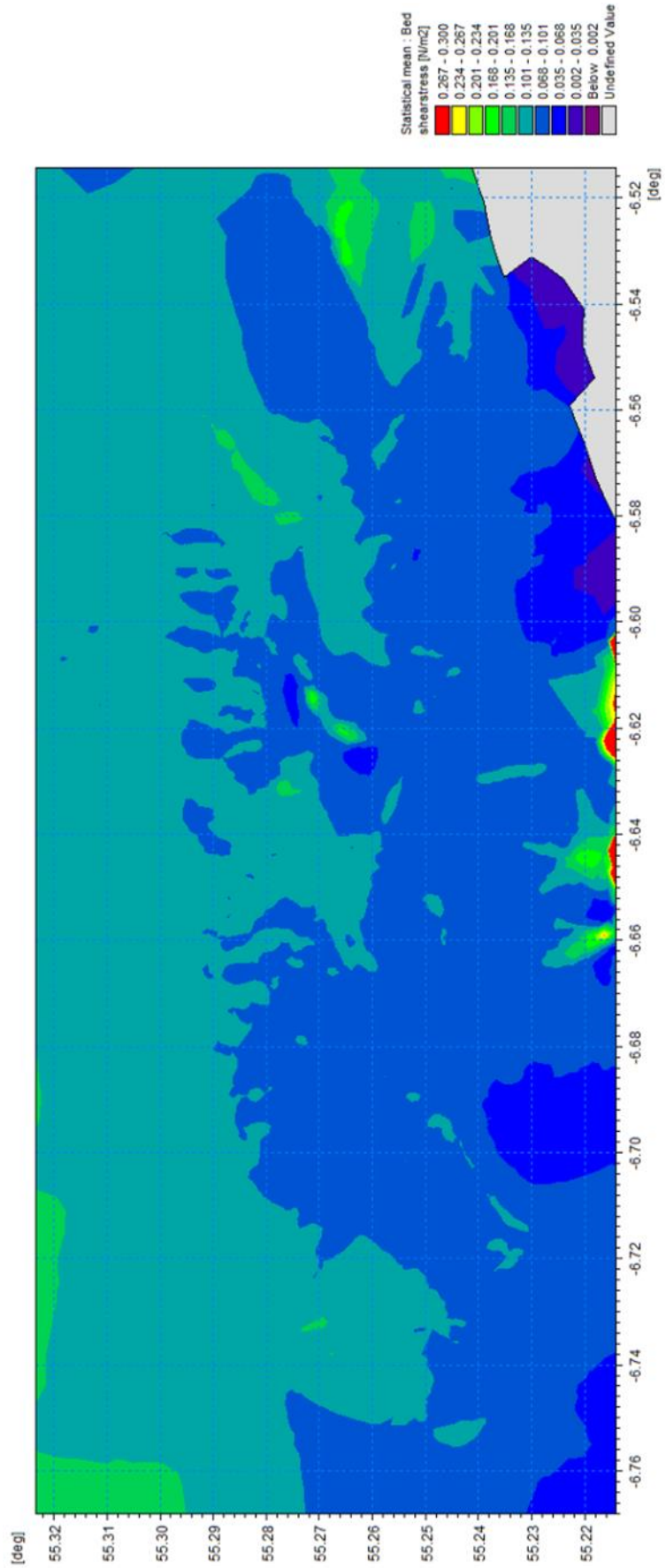

Fig. 5.9. (B) mean bed stress for area B. As with flow velocities, 'The Ridges can be identified offshore by isolated peak stresses.

Barchan Field

A field of barchan dunes is situated to the northwest of Area B (Fig. 5.3A). Typical migration rates for these bedforms were between 5 m and 15 m in an easterly direction during the 6-year time lapse. Maximum flow velocities across this zone peak at 0.43 m/s on the dune crests, with the surrounding seafloor experiencing reduced flows of 0.34 m/s. Similarly mean flows in this area peak at 0.13 m/s over the barchans dunes furthest offshore. Mean velocities of 0.1m/s are simulated on the open shelf between waves. Analysis of current direction for this zone illustrates a bi-directional flow regime with a dominant trend to the east peaking at 0.4 m/s (Fig. 5.8). Bed stresses are more evenly distributed across the zone with individual waves not clearly defined (Fig. 5.9). Maximum bed stress values of up to 0.56 N/m2 are typical throughout the field, with mean bed stress ranging from 0.06 N/m2 to 0.13 N/m2.

West Ridges

The area named ‘West Ridges’ (Fig. 5.3A) is defined by two sediment wave trains separated by a smooth sediment ridge which terminates in the east where both wave trains join close to ‘The Ridges’ outcrop. Average migration for the northern of these sediment waves is 15 m with maximums of 40 m for some isolated crests. The southern sediment waves display lower displacement distances of 5 – 10 m on average, with isolated maximums of 30 m (Chapter 3 & Fig. 5.3). A maximum flow rate of 0.39 m/s occurs over the northern sediment waves with the southern waves experiencing a smaller maximum flow rate at 0.30 m/s (Fig. 5.8A). Mean flow rates are more evenly distributed across the entire zone with both northern and southern wave trains exposed to 0.12 m/s

velocities (Fig. 5.8B). In both maximum and mean velocities there is an increase in flow rate moving eastwards, peaking at the point where wave crests terminate west of ‘The Ridges’ outcrop. These velocities display a bi-directional element with a dominant easterly component

As with flow velocities, maximum bed stresses of 0.6 N/m2 suggest increased hydrodynamic forcing over the northern wave train, compared to 0.5 N/m2 over the southern waves. Mean bed stresses make no distinction between the two sets of waves, with a uniform bed stress energy calculated at 0.08 N/m2, but with a slight increase (as for flow velocity) to the east of this zone with maximums exceeding 1 N/m2 (Fig. 5.9).

Southwest

The southwest zone is characterized by 5 m amplitude waves with measured displacements averaging 10 m, increasing in the southernmost portion of this area to 20 m. Migration is to the northwest is in agreement with bedform asymmetry (Fig. 5.3B). Flow velocities are consistent across the area with a maximum of 0.35 m/s and uniform mean of 0.12 m/s. The currents are however bidirectional, with peak velocities flowing to the southeast, but dominant flow occurring towards the northwest.

Unlike flow regime, there is variation in the distribution of bed stresses (Fig. 5.9). Maximum bed stresses of 0.6 N/m2 occur throughout the area which increases to the east and south up to 0.7 N/m2. The same pattern is followed by the mean bed stresses with the highest values of 0.14 N/m2 occurring in the east and south. These increases coincide with the highest migration rates in this specific area.

Offshore

Migration rates in the offshore zone are highest in the eastern portion of this area, averaging 35 m over 6 years. Migration distances decrease westwards to an average of 12 m north of ‘The Ridges’ outcrop. Peaks in maximum (0.41 m/s) and mean (0.16 m/s) flow rates occur in the eastern section of this area and coincide with the largest migration rates (Fig. 5.8). Moving westwards, they decrease to a maximum value of 0.38 m/s and mean values of approx. 0.15 m/s. A single sediment crest connecting the offshore zone to ’East Ridges’ area is identifiable by a linear band of increased flow velocities peaking at 0.43 m/s. This crest is also easily identified in bedstress data with peak bedstress of 0.7 N/m2 and mean of 0.17 N/m2. Maximum bed stresses show increased energies (up to 0.6 N/m2) in the eastern portion of this area, decreasing westwards to 0.42 N/m2 (Fig. 5.9A). Mean bed stresses however are more uniform, with values of 0.10 N/m2 across the area (Fig. 5.9B).

East Ridges

The ‘East Ridges’ zone displays a wide range of sediment wave types across a range of depths down to 120 m water depth (Fig. 5.3A). Some of the highest migration rates of Area B occur on the slopes to the east of this zone. Sediment waves in 120 m water depth migrated upslope for a distance of 50 m during the 6-year time lapse between surveys. This westerly migration pattern continues to the bathymetric high east of ‘The Ridges’ outcrop, where measured displacement of wave crests reduces significantly to 5 – 10 m. Three single trochoidal waves in the south of this zone and adjacent to the Causeway Bank,

display negligible crest displacement. In the southwest section of this area, sediment waves migrated an average of 10 m between surveys.

Maximum and mean flow velocities in the ‘East Ridges’ zone display similar distributions. Increased maximum (0.38 m/s) and mean (0.13 m/s) occur in the channel containing the upslope migrating sediment waves, continuing to the bathymetric rise east of ‘The Ridges’ outcrop (Fig. 5.9A). These higher flow velocities coincide with the highest measured migration distances in the zone. The trochoidal waves and other sediment waves to the southwest experience lower mean velocities of 0.1 m/s. Flow direction analysis defines a bidirectional flow, exceeding 0.4 m/s in both directions, but with a dominance in flow westwards towards ’The Ridges’ outcrop.

Bed stresses for this zone do not follow the same pattern as the flow regime. Maximum (0.65 N/m2) and mean (0.12 N/m2) energies occur north of the trochoidal waves, but do not extend into the deeper waters to the east. Isolated patches of these elevated stresses do occur however at the crest centres of the trochoidal waves. Maximum bed stress modelled data also indicate elevated energy continuing to the southwest wave field. This is not replicated in mean stress data with a 0.068 N/m2 energy value present across the south of the east ridges zone (Fig. 5.9B).

Causeway Bank

The Causeway Bank is a flat inshore shoal topped by sediment waves. Measured migration of these waves is consistently high for Area B, averaging 22 m with peak migrations reaching 70 m over the 6 years between MBES surveys..

Flow rates are highest in the east of this zone with maximum velocity of 0.42 m/s and mean of 0.14m/s (Fig. 5.8). These values decrease moving westwards to a maximum velocity of 0.30 m/s and a mean of 0.11 m/s. While individual waves cannot be identified in flow-modelled data, points of highest migration >50 m correlate with the areas of peak velocity. Flows on the Causeway bank are heavily dominated by a south-westerly flowing current which exceeds 0.4m/s.

Bed stresses follow similar patterns to flow velocities. Sediment waves to the east of this zone can be identified by areas of maximum bed stress reaching 1 N/m2 followed by reduced levels of 0.48 N/m2 in the wave troughs. These maximum bed stresses gradually reduce westwards to 0.46 N/m2. Mean stresses follow the same trend, reducing from 0.1 N/m2 in the east to 0.07 N/m2 on the west of the bank (Fig. 5.9).

5.5 Discussion

Area A

Overall, it appears that the hydrodynamic conditions influencing the large sand waves in the centre of Area A are connected to the movement of water through Inishtrahull sound (Fig. 5.5). Mean flows between the sound and sediment waves are higher than those to the north and east of these bedforms, averaging 0.36m/s. Flows of this velocity are capable of mobilising sediments up to very coarse sand which would account for the prevalence of bedrock and gravel-sized sediments across this section of shelf and (Fig. 3.5B)(Hjulstrom, 1935, Miller et al., 1977). The ability of modelled flow to mobilise the sediments and maintain the formation over a period of time supports the hypothesis that hydrodynamics are the mechanism for formation and retention of these large-scale sediment waves.

This is effect and the seafloor morphology are consistent with the classification of the feature upon which these waves have formed as an offshore tidal sandbank (Caston, 1972, Nielsen, 1979, Swift et al., 1978).

The large sand waves numbered 1-10 (Fig. 5.3A) are composed largely of coarse sand and shells, coarsening to gravelly sand in the wave troughs and at the outer portion of this area. The wave field in the southeast portion of Area A has consistently coarser sediments, ranging from sandy gravels to pebbles. As a result, there are fewer sedimentary components to consider across Area A compared to Area B when examining relationships between grain size, measure mobility and simulated hydrodynamics.

The correlation between modelled flow data and migration reveal possible indicators of the mechanisms facilitating the formation of these large waves and retention of soft sediments on an otherwise gravel and bedrock dominated section of shelf. These indicators include the rotational migration of sediment waves, the identification of rotation pivot points and potential breakdown in crest profiles outlined previously.

The majority of the large sediment waves (2,4,5,6,7,9 in Fig. 5.2) display a clockwise, rotational element to their migration. Rotary migration around offshore tidal sandbanks has been described on other tidally dominated shelves around the globe, both in field measurements and in hydrodynamic models (Huthnance, 1973, Sanay et al., 2007, Williams et al., 2000). This rotation is characterised by increased movement (and in most cases hydrodynamic energy), close to the crest ends. It is also typical for the southwest portion of the crests (migrating to the northwest) to display larger movement (by >15 m on average) than the northeast crest end. However, it is not always the case that the southwest crest ends experience elevated hydrodynamic energy. More fine sediments are concentrated to the southwest of the large sediment waves (Fig. 3.5B). The northeast crest end of the sediment waves consists of narrow crests of sand surrounded by gravel. It is therefore likely that the increased migration in the southwest is due to the abundance of finer, more easily transported sediments in that location compared to the northwest crest ends of the sediment waves (Hjulstrom, 1935, Miller et al., 1977).

Further to this rotary migration, sediment waves 2, 4, 5 and 7 also display changes in crest profile. In the case of waves 2, 4 and 5, this change manifests as a rounding of the crest profile, which is typically sharp elsewhere in the

sediment waves in this bedform. Sediment wave 7 displays a distinct break in crest continuity. These changes in crest profile have been identified as locations of reduced or negligible migration, which in some instances correlate with an associated reduction in hydrodynamic forces (Lefebvre et al., 2014). Therefore, these low migration, rounded crest points have been identified as the pivot points around which sediment wave migration occurs. Each pivot point is found in proximity of the pivot point of the surrounding sediment waves, adding weight to the argument that they define a central axis of rotation across the study area (Williams et al., 2000).

Sediment wave 7 displays similar clockwise rotation to other crests within the area. This sediment wave is, however, the only to exhibit a break in crest profile close to the crest centre (rather than the formation of bifurcations at crest ends). The rotational migration of this sediment wave may be a contributing factor to this crest break and may be an indicator of a larger split in the sediment waveform (Lefebvre et al., 2014). Sediment wave 7 is the last of a set of waves 1 to 7, which are aligned southwest to northeast, before a marked change to the west – east orientation of wave 8. It is therefore possible that sediment wave 7 has reached a location where different shelf hydrodynamic conditions and changes in sediment composition cause a change in orientation, a hypothesis supported by the lack of other sediment waves in the ~1.5 km gap between waves 7 and 8.

Modelled hydrodynamic flow there suggests a link between Inishtrahull Sound and the offshore tidal sandbank upon which giant sandwaves have formed. The rotary currents identified here, and in other literature, rely on this tidally dominated flows to control their velocity and directional (Caston, 1972, Sanay et

al., 2007). It is therefore probable that any influence on this tidal flow may have impacts on this rotary current, and in turn, the sandwaves at Area A. With Inishtrahull Sound identified as a potential location for tidal turbines (Rourke et al., 2010), the far-field impacts of these marine installations should be carefully considered with respect to the unique sandwave features at Area A and the habitat they create (Ahmadian et al., 2012, Neill et al., 2009, Thiébot et al., 2015).

Area B

Area B includes a range of bedforms of differing morphologies, amplitudes and sediment grain sizes. The modelled hydrodynamic flows and bed stresses can in most cases explain the migration rates of these bedforms.

In some sections of seafloor, the bedforms are composed of a mix of sediment types, for example the sediment waves in the 'West Ridges' zone, which are composed of coarse, medium and fine sand over a gravel seafloor. The majority of these waves consist of coarse sand, gradually fining eastwards. With relatively low migration distances, averaging 15 m, coarse sand waves prevalent in the west of the zone are only mobilised during peaks in hydrodynamic forcing, with average conditions not capable of initiating transport. For medium sand waves further east, hydrodynamic means are close to achieving threshold velocity and critical shear stress suggesting that these sediment waves are mobile during period of elevated energy (Buscombe and Conley, 2012, Miller et al., 1977). Two localised points of much higher energy correlate with two pockets of fine sands combining to create much higher crest displacement than in surrounding areas. The differences in migration rates

between the north and south wave trains in west ridges can be explained by similar hydrodynamics in both areas but a higher fine sand fraction in the north sediment waves.

Elsewhere the mean flow velocities and mean bed stresses may not be large enough to mobilise the coarser fraction within the sediment, but may be able to drive the migration of the finer material (Berelson, 2001, Hjulstrom, 1935).

The ‘Southwest’ zone is dominated by fine sediments and fringed by slightly coarser, medium sands. Hydrodynamic forces are calculated as capable of initiating sediment transport during elevated states but not during mean conditions (Hjulstrom, 1935). Current distribution for the area suggests that 30% of flow conditions during the simulated period can cause transport, however it is likely that bidirectional flow reduces net transport. As a result, while sediment may be mobilised frequently during the tidal cycle, migration distances measured are relatively low. To accurately constrain the effects of this bidirectional flow on transport, higher temporal resolution of both MBES and modelled data is required (Smith et al., 2007, Xu et al., 2008). In this way the figure of 30% can be further explored, defining periods of movements during certain months, seasons or even individual tidal phases.

Sediment waves in the ‘Offshore’ zone are composed of fine and medium sand, coarsening to sandy gravels westwards. With decreasing hydrodynamic energies and increasing grain size, it is unsurprising the sediment transport is reduced in this area (Hjulstrom, 1935, Miller et al., 1977). As with other sections of seafloor in Area B, the main sediment fractions are not mobilised during mean hydrodynamic velocity flows.

The ‘East Ridges’ contain widely varying sediment distribution and migration distances. Highest migration occurs in finer grain sand waves in 120 m deep water. A channel constrains these fine sediments, with upslope migration to the crest of the slope driven by a dominant flow from the east. This is consistent with the findings of (Ediger et al., 2002) in the Sicilian Basin who noted upslope migration of sediment waves composed of similar sediments, driven by a bathymetrically constrained current. A reduction in this upslope movement in Area B is marked by a sharp increase in grain size from sands to gravel. These gravels surround the sand to the west and south and it is likely that they act as a barrier to the further migration of sandy sediments. Mean hydrodynamic flows are not sufficient to mobilise even the fine sediments in this area, however, periods of increased flow (~30 % of flow period) did have sufficient energy to cause transport in the finer fractions. As a result, gravels show little migration, increasing the validity of the hypothesis that they act as a control on migration of finer sediments through entrainment or shadowing (Van Landeghem et al., 2012, Weaver et al., 2000). Measured movement of the trochoidal wave crests are minimal, with only peak flows capable of mobilising their sediments. The crest displacement measured between surveys is most likely the result of crest flexing in a bi-directional currents (Knaapen et al., 2005, Smith et al., 2007).

The ‘Causeway Bank’ is covered by gravels and medium sands with sediment wave grain size coarsening offshore. Modelled hydrodynamics are capable of initiating transport of all the sand components on the bank, but not the gravels. This accounts for the increased migration on the inshore side of the bank driven by a heavily dominating flow to the southwest. This also suggests that acoustic

unit 2 (AU2) identified in Fig. 3.13 is likely to be composed of gravelly sediments over which finer materials are migrating.

On occasions the model does not agree well with the measured migration rates. The barchan dunes composed of sandy gravel have moved short distances overall with maximum localised migrations of <15 m. The flow velocity and bed stress modelled here do not reach the values of 1 m/s and >2.7 N/m2 that are required to mobilize sediments of this type (Hjulstrom, 1935, Miller et al., 1977). Given the high accuracy of the repeat surveys and automated measurement of crest displacement, it is unlikely this discrepancy between measured displacement and modelled flow can be attributed errors in the bathymetric data. There are isolated patches of finer sediments throughout the barchan's location and modelled hydrodynamic conditions are capable of initiating transport of these the sand fraction within the dunes themselves. This transport could account for the small migrations that are measured. Modelled flows however cannot explain the initial formation of these features and a number of reasons should be considered. This site was used as a dredge dumpsite for shipping lanes in nearby Lough Foyle. As a result, material not from this area was introduced using non-natural processes, ie. jettisoned from a vessel (Bates, 1996). It is possible that this process has created these barchan dunes through reworking of dredge piles. It is also possible that the bedforms were formed under different hydrodynamic conditions, perhaps related to larger paleotidal ranges or reduced sea levels (Terwindt and Brouwer, 1986, Westley et al., 2011)(Uehara et al., 2006). Lastly, it is possible that the model is not accurately representing actual conditions across the area and requires further refinement. It should be noted however that throughout the rest of this area, modelled result

correlate well with migration direction and distance across a range of sediment types.

This developed understanding of sediment migration (and its drivers) across Area B has a number of practical applications. Sandy beaches broken by basalt and chalk outcrops are prevalent on this section of coastline (Plets et al., 2011). Understanding of the movements of soft sediments offshore may aid management of these beaches as anthropogenic interactions increase and period stripping occurs during seasonal events (Denny et al., 2013, Nordstrom, 2005, Rodríguez and Dean, 2009, Rosati, 2005). There are several harbours and ports on the north Irish coast, should a requirement develop for future dredge disposal sites, modelled information may assist site selection(Casado-Martínez et al., 2006, Sherwood, 1989).

5.6 Conclusions

The combination of high resolution bathymetric, roughness and computational model flexible mesh have increased the ability to analyse specific sections of seafloor, bedforms and individual sediment waves in a manner that would not have been possible using lower resolution data. By increasing the resolution of this model, which is already designed specifically for sediment transport analysis, understanding of the hydrodynamic forces driving the rotational migration of giant sandwaves has been developed to a level not possible using data from Chapters 3 and 4. This work has also contributed to the understanding of how subtle differences in hydrodynamic conditions may contribute to changes in crest profile and overall shape of sediment waves.

The model outputs have also highlighted the interplay between hydrodynamic forces, sediment distribution and migration of sediment waves to a scale where localised obstacles to sediment transport, such as gravel ridges, can be identified and used to explain the isolation of some of the observed bedforms. The pattern of sediment transport across the widely varying grain sizes in the area is now better constrained and it is clear that most of these sediments can be mobilised during times of peak flow and bed stress but not during mean conditions. This is important when considering any possible human interactions with the seafloor and exploitation of marine resources (offshore engineering, maritime archaeology) in this area.

Chapter 6 – Discussion

This work utilised a multidisciplinary approach to further understanding of the formation of bedforms on the northwest Irish shelf, the distribution of sediments across the area and their potential mobility. This approach has adopted a number of techniques, including the classification of these bedforms and sediments in line with standard nomenclature (Allen, 1980, Belderson et al., 1982, Field et al., 1981), measuring rates of change in the seafloor using widely adopted MBES time lapse surveys (Knaapen et al., 2005, Schimel et al., 2015, Schmitt et al., 2008), and the development of a sediment transport specific hydrodynamic model (Davies and Xing, 2002, Németh et al., 2007). In Chapter 2, a range of non-glacial sedimentary bedforms were mapped and classified (Belderson et al., 1982, Van Landeghem et al., 2009b) using MBES data supported by a ground truthed backscatter classification chart (Goff et al., 2000, Lamarche et al., 2011, McGonigle and Collier, 2014). Chapter 3 used repeat MBES survey to measure change in seafloor over time at two selected locations to examine relationships between sediment wave migration and ROMS model data (2 km resolution) (Bøe et al., 2009). Chapter 4 combined the bedform and sediment overview described in Chapter 2 with a Mike by DHI model, developed specifically to examine sediment transport on the northwest Irish shelf. This enabled the potential mobility of bedforms to be investigated by assessing assumptions made on asymmetry and allowing them to be classified as relict or mobile based on the ability of flow energy to transport the sediments of which they are comprised (Terwindt and Brouwer, 1986). Research Chapter 5 focused back to the two areas selected for repeat survey in Chapter 3, utilising a high

resolution (2 m) version of the model used in Chapter 4 which was refined to interrogate hydrodynamics at the near seafloor across the two sites (Legrand et al., 2006, Sheng and Yang, 2010). The result is an ability to analyse individual sediment waves to better describe variation in along crest profile and mobility, the formation of bifurcations and shadowing of lower amplitude sediment waves by larger formations (Lefebvre et al., 2014, Nielsen and Guard, 2011). Each of these chapters generates discussion and draws conclusions as to sedimentary transport processes from a shelf to bedform scale, in some cases challenging or confirming existing assumptions.

6.1 Shelf scale mapping: a new understanding of the seafloor morphology on the north Irish shelf

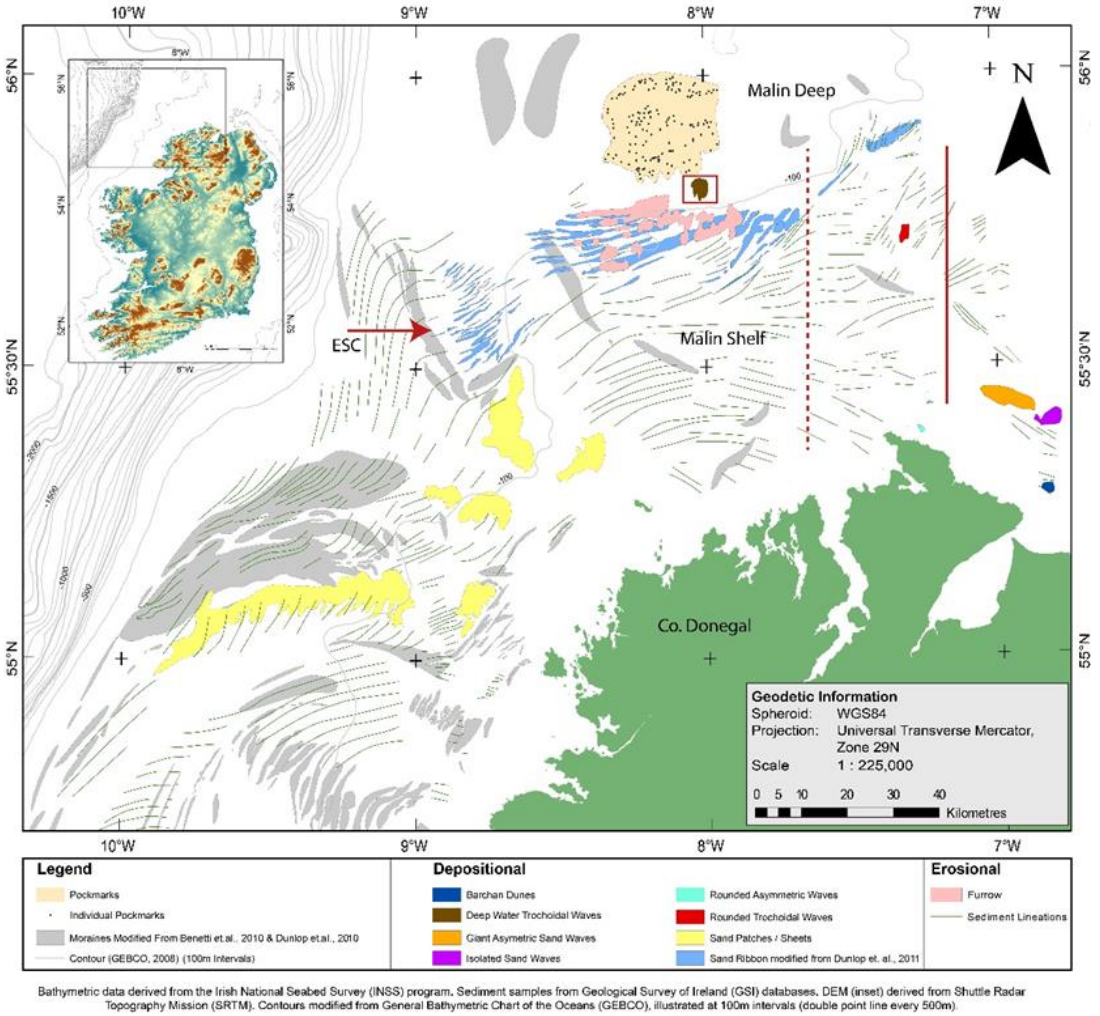

Fig. 6.1 Overview of the features discussed in Chapter 6. Red arrow denotes ingress of ESC onto the shelf. Broken red line indicates location of bedload parting zone suggested by Belderson et. al., 1982, the new location of this feature proposed in this chapter is indicated by the solid red line. Deep water trochoidal waves classified as relict in this chapter are enclosed with a red box.

MBES, backscatter and sediment sample data from the Irish seabed mapping programmes (INSS, INFOMAR and JIBS), were used to investigate the north Irish continental shelf using techniques including hydrodynamic modelling, backscatter classification for the derivation of sediment distribution charts, repeat seafloor survey to measure change, and geomorphological analysis of

bedforms to enable classification and make inferences as to their potential mobility. This multidisciplinary approach, incorporating new techniques for the measurement of sediment wave migration (Chapter 3), provides the most comprehensive study into modern shelf sediments on the northwest Irish shelf to date.

General water depths in Irish water have been understood since early Victorian led soundings (Mayer, 2006, Quinn and Boland, 2010). However widely spaced single soundings only give a general overview of what is the very complex and ever changing marine environment. As a result the spatial resolution required to fully understand shelf features and processes such as bedform classification or indicators of sediment transport such as bedform asymmetry are best achieved with the use of MBES (Barnard et al., 2013, McGonigle et al., 2009, Plets et al., 2011, Shaw et al., 2014).

The overall distribution of water depth across the shelf gives insight into shelf sedimentary processes in a number of ways. Bathymetric depressions such as those identified in Chapter 2 (section 2.4) are proposed as possible sediment traps with greater water depths resulting in reduced flow rates more conducive to the deposition of finer sediments (Berelson, 2001). Bathymetric data also highlights constrictions such as that south of Inishtrahull Island (Fig. 3.1) which increase water velocity and bed stresses and can affect shelf hydrodynamics for a considerable distance (Rourke et al., 2010). Due to the high accuracy of these depth measurements (when used with a precise DGPS positioning system) it is also possible to measure changes between respective surveys with a high degree of confidence in both the vertical and the horizontal (Knaapen and Hulscher, 2002, Ma et al., 2014, Németh et al., 2002). High-resolution

bathymetry also reveals the geometry of sedimentary bedforms, which can allow for specific attributes to be examined in detail such as the ability to measure difference between lee and stoss slopes or asymmetry, an indicator of sediment wave mobility (Van Landeghem et al., 2009b). MBES data clearly defines the shape of sediment waves allowing them to be classified against standard matrixes such as that of (Stow et al., 2009).

The use of slope mapping algorithms and interrogation of bathymetric position indices further serves to identify these features in a quantitative way. Bathymetric Position Indices (BPI) in particular is an effective way to identify more subtle formations such as the sand ribbons with gentle slopes and low vertical profile (Micallef et al., 2012, Verfaillie et al., 2007). By identifying elevation relative to a broader selection of the data set rather than just that adjacent (as is typical when visually interrogating bathymetric charts) these features are clearly defined as a set of positive values (elevations) alongside zero (flat) or negative (depression) values (Micallef et al., 2012). Setup for BPI has been adjusted to identify features at differing scales, clearly identifying ridges, crests and shipwrecks as well as larger features such as moraines on the northwest Irish shelf (Chapter 2, Fig. 2.2).

The analysis of bedform classification, orientation and distribution identified in bathymetric data can indicate shelf sedimentary processes even before supporting sedimentary and hydrodynamic data is introduced (Lo Iacono et al., 2010, Besio et al., 2008b). The occurrence of a bedform in a particular part of the shelf can provide initial information about the sedimentary and hydrodynamic environment. In the first instance, it informs that there is (or was previously) sufficient sediment to facilitate the formation of the bedform.

Secondly, the presence of a bedform suggests a range of near seabed current velocities occurring on the shelf at that location(Allen, 1980, Belderson et al., 1982, Besio, 2004, Stow et al., 2009). Lastly the orientation and asymmetry of these bedforms reveal not only the direction of last known mobility, but also suggest the origin of the primary formative forces (Barnard et al., 2013, Besio, 2004, Van Landeghem et al., 2009b).

Sediment lineations, mapped in Chapter 2, Fig. 2.9, are known to develop under long standing currents (Stow et al., 2009, Hanquiez et al., 2007a). Occurring in parallel across the shelf, these lineations closely follow depth contours. Their location and orientation appear to be in agreement with the sediment pathways suggested by (Kenyon and Stride, 1970) based on side-scan sonar data. In many instances these features are composed of gravelly sand and terminate with a depositional bedform consisting of finer sediments, such as sand patches or sand ribbons. It can thus be inferred that current velocities winnow out finer sediments from these lineations, carrying them downstream to a point where transport of sand sized sediments no longer occurs due to a drop in flow velocity (Berelson, 2001, Lefebvre et al., 2014). It is in these locations that the depositional bedforms such as sand patches form. While sediment lineations fully agree with the pathways suggested by (Kenyon and Stride, 1970) other bedforms such as the giant sand waves (Fig. 2.5) display crest orientations and geometries which do not. It is clear from giant sandwave asymmetry that more localised processes are in effect with some striking results. The rotational migration presented by this bedform (Figs. 3.6A and 3.7C) is a good example of this. The analysis of MBES data has failed to corroborate the location of the bed parting point as suggested by (Kenyon and

Stride, 1970)(Fig.1.8). A break in some sediment lineations is identified in the area previously suggested, however with no significant change in seafloor morphology or bedform distribution or asymmetry, such an interpretation would not be well founded.

Elsewhere, the morphology of deep-water waves presents challenges to other published literature. (Dunlop et al., 2011) describes sandwaves south of the Malin Deep as part of a train of active mobile sediments on the shelf. Analysis of Deep Water Trochoidal Wave geometry suggests low mobility, if any (Chapter 3). Rounded and symmetrical, these low profile crests suggest a breakdown in waveform due to inactivity (Bartholdy et al., 2010c, Belderson et al., 1982, Kenyon and Stride, 1970, Terwindt and Brouwer, 1986).

.

6.2 Backscatter Classification

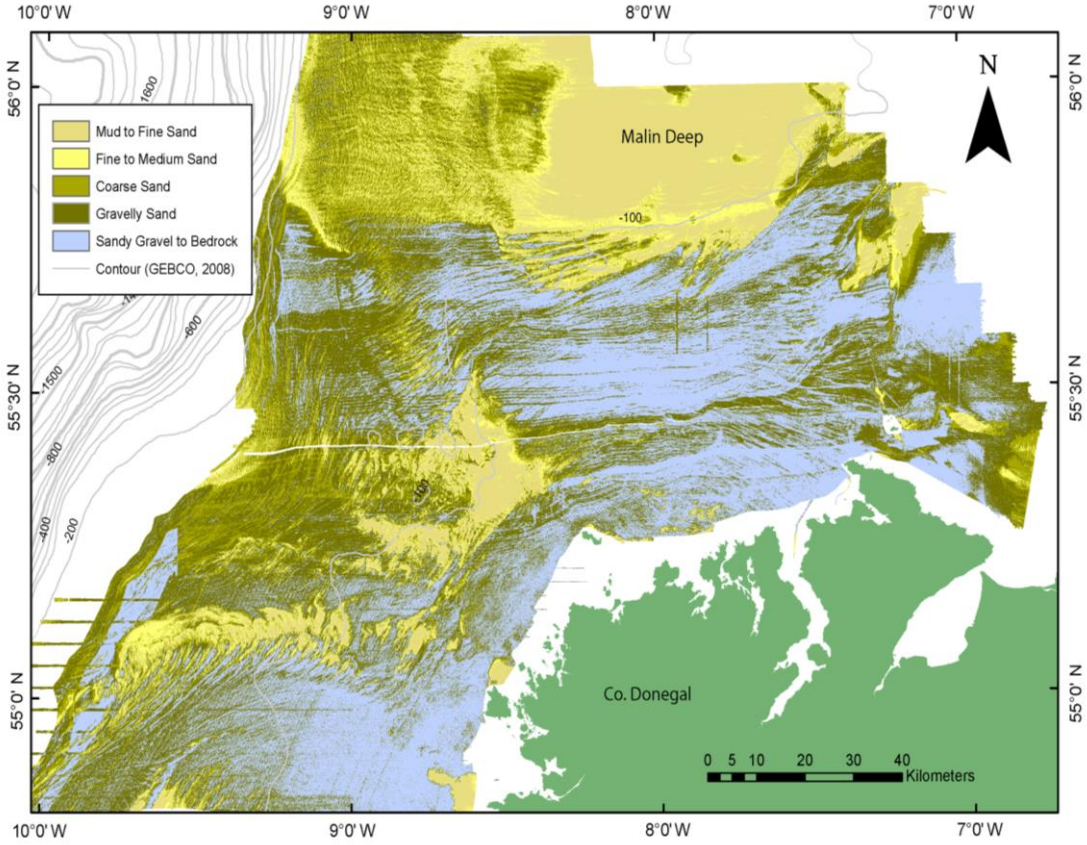

Fig. 6.2 Backscatter classification on the northwest Irish shelf. Evidence of processing issues can be observed through 'striping' artefacts and data gaps. While there are limitations on this data, such as the broad sediment groups, this chart represents the most extensive classification of sediments on this section of Irish shelf.

6.2.1 Potential issues / limitations in the use of backscatter data

The classification of backscatter data has become increasingly used as a key element to seafloor mapping studies (Goff et al., 2000). It has particular relevance to marine sediment studies including marine engineering applications and those interested in defining biological habitats, of which sediment type forms a major component (Brown and Blondel, 2009, Fonseca et al., 2009, McGonigle et al., 2010b). The quality of backscatter signal effects the reliability of classification of this data with poor quality leading to a poor correlation with

actual grain size, striping and other artefacts (Brown et al., 2011, McGonigle et al., 2010a, Rzhanov et al., 2012). Backscatter charts on the northwest Irish shelf utilise data from over 12 differing research cruises. Due to the large range of MBES systems used over these cruises, differences in setup parameters and changes in weather conditions, it is possible for the same section of seafloor to present variations in acoustic backscatter return(McGonigle et al., 2010a, Rzhanov et al., 2012). Further to this, issues caused by the angle of insonification mean that striping artefacts shown in Chapter 3 must be treated with caution and any classification of this signal is unlikely to represent real world sediments. Methods of classifying this data have come under increasing scrutiny as image-based habitat classification becomes the preferred option over field measurements. Issues commonly lie with how the numbers of classifications, or clusters are derived. In this research this has been mitigated by adopting proven methods, an unsupervised classification with a ‘signature’ element to provide some level of supervision to account for the clustering issue (Calvert et al., 2015, Ierodiaconou et al., 2011, Stephens and Diesing, 2014)

It is also worth noting that backscatter signal is a response to surficial sediments only. As a result, a thin soft sediment drape over bedrock will mask the signal of the underlying geology (Bellec et al., 2008). This can give an untrue picture of the distribution of sediments and increases the requirement to incorporate ground truth samples into any classification (Goff et al., 2000, Lamarche et al., 2011). The restriction of backscatter response to surface sediments alone means it is possible for underlying formations or geology to be masked by even a thin sediment drape of differing grain size composition. It is for this reason that even large formations such as the moraines on the

northwest Irish shelf, which are composed of very different materials to the surrounding bedforms, are clearly evident in MBES data but cannot be identified in backscatter data.

6.2.2 Sediment distribution from backscatter data: the interplay between bedforms and substratum

By utilising a combination of geo-acoustic, image analysis and support ground truth samples it is possible to classify backscatter signature into sediment classifications. This study has provided the most comprehensive depiction of shelf sediments in this area to date with backscatter coverage and samples catalogued from multiple research cruises on the northwest Irish shelf. Thanks to standard geological methods for processing of marine sediment samples, many of the catalogued data from the study area could be collated with some standardisation of nomenclature required (Folk, 1954). The Malin Deep presents the largest area of soft sediments within the section of shelf under investigation (Chapter 2, Fig 2.9) (Evans et al., 2015, Szpak et al., 2012). Acoustic response suggests fine-grained sediments which are easily winnowed away by currents (Weaver et al., 2000). It can therefore be assumed that the Malin Deep is an area of low flow velocities and bed stress (Berelson, 2001). Likewise, bedforms which present a ‘hard’ backscatter response (those not identified as bedrock), such as gravel streaks are assumed to experience higher flow rates which winnow away fine sediments and have control over the bedform orientation (Masson et al., 2004). It is therefore possible to examine backscatter for potential erosional and depositional areas with an aim to

elucidating any links between the two (Bellec et al., 2008). This can be exemplified by hard response gravel streaks terminating at an area of soft response sand patches, with high energy flow winnowing finer sediments from the streaks and depositing them as flow intensity reduces (Chapter 2) (Goff et al., 2000).

Backscatter can therefore enable an interpretation of hydrodynamic energy distribution on the northwest Irish shelf, identifying areas likely to experience sediment erosion and deposition. When considering bedforms on the shelf, backscatter data also allows assumptions to be made as to availability of sediments for the formation of specific wave types. It is clear that the sandy sediments required to generate sandwaves are in short supply in the northeast of the study area, however surficial sediments of the required grain size are prevalent in the southwest. Relationships between this data and average flow calculations from hydrodynamic modelling can reveal the provenance of the sediments creating bedforms. These sediments may originate from the large glacial formations on the shelf which are eroded by long standing currents such as the ESC (Kuijpers et al., 2002, White and Bowyer, 1997).

The classifications of Areas A and B in Chapter 3 represent the most accurately classified sections of the seafloor due to the high resolution of sediment sampling and short temporal lapse between backscatter and ground truth acquisition. Backscatter classifications which are constrained by a ground truth element rather than purely model based analysis (such as Angular Response Analysis) are often unable to map sediments down to individual grain sizes (Lamarche et al., 2011). As a result, it is typical for sediment classes to be grouped together, large ranges within these groupings can indicate poor quality

or low resolution data (Brown and Blondel, 2009, Che Hasan et al., 2014) The combination of surveys used to generate the backscatter charts on the northwest Irish shelf and the resultant processing required to merge these datasets has resulted in the need to group sediments within the classification scheme. For example, the similar acoustic responses displayed by boulders and bedrock in this area makes discerning the two classes difficult from backscatter imagery alone. In the case of bedrock, this has been addressed through the use of MBES data. Elsewhere, the varying composition of sands and gravels can create complications when trying to classify these coarse sediment mixtures (Goff et al., 2000). Grouping sediments may appear to be less useful by not classifying sediments down to common geological nomenclature e.g. (Folk, 1954), however, these groupings are more robust and can be validated within the bounds of data resolution.

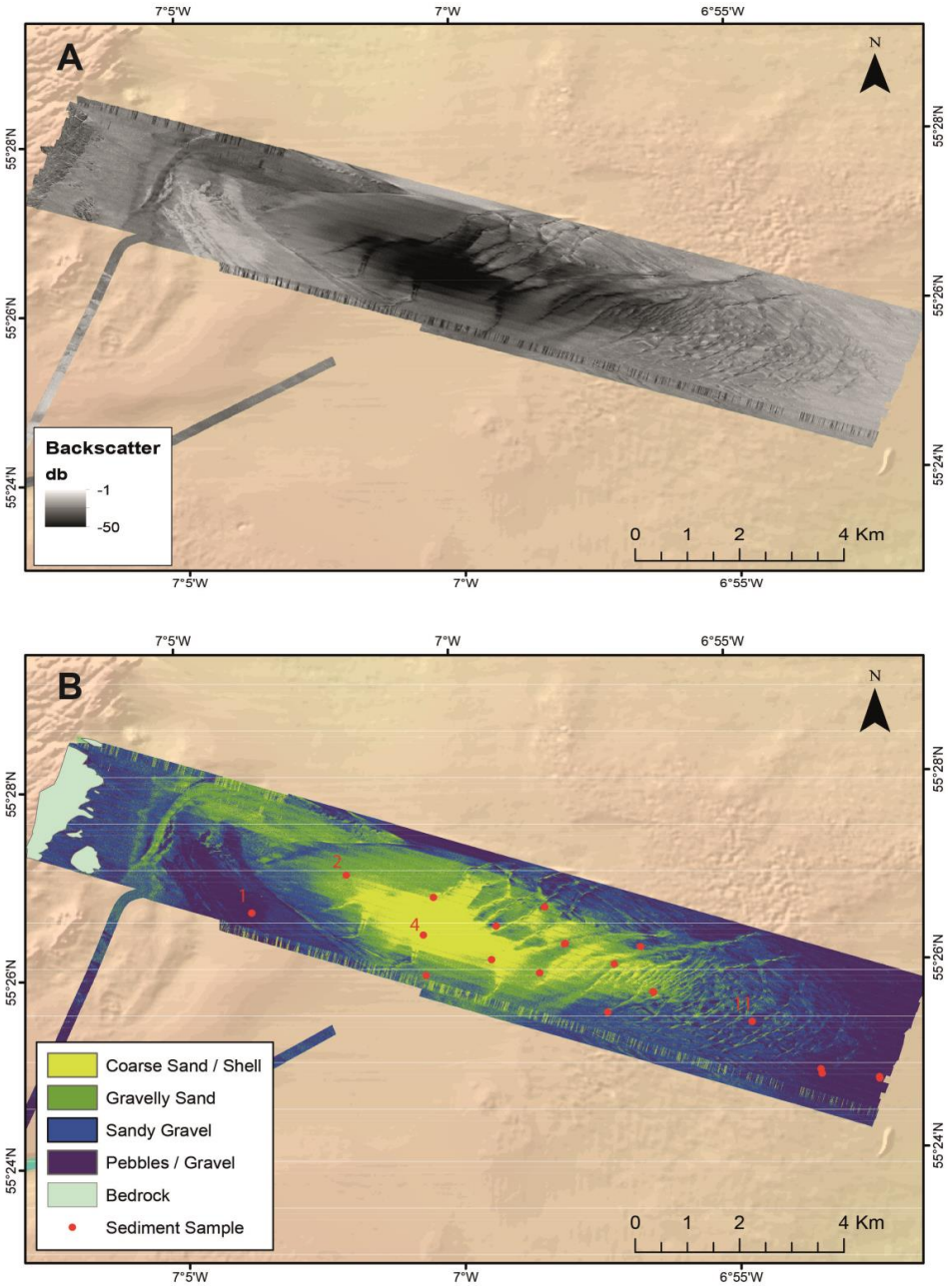

Fig. 6.3 Example of classification derived from a backscatter signal (A) using ground truth data (B) and ESRI Arc GIS software.

Backscatter classification over a single bedform reveals a number of insights when considering the formative processes, composition and other habitat related aspects of the formation at this localised scale. Classified backscatter data such as that presented in Chapter 3 reveal not only the surface composition of the mobile element of the bedform (sandwaves) but also the

surrounding substrate over which the mobile sandwaves are moving (Lamarche et al., 2011). Using knowledge of the sediment grain size, a hjulstrom curve can be used to calculate the minimum flow and bedstress required to make elements of the seafloor mobile (Hjulstrom, 1935, Miller et al., 1977). This can be further analysed by utilising bedform matrices such as that developed by (Stow et al., 2009) to relate this information to the morphology of the bedform observed. Bedform scale classification also reveals small scale differences in sediment type across the formation, such as the increase in grain sizes in the troughs of the sandwaves shown in Chapter 3 Area A. Grain size can also be utilized by benthic ecologists to make inferences as to the suitability of a habitat for a given species (Reise, 2002). In the case of Area A (Chapter 3) it is clear from backscatter classification that the giant sandwaves are composed of finer sediments than the surrounding shelf which is dominated by gravels and exposed bedrock. As a result, this classification reveals a bedform with a sedimentary composition very different to the surrounding shelf suggesting differing hydrodynamics and biological habitat.

Despite the limitations of backscatter classification reduced accuracy due to the grouping of sediments the work presented in Chapters 2 and 3 represent a significant advance in the resolution of classified surface sediments on the northwest Irish shelf at a range of scales.

6.3 Use of Time Lapse Bathymetric data to investigate sediment mobility

Repeat MBES surveys are a recognized method to measure seafloor change in both the vertical and the horizontal over a specified time period (Knaapen and Hulscher, 2002, Knaapen et al., 2005, Ma et al., 2014). The high resolution of modern MBES systems allow for accurate measurements to be made in the displacement of mobile sandwaves or changes in water depths (Schimel et al., 2015, Schmitt et al., 2008). As with most datasets, temporal resolution is a key component to the accuracy of assumptions made about rates of change. As a result, multiple repeat surveys with short temporal spacing generate measurements with the highest confidences (Németh et al., 2002). The accuracy of time-lapse measurements can be adversely affected by an inappropriate temporal resolution that fails to capture changes such as the oscillatory movements of sandwaves between respective surveys (Smith et al., 2007, Xu et al., 2008). In Area B Chapter 3, sandwaves exhibit oscillatory movements from the west to the east and then back to the west in three respective surveys. In this instance, a longer temporal spacing may have suggested movement direction and rates to the west only while shorter time lapses may have enabled this movement to be more accurately quantified. Despite this limitation, repeat survey with a long temporal spacing can be used to gain an overview of bedform migration and net sediment flux across the resurveyed areas. The process of measuring horizontal change has been refined through an automated GIS methodology adapted from terrestrial hydrography research (detailed in Chapter 3) (López-Vicente et al., 2014). This

methodology reduces azimuth bias and other possible user errors as well as presenting a more time effective process compared to manually drawing and measuring multiple sediment wave profiles (Smith and Wise, 2007).

6.4 Hydrodynamic Modelling

An understanding of hydrodynamic forces and their effect on the seafloor is required to be able to understand potential sediment transport and analyse the formative factors which lead to the generation of bedforms on the northwest Irish shelf. Field measurement of these forces is difficult, expensive and in the case of this research, unfeasible given the large area under investigation (Gunn and Stock-Williams, 2013, Legrand et al., 2006). As a result hydrodynamic models validated using real world data can be used to provide insight into flow rate and direction across a large area at a range of varying resolutions. The hydrodynamic model Mike by DHI used in this research features adaptations made to the simulation configuration that allow aspects of water movement to be more accurately simulated in the water column close to the seafloor. The result is a data set that is more applicable to the MBES, backscatter and sedimentary charts developed in this research (Barnard et al., 2013, Liu and Huang, 2009). Hydrodynamic modelling at a shelf scale can be used to examine large scale movements of water bodies, long standing currents and areas of high and low energy (Staneva et al., 2009, Young et al., 2011). They also allow for examination of the relationship between sediment distribution and ocean energy levels on a large scale (Staneva et al., 2009).

The flexible mesh that dictates the resolution of model outputs not only influences outputs in the near-bed portion of the water column but also allows for more data points over bedforms of specific interest. The model developed in this research has data output of <5 m resolution at key points of interest. This enables the flow rate and direction over individual sandwaves to be examined, revealing key information as to the forces contribution to differing bedform morphologies, sedimentary composition and migration. Importantly when considering the mobility of a specific bedform, this high-resolution data coupled with knowledge of grain size distribution can confirm asymmetry based assumptions as to whether a bedform is actively mobile or a relic of previous palaeotidal conditions (Hall and Davies, 2004, Terwindt and Brouwer, 1986). Furthermore, it has been used in this research to confirm not just if the bedform is likely to be mobile but also if the direction of migration assumed from asymmetry matches that of the dominant flow. As a result, both shelf scale and local hydrodynamic forces may be examined from one simulation. The model developed as part of this research is unique in this area of shelf for its emphasis on flow rates and bed stresses in the boundary layer close to the seafloor and the high resolution of data over targeted bedforms.

6.5 Sediment transport processes from a shelf to bedform scale

6.5.1 Sedimentary Record of the European Shelf Current

The European Shelf Current has been observed in multiple oceanographic investigations on the north and western Irish shelf. This barotrophic, geostrophic flow closely follows the shelf edge offshore Ireland (Fernand et al., 2006, White and Bowyer, 1997). There have been also been documented intrusions of this longstanding current onto the northwest Irish shelf between 55ºN and 56ºN, typically during winter months (Booth and Meldrum, 1987, Hill and Mitchelson-Jacob, 1993). Given that measured flow rates of the ESC have exceeded 0.66m/s it is not unfeasible to expect evidence of this current in the MBES, backscatter or model data utilised in this research.

Chapter 3 suggests that the presence of sand ribbons is a sedimentary record of the ESC's ingress onto the northwest Irish shelf similar to the findings of (Kuijpers et al., 2002) when investigating the NSOW and (Hanquiez et al., 2007a) when identifying bedforms relating to the MOQ in the Gulf of Cadiz. These 4 m amplitude, elongate ridges extend for up to 16 km across the shelf in 90 m water depth. Originally mapped in the 1970's by (Bastos et al., 2003)Kenyon, these bedforms typically occur parallel to flow and therefore can be used as indicators of flow direction (Allen, 1980, Evans et al., 2015). The change in orientation of these ridges from southwest – northeast to west – east between 55ºN and 56ºN correlates with the section of shelf where ESC intrusions have been measured. Model simulation data also agrees with

maximum current speeds over the sand ribbons of 0.5m/s, similar to the measured speeds of 0.6m/s in previous studies.

The result of the ESC intrusion is a set of bedforms not evident elsewhere on the shelf despite similar sediments occurring in abundance. The work of (Kenyon and Stride, 1970) suggested a ‘possible’ sediment pathway matching the orientation of these sand ribbon, but with uncertainty as to the dominant direction of transport. This research can confirm the ESC as a major contributing factor to the formation of these sand ribbons and a resulting depositional sediment pathway from west to east. Furthermore, this pathway extends further to the east than originally suggested by (Kenyon and Stride, 1970).

6.5.2 Sediment pathways on the northwest Irish shelf

To date, investigations into sediment pathways on the northwest Irish shelf have been limited. While mapping of glacial formations and their related sediments have been extensive, few studies have specifically examined modern seafloor sediments. (Kenyon and Stride, 1970) attempted to map the transport paths, bedload parting and convergence zones side scan sonar data. While this data suggested pathways with reasonable confidence in the waters of the English Channel, Celtic and Irish Seas, transport processes to the west of Scotland and Ireland could not be as well constrained resulting in classification as ‘probable’ or ‘possible’.

By examining shelf scale model outputs and sediment distribution it is possible to define potential sediment pathways evidenced by datasets which provide an overview that was not possible with the equipment used during these earlier investigations. By mapping, classifying and developing understanding of formative processes and migration pattern of bedforms across the shelf it has been possible to further refine these pathways down to local scales.

This work suggests that the bedload parting point identified by Kenyon located ~ 7º50W (northwest of Malin Head) should be moved further to the east to ~7º20W (north of Malin Head). The pathways suggested by (Kenyon and Stride, 1970) to the west of this point typical follow depth contours and coastline. The identification of sand ribbons and gravel streaks as part of this research agree with this, but also suggest that the direction of movement is from the southwest to the northeast, south of 55º25N and from west to east on areas of the shelf north of this point. East of the Malin Head parting zone, (Kenyon and Stride, 1970) state a ‘known’ pathway moving west to east following depth contours which enters the Irish Sea through the North Channel. The rotary current identified over the giant sandwaves (55º26N, 6º58W) and the dominant flow direction simulated over the isolated sediment waves 6 km to the southeast suggest that sediment pathways may not be as simple as those identified by (Kenyon and Stride, 1970). Further east, at Area B (Chapter 3) off the Causeway Bank, inshore sediment pathways display considerable variation in directionality adding further question to the suggestions made by previous investigations. To further understand movement across the Malin Shelf, more data including better coverage further offshore would be required to properly define sediment pathways on this section of shelf. The work of (Xing and

Davies, 1996) also suggests that the north and northwest Irish shelf not only experiences along shelf transport but also off-shelf sediment movement, particularly on the Malin Hebridean shelf. It is therefore hypothesised that this off-shelf movement may be a contributor to the net loss of sediment measured at the areas resurveyed in Chapter 3.

6.5.3 Mechanisms for sediment deposition and entrapment

Improved understanding of hydrodynamics in the near seafloor zone, including identification of long standing currents such as the ESC make it possible to consider the forces controlling sediment distribution across the northwest Irish shelf. Both the Marine Institute ROMS model and the MIKE by DHI model in these chapters have identified southwest to northeast currents which veer to west to east flows creating similar sedimentary records across the seafloor (Chapter 4). When this flow data is related to grain size distribution and underlying bathymetry a number of trends can be identified. Hydrodynamic models indicate that the bathymetric rise evident in MBES and BPI data between 55º0'N and 55º30'N, classified as a moraine by (Benetti et al., 2010a), experiences southwest to north-easterly dominant flows. The profile of the moraine appears to cause fine to medium sands to be trapped on the southern, up-current side of the moraine. It is therefore hypothesised that these sands have been winnowed out from the gravels evident south of this location and deposited at the southerly base of the moraine.

While a rise in bathymetry can be attributed as a sediment trap, several increases in water depth also appear to trap smaller grain sized sediments. One

such location is situated at 55º20’N 8º30’W where several gravel streaks terminate at a bathymetric depression resulting in a large area characterized by fine and medium sands.

The notion that soft sediments will accumulate in deeper water, which are typically areas of lower hydrodynamic energy, is not unusual (Berelson, 2001). However, in some cases gravel streaks terminate with patches of soft sediment regardless of bathymetric change, e.g. the area in which sand ribbons form between 5º30’N and 55º40’N. This likely reflects that the finer sediments are being winnowed out of the gravel streaks and surrounding shelf over time with the depositional area identifying the point at which flow velocity is reduced. The final mechanism identified for soft sediment deposition on this energetic shelf is the rotary current described over the giant sandwaves to the east of Inishtrahull Island (Fig. 5.1). The high gravel content of the surrounding shelf suggests that finer sediments have been removed by the high-energy flows in that area (Miller et al., 1977, Rourke et al., 2010). This rotational current therefore has acted as a means for retention of finer sediments despite energetic flows across the shelf which would otherwise cause such easily mobilised sediments to be dispersed across the shelf (Caston, 1972, Huthnance, 1973, Williams et al., 2000).

6.5.4 Assessment of bedform mobility: Active and relict bedforms on the northwest Irish shelf.

The early works of (Belderson et al., 1982), (Allen, 1980) and looked to the morphology of a bedform to ascertain how mobile it may be. Characteristics of both mobile bedforms and those considered to be relict (no longer active) were

established and form the basis for many modern sediment transport investigations. These thesis chapters benefit from the ability to utilise a modern multidisciplinary approach to the classification of bedforms as active or relict. Using the foundations established in the 1970's, beform asymmetry can be used as an indicator of mobility (Chapter 2) (Barnard et al., 2013, Bartholdy et al., 2010b, Catano-Lopera and Garcia, 2006). However, in bidirectional current, it is possible for sandwaves to 'flex' around a central point resulting in an almost symmetrical or trochoidal form (Van Landeghem et al., 2009b). The mobility of symmetrical waves can be further classified using the roundness of the crest as an indicator, with sharp, pointed form suggesting increased movement (Lefebvre et al., 2014). It is suggested that more rounded crests suggest degradation of wave profile over time due to processes such as bioturbation (Borsje et al., 2008, Le Hir et al., 2007). This method of classification while robust, is not conclusive.

The research undertaken in Chapter 4 builds upon this morphology-based assessment and includes two further data sets, backscatter derived sediment distribution and outputs from the hydrodynamic model Mike by DHI developed as part of this study. Time lapse measurements can also be used as more definitive method to assess mobility (Knaapen et al., 2005, Smith et al., 2007, Xu et al., 2008), however, as these repeat measurements were not carried out across all bedforms on the shelf they are not included in this section of the discussion. By examining the sedimentary composition of a bedform and the hydrodynamic forces acting near the seafloor it is possible to calculate if energy levels are significant enough to mobilise sediment (Hjulstrom, 1935, Miller et al., 1977). Additionally, this data can also be compared to bedform velocity matrices

such as those devised by (Belderson et al., 1982) and (Stow et al., 2009) to validate classifications. Hydrodynamic flow simulations also define the dominant flow direction and likely path for sediment migration. This is illustrated in Chapter 4 with both the Sand Ribbon and Giant Sand Wave formations. Here model and sediment classification combine to support the morphology-based inferences made in Chapter 2. In contrast, the same multi dataset approach identifies the Deep Water Trochoidal waves to the south of the Malin Deep (Chapter 2 & 3) as relict features. This is first suggested by rounded crests and symmetrical form. Further analysis of sediment grain size and flow rate confirm that energy levels over the bedform are not sufficient to initiate transport at any time during the model duration (Hjulstrom, 1935). This methodology also provides insight into bedforms present in a location which is difficult to explain using morphology alone e.g. the Rounded Trochoidal Waves discussed in 4.5.3. Located in an area of seafloor experiencing lower energies than the surrounding shelf, this bedform could be interpreted as relict. However, model data suggests that periodically, flow rates reach velocities capable of mobilising the sediments of which the bedform is composed. As a result, it is interpreted that the bedform was formed under differing tidal conditions but has a morphology maintained by periodic highs in hydrodynamic energy (Hall and Davies, 2004, Terwindt and Brouwer, 1986). Likewise, analysis of the hydrodynamics and surficial sediments over the large outer moraine mapped and defined as irregular in shape by (Benetti et al., 2010a), reveals that modern conditions are not capable of reworking this feature.

It is therefore suggested that the northwest Irish shelf contains bedforms which:

- are relict and no longer mobile under modern tidal / atmospheric conditions.
- were most likely formed under palaeotidal conditions and are only periodically mobilised by higher than average currents.
- are actively mobile.

Further to this, the use of geomorphology alone to assess bedform mobility is proven not to be comprehensive. This work has led to redefinition of some sediment waves (Deep Water Trochoidal) as relict, which had previously been interpreted as actively mobile by (Dunlop et al., 2011).

6.5.5 Giant sandwaves as an isolated pocket of soft sediments in a unique hydrodynamic regime.

Set upon an offshore tidal bank, giant sandwaves located on the Malin Shelf at 55º26N 6º58W reach amplitudes of 20 m. Large sandwaves typically form in high energy environments (Barnard et al., 2013, Besio, 2004) and while examples can be found globally of waves reaching 10 m amplitudes (Li and King, 2007, Németh et al., 2007), there is little documentation of sediment waves exceeding this (Van Landeghem et al., 2009b) . Sampling has shown these waves to be composed of golden coloured sands with a shell component. Identified in historic admiralty charts and MBES surveys between 2004 and 2014 it is assumed that these sandwaves are a long-standing feature on the

Malin shelf. This formation is also easily identified in backscatter data as an isolated area of soft sediments surrounded by gravels and bedrock (Fig. 3.5 and 6.2). As a result, these sandwaves are remarkable not just due to their large amplitude and high migration rates but also the location on the shelf in which they have formed. The asymmetry of these sandwaves suggests a clockwise, rotational current over the bedform, which is supported both by the 2 km resolution Marine Institute ROMS model and the 5 m Mike by DHI model described in Chapter 5. Model data reveals that there is a bi-directional element to the currents in the area, which has been found to drive rotary currents around tidal sand banks in shelf environments globally (Caston, 1972, Sanay et al., 2007, Williams et al., 2000).

The narrow constriction of Inistrahull Sound 8 km to the west of the bedform creates some of the highest tidal energy levels in Irish Waters (514 G Wh/y) and has been suggested as a possible site for renewable energy tidal turbines(Giorgi and Ringwood, 2013, Rourke et al., 2010). This funnelling of tidal energy undoubtedly increases flow velocities on the shelf areas surrounding Inishtrahull Island and areas close to the giant sandwaves, evidenced by the Mike by DHI model. This flow undoubtedly contributes to the formation of the rotary current over the giant sandwaves and their long-standing presence on this section of shelf. This bedform comprised of coarse sand and shell also represents a habitat for marine species distinct from the surrounding shelf. Rotary currents such as those simulated over this bedform have been known to trap planktonic species within a confined area, leading to increased concentrations of their predators (Hill et al., 1996). Coupled with distinctly different sediments, this section of shelf is capable of supporting benthic and

pelagic organisms, which may be unable to inhabit the gravels on the surrounding shelf (Reise, 2002).

It is typical for any marine renewable feasibility studies to implement hydrodynamic models to measure outputs and potential efficiency of any turbines installed on the seafloor, but also to gauge downstream effects of new structures (Ahmadian et al., 2012, Nash and Phoenix, 2017, Thiébot et al., 2015). In the case of proposals to site marine turbines in Inishtrahull Sound it is possible that an influence on the flow moving through the sound may have an effect on the giant sand waves and other bedforms mapped in the vicinity (Neill et al., 2009). In most cases, reduction in flow velocity creates a hydrodynamic environment more conducive to sedimentary deposition (Berelson, 2001). However, in the case of the giant sand waves, the rotary current has been defined as the mechanism for bedform formation and sediment retention in the area. Should this current be interrupted, this retention mechanism may be affected resulting in a breakdown in the bedform (Sanay et al., 2007). Should a breakdown in bedform occur, accretion of these sediments around any installations in Inishtrahull Sound are unlikely due to surrounding high flow rates. The possibility of smothering of ‘hard’ substrate benthic organisms across the shelf is, however, likely due to the high volumes of soft sediment locked within the bedform (Hendrick et al., 2016). Furthermore, the loss of this habitat unique to this section of shelf may be damaging to the biodiversity of the waters surrounding Inishtrahull.

It is therefore evident that the multidisciplinary approach adopted by this research has enabled effective analysis of sedimentary processes from a shelf

to sediment wave scale and may have future use to proposed marine engineering projects in the area.

Chapter 7 – Conclusions, impact and future work

7.1 Conclusions

This research utilised a multidisciplinary approach to improve knowledge of sedimentary distribution, bedform formation and potential mobility of sediments on the north Irish shelf. By adopting modern techniques for predicting and quantifying seafloor change and using new high-resolution multibeam bathymetry and backscatter data, this research focuses existing data sets on the sedimentary processes and fills knowledge gaps through generation of novel data. To this end, MBES data, sediment grab samples and hydrodynamic models have been combined with insights from previous research into the seafloor on the Irish shelf (Davies and Xing, 2002, Dunlop et al., 2011, Kenyon and Stride, 1970) to provide a more complete analysis of shelf sediments and their mobility.

In **Chapter 2**, using pre-existing INSS multibeam data at 20m resolution and sediment samples and using GIS tools such as the ESRI ArcGIS Hydrology toolbox in a novel way, a new map of the north Irish shelf was generated. The map has revealed the complexity of seafloor morphology and sediment distribution on the northwest Irish shelf:

- Surficial sediments have been classified in five main classes and their distribution mapped in detail.
- Overall eight depositional (Barchan Dunes, Deep Water Trochoidal Waves, Giant Asymmetric Waves, Isolated Sand Waves, Rounded Asymmetric

Waves, Rounded Trochoidal Waves, Sand Patches and Sand Ribbons) and two erosional (Sediment Lineations and Furrows) bedform types were identified and described.

- Some of these bedforms present characteristics typical of mobile, active formations. They include shelf-wide sediment lineations and sand ribbons that are typical of continuous, stable and high-energy current regimes. Their orientation also correlates well with published flow models and measures.
- These modern sediments partially bury and traverse relict, glacial deposits, thus masking their acoustic response and altering the morphology of these glacial features via infilling or overprinting.
- An interaction between modern and relict bedforms due to bottom current reworking of the seafloor is also possible.

In **Chapter 3**, repeat bathymetric surveys at two selected sites were used to calculate horizontal and the vertical charges in bathymetry and to evaluate the mobility of the bedforms found within the sites. A novel method for measuring sediment wave migration was developed and presented. Lastly, sediment distribution across the sites was classified using ground-truthing and backscatter data to examine the possible links between bathymetric changes, sediment grain size and modelled hydrological conditions. In particular:

- Both areas surveyed revealed mobile sediments with distinct migration directions controlled by a primary factor, a rotational current at Area A, and ‘The Ridges’ rock outcrop at Area B. The use of multiple repeat surveys has also highlighted oscillation of sandwaves on at a scale larger than bedform wavelength.

- The results derived from the analysis of bathymetric data are corroborated by existing hydrodynamic models of the area.
- The multi-method approach for the assessment of sediment transport, involving the use of multibeam bathymetric and backscatter data, sediment and seismic data and hydrodynamic models, has proven to be effective for the investigation of a high energy, continental shelf environment.
- The use of ArcGIS hydrology tools in the application of wave crest determination and ET Geowizards scripts for measuring crest displacement has proved to be a time effective and quantitative way to quickly generate information on bedform migration.

In **Chapter 4**, a new hydrodynamic model was developed from the model Mike-3 by DHI using the recently acquired high-resolution bathymetric data and the previous work on sediment distribution on the shelf to generate a higher resolution, sediment transport specific hydrodynamic model for the north Irish shelf. A nested mesh model encompassing an offshore area of 103,000 km^2 was generated with the capability to resolve hydrodynamic conditions at a scale more relevant to bathymetric data. This nested mesh approach allowed shelf-wide measurements of current speed to be calculated at <1 km resolution while in areas of special interest identified from MBES data, maximum resolutions of 5 – 10 m were achieved. Further to this, bed stress simulation accuracy was improved by including sediment grain size distribution as a model input. These outputs, flow velocity and bed stress were then examined in relation to the sediment distribution and bedform morphologies discussed in Chapter 2:

- In general, lower flow velocities coincide with decreased grain size across the model domain with increased flow in inshore areas potentially accounting for the prevalence of coarser material.
- The simulated hydrodynamic forces corroborate well with bedform classifications in Chapter 2, with more sessile, rounded crest formations typically undergoing periods of lower energy exposure than those interpreted as more mobile.
- Simulations over bedforms identified as potentially relict suggest that hydrodynamic forces are not elevated enough to initiate or maintain transport of sediments in these areas.
- The observed relationships are in agreement with many oceanographic current pathways identified by previous investigations in the region, including evidence of possible European Slope Current ingress onto the shelf.

Lastly, in **Chapter 5**, the hydrodynamic model was refined and increased in resolution over the seafloor bedforms, for which sediment mobility was studied in Chapter 3 using time-lapse bathymetric surveys. The resulting outputs enable hydrodynamics and migration to be examined at very localised scales down to individual sediment wave scales.

- The forces driving the rotary migration of sandwaves in Area A are established and linked to wider shelf hydrodynamics, specifically the movement of water through Inishtrahull Sound.

- The significance of rounding of crest profile at specific crest points is examined and related to this rotational migration.
- Trends are established across Area B indicating where hydrodynamic forces are capable of mobilising sediments during mean conditions or peak periods of energy only, suggesting periodic migration.

Overall, this research has highlighted the benefits of a multidisciplinary approach to the investigation of modern seafloor sediments in a shelf environment. The use of bathymetric, backscatter, sediment, seismic and hydrodynamic data has combined to generate the most complete description of modern marine sediment transport on the northwest Irish shelf to date.

7.2 Impact: implications of results for management and exploitation of offshore marine resources

The multidisciplinary approach adopted in this study has resulted in data sets with numerous applications beyond the field of sediment transport research. Some of these applications are here discussed, with an Irish shelf context to the fore. However, many of the points raised are applicable to similar shelf environments around the globe.

Knowledge of near bottom flow, sediment distribution and potential mobility of substrate can have implications for the management of historically significant wrecks found on the seafloor (Quinn et al., 2007). Due to the logistical difficulties associated with raising and maintaining maritime archaeology, the preferred method of site preservation is often to leave the wreck in situ, allowing

surrounding seafloor sediments to encase and protect any remaining structures. However, in some instances, a wreck can undergo periodic erosion and accretion of sediments, allowing structures to be exposed to energetic oceanographic conditions and biological colonization(Quinn and Boland, 2010). These may lead to degradation. Therefore, developing an understanding of hydrodynamic conditions and potential sediment mobility can be used to make predictions as to the level of natural preservation a wreck may experience over time. This is relevant locally on the Irish shelf, where hundreds or wrecks have been found as a result of the seabed mapping programmes INSS, INFOMAR and JIBS (Brady et al., 2012). However, the methodologies outlined here can be applied to wreck sites in any given location in order to monitor exposure to degradation and manage preservation by quantifying sediment accretion or erosion around historical structures.

Our coastlines are becoming an increasingly important area for industry, recreation and tourism (Barnard et al., 2013). This has resulted in a heightened pressure to manage resources in the coastal zone effectively. For ‘soft’ coastlines with tourism reliant on sandy beaches as on the Irish north coast, knowledge of sediment pathways and migratory patterns can be vital in informing management decisions such as coastal defence methods or beach replenishment. Surface difference models presented as part of this study reveal a net loss of sediments across sites monitored on the north Irish coast. The hydrodynamic model used here can be modified to include inshore areas, including spectral waves which may further increase understanding of natural beach stripping and replenishment over time.

Additionally, data presented in this thesis improve the understanding of sediment distribution, potential substrate mobility and hydrodynamic flow on the north Irish shelf. This knowledge is needed by stakeholders to inform decisions on the locations for dumping dredge materials, licensing of aggregate extraction and permissions for coastal engineering works such as harbours or marinas. Applications of this research to the field of marine renewables and associated offshore engineering works are many. Hydrodynamic model outputs and seafloor sediment distribution are typically key components of renewable energy site feasibility studies. The mobility of sediments immediately surrounding installations is of special concern to engineers. Scouring of sediments around structures and pipelines can undermine foundation integrity, expose entrenched cables and effect hydrodynamic flow regime. Equally, excessive accretion of sediment can lead to structural weakness and modify water flow around submerged structures. This study encompasses multiple, proposed marine renewable energy sites, including underwater tidal turbines and offshore wind farms. While these proposed sites undergo intensive, localised site investigations, this study has revealed that sediment mobility over a larger scale must be considered. Some of the mapped largest bedforms have moved >20m yr^{-1} over the last 6 to 9 years. Taking this into consideration, it is not inconceivable that transient waves could migrate through a renewable energy site from beyond the localised boundaries of a feasibility study. This highlights the need for increased understanding of sediment pathways on the shelf. The methodologies presented in this research can be applied to any shelf environment with potentially mobile sediment and proposed marine installations, to provide a baseline for prediction of potentially harmful sediment transport.

Data detailing sediment distribution and hydrodynamic conditions throughout the water column and close to the seafloor have many applications with a biological context. Substrate type (or its presence or absence) is typically the controlling factor for sessile and infaunal organisms. Grain size often dictates the ability of marine organisms, such as *annelida*, to move through substrate, or can prevent attachment or anchoring of sessile creatures (Levin and Dibacco, 1995). Sediment mobility also often dictates the suitability of habitat for some species, with some organisms unable to tolerate any form of smothering by substrate (Freiwald et al., 2002, Levin and Dibacco, 1995). Seafloor composition also drives the location of spawning grounds for commercially important fish stocks (Kloppmann et al., 2001). Hydrodynamic flow is an influential factor affecting species distribution. For example, current speed and direction has particular relevance to planktonic organisms and sessile filter feeders, while some nektonic species may also be influenced by longstanding currents or seasonal variation in dominant flow direction (Freiwald et al., 2002, Levin and Dibacco, 1995, Moll and Radach, 2003). Hydrodynamic models such as the one developed as part of this research may be further modified for specific biological applications. Through development of particle tracking modules, factors such as larval dispersal may be more accurately quantified. This has particular relevance when considering distribution of commercial important shellfish spat but may also be a means to track the expansion of invasive species. Such a model could also be utilised to monitor the formation and movement of Harmful Algal Blooms, which often occur in coastal waters. It is when hydrodynamic data and substrate distribution are combined that a more complete picture of the marine environment is generated and it is these

factors which form the basis of European Union Nature Information System (EUNIS) habitat classifications required as part of the EU's Habitat Directive. The data presented here is adequate to fulfil the elementary layers of this classification system and provide an excellent baseline from which biologists can further quantify habitat suitability for a range of marine species.

7.3 Future work

This work has highlighted the effectiveness of combining repeat bathymetric surveys with a hydrodynamic model of appropriate scale, enabling a comprehensive understanding of shelf sedimentary processes. This research was carried out largely using existing data sets and as such survey design, measurements and sampling strategy were not dedicated to sediment transport applications. Overall similar future research would benefit from targeted repeat MBES and sediment surveys with similar coverage, resolution, system configuration and time-lapse intervals. Uniform design allows transport rate and direction, surface sediment composition and bathymetry to be much better constrained. Data sets acquired concurrently can are more applicable for analysis and similar system configurations remove the need to adjust data to a common format or baseline.

One of the missing aspects of this work is the lack of information about the actual thickness of the sediment bedforms here described with the exception of the seismic data presented in Chapter 3. Analysis of seismic data in conjunction with the analysis of sediment cores would further the understanding of the thickness of sediment facies and bedforms and thus the amount of material available for mobilisation. Seismic data and core stratigraphy descriptions would

also provide greater insight into the relationship between modern, active sediments and underlying seafloor architecture such as glacial formations. Information about the thickness of sediment units on the shelf can also provide further input into Mike by DHI's transport module, defining the depth and volume of a specific sediment type available for mobilisation. This module enables forecasting of sediment migration with the model. As with most research in the area of hydrodynamics, simulated model data is considered inferior to in situ, field measurements. Further work on the hydrodynamics of the Irish shelf would therefore benefit from flow measurements across the shelf using Acoustic Doppler Current Profilers (ADCP) or similar. In particular, an array of such devices spanning the sites described in Chapters 3 and 5 would further constrain model outputs and provide more accurate insights into flow regime along this dynamic marine environment.

The questions raised in Chapter 2 regarding the distortion of glacial landforms and in general the understanding of sedimentary processes over the shelf may be better answered by the generation of a suite of palaeo-hydrodynamic models for this region. Research into the timing and offshore extent of the British-Irish Ice Sheet is informing sea-level models (O'Cofaigh et al., 2012, Peters et al., 2016). As our understanding of changes in sea level and tidal ranges over the shelf since the Last Glacial Maximum (LGM) and during deglaciation improves, the bed stresses could be modelled at relevant time intervals since the LGM. The resulting models, similar to that used in this study, could be utilised to assess how hydrodynamic forces have changed over the shelf with time and the age of formation and modification of the bedforms that were interpreted as

relict. They may also give insight as to the point in time where bed stresses decreased sufficiently to allow previously active bedforms to become dormant. Lastly it is worth pointing out how, given the time and difficulty associated with developing a working hydrodynamic model, the model itself will typically be utilised for multiple applications. The large spatial and temporal coverage of the model here developed, coupled with the range of possible resolutions, make it particularly useful for both large scale processes and localised hydrodynamic interactions. Larval dispersal prediction and harmful contaminant tracking are increasingly popular fields of research with the large volumes of water exchange and chemical weapon disposal in the North Channel making it of special interest to biological scientists. A prevalence of intact shipwrecks and proposed marine renewable sites within the model domain mean it can also be used to simulate high-resolution hydrodynamic processes across small areas.

References

AHMADIAN, R., FALCONER, R. & BOCKELMANN-EVANS, B. 2012. Far-field modelling of the hydro-environmental impact of tidal stream turbines. *Renewable Energy,* 38**,** 107-116.

ALDER, J., CULLIS-SUZUKI, S., KARPOUZI, V., KASCHNER, K., MONDOUX, S., SWARTZ, W., TRUJILLO, P., WATSON, R. & PAULY, D. 2010. Aggregate performance in managing marine ecosystems of 53 maritime countries. *Marine Policy,* 34**,** 468-476.

ALLEN, J. R. L. 1965. Sedimentation to the Lee of Small Underwater Sand Waves: An Experimental Study. *The Journal of Geology,* 73**,** 95-116.

ALLEN, J. R. L. 1980. Sand waves: A model of origin and internal structure. *Sedimentary Geology,* 26**,** 281-328.

BARNARD, P. L., ERIKSON, L. H., ELIAS, E. P. L. & DARTNELL, P. 2013. Sediment transport patterns in the San Francisco Bay Coastal System from cross-validation of bedform asymmetry and modeled residual flux. *Marine Geology,* 345**,** 72-95.

BARRIE, J. V. & CONWAY, K. W. 2014. Seabed characterization for the development of marine renewable energy on the Pacific margin of Canada. *Continental Shelf Research,* 83**,** 45-52.

BARRIE, J. V., CONWAY, K. W., PICARD, K. & GREENE, H. G. 2009. Large-scale sedimentary bedforms and sediment dynamics on a glaciated tectonic continental shelf: Examples from the Pacific margin of Canada. *Continental Shelf Research,* 29**,** 796-806.

BARTHOLDY, J., BARTHOLOMAE, A. & FLEMMING, B. W. 2002. Grain-size control of large compound flow-transverse bedforms in a tidal inlet of the Danish Wadden Sea. *Marine Geology,* 188**,** 391-413.

BARTHOLDY, J., ERNSTSEN, V. B., FLEMMING, B. W., WINTER, C. & BARTHOLOM,ÀÖ¬ß, A. 2010a. A simple model of bedform migration. *Earth Surface Processes and Landforms,* 35**,** 1211-1220.

BARTHOLDY, J., ERNSTSEN, V. B., FLEMMING, B. W., WINTER, C. & BARTHOLOM√§, A. 2010b. A simple model of bedform migration. *Earth Surface Processes and Landforms,* 35**,** 1211-1220.

BARTHOLDY, J., ERNSTSEN, V. B., FLEMMING, B. W., WINTER, C. & BARTHOLOMÄ, A. 2010c. A simple model of bedform migration. *Earth Surface Processes and Landforms,* 35**,** 1211-1220.

BARTLETT, D. & CELLIERS, L. 2016. Geoinformatics for Applied Coastal and Marine Management. *GEOINFORMATICS for Marine and Coastal Management.* CRC Press.

BASSETTI, M. A., JOUET, G., DUFOIS, F., BERNÉ, S., RABINEAU, M. & TAVIANI, M. 2006. Sand bodies at the shelf edge in the Gulf of Lions (Western Mediterranean): Deglacial history and modern processes. *Marine Geology,* 234**,** 93-109.

BASTOS, A. C., COLLINS, M. & KENYON, N. H. 2003. Morphology and internal structure of sand shoals and sandbanks off the Dorset coast, English Channel. *Sedimentology,* 50**,** 1105-1122.

BATES, A. B. 1996. Deepening the Navigation Approach to the Port of Londonderry. *Proceedings of the ICE - Water Maritime and Energy,* 118**,** 1-9.

BELDERSON, R. H., JOHNSON, M. A. & KENYON, N. H. 1982. *Offshore Tidal Sands: Processes and Deposits,* London, Chapman and Hall Ltd.

BELDERSON, R. H. & STRIDE, A. H. 1966. Tidal current fashioning of a basal bed. *Marine Geology,* 4**,** 237-257.

BELLEC, V., WILSON, M., BØE, R., RISE, L., THORSNES, T., BUHL-MORTENSEN, L. & BUHL-MORTENSEN, P. 2008. Bottom currents interpreted from iceberg

ploughmarks revealed by multibeam data at Tromsøflaket, Barents Sea. *Marine Geology,* 249**,** 257-270.

BENETTI, S., DUNLOP, P. & COFAIGH, C. Ì. 2010a. Glacial and glacially-related features on the continental margin of northwest Ireland mapped from marine geophysical data. *Journal of Maps,* 6**,** 14-29.

BENETTI, S., DUNLOP, P. & COFAIGH, C. Ó. 2010b. Glacial and glacially-related features on the continental margin of northwest Ireland mapped from marine geophysical data. *Journal of Maps,* 6**,** 14-29.

BÉRANGER, K., MORTIER, L., GASPARINI, G. P., GERVASIO, L., ASTRALDI, M. & CRÉPON, M. 2004. The dynamics of the Sicily Strait: a comprehensive study from observations and models. *Deep Sea Research Part II: Topical Studies in Oceanography,* 51**,** 411-440.

BERELSON, W. M. 2001. Particle settling rates increase with depth in the ocean. *Deep Sea Research Part II: Topical Studies in Oceanography,* 49**,** 237-251.

BESIO, G. 2004. On the modeling of sand wave migration. *Journal of Geophysical Research,* 109.

BESIO, G., BLONDEAUX, P., BROCCHINI, M., HULSCHER, S. J. M. H., IDIER, D., KNAAPEN, M. A. F., N,ÀÖ¬©METH, A. A., ROOS, P. C. & VITTORI, G. 2008a. The morphodynamics of tidal sand waves: A model overview. *Coastal Engineering,* 55**,** 657-670.

BESIO, G., BLONDEAUX, P., BROCCHINI, M., HULSCHER, S. J. M. H., IDIER, D., KNAAPEN, M. A. F., N√©METH, A. A., ROOS, P. C. & VITTORI, G. 2008b. The morphodynamics of tidal sand waves: A model overview. *Coastal Engineering,* 55**,** 657-670.

BESIO, G., BLONDEAUX, P., BROCCHINI, M., HULSCHER, S. J. M. H., IDIER, D., KNAAPEN, M. A. F., NÉMETH, A. A., ROOS, P. C. & VITTORI, G. 2008c. The morphodynamics of tidal sand waves: A model overview. *Coastal Engineering,* 55**,** 657-670.

BETTERIDGE, K. F. E., THORNE, P. D. & COOKE, R. D. 2008. Calibrating multi-frequency acoustic backscatter systems for studying near-bed suspended sediment transport processes. *Continental Shelf Research,* 28**,** 227-235.

BLONDEL, P. & GÓMEZ SICHI, O. 2009. Textural analyses of multibeam sonar imagery from Stanton Banks, Northern Ireland continental shelf. *Applied Acoustics,* 70**,** 1288-1297.

BLOTT, S. J. & PYE, K. 2001. GRADISTAT: a grain size distribution and statistics package for the analysis of unconsolidated sediments. *Earth Surface Processes and Landforms,* 26**,** 1237-1248.

BØE, R., BELLEC, V. K., DOLAN, M. F. J., BUHL-MORTENSEN, P., BUHL-MORTENSEN, L., SLAGSTAD, D. & RISE, L. 2009. Giant sandwaves in the Hola glacial trough off Vesterålen, North Norway. *Marine Geology,* 267**,** 36-54.

BOOTH, D. A. & MELDRUM, D. T. 1987. Drifting buoys in the Northeast Atlantic. *ICES Journal of Marine Science,* 43**,** 261-267.

BORSJE, B. W., DE VRIES, M. B., HULSCHER, S. & DE BOER, G. J. 2008. Modeling large-scale cohesive sediment transport affected by small-scale biological activity. *Estuarine Coastal and Shelf Science,* 78**,** 468-480.

BRADLEY, S. L., MILNE, G. A., SHENNAN, I. & EDWARDS, R. 2011. An improved glacial isostatic adjustment model for the British Isles. *Journal of Quaternary Science,* 26**,** 541-552.

BRADY, K., MCKEON, C., LYTTLETON, J. & LAWLOR, I. 2012. *Warships, U-Boats & Liners - A Guide to Shipwrecks Mapped in Irish Waters,* Dublin, Ireland, Department of the Arts, Heritage and the Gaeltacht.

BRENNAN, M. L., DAVIS, D., ROMAN, C., BUYNEVICH, I., CATSAMBIS, A., KOFAHL, M., ÜRKMEZ, D., IAN VAUGHN, J., MERRIGAN, M. & DUMAN, M. 2013. Ocean dynamics and anthropogenic impacts along the southern Black Sea shelf examined through the preservation of pre-modern shipwrecks. *Continental Shelf Research,* 53**,** 89-101.

BRIÈRE, C., ABADIE, S., BRETEL, P. & LANG, P. 2007. Assessment of TELEMAC system performances, a hydrodynamic case study of Anglet, France. *Coastal Engineering,* 54**,** 345-356.

BROOKS, A. J., BRADLEY, S. L., EDWARDS, R. J., MILNE, G. A., HORTON, B. & SHENNAN, I. 2008. Postglacial relative sea-level observations from Ireland and their role in glacial rebound modelling. *Journal of Quaternary Science,* 23**,** 175-192.

BROWN, C. J. & BLONDEL, P. 2009. Developments in the application of multibeam sonar backscatter for seafloor habitat mapping. *Applied Acoustics,* 70**,** 1242-1247.

BROWN, C. J., SMITH, S. J., LAWTON, P. & ANDERSON, J. T. 2011. Benthic habitat mapping: A review of progress towards improved understanding of the spatial ecology of the seafloor using acoustic techniques. *Estuarine, Coastal and Shelf Science,* 92**,** 502-520.

BUSCOMBE, D. & CONLEY, D. C. 2012. Effective shear stress of graded sediments. *Water Resources Research,* 48**,** n/a-n/a.

CACCHIONE, D. A., THORNE, P. D., AGRAWAL, Y. & NIDZIEKO, N. J. 2008. Time-averaged near-bed suspended sediment concentrations under waves and currents: Comparison of measured and model estimates. *Continental Shelf Research,* 28**,** 470-484.

CALLAWAY, A., QUINN, R., BROWN, C. J., SERVICE, M. & BENETTI, S. 2011a. Trace metal contamination of Beaufort's Dyke, North Channel, Irish Sea: a legacy of ordnance disposal. *Mar Pollut Bull,* 62**,** 2345-55.

CALLAWAY, A., QUINN, R., BROWN, C. J., SERVICE, M., LONG, D. & BENETTI, S. 2011b. The formation and evolution of an isolated submarine valley in the North Channel, Irish Sea: an investigation of Beaufort's Dyke. *Journal of Quaternary Science,* 26**,** 362-373.

CALVERT, J., STRONG, J. A., SERVICE, M., MCGONIGLE, C. & QUINN, R. 2015. An evaluation of supervised and unsupervised classification techniques for marine benthic habitat mapping using multibeam echosounder data. *Ices Journal of Marine Science,* 72**,** 1498-1513.

CASADO-MARTÍNEZ, M. C., BUCETA, J. L., BELZUNCE, M. J. & DELVALLS, T. A. 2006. Using sediment quality guidelines for dredged material management in commercial ports from Spain. *Environment International,* 32**,** 388-396.

CASTON, V. N. D. 1972. Linear Sand Banks in the Southern North Sea. *Sedimentology,* 18**,** 63-78.

CATAÑO-LOPERA, Y. A. & GARCÍA, M. H. 2006. Geometry and migration characteristics of bedforms under waves and currents. Part 1: Sandwave morphodynamics. *Coastal Engineering,* 53**,** 767-780.

CHE HASAN, R., IERODIACONOU, D., LAURENSON, L. & SCHIMEL, A. 2014. Integrating Multibeam Backscatter Angular Response, Mosaic and Bathymetry Data for Benthic Habitat Mapping. *PLoS ONE,* 9**,** e97339.

CHORIN, A. J. 1997. A Numerical Method for Solving Incompressible Viscous Flow Problems. *Journal of Computational Physics,* 135**,** 118-125.

COOPER, J. A. G., JACKSON, D. W. T., NAVAS, F., MCKENNA, J. & MALVAREZ, G. 2004. Identifying storm impacts on an embayed, high-energy coastline: examples from western Ireland. *Marine Geology,* 210**,** 261-280.

COOPER, J. A. G., KELLEY, J. T., BELKNAP, D. F., QUINN, R. & MCKENNA, J. 2002. Inner shelf seismic stratigraphy off the north coast of Northern Ireland: new data on the depth of the Holocene lowstand. *Marine Geology,* 186**,** 369-387.

CROWDER, D. W. & DIPLAS, P. 2000. Using two-dimensional hydrodynamic models at scales of ecological importance. *Journal of Hydrology,* 230**,** 172-191.

CURRAN, J. C., WATERS, K. A. & CANNATELLI, K. M. 2015. Real time measurements of sediment transport and bed morphology during channel altering flow and sediment transport events. *Geomorphology,* 244**,** 169-179.

DABROWSKI, T., LYONS, K., BERRY, A., CUSACK, C. & NOLAN, G. D. 2014. An operational biogeochemical model of the North-East Atlantic: Model description and skill assessment. *Journal of Marine Systems,* 129**,** 350-367.

DANIELL, J. J. 2015. Bedform facies in western Torres Strait and the influence of hydrodynamics, coastal geometry, and sediment supply on their distribution. *Geomorphology,* 235**,** 118-129.

DAVIES, A. G. & THORNE, P. D. 2008. Advances in the Study of Moving Sediments and Evolving Seabeds. *Surveys in Geophysics,* 29**,** 1-36.

DAVIES, A. M. & GERRITSEN, H. 1994. An intercomparison of three-dimensional tidal hydrodynamic models of the Irish Sea. *Tellus A,* 46**,** 200-221.

DAVIES, A. M. & XING, J. 2002. Processes influencing suspended sediment movement on the Malin–Hebrides shelf. *Continental Shelf Research,* 22**,** 2081-2113.

DE JUAN, S., LO IACONO, C. & DEMESTRE, M. 2013. Benthic habitat characterisation of soft-bottom continental shelves: Integration of acoustic surveys, benthic samples and trawling disturbance intensity. *Estuarine, Coastal and Shelf Science,* 117**,** 199-209.

DENNY, J. F., SCHWAB, W. C., BALDWIN, W. E., BARNHARDT, W. A., GAYES, P. T., MORTON, R. A., WARNER, J. C., DRISCOLL, N. W. & VOULGARIS, G. 2013. Holocene sediment distribution on the inner continental shelf of northeastern South Carolina: Implications for the regional sediment budget and long-term shoreline response. *Continental Shelf Research,* 56**,** 56-70.

DODET, G., BERTIN, X. & TABORDA, R. 2010. Wave climate variability in the North-East Atlantic Ocean over the last six decades. *Ocean Modelling,* 31**,** 120-131.

DONG, L. X., GUAN, W. B., CHEN, Q., LI, X. H., LIU, X. H. & ZENG, X. M. 2011. Sediment transport in the Yellow Sea and East China Sea. *Estuarine, Coastal and Shelf Science,* 93**,** 248-258.

DRAKE, D. E., CACCHIONE, D. A. & KARL, H. A. 1985. Bottom current and sediment transport on San Pedro Shelf, California. *Journal of Sedimentary Research,* 55**,** 15-28.

DUNBAR, R. B., ANDERSON, J. B., DOMACK, E. W. & JACOBS, S. S. 1985. Oceanographic influences on sedimentation along the Antarctic continental shelf. 43**,** 291-312.

DUNLOP, P., SACCHETTI, F., BENETTI, S. & O'COFAIGH, C. 2011. Mapping Ireland's Glaciated Continental Margin Using Marine Geophysical Data. *In:* SMITH, M. J., PARON, P. AND GRIFFITHS, J.S. (ed.) *Geomorphological Mapping: Methods and Applications: A Professional Handbook of Techniques and Applications (Developments in Earth Surface Processes)* Elsevier B.V.

DUNLOP, P., SHANNON, R., MCCABE, M., QUINN, R. & DOYLE, E. 2010. Marine geophysical evidence for ice sheet extension and recession on the Malin Shelf: New evidence for the western limits of the British Irish Ice Sheet. *Marine Geology,* 276**,** 86-99.

EDIGER, V., VELEGRAKIS, A. F. & EVANS, G. 2002. Upper slope sediment waves in the Cilician Basin, northeastern Mediterranean. *Marine Geology,* 192**,** 321-333.

EVANS, W., BENETTI, S., SACCHETTI, F., JACKSON, D. W. T., DUNLOP, P. & MONTEYS, X. 2015. Bedforms on the northwest Irish Shelf: indication of modern active sediment transport and over printing of paleo-glacial sedimentary deposits. *Journal of Maps***,** 1-14.

FELDENS, P., DIESING, M., SCHWARZER, K., HEINRICH, C. & SCHLENZ, B. 2015. Occurrence of flow parallel and flow transverse bedforms in Fehmarn Belt (SW Baltic Sea) related to the local palaeomorphology. *Geomorphology,* 231**,** 53-62.

FELDENS, P., SCHWARZER, K., SAKUNA, D., SZCZUCIŃSKI, W. & SOMPONGCHAIYAKUL, P. 2012. Sediment distribution on the inner

continental shelf off Khao Lak (Thailand) after the 2004 Indian Ocean tsunami. *Earth, Planets and Space,* 64**,** 875-887.

FENSTER, M. S., FITZGERALD, D. M., BOHLEN, W. F., LEWIS, R. S. & BALDWIN, C. T. 1990. Stability of giant sand waves in eastern Long Island Sound, U.S.A. *Marine Geology,* 91**,** 207-225.

FERENTINOS, G. & COLLINS, M. 1979. Tidally induced secondary circulations and their associated sedimentation processes. *Journal of the Oceanographical Society of Japan,* 35**,** 65-74.

FERNAND, L., NOLAN, G. D., RAINE, R., CHAMBERS, C. E., DYE, S. R., WHITE, M. & BROWN, J. 2006. The Irish coastal current: A seasonal jet-like circulation. *Continental Shelf Research,* 26**,** 1775-1793.

FERRET, Y., LE BOT, S., TESSIER, B., GARLAN, T. & LAFITE, R. 2010. Migration and internal architecture of marine dunes in the eastern English Channel over 14 and 56 year intervals: the influence of tides and decennial storms. *Earth Surface Processes and Landforms,* 35**,** 1480-1493.

FERRINI, V. L. & FLOOD, R. D. 2005. A comparison of Rippled Scour Depressions identified with multibeam sonar: Evidence of sediment transport in inner shelf environments. *Continental Shelf Research,* 25**,** 1979-1995.

FERZIGER, J. H. 1987. Simulation of incompressible turbulent flows. *Journal of Computational Physics,* 69**,** 1-48.

FIELD, M. E., NELSON, C. H., CACCHIONE, D. A. & DRAKE, D. E. 1981. Sand Waves on an Epicontinental Shelf: Northern Bering Sea. *In:* NITTROUER, C. A. (ed.) *Developments in Sedimentology.* Elsevier.

FLATHER, R. A. 1976. A tidal model of the northwest European continental shelf. *Mem. Soc. R. Sci. Liege,* 10**,** 141-164.

FOLK, R. L. 1954. The Distinction between Grain Size and Mineral Composition in Sedimentary-Rock Nomenclature. *The Journal of Geology,* 62**,** 344-359.

FONSECA, L., BROWN, C., CALDER, B., MAYER, L. & RZHANOV, Y. 2009. Angular range analysis of acoustic themes from Stanton Banks Ireland: A link between visual interpretation and multibeam echosounder angular signatures. *Applied Acoustics,* 70**,** 1298-1304.

FRANCKEN, F., WARTEL, S., PARKER, R. & TAVERNIERS, E. 2004. Factors influencing subaqueous dunes in the Scheldt Estuary. *Geo-Marine Letters,* 24**,** 14-21.

FREIWALD, A., HÜHNERBACH, V., LINDBERG, B., WILSON, J. & CAMPBELL, J. 2002. The Sula Reef Complex, Norwegian shelf. *Facies,* 47**,** 179-200.

GAVAZZI, G. M., MADRICARDO, F., JANOWSKI, L., KRUSS, A., BLONDEL, P., SIGOVINI, M. & FOGLINI, F. 2016. Evaluation of seabed mapping methods for fine-scale classification of extremely shallow benthic habitats - Application to the Venice Lagoon, Italy. *Estuarine Coastal and Shelf Science,* 170**,** 45-60.

GERKEMA, T. 2000. A linear stability analysis of tidally generated sand waves. *Journal of Fluid Mechanics,* 417**,** 303-322.

GIORGI, S. & RINGWOOD, J. 2013. Can Tidal Current Energy Provide Base Load? *Energies,* 6**,** 2840-2858.

GOFF, J. A., OLSON, H. C. & DUNCAN, C. S. 2000. Correlation of side-scan backscatter intensity with grain-size distribution of shelf sediments, New Jersey margin. *Geo-Marine Letters,* 20**,** 43-49.

GOODWIN, C. E., STRAIN, E. M., EDWARDS, H., BENNETT, S. C., BREEN, J. P. & PICTON, B. E. 2013. Effects of two decades of rising sea surface temperatures on sublittoral macrobenthos communities in Northern Ireland, UK. *Mar Environ Res,* 85**,** 34-44.

GOWEN, R. J., RAINE, R., DICKEY-COLLAS, M. & WHITE, M. 1998. Plankton distributions in relation to physical oceanographic features on the southern Malin Shelf, August 1996. *Ices Journal of Marine Science,* 55**,** 1095-1111.

GUNN, K. & STOCK-WILLIAMS, C. 2013. On validating numerical hydrodynamic models of complex tidal flow. *International Journal of Marine Energy,* 3-4**,** e82-e97.

HALL, P. & DAVIES, A. M. 2004. Modelling tidally induced sediment-transport paths over the northwest European shelf: the influence of sea-level reduction. *Ocean Dynamics,* 54**,** 126-141.

HAND, B. 1988. Internal-Wave Currents as a Mechanism to Account for Large Sand Waves in Navarinsky Canyon Head, Bering Sea. *Journal of Sedimentary Petrology,* 58**,** 760-770.

HANQUIEZ, V., MULDER, T., LECROART, P., GONTHIER, E., MARCH√®S, E. & VOISSET, M. 2007a. High resolution seafloor images in the Gulf of Cadiz, Iberian margin. *Marine Geology,* 246**,** 42-59.

HANQUIEZ, V., MULDER, T., LECROART, P., GONTHIER, E., MARCHÈS, E. & VOISSET, M. 2007b. High resolution seafloor images in the Gulf of Cadiz, Iberian margin. *Marine Geology,* 246**,** 42-59.

HASAN, C. R., IERODIACONOU, D. & MONK, J. 2012. Evaluation of Four Supervised Learning Methods for Benthic Habitat Mapping Using Backscatter from Multi-Beam Sonar. *Remote Sensing,* 4.

HENDRICK, V. J., HUTCHISON, Z. L. & LAST, K. S. 2016. Sediment Burial Intolerance of Marine Macroinvertebrates. *PLoS One,* 11**,** e0149114.

HERMAN, G. 1983. *Coastal Oceanography,* New York, Springer US.

HILL, A. E., BROWN, J. & FERNAND, L. 1996. The western Irish Sea gyre: A retention system for Norway lobster (Nephrops norvegicus)? *Oceanologica Acta,* 19**,** 357-368.

HILL, A. E. & MITCHELSON-JACOB, E. G. 1993. Observations of a poleward-flowing saline core on the continental slope west of Scotland. *Deep Sea Research Part I: Oceanographic Research Papers,* 40**,** 1521-1527.

HJULSTROM, F. 1935. Studies of the morphological activity of rivers as illustrated by the River Fyris, Bulletin. *Geological Institute Upsalsa,* 25**,** 221-527.

HOITINK, A. J. F. & HOEKSTRA, P. 2005. Observations of suspended sediment from ADCP and OBS measurements in a mud-dominated environment. *Coastal Engineering,* 52**,** 103-118.

HOLDAWAY, G. P., THORNE, P. D., FLATT, D., JONES, S. E. & PRANDLE, D. 1999. Comparison between ADCP and transmissometer measurements of suspended sediment concentration. *Continental Shelf Research,* 19**,** 421-441.

HOLT, J., HARLE, J., PROCTOR, R., MICHEL, S., ASHWORTH, M., BATSTONE, C., ALLEN, I., HOLMES, R., SMYTH, T., HAINES, K., BRETHERTON, D. & SMITH, G. 2009. Modelling the global coastal ocean. *Philos Trans A Math Phys Eng Sci,* 367**,** 939-51.

HOVLAND, M. & JUDD, A. G. 1988. Seabed Pockmarks and Seepages. Impact on Geology, Biology and Marine Environment. . *Geological Magazine,* 127**,** 85-86.

HOVLAND, M., SVENSEN, H., FORSBERG, C. F., JOHANSEN, H., FICHLER, C., FOSSÅ, J. H., JONSSON, R. & RUESLÅTTEN, H. 2005. Complex pockmarks with carbonate-ridges off mid-Norway: Products of sediment degassing. *Marine Geology,* 218**,** 191-206.

HUTHNANCE, J. M. 1973. Tidal current asymmetries over the Norfolk Sandbanks. *Estuarine and Coastal Marine Science,* 1**,** 89-99.

HUTHNANCE, J. M. 1995. Circulation, exchange and water masses at the ocean margin: the role of physical processes at the shelf edge. *Progress in Oceanography,* 35**,** 353-431.

HUTHNANCE, J. M., HUMPHERY, J. D., KNIGHT, P. J., CHATWIN, P. G., THOMSEN, L. & WHITE, M. 2002. Near-bed turbulence measurements, stress estimates and sediment mobility at the continental shelf edge. *Progress in Oceanography,* 52**,** 171-194.

IERODIACONOU, D., MONK, J., RATTRAY, A., LAURENSON, L. & VERSACE, V. L. 2011. Comparison of automated classification techniques for predicting benthic biological communities using hydroacoustics and video observations. *Continental Shelf Research,* 31**,** S28-S38.

IHO 2008. International Hydrographic Organisation Standards for Hydrographic Surveys. *Special Publication No.44*.

INALL, M., GILLIBRAND, P., GRIFFITHS, C., MACDOUGAL, N. & BLACKWELL, K. 2009. On the oceanographic variability of the North-West European Shelf to the West of Scotland. *Journal of Marine Systems,* 77**,** 210-226.

IOC, IHO & BODC 2003. Centenary Edition of the GEBCO Digital Atlas published as part of the General Bathymetric Chart of the Oceans. *In:* COMMISION, I. O., ORGANISATION, I. H. & CENTRE, B. O. D. (eds.).

JACKSON, D. W. T., COOPER, J. A. G. & DEL RIO, L. 2005. Geological control of beach morphodynamic state. *Marine Geology,* 216**,** 297-314.

JULIEN, P. Y. 2002. *River Mechanics,* Cambridge, University Press.

KELLEY, J. T., COOPER, J. A. G., JACKSON, D. W. T., BELKNAP, D. F. & QUINN, R. J. 2006. Sea-level change and inner shelf stratigraphy off Northern Ireland. *Marine Geology,* 232**,** 1-15.

KENNEDY, J. F. 2006. The mechanics of dunes and antidunes in erodible-bed channels. *Journal of Fluid Mechanics,* 16**,** 521-544.

KENYON, N. H. & STRIDE, A. H. 1970. The Tide-Swept Continental Shelf Sediments between the Shetland Isles and France. *Sedimentology,* 14**,** 159-173.

KHEIASHY, K. E., MCCORQUODALE, J., GEORGIOU, I. & MESELHE, E. 2010. Three dimensional hydrodynamic modeling over bed forms in open channels. *International Journal of Sediment Research,* 25**,** 431-440.

KING, L. 1969. Submarine End Moraines and Associated Deposits on the Scotian Shelf. *Geological Society of America Bulletin,* 80**,** 83-96.

KING, L. H. & MACLEAN, B. 1970. Pockmarks on the Scotian Shelf. *Geological Society of America Bulletin,* 81**,** 3141-3148.

KLOPPMANN, M., MOHN, C. & BARTSCH, J. 2001. The distribution of blue whiting eggs and larvae on Porcupine Bank in relation to hydrography and currents. *Fisheries Research,* 50**,** 89-109.

KNAAPEN, M. A. F. & HULSCHER, S. J. M. H. 2002. Regeneration of sand waves after dredging. *Coastal Engineering,* 46**,** 277-289.

KNAAPEN, M. A. F., VAN BERGEN HENEGOUW, C. N. & HU, Y. Y. 2005. Quantifying bedform migration using multi-beam sonar. *Geo-Marine Letters,* 25**,** 306-314.

KNIGHT, P. J. & HOWARTH, M. J. 1999. The flow through the north channel of the Irish Sea. *Continental Shelf Research,* 19**,** 693-716.

KUCHAR, J., MILNE, G., HUBBARD, A., PATTON, H., BRADLEY, S., SHENNAN, I. & EDWARDS, R. 2012. Evaluation of a numerical model of the British-Irish ice sheet using relative sea-level data: implications for the interpretation of trimline observations. *Journal of Quaternary Science,* 27**,** 597-605.

KUIJPERS, A., HANSEN, B., HÜHNERBACH, V., LARSEN, B., NIELSEN, T. & WERNER, F. 2002. Norwegian Sea overflow through the Faroe–Shetland gateway as documented by its bedforms. *Marine Geology,* 188**,** 147-164.

LAMARCHE, G., LURTON, X., VERDIER, A.-L. & AUGUSTIN, J.-M. 2011. Quantitative characterisation of seafloor substrate and bedforms using advanced processing of multibeam backscatter—Application to Cook Strait, New Zealand. *Continental Shelf Research,* 31**,** S93-S109.

LE HIR, P., MONBET, Y. & ORVAIN, F. 2007. Sediment erodability in sediment transport modelling: Can we account for biota effects? *Continental Shelf Research,* 27**,** 1116-1142.

LEFEBVRE, A., PAARLBERG, A. J., ERNSTSEN, V. B. & WINTER, C. 2014. Flow separation and roughness lengths over large bedforms in a tidal

environment: A numerical investigation. *Continental Shelf Research,* 91**,** 57-69.

LEGRAND, S., DELEERSNIJDER, E., HANERT, E., LEGAT, V. & WOLANSKI, E. 2006. High-resolution, unstructured meshes for hydrodynamic models of the Great Barrier Reef, Australia. *Estuarine, Coastal and Shelf Science,* 68**,** 36-46.

LEVIN, L. A. & DIBACCO, C. 1995. Influence of Sediment Transport on Short-Term Recolonization by Seamount Infauna. *Marine Ecology Progress Series,* 123**,** 163-175.

LEWIS, E. 1980. The practical salinity scale 1978 and its antecedents. *IEEE Journal of Oceanic Engineering,* 5**,** 3-8.

LI, M. Z. & KING, E. L. 2007. Multibeam bathymetric investigations of the morphology of sand ridges and associated bedforms and their relation to storm processes, Sable Island Bank, Scotian Shelf. *Marine Geology,* 243**,** 200-228.

LI, M. Z., SHERWOOD, C. R. & HILL, P. R. 2012. *Sediments, Morphology and Sedimentary Processes on Continental Shelves: Advances in technologies, research and applications (Special Publication 44 of the IAS)*, John Wiley & Sons.

LIU, X. & HUANG, W. 2009. Modeling sediment resuspension and transport induced by storm wind in Apalachicola Bay, USA. *Environmental Modelling & Software,* 24**,** 1302-1313.

LO IACONO, C., GUILLÉN, J., PUIG, P., RIBÓ, M., BALLESTEROS, M., PALANQUES, A., LÍ FARRÁN, M. & ACOSTA, J. 2010. Large-scale bedforms along a tideless outer shelf setting in the western Mediterranean. *Continental Shelf Research,* 30**,** 1802-1813.

LOBO, F. J., HERNÁNDEZ-MOLINA, F. J., SOMOZA, L., RODERO, J., MALDONADO, A. & BARNOLAS, A. 2000. Patterns of bottom current flow deduced from dune

asymmetries over the Gulf of Cadiz shelf (southwest Spain). *Marine Geology,* 164**,** 91-117.

LÓPEZ-VICENTE, M., PÉREZ-BIELSA, C., LÓPEZ-MONTERO, T., LAMBÁN, L. J. & NAVAS, A. 2014. Runoff simulation with eight different flow accumulation algorithms: Recommendations using a spatially distributed and open-source model. *Environmental Modelling & Software,* 62**,** 11-21.

LOZANO, I., DEVOY, R. J. N., MAY, W. & ANDERSEN, U. 2004. Storminess and vulnerability along the Atlantic coastlines of Europe: analysis of storm records and of a greenhouse gases induced climate scenario. *Marine Geology,* 210**,** 205-225.

LURTON, X. 2002. *An Introduction to Underwater Acoustics - Principles and Applications,* Chichester, UK, Springer.

LYNCH, D. R., SMITH, K. W. & CAHILL, B. 2004. Seasonal mean circulation on the Irish shelf—a model-generated climatology. *Continental Shelf Research,* 24**,** 2215-2244.

MA, X., YAN, J. & FAN, F. 2014. Morphology of submarine barchans and sediment transport in barchans fields off the Dongfang coast in Beibu Gulf. *Geomorphology,* 213**,** 213-224.

MADSEN, P. A., MURRAY, R. & SØRENSEN, O. R. 1991. A new form of the Boussinesq equations with improved linear dispersion characteristics. *Coastal Engineering,* 15**,** 371-388.

MARKS, K. M. & SMITH, W. H. F. 2009. An uncertainty model for deep ocean single beam and multibeam echo sounder data. *Marine Geophysical Researches,* 29**,** 239-250.

MARTIN-SHORT, R., HILL, J., KRAMER, S. C., AVDIS, A., ALLISON, P. A. & PIGGOTT, M. D. 2015. Tidal resource extraction in the Pentland Firth, UK: Potential impacts on flow regime and sediment transport in the Inner Sound of Stroma. *Renewable Energy,* 76**,** 596-607.

MASSON, D. G., WYNN, R. B. & BETT, B. J. 2004. Sedimentary environment of the Faroe-Shetland and Faroe Bank Channels, north-east Atlantic, and the use of bedforms as indicators of bottom current velocity in the deep ocean. *Sedimentology,* 51**,** 1207-1241.

MAYER, L. A. 2006. Frontiers in Seafloor Mapping and Visualization. *Marine Geophysical Researches,* 27**,** 7-17.

MAZUMDER, R. 2003. Sediment transport, aqueous bedform stability and morphodynamics under unidirectional current: a brief overview. *Journal of African Earth Sciences,* 36**,** 1-14.

MCBREEN, F., ASKEW, N., CAMERON, N., CONNOR, D., ELLWOOD, H. & CARTER, A. 2011. UKSeaMap 2010: Predictive mapping of seabed habitats in UK waters.: Joint Nature Conservation Committee.

MCDOWELL, J., KNIGHT, J. & QUINN, R. 2005. High-Resolution Geophysical Investigations Seaward of the Bann Estuary, Northern Ireland Coast. *In:* FITZGERALD, D. & KNIGHT, J. (eds.) *High Resolution Morphodynamics and Sedimentary Evolution of Estuaries.* Springer Netherlands.

MCGONIGLE, C., BROWN, C., QUINN, R. & GRABOWSKI, J. 2009. Evaluation of image-based multibeam sonar backscatter classification for benthic habitat discrimination and mapping at Stanton Banks, UK. *Estuarine, Coastal and Shelf Science,* 81**,** 423-437.

MCGONIGLE, C., BROWN, C. J. & QUINN, R. 2010a. Insonification orientation and its relevance for image-based classification of multibeam backscatter. *ICES Journal of Marine Science,* 67**,** 1010-1023.

MCGONIGLE, C., BROWN, C. J. & QUINN, R. 2010b. Operational Parameters, Data Density and Benthic Ecology: Considerations for Image-Based Classification of Multibeam Backscatter. *Marine Geodesy,* 33**,** 16-38.

MCGONIGLE, C. & COLLIER, J. S. 2014. Interlinking backscatter, grain size and benthic community structure. *Estuarine, Coastal and Shelf Science,* 147**,** 123-136.

MCMAHON, T. 1995. Some oceanographic features of northeastern Atlantic waters west of Ireland. *ICES Journal of Marine Science,* 52**,** 221-232.

MESSAROS, R. C. & BRUNO, M. S. 2010. Laboratory Investigation of Bedform Geometry under Regular and Irregular Surface Gravity Waves. *Journal of Coastal Research***,** 94-103.

MICALLEF, A., LE BAS, T. P., HUVENNE, V. A. I., BLONDEL, P., HÜHNERBACH, V. & DEIDUN, A. 2012. A multi-method approach for benthic habitat mapping of shallow coastal areas with high-resolution multibeam data. *Continental Shelf Research,* 39-40**,** 14-26.

MILLER, M. C., MCCAVE, I. N. & KOMAR, P. D. 1977. Threshold of sediment motion under unidirectional currents. *Sedimentology,* 24**,** 507-527.

MOLL, A. & RADACH, G. 2003. Review of three-dimensional ecological modelling related to the North Sea shelf system. *Progress in Oceanography,* 57**,** 175-217.

MORELISSEN, R., HULSCHER, S. J. M. H., KNAAPEN, M. A. F., NÉMETH, A. A. & BIJKER, R. 2003. Mathematical modelling of sand wave migration and the interaction with pipelines. *Coastal Engineering,* 48**,** 197-209.

MUIR, R. J., FITCHES, W. R. & MALTMAN, A. J. 1994. The Rhinns Complex: Proterozoic basement on Islay and Colonsay, Inner Hebrides, Scotland, and on Inishtrahull, NW Ireland. *Earth and Environmental Science Transactions of the Royal Society of Edinburgh,* 85**,** 77-90.

NASH, S. & PHOENIX, A. 2017. A review of the current understanding of the hydro-environmental impacts of energy removal by tidal turbines. *Renewable and Sustainable Energy Reviews,* 80**,** 648-662.

NEILL, S. P., LITT, E. J., COUCH, S. J. & DAVIES, A. G. 2009. The impact of tidal stream turbines on large-scale sediment dynamics. *Renewable Energy,* 34**,** 2803-2812.

NEILL, S. P., SCOURSE, J. D. & UEHARA, K. 2010. Evolution of bed shear stress distribution over the northwest European shelf seas during the last 12,000 years. *Ocean Dynamics,* 60**,** 1139-1156.

NÉMETH, A. A., HULSCHER, S. J. M. H. & DE VRIEND, H. J. 2002. Modelling sand wave migration in shallow shelf seas. *Continental Shelf Research,* 22**,** 2795-2806.

NÉMETH, A. A., HULSCHER, S. J. M. H. & VAN DAMME, R. M. J. 2007. Modelling offshore sand wave evolution. *Continental Shelf Research,* 27**,** 713-728.

NIELSEN, P. 1979. Some basic concepts of wave sediment transport.

NIELSEN, P. & GUARD, P. A. 2011. Vertical scales and shear stresses in wave boundary layers over movable beds *Coastal Engineering Proceedings; No 32 (2010): Proceedings of 32nd Conference on Coastal Engineering, Shanghai, China, 2010.*

NIO, S. D. 1976. Marine Transgressions as a factor in the formation of sandwave complexes. *Geologie en Mijnbouw***,** 18-40.

NORDSTROM, K. F. 2005. Beach Nourishment and Coastal Habitats: Research Needs to Improve Compatibility. *Restoration Ecology,* 13**,** 215-222.

O'COFAIGH, C., DUNLOP, P. & BENETTI, S. 2012. Marine geophysical evidence for Late Pleistocene ice sheet extent and recession off northwest Ireland. *Quaternary Science Reviews,* 44**,** 147-159.

ODDO, P. & PINARDI, N. 2008. Lateral open boundary conditions for nested limited area models: A scale selective approach. *Ocean Modelling,* 20**,** 134-156.

PAULL, C., USSLER III, W., MAHER, N., GREENE, H. G., REHDER, G., LORENSON, T. & LEE, H. 2002. Pockmarks off Big Sur, California. *Marine Geology,* 181**,** 323-335.

PERILLO, M. M., BEST, J. L., YOKOKAWA, M., SEKIGUCHI, T., TAKAGAWA, T. & GARCIA, M. H. 2014. A unified model for bedform development and equilibrium under unidirectional, oscillatory and combined-flows. *Sedimentology,* 61**,** 2063-2085.

PETERS, J. L., BENETTI, S., DUNLOP, P., Ó COFAIGH, C., MORETON, S. G., WHEELER, A. J. & CLARK, C. D. 2016. Sedimentology and chronology of the advance and retreat of the last British-Irish Ice Sheet on the continental shelf west of Ireland. *Quaternary Science Reviews,* 140**,** 101-124.

PINGREE, R. D. & LE CANN, B. 1989. Celtic and Armorican slope and shelf residual currents. *Progress in Oceanography,* 23**,** 303-338.

PINGREE, R. D. & MADDOCK, L. 1979. The tidal physics of headland flows and offshore tidal bank formation. *Marine Geology,* 32**,** 269-289.

PINGREE, R. D., SINHA, B. & GRIFFITHS, C. R. 1999. Seasonality of the European slope current (Goban Spur) and ocean margin exchange. *Continental Shelf Research,* 19**,** 929-975.

PLETS, R., CLEMENTS, A., QUINN, R., STRONG, J., BREEN, J. & EDWARDS, H. 2012. Marine substratum map of the Causeway Coast, Northern Ireland. *Journal of Maps,* 8**,** 1-13.

PLETS, R., QUINN, R., FORSYTHE, W., WESTLEY, K., BELL, T., BENETTI, S., MCGRATH, F. & ROBINSON, R. 2011. Using Multibeam Echo-Sounder Data to Identify Shipwreck Sites: archaeological assessment of the Joint Irish Bathymetric Survey data. *International Journal of Nautical Archaeology,* 40**,** 87-98.

PROCTOR, R., HOLT, J., ALLEN, J. & BLACKFORD, J. 2003. Nutrient fluxes and budgets for the North West European Shelf from a three-dimensional model. *The Science of The Total Environment,* 314-316**,** 769-785.

QUINN, R. 2000. Marine geophysical investigation of the inshore coastal waters of Northern Ireland. *The International Journal of Nautical Archaeology,* 29**,** 294-298.

QUINN, R. & BOLAND, D. 2010. The role of time-lapse bathymetric surveys in assessing morphological change at shipwreck sites. *Journal of Archaeological Science,* 37**,** 2938-2946.

QUINN, R., FORSYTHE, W., BREEN, C., BOLAND, D., LANE, P. & OMAR, A. L. 2007. Process-based models for port evolution and wreck site formation at Mombasa, Kenya. *Journal of Archaeological Science,* 34**,** 1449-1460.

RAINE, R. 2014. A review of the biophysical interactions relevant to the promotion of HABs in stratified systems: The case study of Ireland. *Deep Sea Research Part II: Topical Studies in Oceanography,* 101**,** 21-31.

REISE, K. 2002. Sediment mediated species interactions in coastal waters. *Journal of Sea Research,* 48**,** 127-141.

RODRÍGUEZ, E. L. & DEAN, R. G. 2009. A Sediment Budget Analysis and Management Strategy for Fort Pierce Inlet, Florida. *Journal of Coastal Research***,** 870-883.

ROSATI, J. D. 2005. Concepts in Sediment Budgets. *Journal of Coastal Research***,** 307-322.

ROURKE, F. O., BOYLE, F. & REYNOLDS, A. 2010. Marine current energy devices: Current status and possible future applications in Ireland. *Renewable and Sustainable Energy Reviews,* 14**,** 1026-1036.

RUBIN, D. M. & IKEDA, H. 1990. Flume experiments on the alignment of transverse, oblique, and longitudinal dunes in directionally varying flows. *Sedimentology,* 37**,** 673-684.

RZHANOV, Y., FONSECA, L. & MAYER, L. 2012. Construction of seafloor thematic maps from multibeam acoustic backscatter angular response data. *Computers & Geosciences,* 41**,** 181-187.

SACCHETTI, F., BENETTI, S., GEORGIOPOULOU, A., DUNLOP, P. & QUINN, R. 2011. Geomorphology of the Irish Rockall Trough, North Atlantic Ocean, mapped from multibeam bathymetric and backscatter Data. *Journal of Maps,* 7**,** 60-81.

SACCHETTI, F., BENETTI, S., GEORGIOPOULOU, A., SHANNON, P. M., O'REILLY, B. M., DUNLOP, P., QUINN, R. & Ó COFAIGH, C. 2012. Deep-water geomorphology of the glaciated Irish margin from high-resolution marine geophysical data. *Marine Geology,* 291-294**,** 113-131.

SANAY, R., VOULGARIS, G. & WARNER, J. C. 2007. Tidal asymmetry and residual circulation over linear sandbanks and their implication on sediment transport: A process-oriented numerical study. *Journal of Geophysical Research,* 112.

SCHIMEL, A. C. G., IERODIACONOU, D., HULANDS, L. & KENNEDY, D. M. 2015. Accounting for uncertainty in volumes of seabed change measured with repeat multibeam sonar surveys. *Continental Shelf Research,* 111**,** 52-68.

SCHMITT, T., MITCHELL, N. C. & RAMSAY, A. T. S. 2008. Characterizing uncertainties for quantifying bathymetry change between time-separated multibeam echo-sounder surveys. *Continental Shelf Research,* 28**,** 1166-1176.

SCHMITT, T., MITCHELL, N. C. & RAMSAY, T. S. 2007. Use of swath bathymetry in the investigation of sand dune geometry and migration around a near shore 'banner' tidal sandbank. *Geological Society, London, Special Publications,* 274**,** 53-64.

SHAN, S., SHENG, J., THOMPSON, K. R. & GREENBERG, D. A. 2011. Simulating the three-dimensional circulation and hydrography of Halifax Harbour using a multi-nested coastal ocean circulation model. *Ocean Dynamics,* 61**,** 951-976.

SHANMUGAM, S., LUCAS, N., PHIPPS, P., RICHARDS, A. & BARNSLEY, M. 2003. Assessment of remote sensing techniques for habitat mapping in coastal dune ecosystems. *Journal of Coastal Research,* 19**,** 64-75.

SHAW, J., TODD, B. J. & LI, M. Z. 2014. Geologic insights from multibeam bathymetry and seascape maps of the Bay of Fundy, Canada. *Continental Shelf Research,* 83**,** 53-63.

SHENG, J. Y. & YANG, B. 2010. A Nested-Grid Ocean Circulation Model for Simulating Three-Dimensional Circulation and Hydrography over Canadian Atlantic Coastal Waters. *Terrestrial Atmospheric and Oceanic Sciences,* 21**,** 27-44.

SHERWOOD, C. R. Year. Use Of Sediment Transport Calculations In Dredged Material Disposal Site Selection. *In:* Proceedings OCEANS, 18-21 Sept. 1989 1989. 326-332.

SHIELDS, A. 1936. Application of similarity principles and turbulence research to bed-load movement. *Mitteilunger der Preussischen Versuchsanstalt für Wasserbau und Schiffbau,* 26**,** 5-24.

SIDDORN, J. R., ALLEN, J. I., BLACKFORD, J. C., GILBERT, F. J., HOLT, J. T., HOLT, M. W., OSBORNE, J. P., PROCTOR, R. & MILLS, D. K. 2007. Modelling the hydrodynamics and ecosystem of the North-West European continental shelf for operational oceanography. *Journal of Marine Systems,* 65**,** 417-429.

SINGLETON, G. H. 2001. Marine Aggregate Dredging in the UK: A Review. *Underwater Technology,* 25**,** 3-14.

SINHA, B. & PINGREE, R. D. 1997. The principal lunar semidiurnal tide and its harmonics: baseline solutions for M2 and M4 constituents on the North-West European Continental Shelf. *Continental Shelf Research,* 17**,** 1321-1365.

SLEIGH, P. A., GASKELL, P. H., BERZINS, M. & WRIGHT, N. G. 1998. An unstructured finite-volume algorithm for predicting flow in rivers and estuaries. *Computers & Fluids,* 27**,** 479-508.

SMITH, D. P., KVITEK, R., IAMPIETRO, P. J. & WONG, K. 2007. Twenty-nine months of geomorphic change in upper Monterey Canyon (2002–2005). *Marine Geology,* 236**,** 79-94.

SMITH, M. J. & CLARK, C. D. 2005. Methods for the visualization of digital elevation models for landform mapping. *Earth Surface Processes and Landforms,* 30**,** 885-900.

SMITH, M. J. & WISE, S. M. 2007. Problems of bias in mapping linear landforms from satellite imagery. *International Journal of Applied Earth Observation and Geoinformation,* 9**,** 65-78.

SONG, Y. & HAIDVOGEL, D. 1994. A Semi-implicit Ocean Circulation Model Using a Generalized Topography-Following Coordinate System. *Journal of Computational Physics,* 115**,** 228-244.

SOUZA, A. J., SIMPSON, J. H., HARIKRISHNAN, M. & MALARKEY, J. 2001. Flow structure and seasonalityin the Hebridean slope current. *Oceanologica Acta,* 24**,** 63-76.

STANEVA, J., STANEV, E. V., WOLFF, J.-O., BADEWIEN, T. H., REUTER, R., FLEMMING, B., BARTHOLOMÄ, A. & BOLDING, K. 2009. Hydrodynamics and sediment dynamics in the German Bight. A focus on observations and numerical modelling in the East Frisian Wadden Sea. *Continental Shelf Research,* 29**,** 302-319.

STEPHENS, D. & DIESING, M. 2014. A comparison of supervised classification methods for the prediction of substrate type using multibeam acoustic and legacy grain-size data. *PLoS One,* 9**,** e93950.

STOW, D. A. V., HERNANDEZ-MOLINA, F. J., LLAVE, E., SAYAGO-GIL, M., DIAZ DEL RIO, V. & BRANSON, A. 2009. Bedform-velocity matrix: The estimation of bottom current velocity from bedform observations. *Geology,* 37**,** 327-330.

SWIFT, D. J. P., PARKER, G., LANFREDI, N. W., PERILLO, G. & FIGGE, K. 1978. Shoreface-connected sand ridges on American and European shelves: A comparison. *Estuarine and Coastal Marine Science,* 7**,** 257-273.

SZPAK, M. T., MONTEYS, X., O'REILLY, S., SIMPSON, A. J., GARCIA, X., EVANS, R. L., ALLEN, C. C. R., MCNALLY, D. J., COURTIER-MURIAS, D. & KELLEHER, B. P. 2012. Geophysical and geochemical survey of a large marine pockmark on the Malin Shelf, Ireland. *Geochemistry, Geophysics, Geosystems,* 13**,** n/a-n/a.

TERWINDT, J. H. J. 1971. Sand waves in the southern bight of the North Sea. *Marine Geology,* 10**,** 51-67.

TERWINDT, J. H. J. & BROUWER, M. J. N. 1986. The behaviour of intertidal sandwaves during neap-spring tide cycles and the relevance for palaeoflow reconstructions. *Sedimentology,* 33**,** 1-31.

THIÉBOT, J., BAILLY DU BOIS, P. & GUILLOU, S. 2015. Numerical modeling of the effect of tidal stream turbines on the hydrodynamics and the sediment transport – Application to the Alderney Race (Raz Blanchard), France. *Renewable Energy,* 75**,** 356-365.

THORNE, P. D. & HANES, D. M. 2002. A review of acoustic measurement of small-scale sediment processes. *Continental Shelf Research,* 22**,** 603-632.

UEHARA, K., SCOURSE, J. D., HORSBURGH, K. J., LAMBECK, K. & PURCELL, A. P. 2006. Tidal evolution of the northwest European shelf seas from the Last Glacial Maximum to the present. *Journal of Geophysical Research,* 111.

VAN LANDEGHEM, K. J. J., BAAS, J. H., MITCHELL, N. C., WILCOCKSON, D. & WHEELER, A. J. 2012. Reversed sediment wave migration in the Irish Sea, NW Europe: A reappraisal of the validity of geometry-based predictive modelling and assumptions. *Marine Geology,* 295-298**,** 95-112.

VAN LANDEGHEM, K. J. J., UEHARA, K., WHEELER, A. J., MITCHELL, N. C. & SCOURSE, J. D. 2009a. Post-glacial sediment dynamics in the Irish Sea and sediment wave morphology: Data–model comparisons. *Continental Shelf Research,* 29**,** 1723-1736.

VAN LANDEGHEM, K. J. J., WHEELER, A. J., MITCHELL, N. C. & SUTTON, G. 2009b. Variations in sediment wave dimensions across the tidally dominated Irish Sea, NW Europe. *Marine Geology,* 263**,** 108-119.

VARELA, R. A. D., REGO, P. R., IGLESIAS, S. C. & SOBRINO, C. M. 2008. Automatic habitat classification methods based on satellite images: A practical assessment in the NW Iberia coastal mountains. *Environmental Monitoring and Assessment,* 144**,** 229-250.

VERFAILLIE, E., DOORNENBAL, P., MITCHELL, A. J., WHITE, J. & VAN LANCKER, V. 2007. The bathymetric position index (BPI) as a support tool for habitat mapping. . *Worked example for the MESH Final Guidance.*

.

WAKELIN, S. L., HOLT, J. T. & PROCTOR, R. 2008. The influence of initial conditions and open boundary conditions on shelf circulation in a 3D ocean-shelf model of the North East Atlantic. *Ocean Dynamics,* 59**,** 67-81.

WARD, S. L., NEILL, S. P., SCOURSE, J. D., BRADLEY, S. L. & UEHARA, K. 2016. Sensitivity of palaeotidal models of the northwest European shelf seas to glacial isostatic adjustment since the Last Glacial Maximum. *Quaternary Science Reviews,* 151**,** 198-211.

WARD, S. L., NEILL, S. P., VAN LANDEGHEM, K. J. J. & SCOURSE, J. D. 2015. Classifying seabed sediment type using simulated tidal-induced bed shear stress. *Marine Geology,* 367**,** 94-104.

WARNER, J. C., SHERWOOD, C. R., ARANGO, H. G. & SIGNELL, R. P. 2005. Performance of four turbulence closure models implemented using a generic length scale method. *Ocean Modelling,* 8**,** 81-113.

WEAVER, P. P. E., WYNN, R. B., KENYON, N. H. & EVANS, J. 2000. Continental margin sedimentation, with special reference to the north-east Atlantic margin. *Sedimentology,* 47**,** 239-256.

WESTLEY, K., QUINN, R., FORSYTHE, W., PLETS, R., BELL, T., BENETTI, S., MCGRATH, F. & ROBINSON, R. 2011. Mapping Submerged Landscapes Using Multibeam Bathymetric Data: a case study from the north coast of Ireland. *International Journal of Nautical Archaeology,* 40**,** 99-112.

WEWETZER, S. F. K. 1999. Side-scan sonar mapping of bedforms in the middle Tay Estuary, Scotland. *International Journal of Remote Sensing,* 20**,** 511-522.

WHITE, M. & BOWYER, P. 1997. The shelf-edge current north-west of Ireland. *Annales Geophysicae,* 15**,** 1076-1083.

WILCOCK, P. 1993. Critical shear stress of natural sediments. *Journal of Hydraulic Engineering,* 119**,** 491-505.

WILLIAMS, J. J., MACDONALD, N. J., O'CONNOR, B. A. & PAN, S. 2000. Offshore sand bank dynamics. *Journal of Marine Systems,* 24**,** 153-173.

WRIGHT, D. J., PENDLETON, M., BOULWARE, J., WALBRIDGE, S., GERLT, B., ESLINGER, D., SAMPSON, D. & HUNTLEY, E. 2012. ArcGIS Benthic Terrain Modeler (BTM), v. 3.0. *Environmental Systems Research Institute, NOAA Coastal Services Center, Massachusetts Office of Coastal Zone Management. Available online at http://esriurl.com/5754.*

WU, Y., CHAFFEY, J., GREENBERG, D. A., COLBO, K. & SMITH, P. C. 2011. Tidally-induced sediment transport patterns in the upper Bay of Fundy: A numerical study. *Continental Shelf Research,* 31**,** 2041-2053.

WWW.GSISEABED.IE. *Irish National Seabed Survey - Mapping the Irish Seabed* [Online]. [Accessed January 2016].

WWW.INFOMAR.IE. 2016. *INtegrated Mapping FOr the Sustainable Development of Ireland's MArine Resource* [Online]. [Accessed January 2016].

WYNN, R. B. & STOW, D. A. V. 2002. Classification and characterisation of deep-water sediment waves. *Marine Geology,* 192**,** 7-22.

XING, J. & DAVIES, A. M. 1996. A numerical model of the long term flow along the Malin-Hebrides shelf. *Journal of Marine Systems,* 8**,** 191-218.

XING, J. & DAVIES, A. M. 1998. A three-dimensional model of internal tides on the Malin-Hebrides shelf and shelf edge. *Journal of Geophysical Research,* 103**,** 27821.

XING, J. & DAVIES, A. M. 2001. The influence of shelf edge flows and wind upon the circulation on the Malin Shelf and in the Irish Sea. *Continental Shelf Research,* 21**,** 21-45.

XU, J., LI, G., DONG, P. & SHI, J. 2010. Bedform evolution around a submarine pipeline and its effects on wave-induced forces under regular waves. *Ocean Engineering,* 37**,** 304-313.

XU, J. P., WONG, F. L., KVITEK, R., SMITH, D. P. & PAULL, C. K. 2008. Sandwave migration in Monterey Submarine Canyon, Central California. *Marine Geology,* 248**,** 193-212.

XU, W., MILLER, P. I., QUARTLY, G. D. & PINGREE, R. D. 2015. Seasonality and interannual variability of the European Slope Current from 20years of altimeter data compared with in situ measurements. *Remote Sensing of Environment,* 162**,** 196-207.

YOUNG, E. F., ALDRIDGE, J. N. & BROWN, J. 2000. Development and validation of a three-dimensional curvilinear model for the study of fluxes through the North Channel of the Irish Sea. *Continental Shelf Research,* 20**,** 997-1035.

YOUNG, E. F., MEREDITH, M. P., MURPHY, E. J. & CARVALHO, G. R. 2011. High-resolution modelling of the shelf and open ocean adjacent to South Georgia, Southern Ocean. *Deep Sea Research Part II: Topical Studies in Oceanography,* 58**,** 1540-1552.

ZACHARIOUDAKI, A., PAN, S., SIMMONDS, D., MAGAR, V. & REEVE, D. E. 2011. Future wave climate over the west-European shelf seas. *Ocean Dynamics,* 61**,** 807-827.

ZANUTTIGH, B. 2007. Numerical modelling of the morphological response induced by low-crested structures in Lido di Dante, Italy. *Coastal Engineering,* 54**,** 31-47.

ZHU, Y. & CHANG, R. 2000. Preliminary Study of the Dynamic Origin of the Distribution Pattern of Bottom Sediments on the Continental Shelves of the Bohai Sea, Yellow Sea and East China Sea. *Estuarine, Coastal and Shelf Science,* 51**,** 663-680.

Appendix 1 - Modern Bedform and Sediment Distribution on the North West Irish Shelf

Presented at 56th Irish Geological Research Meeting 2013, Derry.

Will Evans[1]*, Sara Benetti[1], Derek Jackson[1], Xavier Monteys[2].

[1]School of Environmental Sciences, University of Ulster, Coleraine, United Kingdom

[2]Geological Survey of Ireland, Beggars Bush, Dublin, Ireland

The NW Irish shelf has undergone intensive surveying in recent years. Multibeam echosounder data, gathered as part of the Marine Institute's Irish National Seabed Survey (INSS - http://www.gsiseabed.ie) has revealed bedforms of diverse size and structure. Some of these bedforms may be interpreted as glacial structures associated with the advance and retreat of the British Irish Ice Sheet while others present geomorphlogy associated with more modern marine environments. Backscatter images also present in this data set allow interpretation of not just morphology but also the surface sediments of which these bedforms are comprised. Extensive ground truthing samples taken as part of the INSS survey and on other research cruises in the area, allow these backscatter images to be calibrated to enable mapping of shelf sediments on a large scale, but at high resolution. This poster displays charts illustrating the location and geomorphology of the aforementioned modern sediments. Backscatter classification has been carried and calibrated with the Geological Survey of Ireland's sediment database to present a shelf wide sediment map. Probable relationships between sediment distribution, modern and glacial bedforms are also discussed.

Modern Bedform and Sediment Distribution on the Northwest Irish Shelf

Will Evans[1], Sara Benetti[1], Derek Jackson[1], Xavier Moneys[2], Kieran Lyons[3]
[1]University of Ulster; [2]Geological Survey of Ireland; [3]Marine Institute

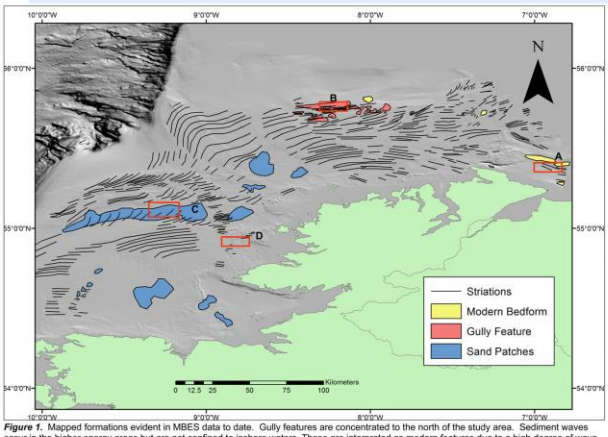

Figure 1. Mapped formations evident in MBES data to date. Gully features are concentrated to the north of the study area. Sediment waves occur in the higher energy areas but are not confined to inshore waters. These are interpreted as modern features due to a high degree of wave asymmetry. Sand patches are evident throughout much of the study area, typically in lower energy environments. Striations were mapped to allow possible correlation between surface sediment streaks and any modelled current data. All features are in depths between 30m and 180m. Case Study locations are also shown .

Introduction

The northwest area of the Irish Shelf has undergone intensive surveying in recent years. Multibeam echosounder data gathered as part of the Irish National Seabed Survey (INSS) has revealed bedforms of diverse size and structure. Some of these bedforms may be interpreted as glacial structures associated with the advance and retreat of the British Irish Ice Sheet. The focus of this study however is the formations which present characteristics associated with a more modern marine environment.

Applications

- Habitat Mapping
- Fisheries Management / Spawning Grounds
- Maritime Archaeology Site Management
- Coastal and Offshore Engineering
- Marine Renewable Site Selection

Data Sets

- Irish National Seabed Survey (INSS) Multibeam Echosounder Data (MBES)
- Geological Survey of Ireland (GSI) Sedimentary Records Database
- Marine Institute Regional Ocean Modelling System (ROMS) outputs as annual peak bottom velocities (m/s)

Methodology

- MBES Data was interrogated using IVS Fledermaus 3D using a variety of azimuths and shading.
- Features were then mapped using ESRI ArcGIS 10.
- Regional Ocean Modelling System (ROMS) model data was processed using MATLAB and plotted using ESRI ArcGIS 10.

Case Studies

A - Sediment Waves; B - Gully Features; C - Sand Patches;
D - Scouring at an object

All case study images were gathered using IVS Fledermaus 3D, with an azimuth of 315 and an elevation of 45. A vertical exaggeration of 6 was used.

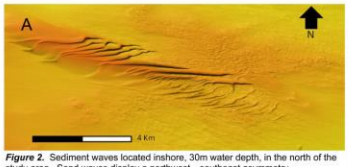

Figure 2. Sediment waves located inshore, 30m water depth, in the north of the study area. Sand waves display a northwest—southeast asymmetry. Wavelengths range from 400m to 200m and the largest wave displays an amplitude of 20m. Such bedforms are expected in these shallower water depths with increased current flow

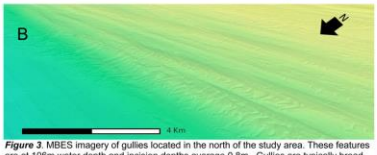

Figure 3. MBES imagery of gullies located in the north of the study area. These features are at 106m water depth and incision depths average 0.8m. Gullies are typically broad at the head, narrowing down-slope and in some instances closing out. Feature orientation is perpendicular to the direction of the dominant flow in the area (see ***Figure 6***.

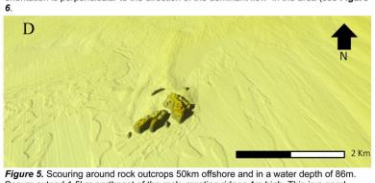

Figure 5. Scouring around rock outcrops 50km offshore and in a water depth of 86m. Scours extend 1.5km northeast of the rock, creating ridges 4m high. This is a good indicator of sediment mobility in the area and correlates well with observed bedforms and modelled flow rates in the area (see ***Figure 6***).

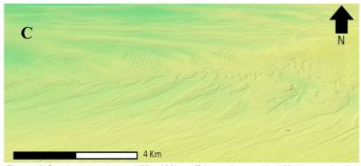

Figure 4. Sand patches located 75—100km offshore. Located in 100m water depth, these patches are up to 1m thick, the largest of which is 1km wide. Belderson (1982) suggested these formations are generated by low energy conditions with a peak flow of around 0.5m/s.

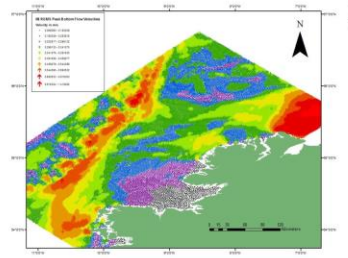

Figure 6. Peak bottom flow velocities simulated by the Marine Institute ROMS model. Note the north running current along the shelf break. Velocities correlate well with sediment striations mapped in ***Figure 1***. Highest energies (1.4 m/s) are recorded in the areas surrounding ***Figure 2***. This model is validated by tidal gauges, satellite imagery and Argos floats on a regular basis.

Future Work

- Complete mapping of remaining features evident in INSS multibeam data.
- Mosaic of backscatter data for entire study area.
- Classification of backscatter data using GSI sediment database as ground truthing.
- Integration of this sediment chart into a hydrodynamic model to enhance accuracy of sediment transport simulation.
- Run model simulations using DHI MIKE to gauge sediment mobility across the Northwest Irish Shelf.

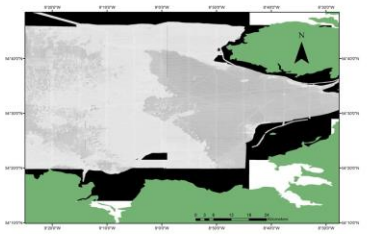

Figure 7. Backscatter imagery of Donegal Bay. The greyscale presents different levels in hardness of surface sediment. Backscatter can be calibrated using sediment samples to create a sediment distribution chart.

References

Belderson, R.H., Johnson, M.A., Kenyon, N.H., 1982. Bedforms. In: Stride, A.H. (Ed.), Offshore Tidal Sands; Processes and Deposits. Chapman & Hall, London, pp. 27–58

Appendix 2 – Erosional and Depositional Features on the northwest Irish shelf.

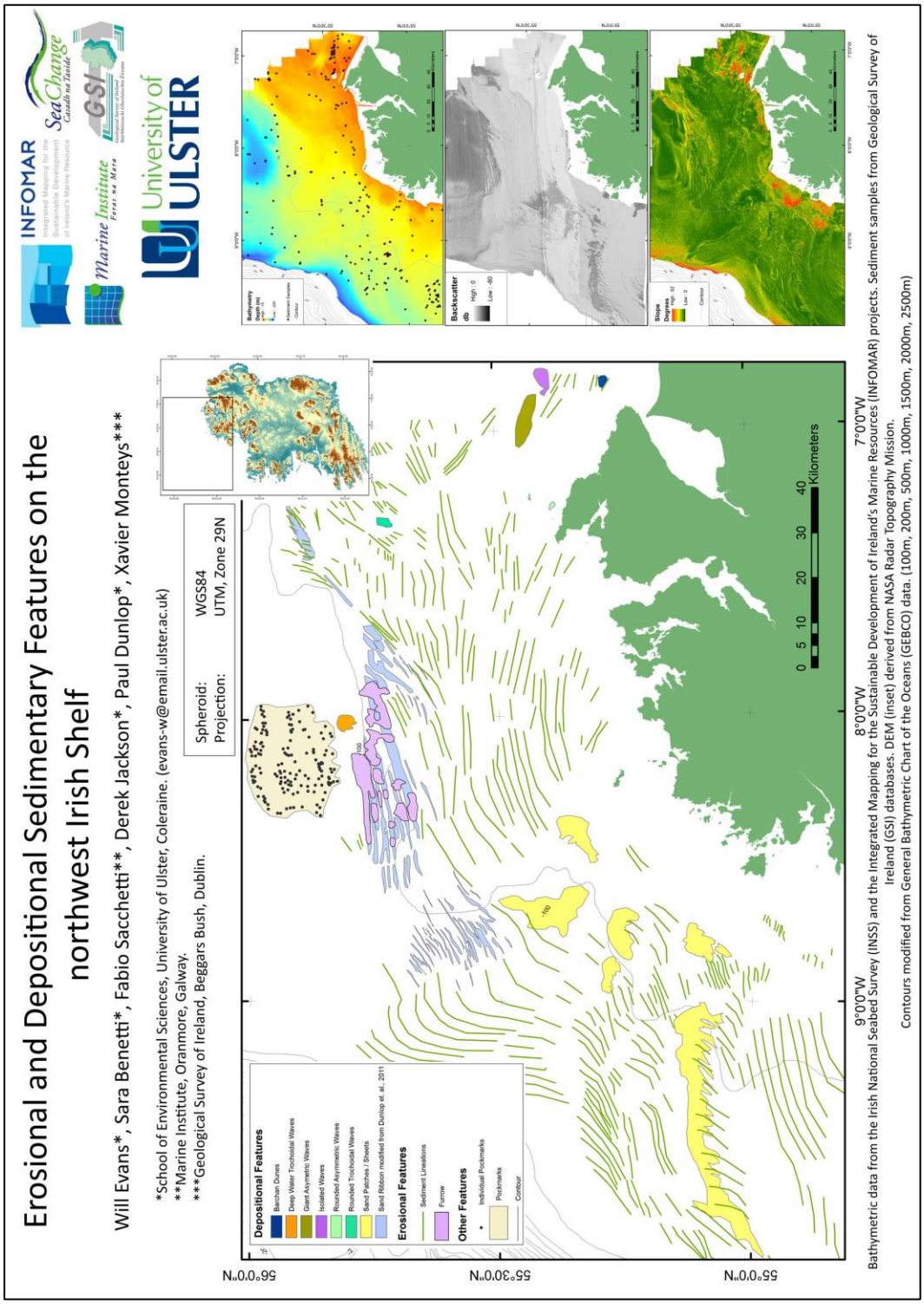

Appendix 3 – Observation of bathymetric change using time-separated MBES surveys on the north Irish shelf

Observation of bathymetric change using time-separated multibeam bathymetric surveys on the north Irish shelf

Will Evans[1], Sara Benetti[1], Fabio Sacchetti[2], Derek Jackson[1].
[1]University of Ulster, Coleraine, Northern Ireland. [2]Marine Institute, Galway, Ireland.

Spheroid : WGS84
Projection : UTM, Zone 29N

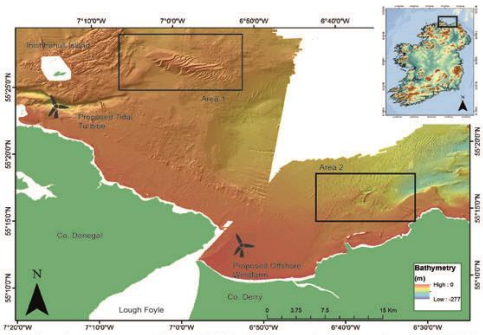

Overview of areas resurveyed aboard R.V. Celtic Voyager during research cruise CV13030. Proposed marine renewable energy sites are illustrated. Bathymetry data processed using Caris Hips and exported to ESRI ArcGIS v10.1 for data set integration.

Inset DEM derived from Shuttle Radar Topography Mission

Repeat multibeam as a means to measure sediment transport.

Applications for:
- Fisheries Management
- Dredge Disposal
- Shipwreck Management

Special relevance to offshore engineering on north Irish shelf:
- Marine Cables
- Proposed Marine Renewables

Existing high-resolution multibeam data sets:
- Irish National Seabed Survey (INSS, 2004).
- Joint Irish Bathymetric Survey (JIBS, 2007).

R.V. Celtic Voyager used for research survey CV13030. A SIMRAD EM3002 system was used to collect bathymetric data. On board systems compenstated fully for heave, roll and pitch. DGPS navigation was used for high location accuracy.

(www.marine.ie)

Methodology

- Acoustic survey aboard R.V. Celtic Voyager to collect repeat high-resolution multibeam data.
- Area 1 - INSS data represents 10 year time separation.
- Area 2 - JIBS data represents 7 year time lapse
- All data corrected and processed using Caris Hips.
- Surface difference between surveys (vertical) calculated using Caris Base Editor.
- Bedform crests digitised for each survey and displacement distance / direction calculated in ESRI ArcGIS V10.1.

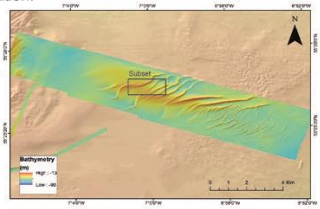

Area 1 survey data from CV13030, processed in Caris Hips (49 Km^2). Sand waves reach amplitudes of 20m with crests extending for up to 5km. Bedrock was included to provided datum for survey comparison. Crest displacement subset location shown.

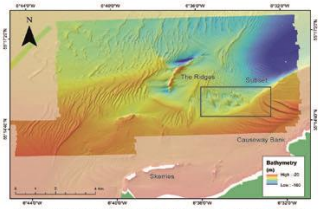

Area 2 data (83 Km^2) displays a wide range of bedform types including three, 18m amplitude trochoidal waves. 'The Ridges' rock outcrops provided datum for data comparison. Location of surface difference subset also illustrated.

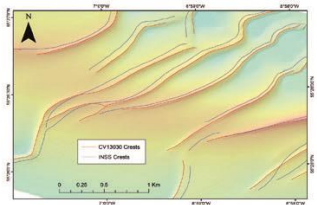

Digitised crest displacement between INSS and CV13030 surveys allowing bedform migration to be measured.

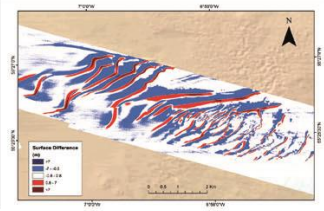

Area 1 Surface difference analysis carried out using Caris Base Editor. Areas of erosion (blue) with accretion (red) to the SE suggests wave migration in this direction.

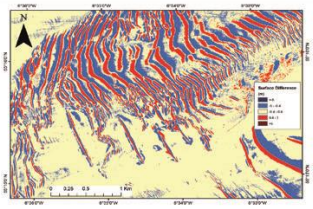

Area 2 surface difference analysis is more complex. Significant change is recorded in sequences consistent with bedform migration, though directionality varies across the region resurveyed. A net decrease in surface elevation is also measured.

Results

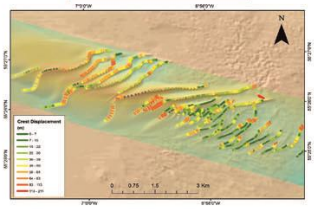

Example of measured crest displacement across Area 1. 70m crest migration is recorded over the large sandwaves to the NW. One barchan dune (NE) shows migration of +200m. Avg. displacement over 10 year lapse is 32m.

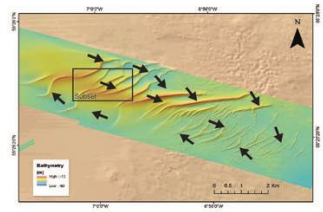

Area 1. Direction of sediment migration as indicated by crest displacement and surface difference calculations. A clockwise circulatory movement is suggested, possibly influenced by Inishtrahull Island to the west.

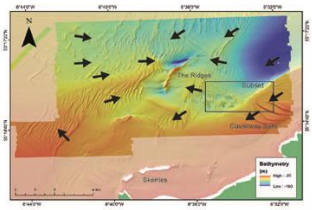

Area 2. 'The Ridges' rock outcrop appears to separate two differing sediment transport patterns, with an easterly movement to the N and W. Further inshore and to the E of the ridge, migration is orientated to the W and SW.

The north Irish shelf has undergone intensive surveying in recent years. Multibeam echosounder data gathered as part of the Irish National Seabed Survey (2004) and the Joint Irish Bathymetric Survey (2007) have revealed bedforms of diverse size and structure. How these bedforms migrate across the seafloor has implications for the siting of marine renewable installations, routing of cables, preservation of maritime archaeology and marine habitat designations. Repeat multibeam surveys are a useful method to monitor this migration over time as differences between successive surveys can indicate transport rate and direction of sediments. In 2013, 158km^2 of seafloor on the north Irish shelf was resurveyed using multibeam echosounder, seismics and sediment sampling techniques. Areas resurveyed were selected based on proximity to proposed marine renewable sites and Special Areas of Conservation, as well as displaying variety of bedform type. This poster presents differences in seabed morphology between this survey and previous mapping programs resulting in time-lapse data of between 7 and 9 years. Caris Hips & Sips 7.1 was used to create surface difference charts, indicating overall sediment flux and any change in the amplitudes of bedforms observed. ESRI ArcGIS 10.1 was then used to digitise and measure movement of bedform crestlines to generate a chart indicating rate and direction of migration. The magnitude and possible implications of this movement, are discussed.

Appendix 4 – CV13030 Shiptime Report

National Research Vessels

SHIP-TIME PROGRAMME

Survey Code:	Survey Name:	Chief Scientist/ Institution
CV13030	Sediment Transport Assessment, Irish North Coast	Will Evans, University of Ulster

Section A: Award Summary

Title of Research Survey and Survey Code:	Sediment Transport Assessment, Irish North Coast CV13030	
Co-Ordinator/ Chief Scientist:	Will Evans	
Vessel used for ship-time:	*RV Celtic Voyager* ☒ *RV Celtic Explorer* ☐	
Total number of days at sea:	5 Days	
Total number of grant-aided ship-time days awarded:	5 Days	
Dates of survey:	27/09/13 – 01/10/13	
Mobilisation/Demobilisation Ports	Rathmullan / Lisahally	
Survey Personnel:	*No. of Scientists* *3*	*No. of Students* *2*
Final Report Completed by:	Will Evans	**Date**: 20/10/13

Section B: Description of the Research Survey

B1 Overview of survey personnel

Names	***Institute/ Department/ Course***	***Position (undergraduate/ post graduate etc)***	***Number of Days***
Scientists			
Will Evans	***University of Ulster***	***Postgraduate***	***5***
Fabio Sacchetti	***Marine Institute***	***Postdoctorate***	***5***
Jay Calvert	***University of Ulster***	***Postgraduate***	***5***
Students			
Stephen Ramsay	***University of Ulster***	***Undergraduate***	***5***
James Burns	***University of Ulster***	***Undergraduate***	***5***

B2 Objectives

Briefly outline the overall objectives of the research survey.
Please state if objectives have changed from the original proposal. If survey included a training element please outline clearly.

Recent programmes in Irish coastal waters such as Irish National Seabed Survey (INSS), Integrated Mapping For the Sustained Development of Ireland's Marine Resources (INFOMAR) and Joint Irish Bathymetry Survey (JIBS) have created very high-resolution data sets which have revealed a wide variety of sedimentary bedforms. These bedforms typically display geometrical characteristics consistent with migration. Multibeam Echosounder (MBES) data, while excellent at detailing these geometrics at high accuracy, can only provide a single snapshot of bathymetry. The result is that any rate or direction of migration can only be assumed. The relationship between these geometric characteristics and rates of migration have been increasingly contested in recent years based on evidence from time-lapse surveys. Given the high diversity and density of bedform types, high energy hydrodynamic regime and multi-disciplinary interest, the JIBS / INSS data sets present an excellent opportunity to carry out sediment transport assessment via repeat MBES surveys.

The main aim of this survey was to assess sediment transport in four selected areas based on significant changes in bathymetry. Repeat survey of these areas should allow the conventional relationship between bedform asymmetry and migration direction to be tested. It is hoped that the data collected as part of this cruise will increase knowledge of sediment pathways on the shelf and sediment budget for sections of coastline.

In line with recommendations made by Marine Institute as part of the shiptime application review process, a benthic biology assessment was also included in the survey. As such, fauna >1mm were removed from the sediment and preserved for further classification. This data will be used to further understanding of benthic, faunal biodiversity and distribution across a range of depths and sediment types.

Two students on board received training in treatment and processing of sediment and benthic ecology samples. Fabio Sacchetti also provided instruction in the operation of multibeam, pinger and castaway Conductivity Temperature Density (CTD) systems.

Specific objectives of the survey were:

- To repeat MBES surveys in selected areas of the JIBS and INSS data sets for evidence of bathymetric change.
- To relate any change in bathymetry to potential sediment transport with emphasis on the migration of sandwaves.
- To ground truth MBES data using sediment grabs to aid classification of backscatter data. This will also supplement the low-resolution sediment data in the area.
- To collect biological information to accompany the new sediment and bathymetric data.
- To provide multidisciplinary training for undergraduate students.

B3 Overview of research survey

Provide a narrative overview of the research survey including survey timelines
The information provided in this section should not exceed 5 pages (excluding tables and maps)

27th October

11:15 Scientific party arrived Rathmullan. Cores from CV13031 were removed for transit to University of Ulster Coleraine. **11:45** Safety brief and lunch followed by muster. **13:15** Depart Rathmullan. After discussion with the Captain, the decision was made to survey sites 3 + 4 (see Fig.1), then proceed into UK waters. This decision was designed to reduce transit times and to take into account increasing weather conditions in the forecast. **16:00** Arrival at first sediment sampling station (1/13, Area 3). Weather condtions were favourable and the Day Grab was deployed. **16:45** Final sediment sample of the day carried out (3/13, Area 3). **17:05** MBES and Pinger initiated for Area 3, beginning with a soft start. **17:15** R.V. Celtic Voyager fouled on fishing gear. MBES + Pinger stopped. **17:50** Foul cleared and MBES + Pinger resumed. **19:30** Decision made to move to Area 4 due to

prevalence of fishing gear with excessively long, floating lines. Plan to return and survey Area 3 in hours of daylight. **20:00** Multibeam + Pinger initiated Area 4.

28th October

11:30 MBES + Pinger operations ceased. Acoustic survey of Area 4 completed. **12:00** On station for sediment sample (1/17, Area 4). The decision was made to continue with sampling with the Day Grab given the good recoveries made on the 27th. **16:30** Final sediment sample of the day taken, (17/17, Area 4). **16:45** Transit to Area 3. **17:30** MBES + Pinger started. Areas with fishing gear surveyed first (daylight hours) to reduce risk of fouling on long floating lines.

29th October

09:30 MBES + Pinger operations ceased. Acoustic survey of Area 3 complete. Some small gaps remained in MBES to be filled before transit to UK waters. **10:15** On station (4/14, Area 3), continued use of Day Grab for sediment sampling. **11:10** Final sediment sample taken for Area 3 (13/13**). 11:10** Gaps in MBES data filled. **11:30** Transit to Area 2 in UK waters. **14:00** Arrive Area 2 at first sediment sample location (1/46). **16:30** Final sediment sample of the day (9/46). **16:30** After discussion with the Captain, survey Areas 1 & 2 were joined into one continuous survey area. This not only increased MBES coverage for the area but also created longer, straight survey lines resulting in less complicated navigation. **16:40** MBES + Pinger operations started on the furthest offshore survey lines due to gradually increasing weather conditions forecast for the remainder of the cruise.

30th October

09:00 MBES + Pinger operations ceased. **09:30** On station for Day Grab sample (10/46). **16:30** Sediment sampling operations finished for the day (38/46). Day Grab performed excellently across a wide variety of depths and sediment types, despite increasing weather conditions. Crew and scientists worked well together to sample these 28 sites (with occasional repeat sampling). **16:35** MBES + Pinger resumed.

1st November

10:00 MBES + Pinger operations ceased. Acoustic survey of Areas 1 + 2 (merged) complete. **10:45** On station for Day Grab (39/46). **11:00** Final sediment sample recovered (46/46) and began transit to Lisahally. **13:30** Arrive Lisahally. **15:00** Full Demob and departure of scientists.

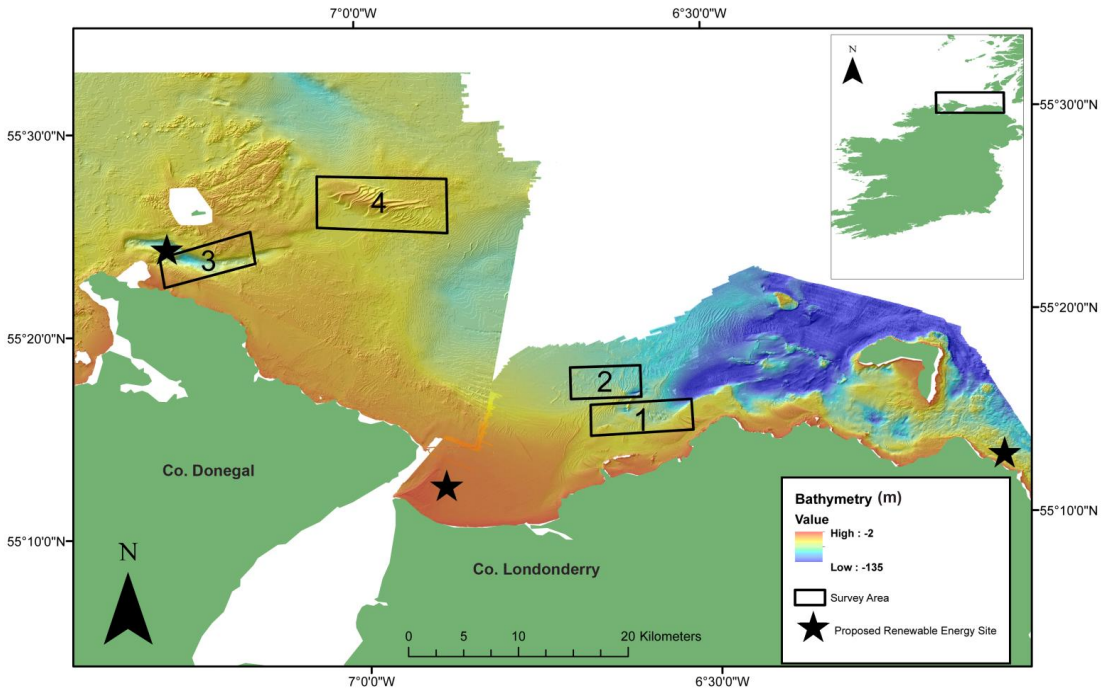

Fig.1 Outline of proposed survey areas and proximity to proposed renewable energy sites.

B4 Benefits, impact and contribution of the outputs to marine research and the marine sector in general.

Outline clearly the specific outcomes and benefits of the research survey.
The information provided in this section should not exceed 1/2 page (excluding tables and maps)

Several benefits to the survey results are predicted. While the majority of data has yet to be processed several potential impacts have been identified based on themes.

Publications

The data collected as part of this research cruise is expected to form the basis for at least one peer-reviewed article in an international journal as part of a PhD project in sediment transport (Will Evans). Repeat MBES survey across such a large area and range of sediment wave types is uncommon in scientific literature. It is hoped that the processed data will provide a novel insight into shelf sediment transport potential. Benthic ecology data collected is also expected to feed into a second PhD (Jay Calvert) examining faunal communities across different acoustic backscatter ranges, again, with peer reviewed publications.

Marine Renewables and Offshore Engineering

Knowledge of sediment mobility is highly important when considering any marine engineering. Mobile sediments can cause erosion or accretion of sediments against installations, potential reducing structural integrity. Not only is the main harnessing equipment such as a tidal turbine or wind turbine base to be considered, but also associated cables and anchors. Increased knowledge of volumes and rates of

sediment flux generated by this survey may further inform the decision-making processes for the proposed tidal energy site at Inishtrahull and the proposed wind turbine site at Tuns Bank (Fig.1). Early analysis of the Inishtrahull Sound area suggests that inshore sediment waves appear to be mobile, with new waves apparent in the cruise data that did not exist at the time of the JIBS survey (Fig.3).

Hydrodynamic Model

Due to the high costs of conventional analysis of sediment mobility (repeat survey, seabed landers, moored equipment), hydrodynamic models are being utilised to great effect with widespread applications. Such models can also support arguments for sediment mobility derived from geomorphological features observed in MBES or backscatter data sets. One of the most common of these is bedform asymmetry evident in sand waves. A hydrodynamic model has been developed by Will Evans as part of his PhD project on sediment transport. Backscatter and ground-truthing data from this survey will be combined to produce a roughness chart which will provide an important input into this model. This input will allow the sediment transport module within the software to more accurately simulate bed stresses across the shelf, allowing for forecasting of probable sediment mobility. This has multiple applications including habitat mapping, and wreck site management. Three proposed marine renewable sites are located within the boundaries of this hydrodynamic model, including two tidal turbine sites. Knowledge of bed stresses not only within the boundaries of these sites, but also the extended region around them may provide insight into the long-term viability of engineering installations. Ultimately this combined approach of computational analysis and site resurvey may form the basis of a common research strategy for management of sediment on a shelf-wide scale.

Coastal Zone Management

Bathymetric difference models generated from MBES repeat survey will indicate trends in sediment budget for the selected areas of the north Irish Shelf. This is of particular importance for Areas 1 & 2**,** where good coastal zone management is becoming increasingly vital due to the high economic reliance on tourism attracted by beaches and watersports. Knowledge of sediment budget offshore may influence management of beaches, hard and soft coastal defences and future aggregate extraction licensing. This relates directly to several 'Environmental Impacts' outlined in the MI Sea Change Strategy including environmental management planning. An increase in marine tourism was also identified as a target under the strategies 'Economic Impacts'.

Other Impacts

Data acquired as part of this cruise may be used for future research in other disciplines. The Irish North Coast has an abundance of wreck sites and areas of interest to maritime archaeology. Knowledge of sediment accretion or erosion may influence wreck site management or future survey design.

Seafloor substrate type, mobility and hydrodynamic conditions are all key components in defining a marine habitat. Data from this cruise may affect the validity of previous habitat mapping carried out as part of the European Habitat Mapping Directive. This is of particular importance given that much of the MBES and sedimentary data collected in Area 1 is within the candidate Special Area of Conservation (cSAC) 'Skerries and Causeway'. The combination of significantly

improved backscatter data and density of sediment samples will allow substrate maps for the area to be improved. Biological sampling within the area also presents a suite data with which to further inform any special designations attached to this area of conservation.

Future Scientists

It is envisaged that the data sets collected as part of this cruise will be utilised for teaching at University of Ulster. Acoustic and sedimentary data is directly applicable to modules in seafloor mapping, GIS training and data set integration and as part of dissertation projects. Biological samples will be stored to provide a catalog of marine invertebrates available for student training in identification techniques.

B5 Data

Provide a description of the data collected from the research survey, the usage of the data and how it will be stored.
The information provided in this section should not exceed 1/2 page (excluding tables and maps)

Multibeam Data

The primary objective of the research cruise was to carry out repeat MBES surveys over selected areas. These areas were chosen based on proximity to marine renewable energy sites, sediment transport potential and previous repeat survey coverage. Before initiating any of the acoustic surveying equipment aboard, a soft start was carried out, in line with the recommendations made during the JNCC review process. A total of 157.47 km^2 repeat MBES coverage was achieved, exceeding the objectives outlined in the original shiptime application. Some 5 km^2 of this had previously been resurveyed as part of University of Ulster student training cruises in 2009 and 2010 (Fig.4). The result is excellent repeat coverage in key areas of INSS and JIBS data on the Irish North Coast. This data will be compared to earlier MBES surveys and surface difference analysis carried out. This process is aided by the inclusion of datum objects, such as bedrock, within the survey design which allow multiple data sets to be compared more accurately. Sediment wave crestlines will be mapped and compared to those identified as part of previous research, allowing some inferences to be made as to sediment transport in the horizontal as well as the vertical. This data will form part of at least one peer reviewed article and will provide a significant component of the PhD thesis of Will Evans.

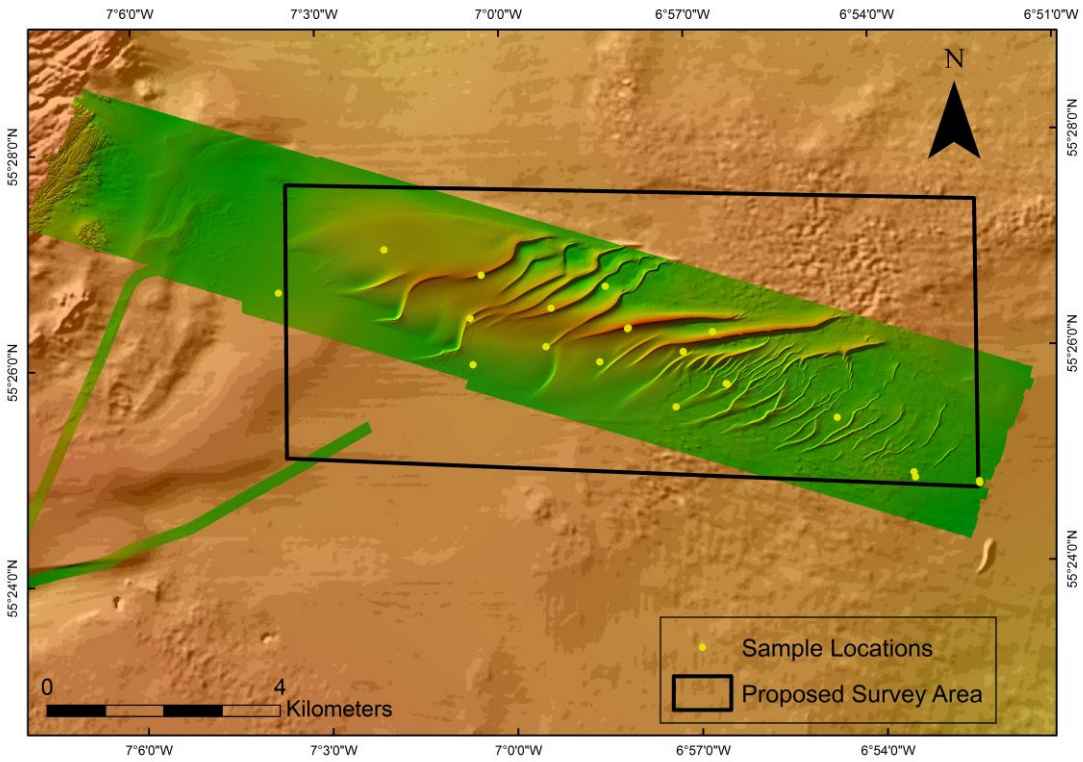

Fig.2 Area 4, large offshore sandwaves. Area of survey was adjusted from original proposal to improve coverage of the bedform.

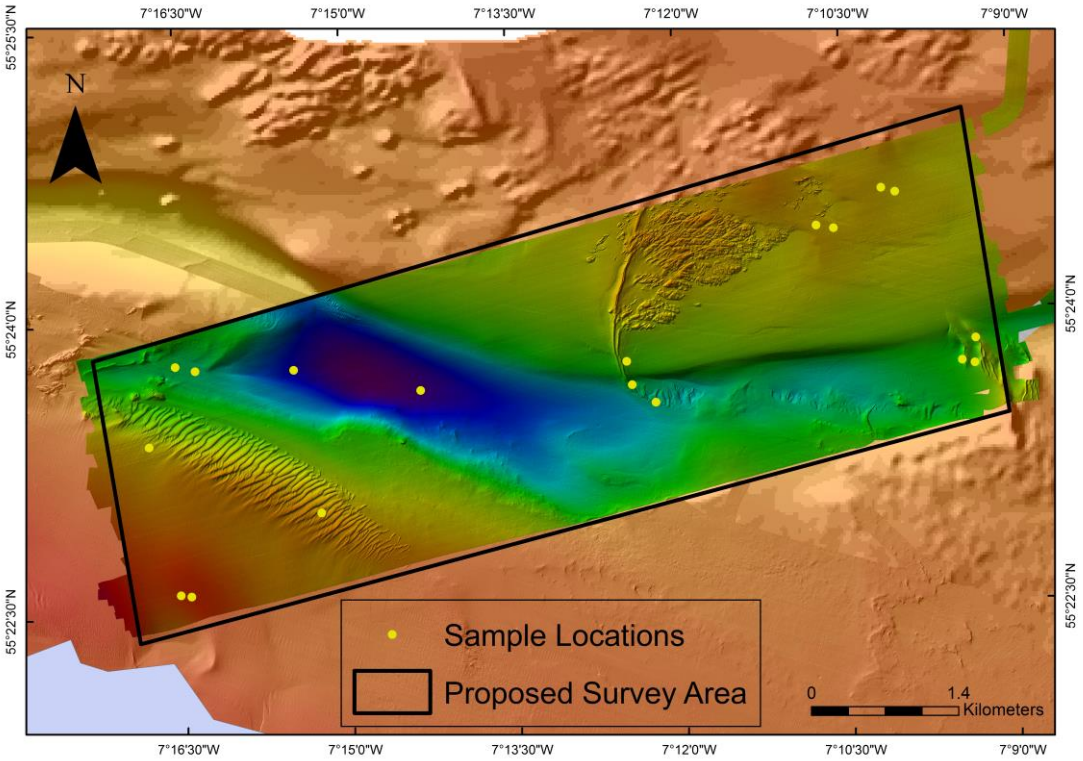

Fig.3 Area 3, Inishtrahull Sound MBES coverage.

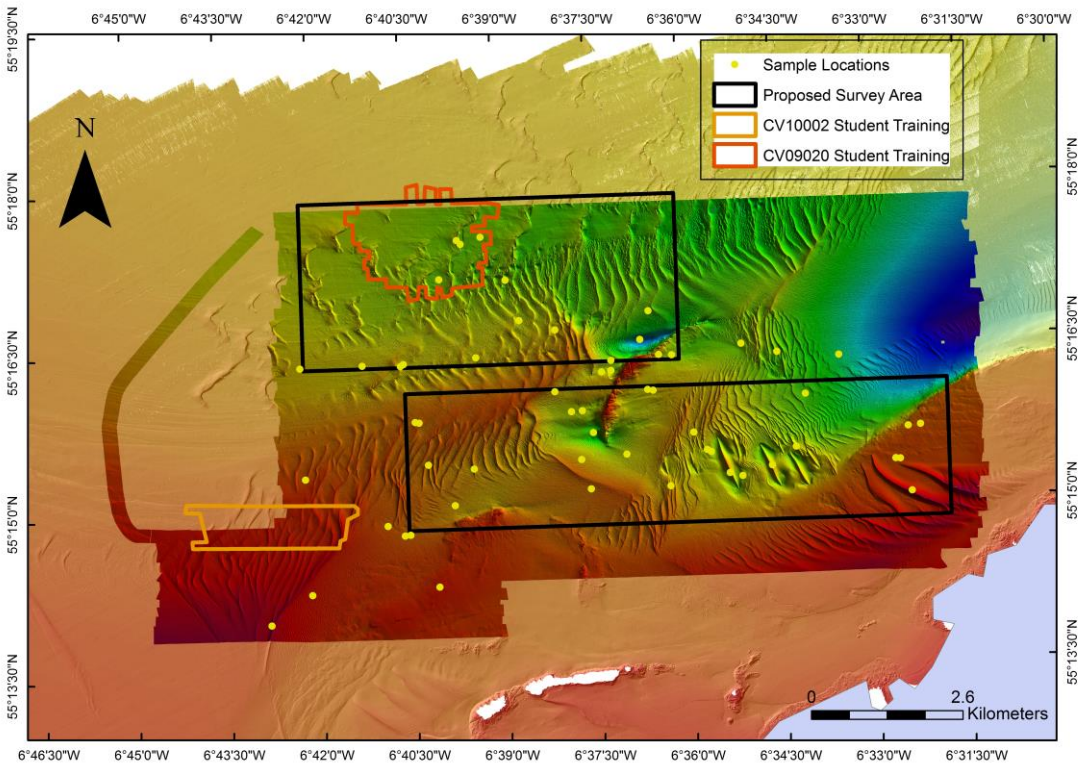

Fig.4 MBES coverage and sediment sample locations in the JIBS data (Areas 3 + 4). The survey area differs greatly from the original proposal. Previously resurvey locations are boxed Red (2010) and Orange (2009)

Backscatter

The backscatter data collected simutaneously with bathymetric data allows important inferences to be made as to the composition of surface sediments in the surveyed areas. Sediment samples acquired will be used to ground truth this data, allowing similar backscatter responsed to be classifed by sediment type. This backscatter classification chart will have numerous applications, initally forming a key dataset for a journal article assessing the variation and migration rates of bedforms and how these may relate to substrate type. Further to this, sediment distribution will form a seabed roughness input for the hydrodynamic model of the area, enabling more accurate simulation of bed stresses. This data will be stored digitally at University of Ulster.

Sediment Samples

Throughout the duration of the cruise, the Day Grab was used for sediment sampling. Processed backscatter data was used to target sample sites on areas of differing backscatter response (see Figs. 2, 3, 4). This in turn will enable more accurate mapping of backscatter classification and sediment distribution. 92 attempts were made with the Day Grab with 14 'no recovery' sites. The equipment performed excellently given the range of sediment types sampled.

Station	Equipment	Longitude	Latitude	Depth
IT 1	Day Grab	-7°16'47.44"	55°23'22.70"	36m
IT 2	Day Grab	-7°15'15.22"	55 23'1.36"	32m
IT 3	Day Grab	-7°12'13.38"	55°23'32.88"	60m
IT 4	Day Grab	-7°10'1.45"	55°24'35.94"	35.5m
IT 4A	Day Grab	-7°10'8.92"	55°24'37.29"	34.5m
IT 5	Day Grab	-7°10'35.12"	55°24'25.17"	33.7m
IT 5A	Day Grab	-7°10'44.44"	55°24'26.18"	33.5m
IT 6	Day Grab	-7°9'19.80"	55°23'50.43"	42.8m
IT 7	Day Grab	-7°9'20.62"	55°23'42.73"	47.3m
IT 7A	Day Grab	-7°9'27.37"	55°23'43.67"	48.2m
IT 8	Day Grab	-7°12'25.88"	55°23'38.45"	58.7m
IT 9	Day Grab	-7°12'28.57"	55°23'45.66"	46.1m
IT 10	Day Grab	-7°14'20.15"	55°23'38.30"	87.7m
IT 11	Day Grab	-7°15'28.45"	55°23'45.51"	81.2m
IT 12	Day Grab	-7°16'21.66"	55°23'45.85"	60.3m
IT 12A	Day Grab	-7°16'32.41"	55°23'47.26"	58m
IT 13	Day Grab	-7°16'26.45"	55°22'36.44"	21.7m
IT 13A	Day Grab	-7°16'32.11"	55°22'36.91"	22.1m
NI 1	Day Grab	-6°39'56.67"	55°17'8.91"	78.9m
NI 2	Day Grab	-6°38'5.58"	55°16'38.85"	64.5m
NI 3	Day Grab	-6°37'12.11"	55°16'20.91"	74.4m
NI 4	Day Grab	-6°36'37.43"	55°16'4.03"	63.7m
NI 4A	Day Grab	-6°36'32.01"	55°16'3.55"	64.8m
NI 5	Day Grab	-6°35'54.03"	55°15'39.44"	58.8m
NI 6	Day Grab	-6°35'37.42"	55°15'28.28"	69.4M
NI 6A	Day Grab	-6°35'41.30"	55°15'29.52"	68.6M
NI 7	Day Grab	-6°35'19.96"	55°15'16.34"	52.6M
NI 8	Day Grab	-6°42'14.56"	55°16'21.73"	62.9m
NI 9	Day Grab	-6°41'14.01"	55°16'22.20"	63.6m
NI 10	Day Grab	-6°40'33.88"	55°16'22.42"	64.2m
NI 10A	Day Grab	-6°40'36.84"	55°16'21.34"	64.1m
NI 11	Day Grab	-6°39'23.33"	55°16'24.83"	63.9m
NI 12	Day Grab	-6°40'20.41"	55°15'49.51"	47.5m
NI 12A	Day Grab	-6°40'24.17"	55°15'49.96"	47.8m
NI 13	Day Grab	-6°42'12.57"	55°15'19.96"	42.7m
NI 14	Day Grab	-6°40'53.78"	55°14'52.68"	46.6m
NI 15	Day Grab	-6°40'32.09"	55°14'47.35"	48.6m
NI 15A	Day Grab	-6°40'37.41"	55°14'47.04"	47.4m
NI 16	Day Grab	-6°39'47.89"	55°15'2.97"	57.3m
NI 17	Day Grab	-6°40'12.65"	55°15'25.89"	49.4m
NI 18	Day Grab	-6°39'28.34"	55°15'23.01"	51.2m
NI 19	Day Grab	-6°38'7.60"	55°16'4.48"	58.4m
NI 20	Day Grab	-6°37'12.29"	55°16'15.24"	76.2m
NI 20A	Day Grab	-6°37'21.58"	55°16'14.63"	67.6m
NI 21	Day Grab	-6°36'43.33"	55°16'32.02"	117.3m
NI 22	Day Grab	-6°36'13.09"	55°16'22.89"	74.9m
NI 22A	Day Grab	-6°36'25.53"	55°16'23.31"	64.8m
NI 23	Day Grab	-6°37'41.44"	55°15'53.48"	70.1m
NI 23A	Day Grab	-6°37'52.07"	55°15'53.05"	70.3m

NI 24	Day Grab	-6°37'31.38"	55°15'41.04"	85.8m
NI 25	Day Grab	-6°36'59.65"	55°15'28.47"	67.8m
NI 26	Day Grab	-6°37'43.66"	55°15'26.30"	59.3
NI 27	Day Grab	-6°37'35.35"	55°15'9.83"	50.1m
NI 28	Day Grab	-6°36'17.95"	55°15'10.05"	55.9m
NI 29	Day Grab	-6°35'7.78"	55°15'14.35"	71.1m
NI 30	Day Grab	-6°34'38.61"	55°15'19.77"	57.5m
NI 31	Day Grab	-6°34'14.94"	55°15'29.67"	63.3m
NI 32	Day Grab	-6°32'23.68"	55°15'3.15"	28.1m
NI 33	Day Grab	-6°32'34.20"	55°15'21.17"	43.2m
NI 33A	Day Grab	-6°32'38.52"	55°15'21.33"	43.2m
NI 34	Day Grab	-6°32'13.54"	55°15'39.92"	46.3m
NI 34A	Day Grab	-6°32'25.46"	55°15'39.28"	45.2m
NI 35	Day Grab	-6°34'4.30"	55°15'58.90"	87.5m
NI 36	Day Grab	-6°33'30.55"	55°16'19.99"	105.2m
Ni 37	Day Grab	-6°34'30.63"	55°16'22.77"	81.3m
NI 38	Day Grab	-6°35'5.19"	55°16'27.96"	77.3m
NI 39	Day Grab	-6°36'34.41"	55°16'47.82"	83.1m
NI 40	Day Grab	-6°38'40.25"	55°16'44.69"	71.8m
NI 41	Day Grab	-6°38'52.41"	55°17'7.41"	75.0m
NI 42	Day Grab	-6°39'15.24"	55°17'31.75"	79.6m
NI 43	Day Grab	-6°39'34.80"	55°17'28.26"	81.5m
NI 43A	Day Grab	-6°39'38.33"	55°17'30.41"	71.3m
NI 44	Day Grab	-6°40'5.49"	55°14'17.95"	35.5m
NI 45	Day Grab	-6°42'9.24"	55°14'15.59"	34.5m
NI 46	Day Grab	-6°42'49.81"	55°13'59.45"	25.5m
OF 1	Day Grab	-7°3'42.07"	55°26'40.50"	46.3m
OF 2	Day Grab	-7°1'57.86"	55°27'2.93"	37.2m
OF 3	Day Grab	-7°0'23.68"	55°26'47.29"	27.4m
OF 4	Day Grab	-7°0'35.69"	55°26'23.48"	31.3m
OF 5	Day Grab	-6°59'16.21"	55°26'27.90"	31.5m
OF 6	Day Grab	-6°58'22.78"	55°26'39.17"	49.8m
OF 6A	Day Grab	-6°58'22.81"	55°26'39.18"	50m
OF 7	Day Grab	-6°58'1.44"	55°26'15.67"	27.8m
OF 7A	Day Grab	-6°58'2.22"	55°26'15.24"	26m
OF 8	Day Grab	-6°56'39.48"	55°26'12.30"	40.4m
OF 9	Day Grab	-6°57'8.57"	55°26'1.64"	39m
OF 10	Day Grab	-6°56'27.64"	55°25'43.10"	45.8m
OF 10A	Day Grab	-6°56'26.68"	55°25'42.93"	46.6m
OF 11	Day Grab	-6°54'40.28"	55°25'22.51"	47.1m
OF 12	Day Grab	-6°52'23.45"	55°24'44.90"	52m
OF 12A	Day Grab	-6°52'23.27"	55°24'43.87"	52.1m
OF 13	Day Grab	-6°53'26.94"	55°24'50.93"	58.8m
OF 13A	Day Grab	-6°53'25.78"	55°24'48.12"	49.6m
OF 14	Day Grab	-6°57'17.21"	55°25'30.97"	44.4m
OF 15	Day Grab	-6°58'30.25"	55°25'57.31"	42.1m
OF 16	Day Grab	-6°59'22.28"	55°26'6.56"	38.1m
OF 17	Day Grab	-7°0'34.02"	55°25'57.65"	46.6m

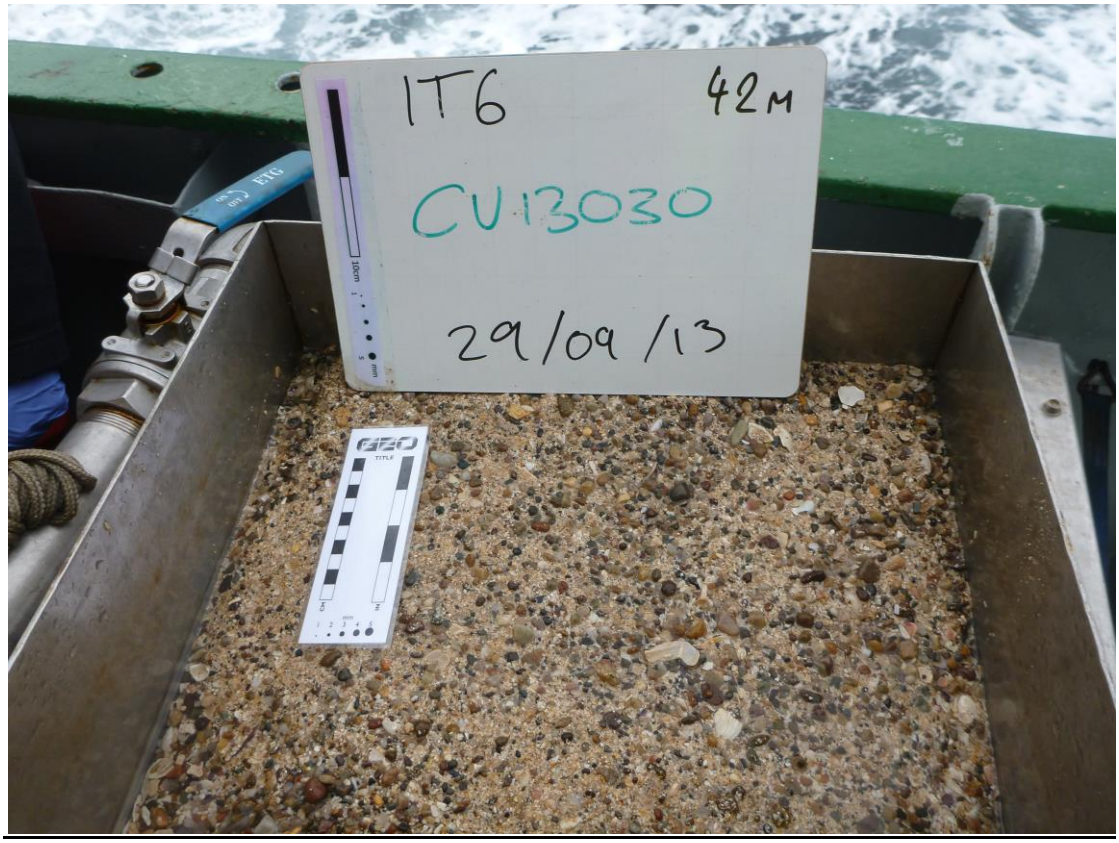

Picture 1. Typical Day Grab performance throughout the cruise duration, resulting in sufficient sediment recovery for both geological and biological sampling to be carried out.

Pinger

Simultaneous to MBES data acquisition, pinger sub-bottom data was also aquired. Selected lines transversing key bedforms will be used to interrogate the integral structure of sandwaves which may give further indication as to probable sediment mobility. Pinger data will also indicate thicknesses of sediment in the area. This data will be stored digitally at University of Ulster.

SAMPLE STATISTICS

SAMPLE IDENTITY: **NI2**

ANALYST & DATE: ,

SAMPLE TYPE: Trimodal, Poorly Sorted

TEXTURAL GROUP: Sandy Gravel

SEDIMENT NAME: Sandy Very Fine Gravel

	μm	ϕ
MODE 1:	2400.0	-1.243
MODE 2:	302.5	1.747
MODE 3:	4800.0	-2.243
D_{10}:	272.7	-1.445
MEDIAN or D_{50}:	1115.0	-0.157
D_{90}:	2721.9	1.875
(D_{90} / D_{10}):	9.982	-1.298
(D_{90} - D_{10}):	2449.2	3.319
(D_{75} / D_{25}):	5.163	-1.124
(D_{75} - D_{25}):	1746.4	2.368

GRAIN SIZE DISTRIBUTION

GRAVEL:	30.2%	COARSE SAND:	15.7%
SAND:	69.7%	MEDIUM SAND:	24.0%
MUD:	0.1%	FINE SAND:	6.6%
		V FINE SAND:	0.3%
V COARSE GRAVEL:	0.0%	V COARSE SILT:	0.0%
COARSE GRAVEL:	0.0%	COARSE SILT:	0.0%
MEDIUM GRAVEL:	0.0%	MEDIUM SILT:	0.0%
FINE GRAVEL:	8.1%	FINE SILT:	0.0%
V FINE GRAVEL:	22.1%	V FINE SILT:	0.0%
V COARSE SAND:	23.1%	CLAY:	0.0%

	METHOD OF MOMENTS			FOLK & WARD METHOD		
	Arithmetic μm	Geometric μm	Logarithmic ϕ	Geometric μm	Logarithmic ϕ	Description
MEAN ($\bar{x}$) :	1479.1	980.1	0.029	963.7	0.053	Coarse Sand
SORTING (σ):	1265.7	2.579	1.367	2.637	1.399	Poorly Sorted
SKEWNESS (Sk):	1.282	-0.237	0.237	-0.143	0.143	Fine Skewed
KURTOSIS (K):	4.164	2.359	2.359	0.757	0.757	Platykurtic

GRAIN SIZE DISTRIBUTION

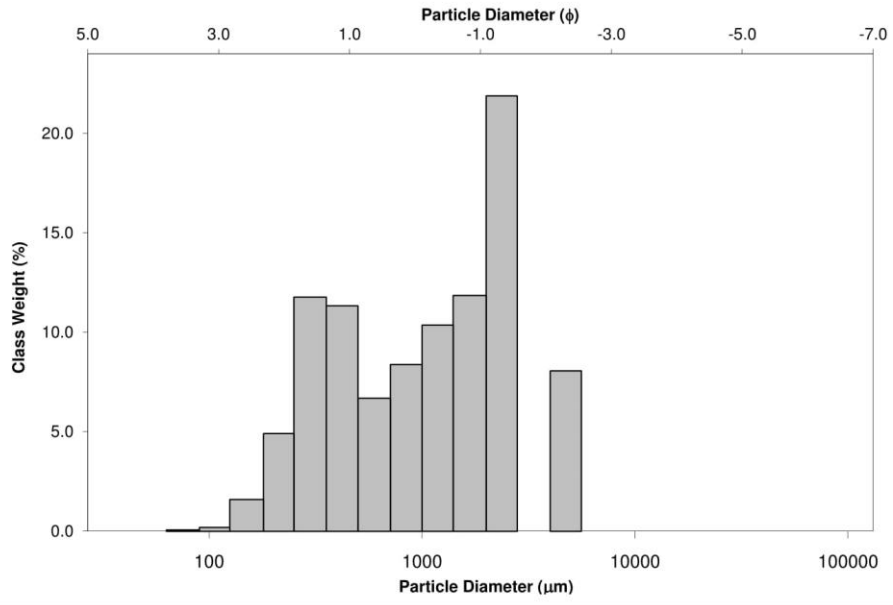

SAMPLE STATISTICS

SAMPLE IDENTITY: **NI3** ANALYST & DATE: ,

SAMPLE TYPE: Unimodal, Well Sorted TEXTURAL GROUP: Slightly Gravelly Sand

SEDIMENT NAME: Slightly Very Fine Gravelly Medium Sand

	μm	ϕ
MODE 1:	302.5	1.747
MODE 2:		
MODE 3:		
D_{10}:	207.1	1.037
MEDIAN or D_{50}:	329.1	1.604
D_{90}:	487.5	2.272
(D_{90} / D_{10}):	2.354	2.192
(D_{90} - D_{10}):	280.4	1.235
(D_{75} / D_{25}):	1.615	1.553
(D_{75} - D_{25}):	160.0	0.692

GRAIN SIZE DISTRIBUTION

GRAVEL:	0.0%	COARSE SAND:	7.2%
SAND:	99.9%	MEDIUM SAND:	71.7%
MUD:	0.0%	FINE SAND:	20.4%
		V FINE SAND:	0.4%
V COARSE GRAVEL:	0.0%	V COARSE SILT:	0.0%
COARSE GRAVEL:	0.0%	COARSE SILT:	0.0%
MEDIUM GRAVEL:	0.0%	MEDIUM SILT:	0.0%
FINE GRAVEL:	0.0%	FINE SILT:	0.0%
V FINE GRAVEL:	0.0%	V FINE SILT:	0.0%
V COARSE SAND:	0.2%	CLAY:	0.0%

	METHOD OF MOMENTS			FOLK & WARD METHOD		
	Arithmetic μm	Geometric μm	Logarithmic ϕ	Geometric μm	Logarithmic ϕ	Description
MEAN ($\bar{x}$) :	352.6	327.8	1.609	326.3	1.616	Medium Sand
SORTING (σ):	131.6	1.408	0.494	1.405	0.491	Well Sorted
SKEWNESS (Sk):	4.509	-0.429	0.429	-0.016	0.016	Symmetrical
KURTOSIS (K):	102.9	8.997	8.997	0.944	0.944	Mesokurtic

GRAIN SIZE DISTRIBUTION

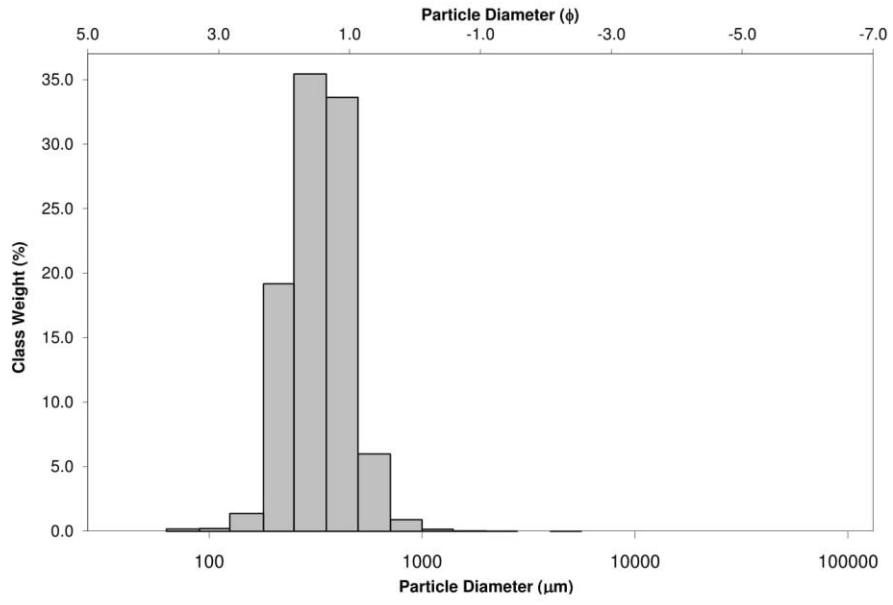

SAMPLE STATISTICS

SAMPLE IDENTITY: **NI 5** ANALYST & DATE: ,

SAMPLE TYPE: Bimodal, Poorly Sorted TEXTURAL GROUP: Gravelly Sand

SEDIMENT NAME: Very Fine Gravelly Coarse Sand

	μm	ϕ
MODE 1:	855.0	0.247
MODE 2:	427.5	1.247
MODE 3:		
D_{10}:	296.2	-0.997
MEDIAN or D_{50}:	783.6	0.352
D_{90}:	1995.6	1.756
(D_{90} / D_{10}):	6.738	-1.761
(D_{90} - D_{10}):	1699.4	2.752
(D_{75} / D_{25}):	2.753	-3.680
(D_{75} - D_{25}):	790.5	1.461

GRAIN SIZE DISTRIBUTION

GRAVEL:	9.9%	COARSE SAND:	35.9%
SAND:	90.0%	MEDIUM SAND:	23.7%
MUD:	0.0%	FINE SAND:	5.6%
		V FINE SAND:	0.2%
V COARSE GRAVEL:	0.0%	V COARSE SILT:	0.0%
COARSE GRAVEL:	0.0%	COARSE SILT:	0.0%
MEDIUM GRAVEL:	0.0%	MEDIUM SILT:	0.0%
FINE GRAVEL:	2.4%	FINE SILT:	0.0%
V FINE GRAVEL:	7.6%	V FINE SILT:	0.0%
V COARSE SAND:	24.6%	CLAY:	0.0%

	METHOD OF MOMENTS			FOLK & WARD METHOD		
	Arithmetic μm	Geometric μm	Logarithmic ϕ	Geometric μm	Logarithmic ϕ	Description
MEAN ($\bar{x}$) :	1012.6	765.3	0.386	773.1	0.371	Coarse Sand
SORTING (σ):	836.7	2.070	1.049	2.070	1.050	Poorly Sorted
SKEWNESS (Sk):	2.418	0.011	-0.011	-0.027	0.027	Symmetrical
KURTOSIS (K):	10.69	3.170	3.170	0.961	0.961	Mesokurtic

GRAIN SIZE DISTRIBUTION

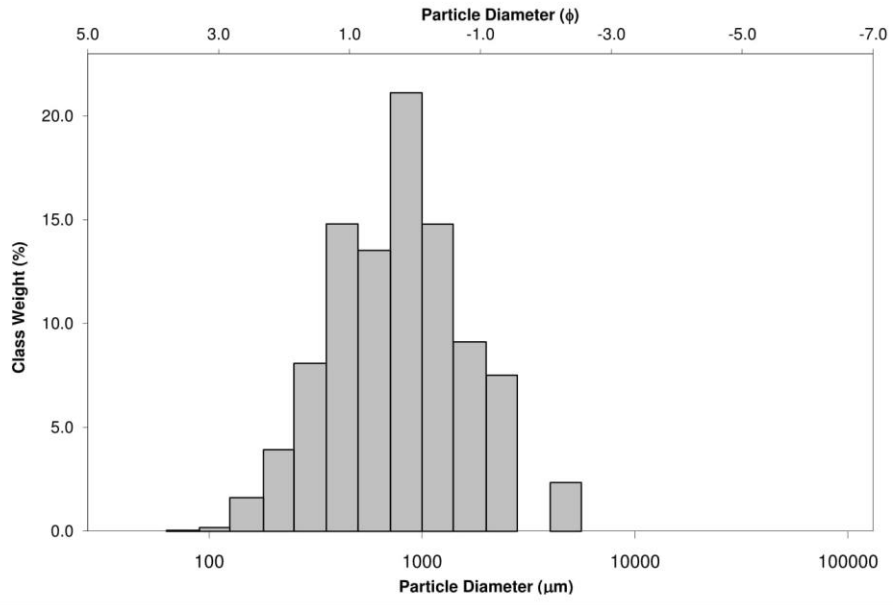

SAMPLE STATISTICS

SIEVING ERROR: 1.9%

SAMPLE IDENTITY: **NI 7**

ANALYST & DATE: ,

SAMPLE TYPE: Unimodal, Moderately Sorted

TEXTURAL GROUP: Sandy Gravel

SEDIMENT NAME: Sandy Very Fine Gravel

	µm	ϕ
MODE 1:	2400.0	-1.243
MODE 2:		
MODE 3:		
D_{10}:	646.2	-1.387
MEDIAN or D_{50}:	1657.9	-0.729
D_{90}:	2614.9	0.630
(D_{90} / D_{10}):	4.047	-0.454
(D_{90} - D_{10}):	1968.7	2.017
(D_{75} / D_{25}):	2.199	0.043
(D_{75} - D_{25}):	1242.9	1.137

GRAIN SIZE DISTRIBUTION

GRAVEL:	39.3%	COARSE SAND:	15.9%
SAND:	60.7%	MEDIUM SAND:	2.9%
MUD:	0.1%	FINE SAND:	3.8%
		V FINE SAND:	0.6%
V COARSE GRAVEL:	0.0%	V COARSE SILT:	0.0%
COARSE GRAVEL:	0.0%	COARSE SILT:	0.0%
MEDIUM GRAVEL:	0.0%	MEDIUM SILT:	0.0%
FINE GRAVEL:	2.5%	FINE SILT:	0.0%
V FINE GRAVEL:	36.7%	V FINE SILT:	0.0%
V COARSE SAND:	37.5%	CLAY:	0.0%

	METHOD OF MOMENTS			FOLK & WARD METHOD		
	Arithmetic µm	Geometric µm	Logarithmic ϕ	Geometric µm	Logarithmic ϕ	Description
MEAN ($\bar{x}$) :	1700.5	1402.2	-0.488	1496.8	-0.582	Very Coarse Sand
SORTING (σ):	867.3	2.005	1.003	1.850	0.887	Moderately Sorted
SKEWNESS (Sk):	0.779	-1.645	1.645	-0.414	0.414	Very Fine Skewed
KURTOSIS (K):	5.101	7.066	7.066	1.160	1.160	Leptokurtic

GRAIN SIZE DISTRIBUTION

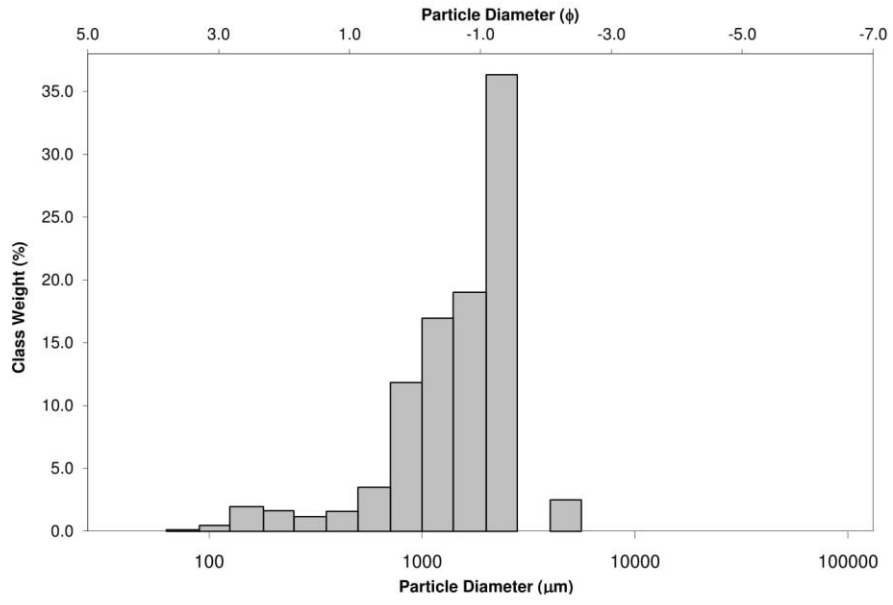

SAMPLE STATISTICS

SAMPLE IDENTITY: **NI12A** ANALYST & DATE: ,

SAMPLE TYPE: Bimodal, Poorly Sorted TEXTURAL GROUP: Gravelly Sand

SEDIMENT NAME: Very Fine Gravelly Medium Sand

	μm	ϕ
MODE 1:	302.5	1.747
MODE 2:	1200.0	-0.243
MODE 3:		
D_{10}:	200.9	-0.938
MEDIAN or D_{50}:	413.9	1.273
D_{90}:	1916.3	2.316
(D_{90} / D_{10}):	9.540	-2.468
(D_{90} - D_{10}):	1715.4	3.254
(D_{75} / D_{25}):	4.006	-18.267
(D_{75} - D_{25}):	806.4	2.002

GRAIN SIZE DISTRIBUTION

GRAVEL:	9.0%	COARSE SAND:	16.2%
SAND:	90.9%	MEDIUM SAND:	36.6%
MUD:	0.1%	FINE SAND:	19.6%
		V FINE SAND:	0.4%
V COARSE GRAVEL:	0.0%	V COARSE SILT:	0.0%
COARSE GRAVEL:	0.0%	COARSE SILT:	0.0%
MEDIUM GRAVEL:	0.0%	MEDIUM SILT:	0.0%
FINE GRAVEL:	2.1%	FINE SILT:	0.0%
V FINE GRAVEL:	6.9%	V FINE SILT:	0.0%
V COARSE SAND:	18.1%	CLAY:	0.0%

	METHOD OF MOMENTS			FOLK & WARD METHOD		
	Arithmetic μm	Geometric μm	Logarithmic ϕ	Geometric μm	Logarithmic ϕ	Description
MEAN ($\bar{x}$) :	810.8	529.4	0.918	520.0	0.943	Coarse Sand
SORTING (σ):	863.4	2.393	1.259	2.367	1.243	Poorly Sorted
SKEWNESS (Sk):	2.441	0.445	-0.445	0.363	-0.363	Very Coarse Skewed
KURTOSIS (K):	10.42	2.735	2.735	0.768	0.768	Platykurtic

GRAIN SIZE DISTRIBUTION

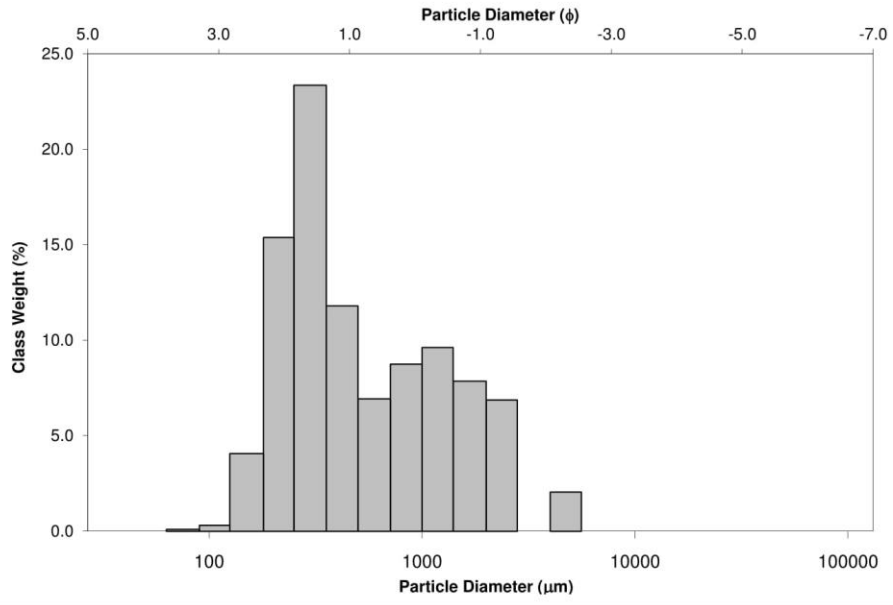

SAMPLE STATISTICS

SAMPLE IDENTITY: **NI13** ANALYST & DATE: ,

SAMPLE TYPE: Unimodal, Poorly Sorted TEXTURAL GROUP: Gravelly Sand

SEDIMENT NAME: Very Fine Gravelly Medium Sand

	μm	ϕ
MODE 1:	302.5	1.747
MODE 2:		
MODE 3:		
D_{10}:	197.4	-0.839
MEDIAN or D_{50}:	391.4	1.353
D_{90}:	1788.9	2.341
(D_{90} / D_{10}):	9.061	-2.790
(D_{90} - D_{10}):	1591.4	3.180
(D_{75} / D_{25}):	3.080	6.834
(D_{75} - D_{25}):	556.9	1.623

GRAIN SIZE DISTRIBUTION

GRAVEL:	8.0%	COARSE SAND:	16.4%
SAND:	90.5%	MEDIUM SAND:	42.5%
MUD:	1.5%	FINE SAND:	18.4%
		V FINE SAND:	0.3%
V COARSE GRAVEL:	0.0%	V COARSE SILT:	0.2%
COARSE GRAVEL:	0.0%	COARSE SILT:	0.2%
MEDIUM GRAVEL:	0.0%	MEDIUM SILT:	0.2%
FINE GRAVEL:	2.0%	FINE SILT:	0.2%
V FINE GRAVEL:	6.0%	V FINE SILT:	0.2%
V COARSE SAND:	13.0%	CLAY:	0.2%

	METHOD OF MOMENTS			FOLK & WARD METHOD		
	Arithmetic μm	Geometric μm	Logarithmic ϕ	Geometric μm	Logarithmic ϕ	Description
MEAN ($\bar{x}$) :	732.9	465.4	1.104	486.0	1.041	Medium Sand
SORTING (σ):	834.6	2.592	1.374	2.313	1.210	Poorly Sorted
SKEWNESS (Sk):	2.795	-0.540	0.540	0.362	-0.362	Very Coarse Skewed
KURTOSIS (K):	12.38	6.707	6.707	0.971	0.971	Mesokurtic

GRAIN SIZE DISTRIBUTION

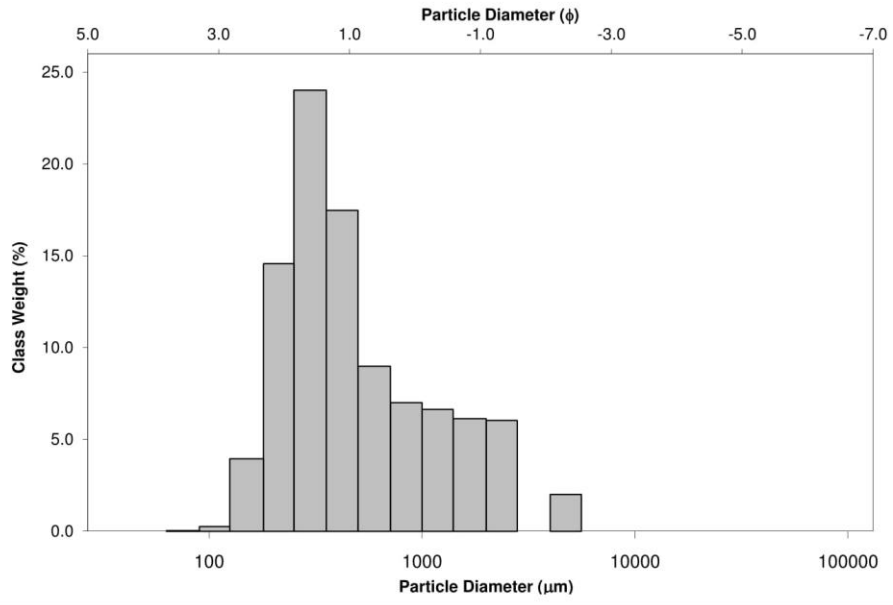

SAMPLE STATISTICS

SAMPLE IDENTITY: **NI14** ANALYST & DATE: ,

SAMPLE TYPE: Bimodal, Moderately Sorted TEXTURAL GROUP: Slightly Gravelly Sand

SEDIMENT NAME: Slightly Very Fine Gravelly Medium Sand

	μm	ϕ
MODE 1:	302.5	1.747
MODE 2:	855.0	0.247
MODE 3:		
D_{10}:	193.4	-0.025
MEDIAN or D_{50}:	317.6	1.655
D_{90}:	1017.4	2.370
(D_{90} / D_{10}):	5.261	-95.115
(D_{90} - D_{10}):	824.0	2.395
(D_{75} / D_{25}):	1.958	1.935
(D_{75} - D_{25}):	238.6	0.969

GRAIN SIZE DISTRIBUTION

GRAVEL:	1.5%	COARSE SAND:	13.6%
SAND:	98.5%	MEDIUM SAND:	50.8%
MUD:	0.0%	FINE SAND:	24.8%
		V FINE SAND:	0.4%
V COARSE GRAVEL:	0.0%	V COARSE SILT:	0.0%
COARSE GRAVEL:	0.0%	COARSE SILT:	0.0%
MEDIUM GRAVEL:	0.0%	MEDIUM SILT:	0.0%
FINE GRAVEL:	0.1%	FINE SILT:	0.0%
V FINE GRAVEL:	1.4%	V FINE SILT:	0.0%
V COARSE SAND:	8.8%	CLAY:	0.0%

	METHOD OF MOMENTS			FOLK & WARD METHOD		
	Arithmetic μm	Geometric μm	Logarithmic ϕ	Geometric μm	Logarithmic ϕ	Description
MEAN ($\bar{x}$) :	480.9	373.0	1.423	371.2	1.430	Medium Sand
SORTING (σ):	427.9	1.877	0.908	1.878	0.909	Moderately Sorted
SKEWNESS (Sk):	2.874	0.957	-0.957	0.389	-0.389	Very Coarse Skewed
KURTOSIS (K):	14.90	3.818	3.818	1.271	1.271	Leptokurtic

GRAIN SIZE DISTRIBUTION

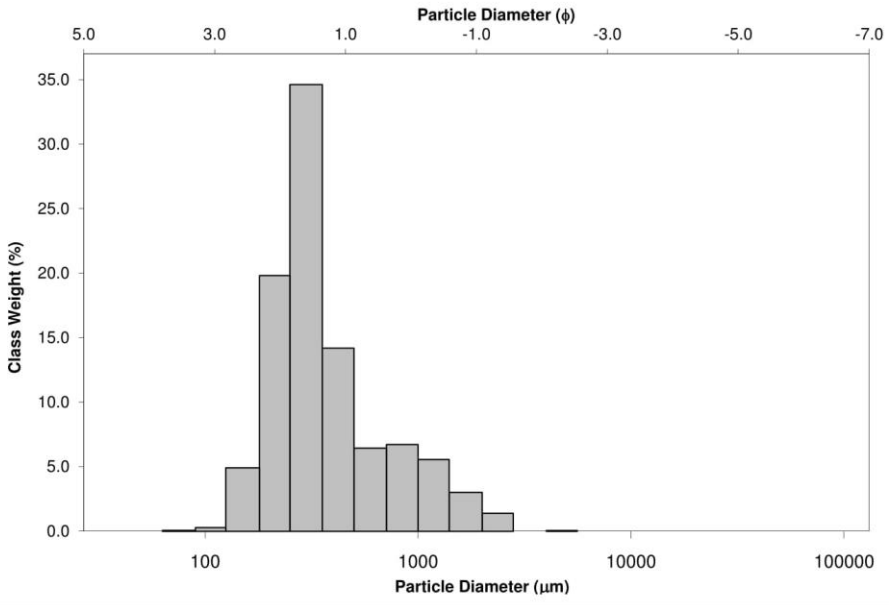

SAMPLE STATISTICS

SAMPLE IDENTITY: **NI15**

ANALYST & DATE: ,

SAMPLE TYPE: Unimodal, Well Sorted

TEXTURAL GROUP: Sand

SEDIMENT NAME: Well Sorted Fine Sand

	μm	ϕ
MODE 1:	215.0	2.237
MODE 2:		
MODE 3:		
D_{10}:	139.4	1.692
MEDIAN or D_{50}:	209.4	2.255
D_{90}:	309.5	2.843
(D_{90} / D_{10}):	2.220	1.680
(D_{90} - D_{10}):	170.1	1.151
(D_{75} / D_{25}):	1.417	1.249
(D_{75} - D_{25}):	72.68	0.502

GRAIN SIZE DISTRIBUTION

GRAVEL: 0.0%	COARSE SAND: 0.3%
SAND: 100.0%	MEDIUM SAND: 22.8%
MUD: 0.0%	FINE SAND: 74.0%
	V FINE SAND: 2.7%
V COARSE GRAVEL: 0.0%	V COARSE SILT: 0.0%
COARSE GRAVEL: 0.0%	COARSE SILT: 0.0%
MEDIUM GRAVEL: 0.0%	MEDIUM SILT: 0.0%
FINE GRAVEL: 0.0%	FINE SILT: 0.0%
V FINE GRAVEL: 0.0%	V FINE SILT: 0.0%
V COARSE SAND: 0.2%	CLAY: 0.0%

	METHOD OF MOMENTS			FOLK & WARD METHOD		
	Arithmetic μm	Geometric μm	Logarithmic ϕ	Geometric μm	Logarithmic ϕ	Description
MEAN ($\bar{x}$) :	221.6	208.4	2.263	207.8	2.267	Fine Sand
SORTING (σ):	84.33	1.347	0.430	1.346	0.429	Well Sorted
SKEWNESS (Sk):	7.456	-0.088	0.088	-0.025	0.025	Symmetrical
KURTOSIS (K):	114.5	12.66	12.66	1.121	1.121	Leptokurtic

GRAIN SIZE DISTRIBUTION

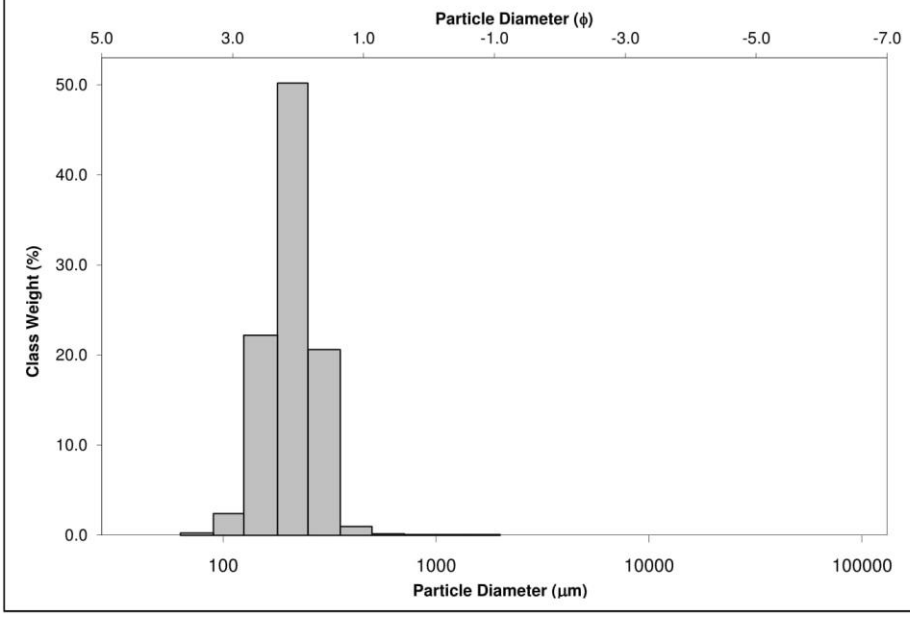

SAMPLE STATISTICS

SIEVING ERROR: 1.8%

SAMPLE IDENTITY: **NI 15A**

ANALYST & DATE: ,

SAMPLE TYPE: Unimodal, Well Sorted

TEXTURAL GROUP: Sand

SEDIMENT NAME: Well Sorted Fine Sand

	μm	ϕ
MODE 1:	215.0	2.237
MODE 2:		
MODE 3:		
D_{10}:	139.4	1.692
MEDIAN or D_{50}:	209.4	2.255
D_{90}:	309.5	2.843
(D_{90} / D_{10}):	2.220	1.680
(D_{90} - D_{10}):	170.1	1.151
(D_{75} / D_{25}):	1.417	1.249
(D_{75} - D_{25}):	72.68	0.502

GRAIN SIZE DISTRIBUTION

GRAVEL: 0.0%	COARSE SAND: 0.3%
SAND: 100.0%	MEDIUM SAND: 22.8%
MUD: 0.0%	FINE SAND: 74.0%
	V FINE SAND: 2.7%
V COARSE GRAVEL: 0.0%	V COARSE SILT: 0.0%
COARSE GRAVEL: 0.0%	COARSE SILT: 0.0%
MEDIUM GRAVEL: 0.0%	MEDIUM SILT: 0.0%
FINE GRAVEL: 0.0%	FINE SILT: 0.0%
V FINE GRAVEL: 0.0%	V FINE SILT: 0.0%
V COARSE SAND: 0.2%	CLAY: 0.0%

	METHOD OF MOMENTS			FOLK & WARD METHOD		
	Arithmetic μm	Geometric μm	Logarithmic ϕ	Geometric μm	Logarithmic ϕ	Description
MEAN ($\bar{x}$) :	221.6	208.4	2.263	207.8	2.267	Fine Sand
SORTING (σ):	84.33	1.347	0.430	1.346	0.429	Well Sorted
SKEWNESS (Sk):	7.456	-0.088	0.088	-0.025	0.025	Symmetrical
KURTOSIS (K):	114.5	12.66	12.66	1.121	1.121	Leptokurtic

GRAIN SIZE DISTRIBUTION

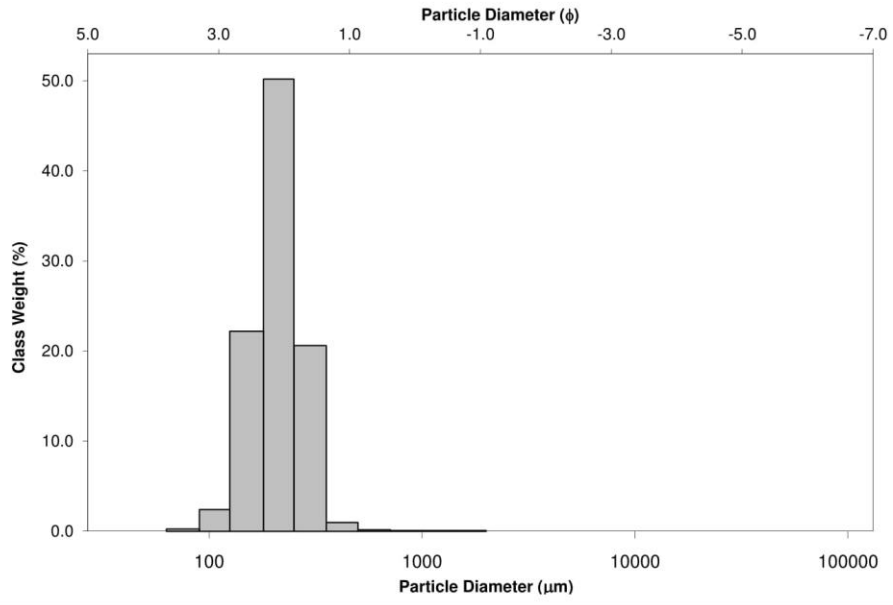

SAMPLE STATISTICS

SAMPLE IDENTITY: **NI16** ANALYST & DATE: ,

SAMPLE TYPE: Unimodal, Well Sorted TEXTURAL GROUP: Slightly Gravelly Sand

SEDIMENT NAME: Slightly Fine Gravelly Fine Sand

	μm	ϕ
MODE 1:	215.0	2.237
MODE 2:		
MODE 3:		
D_{10}:	139.4	1.597
MEDIAN or D_{50}:	210.6	2.247
D_{90}:	330.5	2.843
(D_{90} / D_{10}):	2.371	1.780
(D_{90} - D_{10}):	191.1	1.245
(D_{75} / D_{25}):	1.547	1.325
(D_{75} - D_{25}):	92.50	0.629

GRAIN SIZE DISTRIBUTION

GRAVEL:	0.3%	COARSE SAND:	0.6%
SAND:	99.7%	MEDIUM SAND:	27.0%
MUD:	0.0%	FINE SAND:	70.5%
		V FINE SAND:	1.5%
V COARSE GRAVEL:	0.0%	V COARSE SILT:	0.0%
COARSE GRAVEL:	0.0%	COARSE SILT:	0.0%
MEDIUM GRAVEL:	0.0%	MEDIUM SILT:	0.0%
FINE GRAVEL:	0.2%	FINE SILT:	0.0%
V FINE GRAVEL:	0.1%	V FINE SILT:	0.0%
V COARSE SAND:	0.1%	CLAY:	0.0%

	METHOD OF MOMENTS			FOLK & WARD METHOD		
	Arithmetic μm	Geometric μm	Logarithmic ϕ	Geometric μm	Logarithmic ϕ	Description
MEAN ($\bar{x}$) :	239.7	215.1	2.217	212.2	2.237	Fine Sand
SORTING (σ):	234.7	1.427	0.513	1.390	0.475	Well Sorted
SKEWNESS (Sk):	16.45	1.732	-1.732	0.053	-0.053	Symmetrical
KURTOSIS (K):	312.7	18.07	18.07	0.969	0.969	Mesokurtic

GRAIN SIZE DISTRIBUTION

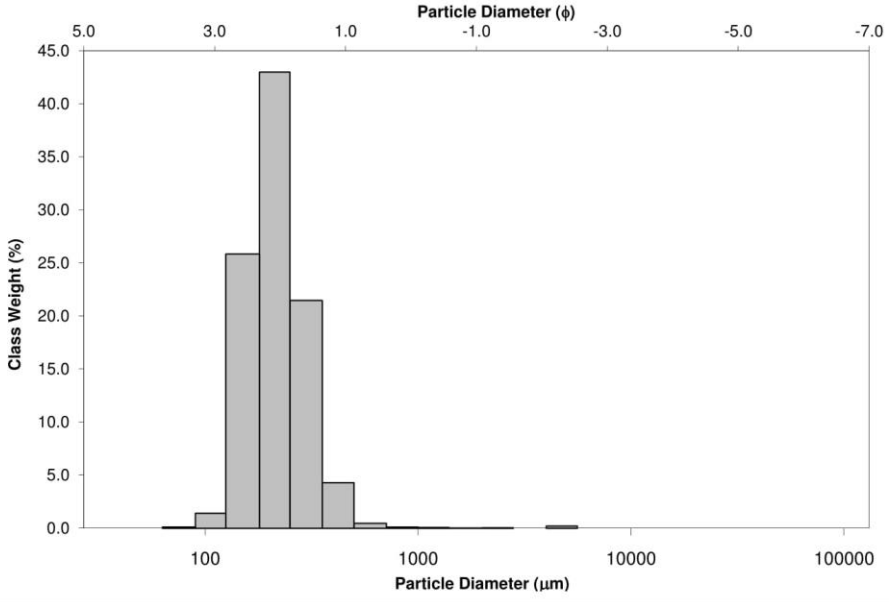

SAMPLE STATISTICS

SAMPLE IDENTITY: **NI17** ANALYST & DATE: ,

SAMPLE TYPE: Unimodal, Moderately Sorted TEXTURAL GROUP: Gravelly Sand

SEDIMENT NAME: Very Fine Gravelly Medium Sand

	μm	ϕ
MODE 1:	427.5	1.247
MODE 2:		
MODE 3:		
D_{10}:	304.5	-0.818
MEDIAN or D_{50}:	619.0	0.692
D_{90}:	1763.1	1.715
(D_{90} / D_{10}):	5.789	-2.097
(D_{90} - D_{10}):	1458.6	2.533
(D_{75} / D_{25}):	2.774	-7.367
(D_{75} - D_{25}):	722.5	1.472

GRAIN SIZE DISTRIBUTION

GRAVEL:	6.4%	COARSE SAND:	29.5%
SAND:	92.2%	MEDIUM SAND:	36.5%
MUD:	1.4%	FINE SAND:	2.7%
		V FINE SAND:	0.1%
V COARSE GRAVEL:	0.0%	V COARSE SILT:	0.2%
COARSE GRAVEL:	0.0%	COARSE SILT:	0.2%
MEDIUM GRAVEL:	0.0%	MEDIUM SILT:	0.2%
FINE GRAVEL:	0.4%	FINE SILT:	0.2%
V FINE GRAVEL:	6.0%	V FINE SILT:	0.2%
V COARSE SAND:	23.4%	CLAY:	0.2%

	METHOD OF MOMENTS			FOLK & WARD METHOD		
	Arithmetic μm	Geometric μm	Logarithmic ϕ	Geometric μm	Logarithmic ϕ	Description
MEAN ($\bar{x}$) :	857.0	646.5	0.629	684.5	0.547	Coarse Sand
SORTING (σ):	631.6	2.294	1.198	1.947	0.961	Moderately Sorted
SKEWNESS (Sk):	1.791	-1.800	1.800	0.197	-0.197	Coarse Skewed
KURTOSIS (K):	8.135	11.95	11.95	0.856	0.856	Platykurtic

GRAIN SIZE DISTRIBUTION

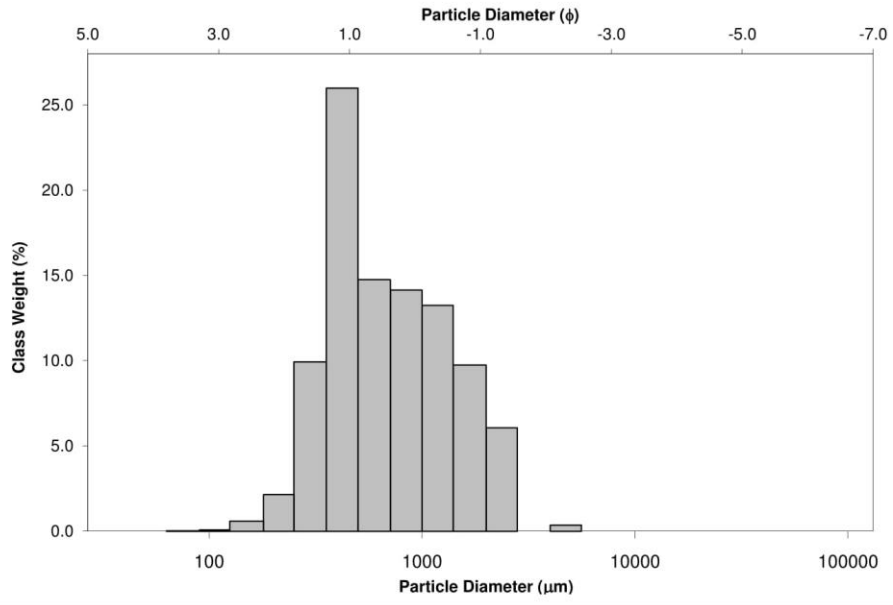

SAMPLE STATISTICS

SAMPLE IDENTITY: **NI18** ANALYST & DATE: ,

SAMPLE TYPE: Unimodal, Moderately Sorted TEXTURAL GROUP: Slightly Gravelly Sand

SEDIMENT NAME: Slightly Very Fine Gravelly Medium Sand

	μm	ϕ
MODE 1:	427.5	1.247
MODE 2:		
MODE 3:		
D_{10}:	230.5	0.238
MEDIAN or D_{50}:	397.4	1.331
D_{90}:	847.7	2.117
(D_{90} / D_{10}):	3.677	8.883
(D_{90} - D_{10}):	617.2	1.879
(D_{75} / D_{25}):	1.640	1.696
(D_{75} - D_{25}):	191.7	0.713

GRAIN SIZE DISTRIBUTION

GRAVEL:	2.1%	COARSE SAND:	15.9%
SAND:	97.9%	MEDIUM SAND:	64.6%
MUD:	0.0%	FINE SAND:	12.2%
		V FINE SAND:	0.2%
V COARSE GRAVEL:	0.0%	V COARSE SILT:	0.0%
COARSE GRAVEL:	0.0%	COARSE SILT:	0.0%
MEDIUM GRAVEL:	0.0%	MEDIUM SILT:	0.0%
FINE GRAVEL:	0.4%	FINE SILT:	0.0%
V FINE GRAVEL:	1.8%	V FINE SILT:	0.0%
V COARSE SAND:	5.0%	CLAY:	0.0%

	METHOD OF MOMENTS			FOLK & WARD METHOD		
	Arithmetic μm	Geometric μm	Logarithmic ϕ	Geometric μm	Logarithmic ϕ	Description
MEAN ($\bar{x}$) :	510.8	418.5	1.257	406.2	1.300	Medium Sand
SORTING (σ):	452.9	1.715	0.778	1.656	0.728	Moderately Sorted
SKEWNESS (Sk):	4.816	1.085	-1.085	0.154	-0.154	Coarse Skewed
KURTOSIS (K):	36.11	6.056	6.056	1.545	1.545	Very Leptokurtic

GRAIN SIZE DISTRIBUTION

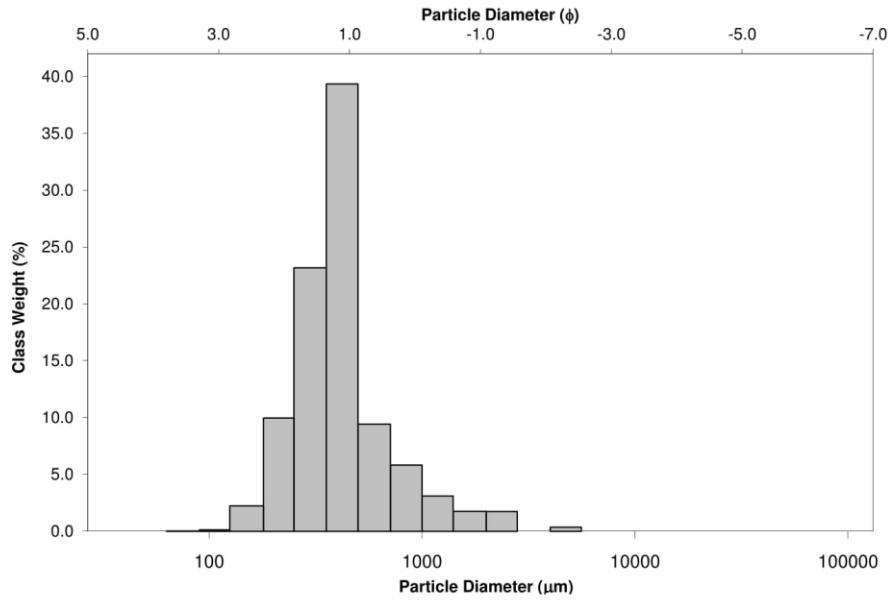

SAMPLE STATISTICS

SAMPLE IDENTITY: **NI19** ANALYST & DATE: ,

SAMPLE TYPE: Unimodal, Well Sorted TEXTURAL GROUP: Slightly Gravelly Sand

SEDIMENT NAME: Slightly Very Fine Gravelly Medium Sand

	μm	ϕ
MODE 1:	215.0	2.237
MODE 2:		
MODE 3:		
D_{10}:	173.1	1.303
MEDIAN or D_{50}:	253.2	1.982
D_{90}:	405.2	2.530
(D_{90} / D_{10}):	2.340	1.941
(D_{90} - D_{10}):	232.0	1.227
(D_{75} / D_{25}):	1.580	1.402
(D_{75} - D_{25}):	117.8	0.660

GRAIN SIZE DISTRIBUTION

GRAVEL:	0.0%	COARSE SAND:	2.9%
SAND:	100.0%	MEDIUM SAND:	48.4%
MUD:	0.0%	FINE SAND:	48.1%
		V FINE SAND:	0.5%
V COARSE GRAVEL:	0.0%	V COARSE SILT:	0.0%
COARSE GRAVEL:	0.0%	COARSE SILT:	0.0%
MEDIUM GRAVEL:	0.0%	MEDIUM SILT:	0.0%
FINE GRAVEL:	0.0%	FINE SILT:	0.0%
V FINE GRAVEL:	0.0%	V FINE SILT:	0.0%
V COARSE SAND:	0.1%	CLAY:	0.0%

	METHOD OF MOMENTS			FOLK & WARD METHOD		
	Arithmetic μm	Geometric μm	Logarithmic ϕ	Geometric μm	Logarithmic ϕ	Description
MEAN ($\bar{x}$) :	277.7	257.9	1.955	255.2	1.970	Medium Sand
SORTING (σ):	106.4	1.402	0.487	1.395	0.480	Well Sorted
SKEWNESS (Sk):	2.810	0.110	-0.110	0.048	-0.048	Symmetrical
KURTOSIS (K):	27.08	6.913	6.913	1.050	1.050	Mesokurtic

GRAIN SIZE DISTRIBUTION

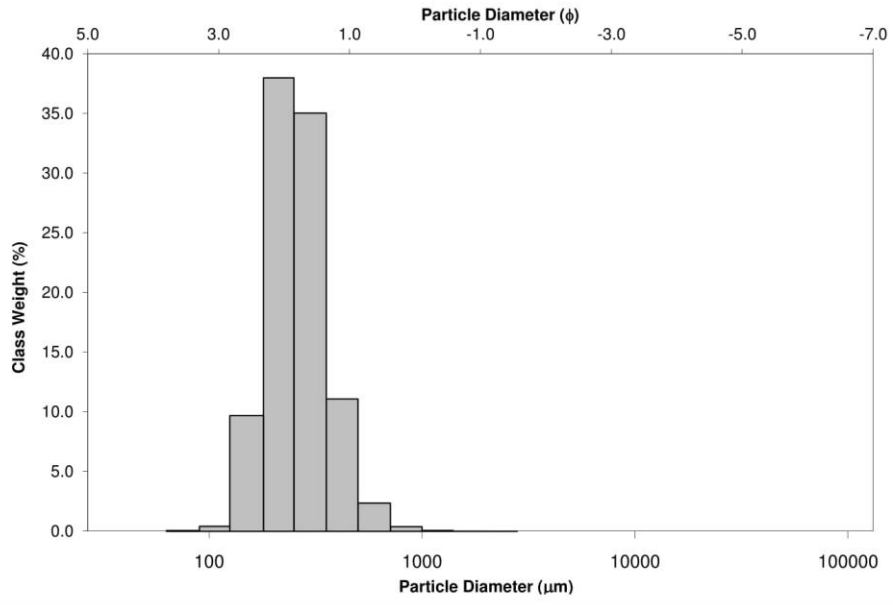

SAMPLE STATISTICS

SIEVING ERROR: 2.2%

SAMPLE IDENTITY: **NI 21**

ANALYST & DATE: ,

SAMPLE TYPE: Unimodal, Well Sorted

TEXTURAL GROUP: Slightly Gravelly Sand

SEDIMENT NAME: Slightly Very Fine Gravelly Fine Sand

	μm	ϕ
MODE 1:	215.0	2.237
MODE 2:		
MODE 3:		
D_{10}:	153.6	1.498
MEDIAN or D_{50}:	243.9	2.036
D_{90}:	354.0	2.702
(D_{90} / D_{10}):	2.304	1.804
(D_{90} - D_{10}):	200.3	1.204
(D_{75} / D_{25}):	1.578	1.387
(D_{75} - D_{25}):	112.7	0.658

GRAIN SIZE DISTRIBUTION

GRAVEL:	0.1%	COARSE SAND:	2.2%
SAND:	99.9%	MEDIUM SAND:	44.7%
MUD:	0.1%	FINE SAND:	50.7%
		V FINE SAND:	2.0%
V COARSE GRAVEL:	0.0%	V COARSE SILT:	0.0%
COARSE GRAVEL:	0.0%	COARSE SILT:	0.0%
MEDIUM GRAVEL:	0.0%	MEDIUM SILT:	0.0%
FINE GRAVEL:	0.0%	FINE SILT:	0.0%
V FINE GRAVEL:	0.1%	V FINE SILT:	0.0%
V COARSE SAND:	0.3%	CLAY:	0.0%

	METHOD OF MOMENTS			FOLK & WARD METHOD		
	Arithmetic μm	Geometric μm	Logarithmic ϕ	Geometric μm	Logarithmic ϕ	Description
MEAN ($\bar{x}$) :	266.0	244.3	2.033	244.8	2.030	Fine Sand
SORTING (σ):	124.2	1.441	0.527	1.399	0.485	Well Sorted
SKEWNESS (Sk):	6.166	-0.167	0.167	0.012	-0.012	Symmetrical
KURTOSIS (K):	82.07	11.13	11.13	1.071	1.071	Mesokurtic

GRAIN SIZE DISTRIBUTION

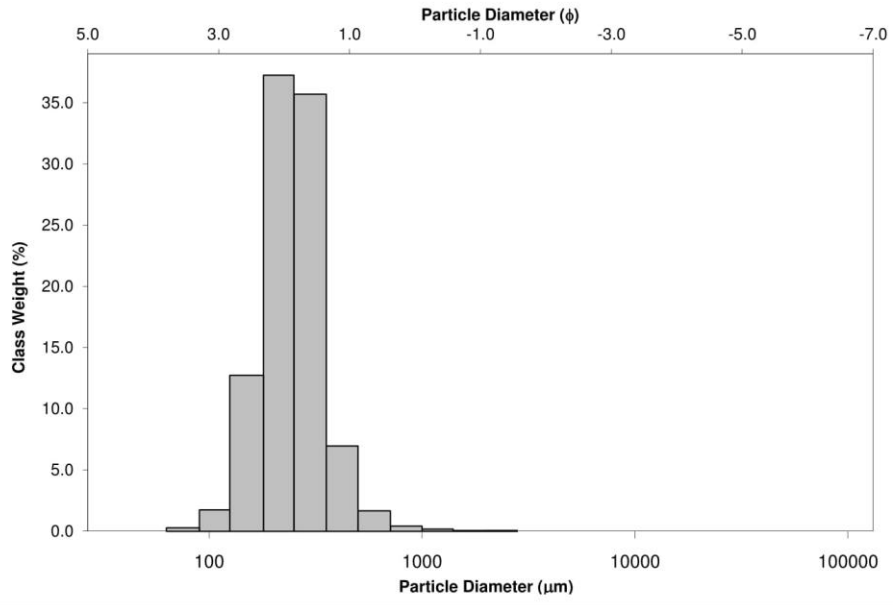

SAMPLE STATISTICS

SAMPLE IDENTITY: **NI25** ANALYST & DATE: ,

SAMPLE TYPE: Unimodal, Well Sorted TEXTURAL GROUP: Slightly Gravelly Sand

SEDIMENT NAME: Slightly Very Fine Gravelly Medium Sand

	μm	ϕ
MODE 1:	302.5	1.747
MODE 2:		
MODE 3:		
D_{10}:	208.5	1.022
MEDIAN or D_{50}:	313.5	1.673
D_{90}:	492.4	2.262
(D_{90} / D_{10}):	2.362	2.213
(D_{90} - D_{10}):	283.9	1.240
(D_{75} / D_{25}):	1.562	1.489
(D_{75} - D_{25}):	144.6	0.643

GRAIN SIZE DISTRIBUTION

GRAVEL:	0.0%	COARSE SAND:	8.5%
SAND:	100.0%	MEDIUM SAND:	69.9%
MUD:	0.0%	FINE SAND:	21.2%
		V FINE SAND:	0.1%
V COARSE GRAVEL:	0.0%	V COARSE SILT:	0.0%
COARSE GRAVEL:	0.0%	COARSE SILT:	0.0%
MEDIUM GRAVEL:	0.0%	MEDIUM SILT:	0.0%
FINE GRAVEL:	0.0%	FINE SILT:	0.0%
V FINE GRAVEL:	0.0%	V FINE SILT:	0.0%
V COARSE SAND:	0.3%	CLAY:	0.0%

	METHOD OF MOMENTS			FOLK & WARD METHOD		
	Arithmetic μm	Geometric μm	Logarithmic ϕ	Geometric μm	Logarithmic ϕ	Description
MEAN ($\bar{x}$) :	348.4	323.1	1.630	319.7	1.645	Medium Sand
SORTING (σ):	149.0	1.393	0.479	1.410	0.495	Well Sorted
SKEWNESS (Sk):	7.039	0.706	-0.706	0.115	-0.115	Coarse Skewed
KURTOSIS (K):	157.5	4.868	4.868	1.050	1.050	Mesokurtic

GRAIN SIZE DISTRIBUTION

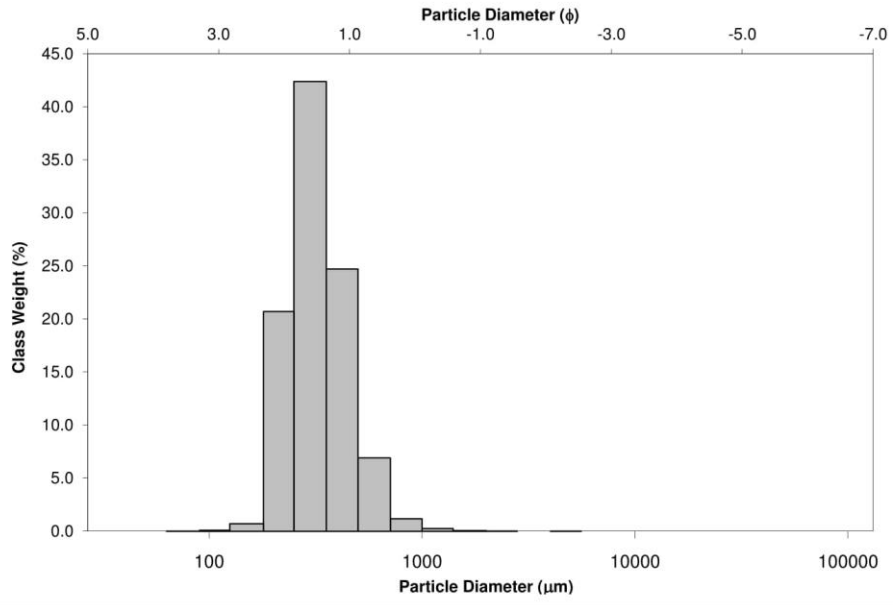

SAMPLE STATISTICS

SIEVING ERROR: 1.7%

SAMPLE IDENTITY: **NI 27**

ANALYST & DATE: ,

SAMPLE TYPE: Unimodal, Well Sorted

TEXTURAL GROUP: Sand

SEDIMENT NAME: Well Sorted Fine Sand

	μm	ϕ
MODE 1:	215.0	2.237
MODE 2:		
MODE 3:		
D_{10}:	155.1	1.618
MEDIAN or D_{50}:	222.2	2.170
D_{90}:	325.8	2.689
(D_{90} / D_{10}):	2.100	1.662
(D_{90} - D_{10}):	170.7	1.071
(D_{75} / D_{25}):	1.418	1.266
(D_{75} - D_{25}):	79.44	0.504

GRAIN SIZE DISTRIBUTION

GRAVEL:	0.0%	COARSE SAND:	0.5%
SAND:	99.9%	MEDIUM SAND:	30.5%
MUD:	0.1%	FINE SAND:	67.9%
		V FINE SAND:	1.1%
V COARSE GRAVEL:	0.0%	V COARSE SILT:	0.0%
COARSE GRAVEL:	0.0%	COARSE SILT:	0.0%
MEDIUM GRAVEL:	0.0%	MEDIUM SILT:	0.0%
FINE GRAVEL:	0.0%	FINE SILT:	0.0%
V FINE GRAVEL:	0.0%	V FINE SILT:	0.0%
V COARSE SAND:	0.0%	CLAY:	0.0%

	METHOD OF MOMENTS			FOLK & WARD METHOD		
	Arithmetic μm	Geometric μm	Logarithmic ϕ	Geometric μm	Logarithmic ϕ	Description
MEAN ($\bar{x}$) :	236.8	224.6	2.154	229.2	2.125	Fine Sand
SORTING (σ):	70.20	1.322	0.403	1.311	0.390	Well Sorted
SKEWNESS (Sk):	2.525	-0.685	0.685	0.071	-0.071	Symmetrical
KURTOSIS (K):	22.99	14.85	14.85	1.088	1.088	Mesokurtic

GRAIN SIZE DISTRIBUTION

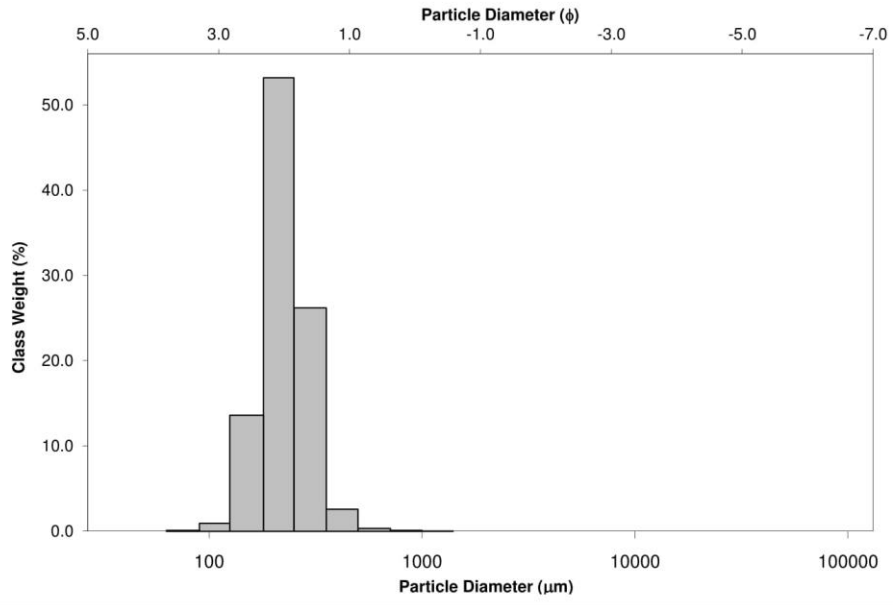

SAMPLE STATISTICS

SAMPLE IDENTITY: **NI28** ANALYST & DATE: ,

SAMPLE TYPE: Polymodal, Poorly Sorted TEXTURAL GROUP: Gravelly Sand

SEDIMENT NAME: Very Fine Gravelly Medium Sand

	μm	ϕ
MODE 1:	427.5	1.247
MODE 2:	215.0	2.237
MODE 3:	2400.0	-1.243
D_{10}:	192.5	-1.057
MEDIAN or D_{50}:	504.8	0.986
D_{90}:	2080.3	2.377
(D_{90} / D_{10}):	10.81	-2.249
(D_{90} - D_{10}):	1887.7	3.434
(D_{75} / D_{25}):	3.031	25.87
(D_{75} - D_{25}):	640.8	1.600

GRAIN SIZE DISTRIBUTION

GRAVEL:	10.8%	COARSE SAND:	26.8%
SAND:	89.2%	MEDIUM SAND:	31.4%
MUD:	0.1%	FINE SAND:	17.4%
		V FINE SAND:	0.7%
V COARSE GRAVEL:	0.0%	V COARSE SILT:	0.0%
COARSE GRAVEL:	0.0%	COARSE SILT:	0.0%
MEDIUM GRAVEL:	0.0%	MEDIUM SILT:	0.0%
FINE GRAVEL:	4.3%	FINE SILT:	0.0%
V FINE GRAVEL:	6.5%	V FINE SILT:	0.0%
V COARSE SAND:	12.9%	CLAY:	0.0%

	METHOD OF MOMENTS			FOLK & WARD METHOD		
	Arithmetic μm	Geometric μm	Logarithmic ϕ	Geometric μm	Logarithmic ϕ	Description
MEAN ($\bar{x}$) :	886.9	571.1	0.808	552.4	0.856	Coarse Sand
SORTING (σ):	1016.3	2.400	1.263	2.426	1.278	Poorly Sorted
SKEWNESS (Sk):	2.596	0.450	-0.450	0.162	-0.162	Coarse Skewed
KURTOSIS (K):	9.855	3.164	3.164	1.056	1.056	Mesokurtic

GRAIN SIZE DISTRIBUTION

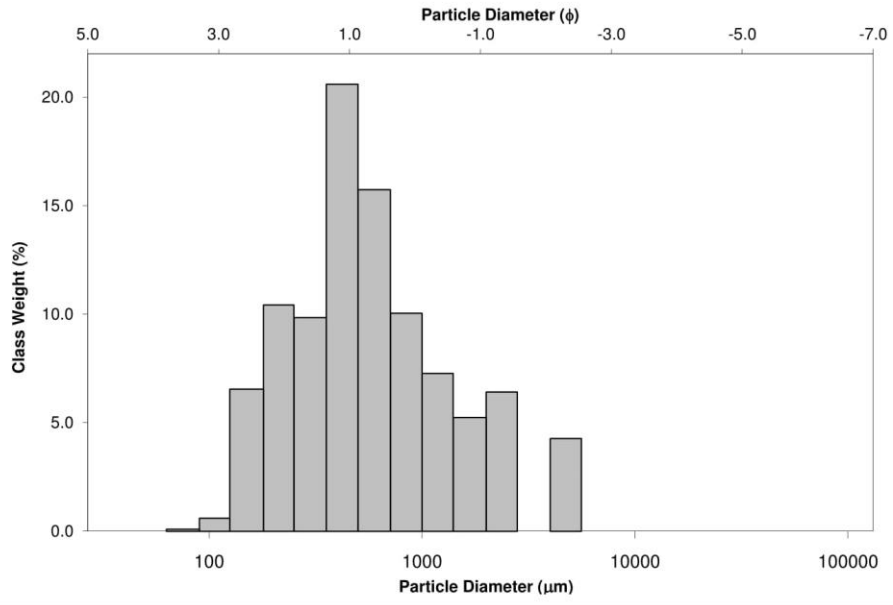

SAMPLE STATISTICS

SAMPLE IDENTITY: **NI 30** ANALYST & DATE: ,

SAMPLE TYPE: Trimodal, Poorly Sorted TEXTURAL GROUP: Gravelly Sand

SEDIMENT NAME: Very Fine Gravelly Coarse Sand

	μm	ϕ
MODE 1:	2400.0	-1.243
MODE 2:	855.0	0.247
MODE 3:	4800.0	-2.243
D_{10}:	395.2	-1.426
MEDIAN or D_{50}:	1207.0	-0.271
D_{90}:	2687.8	1.340
(D_{90} / D_{10}):	6.802	-0.939
(D_{90} - D_{10}):	2292.6	2.766
(D_{75} / D_{25}):	2.991	-0.431
(D_{75} - D_{25}):	1431.5	1.580

GRAIN SIZE DISTRIBUTION

GRAVEL:	29.9%	COARSE SAND:	30.1%
SAND:	69.9%	MEDIUM SAND:	7.0%
MUD:	0.2%	FINE SAND:	5.1%
		V FINE SAND:	0.6%
V COARSE GRAVEL:	0.0%	V COARSE SILT:	0.0%
COARSE GRAVEL:	0.0%	COARSE SILT:	0.0%
MEDIUM GRAVEL:	0.0%	MEDIUM SILT:	0.0%
FINE GRAVEL:	7.2%	FINE SILT:	0.0%
V FINE GRAVEL:	22.6%	V FINE SILT:	0.0%
V COARSE SAND:	27.2%	CLAY:	0.0%

	METHOD OF MOMENTS			FOLK & WARD METHOD		
	Arithmetic μm	Geometric μm	Logarithmic ϕ	Geometric μm	Logarithmic ϕ	Description
MEAN ($\bar{x}$) :	1555.3	1143.3	-0.193	1178.4	-0.237	Very Coarse Sand
SORTING (σ):	1160.7	2.304	1.204	2.279	1.188	Poorly Sorted
SKEWNESS (Sk):	1.391	-0.801	0.801	-0.085	0.085	Symmetrical
KURTOSIS (K):	4.760	4.928	4.928	1.111	1.111	Leptokurtic

GRAIN SIZE DISTRIBUTION

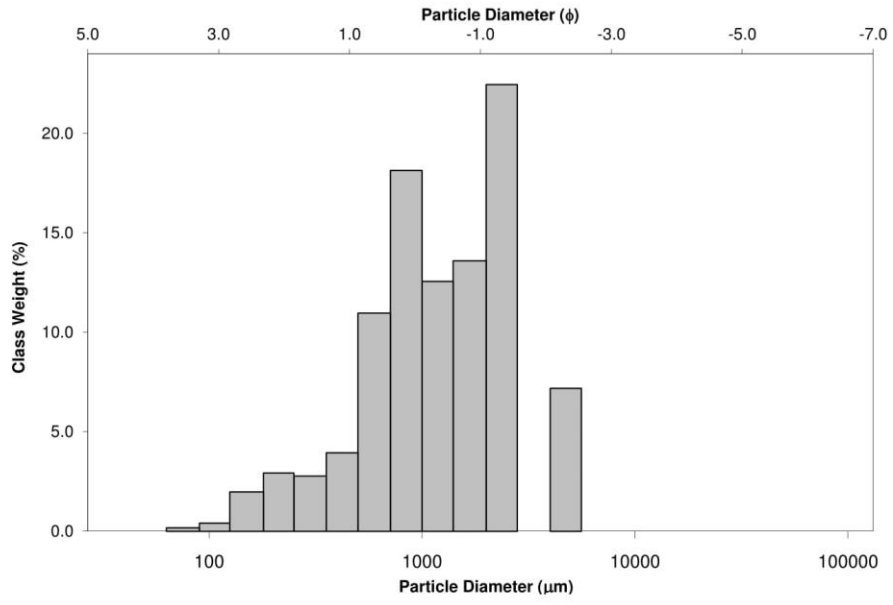

SAMPLE STATISTICS

SAMPLE IDENTITY: **NI31** ANALYST & DATE: ,

SAMPLE TYPE: Bimodal, Poorly Sorted TEXTURAL GROUP: Gravelly Sand

SEDIMENT NAME: Very Fine Gravelly Very Coarse Sand

	μm	ϕ
MODE 1:	2400.0	-1.243
MODE 2:	4800.0	-2.243
MODE 3:		
D_{10}:	394.5	-1.384
MEDIAN or D_{50}:	1248.3	-0.320
D_{90}:	2610.0	1.342
(D_{90} / D_{10}):	6.615	-0.969
(D_{90} - D_{10}):	2215.5	2.726
(D_{75} / D_{25}):	3.219	-0.566
(D_{75} - D_{25}):	1454.6	1.687

GRAIN SIZE DISTRIBUTION

GRAVEL:	28.8%	COARSE SAND:	25.0%
SAND:	71.1%	MEDIUM SAND:	12.5%
MUD:	0.1%	FINE SAND:	3.1%
		V FINE SAND:	0.3%
V COARSE GRAVEL:	0.0%	V COARSE SILT:	0.0%
COARSE GRAVEL:	0.0%	COARSE SILT:	0.0%
MEDIUM GRAVEL:	0.0%	MEDIUM SILT:	0.0%
FINE GRAVEL:	5.0%	FINE SILT:	0.0%
V FINE GRAVEL:	23.7%	V FINE SILT:	0.0%
V COARSE SAND:	30.2%	CLAY:	0.0%

	METHOD OF MOMENTS			FOLK & WARD METHOD		
	Arithmetic μm	Geometric μm	Logarithmic ϕ	Geometric μm	Logarithmic ϕ	Description
MEAN ($\bar{x}$) :	1496.6	1129.0	-0.175	1142.7	-0.192	Very Coarse Sand
SORTING (σ):	1060.9	2.201	1.138	2.209	1.143	Poorly Sorted
SKEWNESS (Sk):	1.357	-0.694	0.694	-0.142	0.142	Fine Skewed
KURTOSIS (K):	5.178	4.504	4.504	0.925	0.925	Mesokurtic

GRAIN SIZE DISTRIBUTION

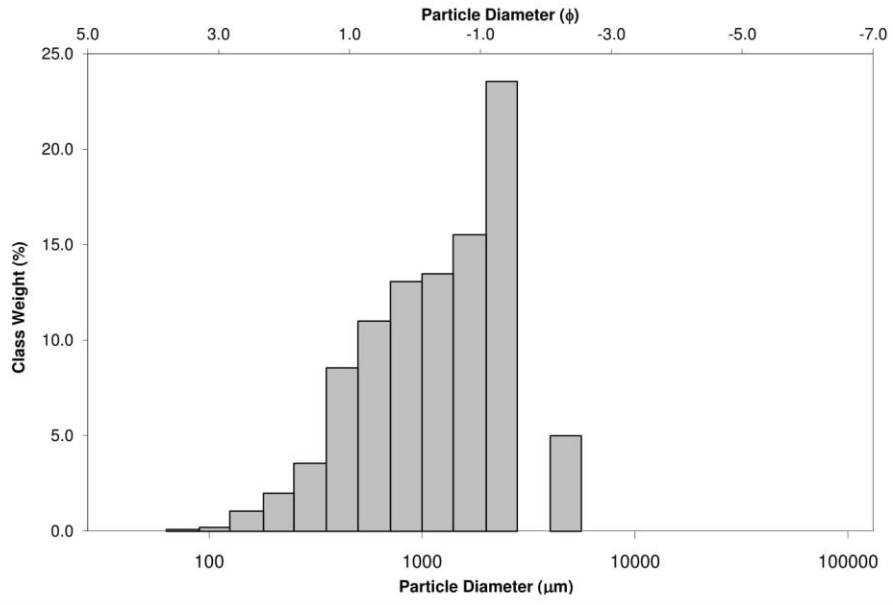

SAMPLE STATISTICS

SAMPLE IDENTITY: **NI33A** ANALYST & DATE: ,

SAMPLE TYPE: Trimodal, Poorly Sorted TEXTURAL GROUP: Sandy Gravel

SEDIMENT NAME: Sandy Fine Gravel

	μm	ϕ
MODE 1:	4800.0	-2.243
MODE 2:	302.5	1.747
MODE 3:	2400.0	-1.243
D_{10}:	235.0	-2.381
MEDIAN or D_{50}:	2432.8	-1.283
D_{90}:	5208.6	2.089
(D_{90} / D_{10}):	22.16	-0.877
(D_{90} - D_{10}):	4973.6	4.470
(D_{75} / D_{25}):	14.42	-0.731
(D_{75} - D_{25}):	4348.2	3.850

GRAIN SIZE DISTRIBUTION

GRAVEL:	55.0%	COARSE SAND:	4.7%
SAND:	44.9%	MEDIUM SAND:	22.6%
MUD:	0.1%	FINE SAND:	10.6%
		V FINE SAND:	0.5%
V COARSE GRAVEL:	0.0%	V COARSE SILT:	0.0%
COARSE GRAVEL:	0.0%	COARSE SILT:	0.0%
MEDIUM GRAVEL:	0.0%	MEDIUM SILT:	0.0%
FINE GRAVEL:	46.4%	FINE SILT:	0.0%
V FINE GRAVEL:	8.5%	V FINE SILT:	0.0%
V COARSE SAND:	6.4%	CLAY:	0.0%

	METHOD OF MOMENTS			FOLK & WARD METHOD		
	Arithmetic μm	Geometric μm	Logarithmic ϕ	Geometric μm	Logarithmic ϕ	Description
MEAN ($\bar{x}$) :	2658.1	1414.2	-0.500	1491.2	-0.576	Very Coarse Sand
SORTING (σ):	2079.7	3.748	1.906	3.446	1.785	Poorly Sorted
SKEWNESS (Sk):	-0.053	-0.497	0.497	-0.516	0.516	Very Fine Skewed
KURTOSIS (K):	1.151	1.737	1.737	0.518	0.518	Very Platykurtic

GRAIN SIZE DISTRIBUTION

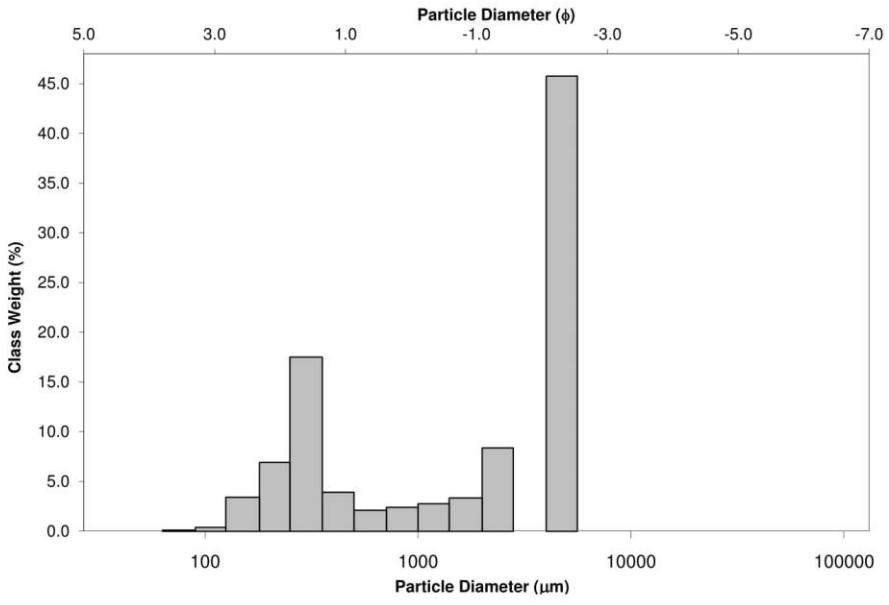

SAMPLE STATISTICS

SAMPLE IDENTITY: **NI35** ANALYST & DATE: ,

SAMPLE TYPE: Unimodal, Well Sorted TEXTURAL GROUP: Slightly Gravelly Sand

SEDIMENT NAME: Slightly Very Fine Gravelly Medium Sand

	μm	ϕ
MODE 1:	302.5	1.747
MODE 2:		
MODE 3:		
D_{10}:	262.2	0.847
MEDIAN or D_{50}:	338.2	1.564
D_{90}:	555.8	1.931
(D_{90} / D_{10}):	2.120	2.280
(D_{90} - D_{10}):	293.7	1.084
(D_{75} / D_{25}):	1.501	1.485
(D_{75} - D_{25}):	144.5	0.586

GRAIN SIZE DISTRIBUTION

GRAVEL:	0.9%	COARSE SAND:	10.2%
SAND:	99.0%	MEDIUM SAND:	85.1%
MUD:	0.0%	FINE SAND:	2.3%
		V FINE SAND:	0.2%
V COARSE GRAVEL:	0.0%	V COARSE SILT:	0.0%
COARSE GRAVEL:	0.0%	COARSE SILT:	0.0%
MEDIUM GRAVEL:	0.0%	MEDIUM SILT:	0.0%
FINE GRAVEL:	0.5%	FINE SILT:	0.0%
V FINE GRAVEL:	0.5%	V FINE SILT:	0.0%
V COARSE SAND:	1.2%	CLAY:	0.0%

	METHOD OF MOMENTS			FOLK & WARD METHOD		
	Arithmetic μm	Geometric μm	Logarithmic ϕ	Geometric μm	Logarithmic ϕ	Description
MEAN ($\bar{x}$) :	416.6	365.6	1.452	353.5	1.500	Medium Sand
SORTING (σ):	367.4	1.489	0.575	1.342	0.424	Well Sorted
SKEWNESS (Sk):	8.804	1.803	-1.803	0.333	-0.333	Very Coarse Skewed
KURTOSIS (K):	97.64	16.26	16.26	1.014	1.014	Mesokurtic

GRAIN SIZE DISTRIBUTION

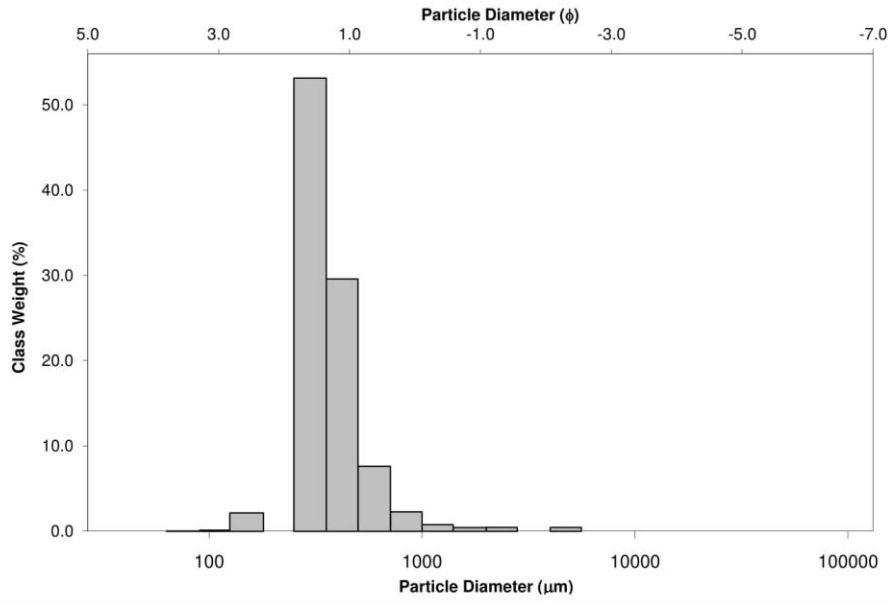

SAMPLE STATISTICS

SAMPLE IDENTITY: **NI37** ANALYST & DATE: ,

SAMPLE TYPE: Trimodal, Poorly Sorted TEXTURAL GROUP: Gravelly Sand

SEDIMENT NAME: Very Fine Gravelly Coarse Sand

	μm	ϕ
MODE 1:	427.5	1.247
MODE 2:	2400.0	-1.243
MODE 3:	4800.0	-2.243
D_{10}:	274.8	-1.118
MEDIAN or D_{50}:	602.8	0.730
D_{90}:	2170.2	1.864
(D_{90} / D_{10}):	7.898	-1.667
(D_{90} - D_{10}):	1895.5	2.982
(D_{75} / D_{25}):	2.757	-10.091
(D_{75} - D_{25}):	698.3	1.463

GRAIN SIZE DISTRIBUTION

GRAVEL:	12.0%	COARSE SAND:	33.0%
SAND:	87.9%	MEDIUM SAND:	32.6%
MUD:	0.1%	FINE SAND:	6.7%
		V FINE SAND:	0.4%
V COARSE GRAVEL:	0.0%	V COARSE SILT:	0.0%
COARSE GRAVEL:	0.0%	COARSE SILT:	0.0%
MEDIUM GRAVEL:	0.0%	MEDIUM SILT:	0.0%
FINE GRAVEL:	3.6%	FINE SILT:	0.0%
V FINE GRAVEL:	8.4%	V FINE SILT:	0.0%
V COARSE SAND:	15.3%	CLAY:	0.0%

	METHOD OF MOMENTS			FOLK & WARD METHOD		
	Arithmetic μm	Geometric μm	Logarithmic ϕ	Geometric μm	Logarithmic ϕ	Description
MEAN ($\bar{x}$) :	966.8	679.1	0.558	689.7	0.536	Coarse Sand
SORTING (σ):	964.8	2.198	1.136	2.174	1.120	Poorly Sorted
SKEWNESS (Sk):	2.474	0.368	-0.368	0.216	-0.216	Coarse Skewed
KURTOSIS (K):	9.605	3.499	3.499	1.018	1.018	Mesokurtic

GRAIN SIZE DISTRIBUTION

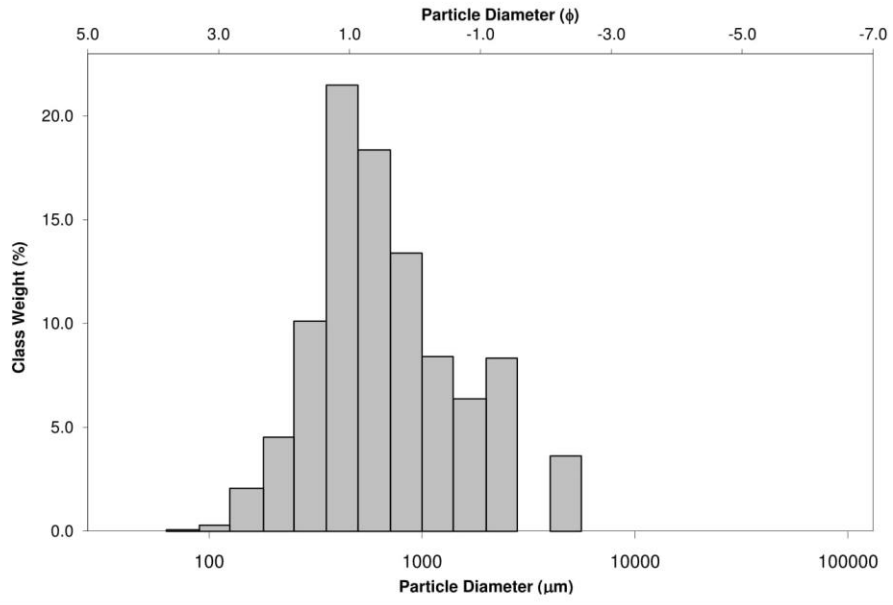

SAMPLE STATISTICS

SAMPLE IDENTITY: **NI38** ANALYST & DATE: ,

SAMPLE TYPE: Unimodal, Moderately Well Sorted TEXTURAL GROUP: Slightly Gravelly Sand

SEDIMENT NAME: Slightly Very Fine Gravelly Medium Sand

	μm	ϕ
MODE 1:	302.5	1.747
MODE 2:		
MODE 3:		
D_{10}:	194.3	0.760
MEDIAN or D_{50}:	316.7	1.659
D_{90}:	590.4	2.364
(D_{90} / D_{10}):	3.039	3.109
(D_{90} - D_{10}):	396.1	1.604
(D_{75} / D_{25}):	1.697	1.620
(D_{75} - D_{25}):	174.9	0.763

GRAIN SIZE DISTRIBUTION

GRAVEL:	0.6%	COARSE SAND:	11.1%
SAND:	99.4%	MEDIUM SAND:	61.6%
MUD:	0.1%	FINE SAND:	24.2%
		V FINE SAND:	0.3%
V COARSE GRAVEL:	0.0%	V COARSE SILT:	0.0%
COARSE GRAVEL:	0.0%	COARSE SILT:	0.0%
MEDIUM GRAVEL:	0.0%	MEDIUM SILT:	0.0%
FINE GRAVEL:	0.0%	FINE SILT:	0.0%
V FINE GRAVEL:	0.5%	V FINE SILT:	0.0%
V COARSE SAND:	2.1%	CLAY:	0.0%

	METHOD OF MOMENTS			FOLK & WARD METHOD		
	Arithmetic μm	Geometric μm	Logarithmic ϕ	Geometric μm	Logarithmic ϕ	Description
MEAN ($\bar{x}$) :	383.9	332.2	1.590	321.0	1.639	Medium Sand
SORTING (σ):	266.7	1.600	0.678	1.537	0.620	Moderately Well Sorted
SKEWNESS (Sk):	4.785	0.667	-0.667	0.121	-0.121	Coarse Skewed
KURTOSIS (K):	40.43	7.572	7.572	1.162	1.162	Leptokurtic

GRAIN SIZE DISTRIBUTION

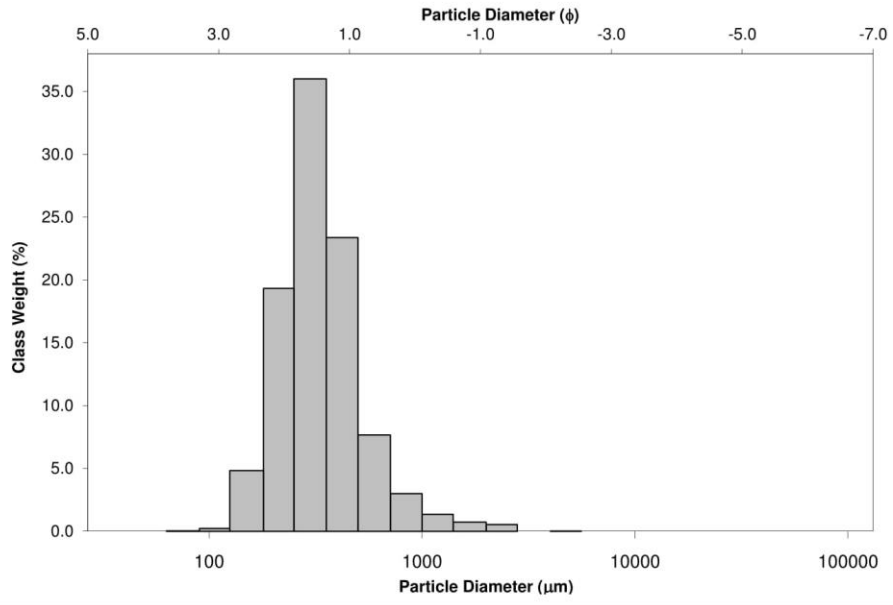

SAMPLE STATISTICS

SAMPLE IDENTITY: **NI39** ANALYST & DATE: ,

SAMPLE TYPE: Unimodal, Well Sorted TEXTURAL GROUP: Slightly Gravelly Sand

SEDIMENT NAME: Slightly Very Fine Gravelly Medium Sand

	μm	ϕ
MODE 1:	302.5	1.747
MODE 2:		
MODE 3:		
D_{10}:	250.6	1.254
MEDIAN or D_{50}:	302.3	1.726
D_{90}:	419.2	1.996
(D_{90} / D_{10}):	1.673	1.592
(D_{90} - D_{10}):	168.6	0.742
(D_{75} / D_{25}):	1.264	1.217
(D_{75} - D_{25}):	71.02	0.338

GRAIN SIZE DISTRIBUTION

GRAVEL:	0.1%	COARSE SAND:	3.5%
SAND:	99.9%	MEDIUM SAND:	86.6%
MUD:	0.0%	FINE SAND:	9.0%
		V FINE SAND:	0.4%
V COARSE GRAVEL:	0.0%	V COARSE SILT:	0.0%
COARSE GRAVEL:	0.0%	COARSE SILT:	0.0%
MEDIUM GRAVEL:	0.0%	MEDIUM SILT:	0.0%
FINE GRAVEL:	0.0%	FINE SILT:	0.0%
V FINE GRAVEL:	0.1%	V FINE SILT:	0.0%
V COARSE SAND:	0.4%	CLAY:	0.0%

	METHOD OF MOMENTS			FOLK & WARD METHOD		
	Arithmetic μm	Geometric μm	Logarithmic ϕ	Geometric μm	Logarithmic ϕ	Description
MEAN ($\bar{x}$) :	321.3	300.3	1.736	302.3	1.726	Medium Sand
SORTING (σ):	134.6	1.370	0.454	1.293	0.371	Well Sorted
SKEWNESS (Sk):	8.749	-0.162	0.162	-0.097	0.097	Symmetrical
KURTOSIS (K):	179.0	12.99	12.99	2.049	2.049	Very Leptokurtic

GRAIN SIZE DISTRIBUTION

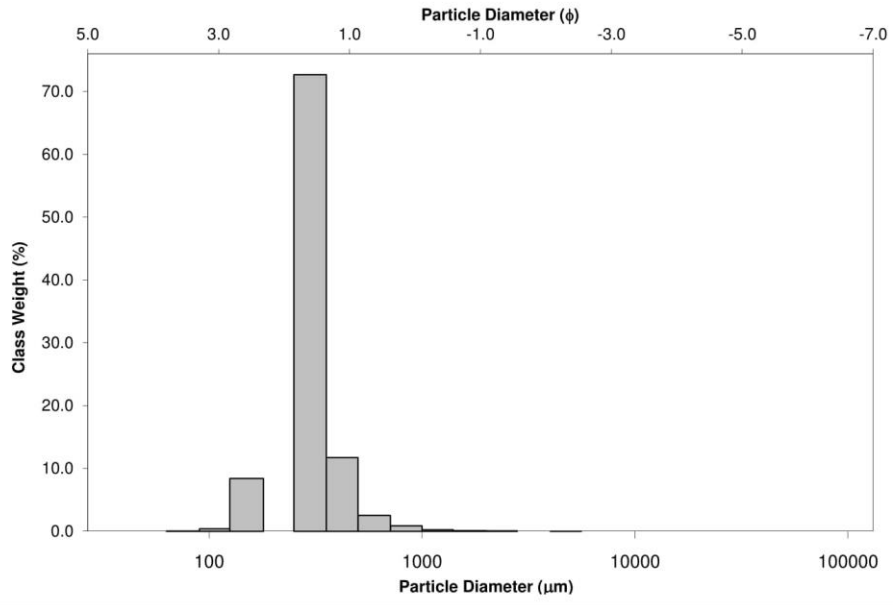

SAMPLE STATISTICS

SAMPLE IDENTITY: **NI40** ANALYST & DATE: ,

SAMPLE TYPE: Unimodal, Well Sorted TEXTURAL GROUP: Slightly Gravelly Sand

SEDIMENT NAME: Slightly Very Fine Gravelly Medium Sand

	μm	ϕ
MODE 1:	302.5	1.747
MODE 2:		
MODE 3:		
D_{10}:	254.6	1.046
MEDIAN or D_{50}:	313.3	1.674
D_{90}:	484.2	1.974
(D_{90} / D_{10}):	1.902	1.887
(D_{90} - D_{10}):	229.7	0.928
(D_{75} / D_{25}):	1.313	1.268
(D_{75} - D_{25}):	86.19	0.393

GRAIN SIZE DISTRIBUTION

GRAVEL:	0.2%	COARSE SAND:	7.5%
SAND:	99.8%	MEDIUM SAND:	85.1%
MUD:	0.0%	FINE SAND:	6.1%
		V FINE SAND:	0.3%
V COARSE GRAVEL:	0.0%	V COARSE SILT:	0.0%
COARSE GRAVEL:	0.0%	COARSE SILT:	0.0%
MEDIUM GRAVEL:	0.0%	MEDIUM SILT:	0.0%
FINE GRAVEL:	0.1%	FINE SILT:	0.0%
V FINE GRAVEL:	0.1%	V FINE SILT:	0.0%
V COARSE SAND:	0.7%	CLAY:	0.0%

	METHOD OF MOMENTS			FOLK & WARD METHOD		
	Arithmetic μm	Geometric μm	Logarithmic ϕ	Geometric μm	Logarithmic ϕ	Description
MEAN ($\bar{x}$) :	354.2	324.7	1.623	328.5	1.606	Medium Sand
SORTING (σ):	199.4	1.421	0.507	1.381	0.466	Well Sorted
SKEWNESS (Sk):	10.62	0.441	-0.441	0.153	-0.153	Coarse Skewed
KURTOSIS (K):	199.4	13.68	13.68	1.976	1.976	Very Leptokurtic

GRAIN SIZE DISTRIBUTION

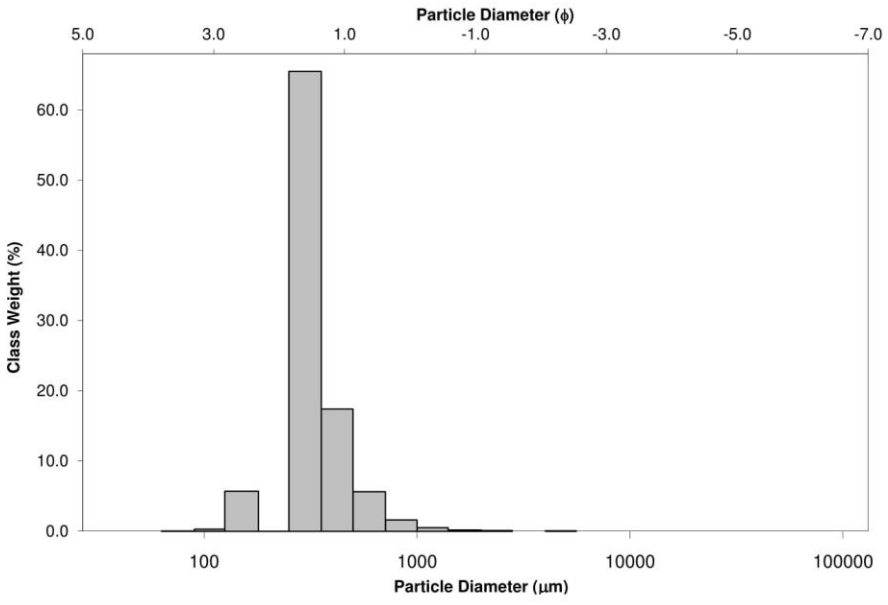

SAMPLE STATISTICS

SAMPLE IDENTITY: **NI 41** ANALYST & DATE: ,

SAMPLE TYPE: Unimodal, Moderately Sorted TEXTURAL GROUP: Slightly Gravelly Sand

SEDIMENT NAME: Slightly Very Fine Gravelly Medium Sand

	μm	ϕ
MODE 1:	427.5	1.247
MODE 2:		
MODE 3:		
D_{10}:	378.8	-0.516
MEDIAN or D_{50}:	602.7	0.730
D_{90}:	1429.9	1.401
(D_{90} / D_{10}):	3.775	-2.715
(D_{90} - D_{10}):	1051.1	1.916
(D_{75} / D_{25}):	2.215	26.20
(D_{75} - D_{25}):	531.5	1.147

GRAIN SIZE DISTRIBUTION

GRAVEL:	3.6%	COARSE SAND:	37.6%
SAND:	96.3%	MEDIUM SAND:	37.9%
MUD:	0.0%	FINE SAND:	1.0%
		V FINE SAND:	0.0%
V COARSE GRAVEL:	0.0%	V COARSE SILT:	0.0%
COARSE GRAVEL:	0.0%	COARSE SILT:	0.0%
MEDIUM GRAVEL:	0.0%	MEDIUM SILT:	0.0%
FINE GRAVEL:	0.6%	FINE SILT:	0.0%
V FINE GRAVEL:	3.1%	V FINE SILT:	0.0%
V COARSE SAND:	19.8%	CLAY:	0.0%

	METHOD OF MOMENTS			FOLK & WARD METHOD		
	Arithmetic μm	Geometric μm	Logarithmic ϕ	Geometric μm	Logarithmic ϕ	Description
MEAN ($\bar{x}$) :	803.2	672.2	0.573	664.2	0.590	Coarse Sand
SORTING (σ):	557.1	1.716	0.779	1.690	0.757	Moderately Sorted
SKEWNESS (Sk):	2.952	0.582	-0.582	0.319	-0.319	Very Coarse Skewed
KURTOSIS (K):	17.34	4.188	4.188	0.845	0.845	Platykurtic

GRAIN SIZE DISTRIBUTION

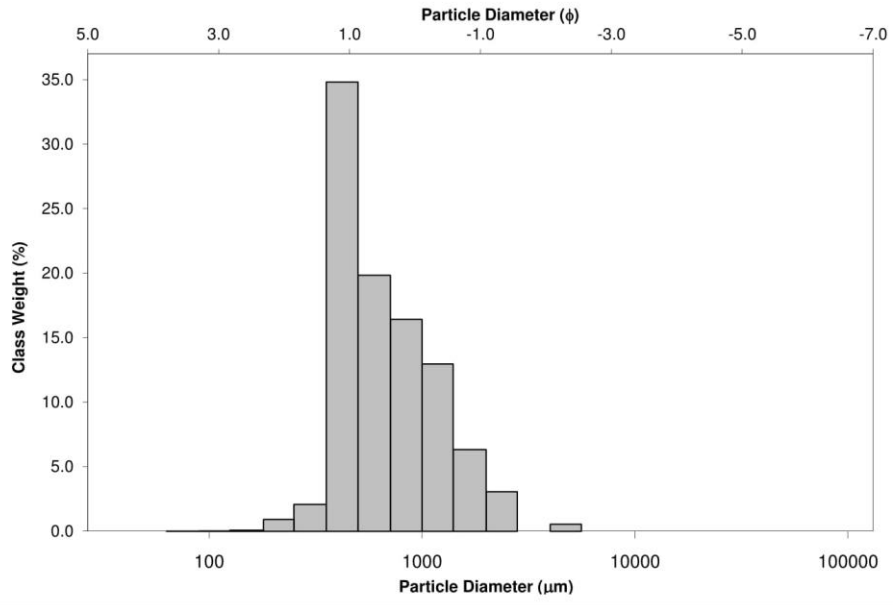

SAMPLE STATISTICS

SAMPLE IDENTITY: **NI 43 A** ANALYST & DATE: ,

SAMPLE TYPE: Bimodal, Moderately Sorted TEXTURAL GROUP: Sandy Gravel

SEDIMENT NAME: Sandy Very Fine Gravel

	µm	ϕ
MODE 1:	2400.0	-1.243
MODE 2:	4800.0	-2.243
MODE 3:		
D_{10}:	574.6	-1.418
MEDIAN or D_{50}:	1493.2	-0.578
D_{90}:	2672.7	0.799
(D_{90} / D_{10}):	4.651	-0.564
(D_{90} - D_{10}):	2098.0	2.218
(D_{75} / D_{25}):	2.372	-0.089
(D_{75} - D_{25}):	1277.9	1.246

GRAIN SIZE DISTRIBUTION

GRAVEL:	32.9%	COARSE SAND:	20.6%
SAND:	67.1%	MEDIUM SAND:	6.0%
MUD:	0.0%	FINE SAND:	1.1%
		V FINE SAND:	0.1%
V COARSE GRAVEL:	0.0%	V COARSE SILT:	0.0%
COARSE GRAVEL:	0.0%	COARSE SILT:	0.0%
MEDIUM GRAVEL:	0.0%	MEDIUM SILT:	0.0%
FINE GRAVEL:	6.3%	FINE SILT:	0.0%
V FINE GRAVEL:	26.5%	V FINE SILT:	0.0%
V COARSE SAND:	39.3%	CLAY:	0.0%

	METHOD OF MOMENTS			FOLK & WARD METHOD		
	Arithmetic µm	Geometric µm	Logarithmic ϕ	Geometric µm	Logarithmic ϕ	Description
MEAN ($\bar{x}$) :	1701.2	1384.6	-0.469	1400.5	-0.486	Very Coarse Sand
SORTING (σ):	1047.4	1.927	0.947	1.924	0.944	Moderately Sorted
SKEWNESS (Sk):	1.390	-0.692	0.692	-0.127	0.127	Fine Skewed
KURTOSIS (K):	5.260	4.785	4.785	1.106	1.106	Mesokurtic

GRAIN SIZE DISTRIBUTION

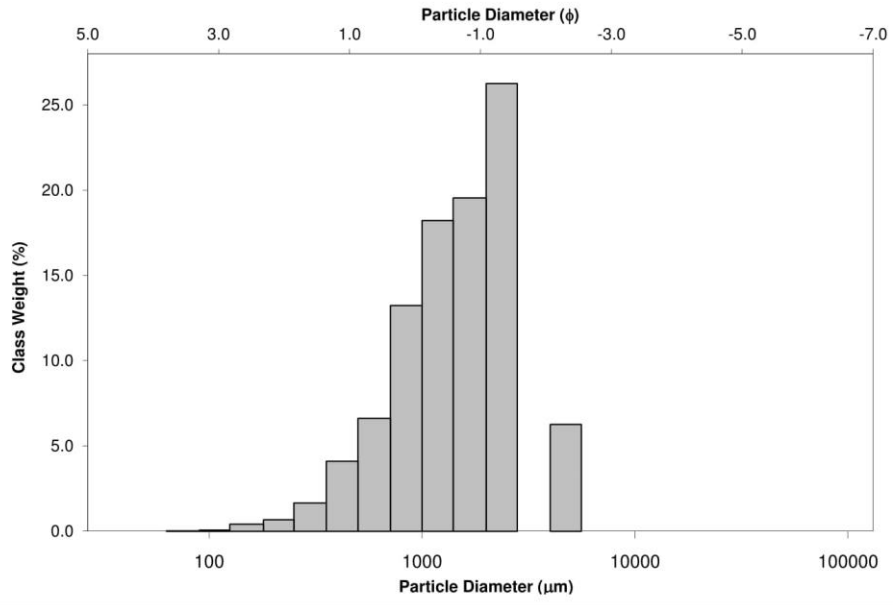

SAMPLE STATISTICS

SAMPLE IDENTITY: **NI44** ANALYST & DATE: ,

SAMPLE TYPE: Bimodal, Very Poorly Sorted TEXTURAL GROUP: Sandy Gravel

SEDIMENT NAME: Sandy Fine Gravel

	μm	ϕ
MODE 1:	4800.0	-2.243
MODE 2:	215.0	2.237
MODE 3:		
D_{10}:	145.0	-2.357
MEDIAN or D_{50}:	291.8	1.777
D_{90}:	5122.9	2.785
(D_{90} / D_{10}):	35.32	-1.182
(D_{90} - D_{10}):	4977.9	5.142
(D_{75} / D_{25}):	23.53	-1.105
(D_{75} - D_{25}):	4291.9	4.556

GRAIN SIZE DISTRIBUTION

GRAVEL:	38.8%	COARSE SAND:	0.8%
SAND:	61.1%	MEDIUM SAND:	15.4%
MUD:	0.1%	FINE SAND:	41.8%
		V FINE SAND:	2.3%
V COARSE GRAVEL:	0.0%	V COARSE SILT:	0.0%
COARSE GRAVEL:	0.0%	COARSE SILT:	0.0%
MEDIUM GRAVEL:	0.0%	MEDIUM SILT:	0.0%
FINE GRAVEL:	37.8%	FINE SILT:	0.0%
V FINE GRAVEL:	1.0%	V FINE SILT:	0.0%
V COARSE SAND:	0.8%	CLAY:	0.0%

	METHOD OF MOMENTS			FOLK & WARD METHOD		
	Arithmetic μm	Geometric μm	Logarithmic ϕ	Geometric μm	Logarithmic ϕ	Description
MEAN ($\bar{x}$) :	1986.1	703.1	0.508	613.8	0.704	Coarse Sand
SORTING (σ):	2207.9	4.677	2.226	4.096	2.034	Very Poorly Sorted
SKEWNESS (Sk):	0.473	0.331	-0.331	0.614	-0.614	Very Coarse Skewed
KURTOSIS (K):	1.245	1.298	1.298	0.481	0.481	Very Platykurtic

GRAIN SIZE DISTRIBUTION

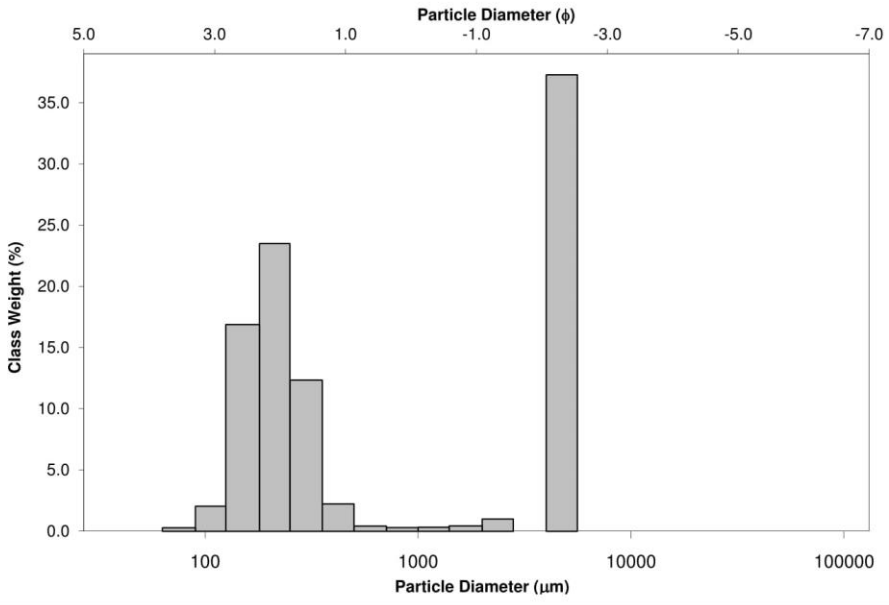

SAMPLE STATISTICS

SAMPLE IDENTITY: **NI46** ANALYST & DATE: ,

SAMPLE TYPE: Bimodal, Moderately Well Sorted TEXTURAL GROUP: Slightly Gravelly Sand

SEDIMENT NAME: Slightly Very Fine Gravelly Medium Sand

	μm	ϕ
MODE 1:	302.5	1.747
MODE 2:	152.5	2.737
MODE 3:		
D_{10}:	152.5	1.012
MEDIAN or D_{50}:	314.3	1.670
D_{90}:	495.9	2.713
(D_{90} / D_{10}):	3.252	2.682
(D_{90} - D_{10}):	343.4	1.701
(D_{75} / D_{25}):	1.502	1.440
(D_{75} - D_{25}):	132.6	0.587

GRAIN SIZE DISTRIBUTION

GRAVEL:	0.1%	COARSE SAND:	8.8%
SAND:	99.8%	MEDIUM SAND:	73.4%
MUD:	0.1%	FINE SAND:	15.6%
		V FINE SAND:	1.4%
V COARSE GRAVEL:	0.0%	V COARSE SILT:	0.0%
COARSE GRAVEL:	0.0%	COARSE SILT:	0.0%
MEDIUM GRAVEL:	0.0%	MEDIUM SILT:	0.0%
FINE GRAVEL:	0.0%	FINE SILT:	0.0%
V FINE GRAVEL:	0.1%	V FINE SILT:	0.0%
V COARSE SAND:	0.5%	CLAY:	0.0%

	METHOD OF MOMENTS			FOLK & WARD METHOD		
	Arithmetic μm	Geometric μm	Logarithmic ϕ	Geometric μm	Logarithmic ϕ	Description
MEAN ($\bar{x}$) :	344.1	307.6	1.701	292.4	1.774	Medium Sand
SORTING (σ):	182.5	1.553	0.635	1.596	0.674	Moderately Well Sorted
SKEWNESS (Sk):	6.897	-0.376	0.376	-0.167	0.167	Fine Skewed
KURTOSIS (K):	125.4	6.884	6.884	1.529	1.529	Very Leptokurtic

GRAIN SIZE DISTRIBUTION

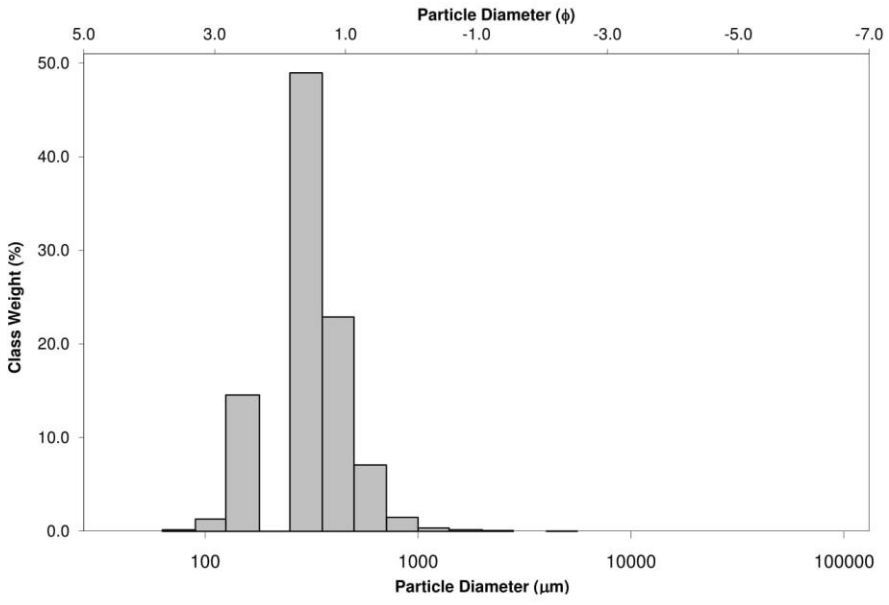

SAMPLE STATISTICS

SAMPLE IDENTITY: **OF 2** ANALYST & DATE: ,

SAMPLE TYPE: Bimodal, Poorly Sorted TEXTURAL GROUP: Gravelly Sand

SEDIMENT NAME: Very Fine Gravelly Very Coarse Sand

	μm	ϕ
MODE 1:	427.5	1.247
MODE 2:	1200.0	-0.243
MODE 3:		
D_{10}:	335.6	-1.090
MEDIAN or D_{50}:	863.0	0.213
D_{90}:	2129.4	1.575
(D_{90} / D_{10}):	6.345	-1.445
(D_{90} - D_{10}):	1793.8	2.666
(D_{75} / D_{25}):	3.190	-1.927
(D_{75} - D_{25}):	1020.3	1.674

GRAIN SIZE DISTRIBUTION

GRAVEL:	12.1%	COARSE SAND:	27.5%
SAND:	86.0%	MEDIUM SAND:	26.3%
MUD:	2.0%	FINE SAND:	0.3%
		V FINE SAND:	0.0%
V COARSE GRAVEL:	0.0%	V COARSE SILT:	0.3%
COARSE GRAVEL:	0.0%	COARSE SILT:	0.3%
MEDIUM GRAVEL:	0.0%	MEDIUM SILT:	0.3%
FINE GRAVEL:	1.0%	FINE SILT:	0.3%
V FINE GRAVEL:	11.0%	V FINE SILT:	0.3%
V COARSE SAND:	31.9%	CLAY:	0.3%

	METHOD OF MOMENTS			FOLK & WARD METHOD		
	Arithmetic μm	Geometric μm	Logarithmic ϕ	Geometric μm	Logarithmic ϕ	Description
MEAN ($\bar{x}$) :	1078.3	791.3	0.338	849.5	0.235	Coarse Sand
SORTING (σ):	766.1	2.540	1.345	2.052	1.037	Poorly Sorted
SKEWNESS (Sk):	1.546	-2.203	2.203	-0.033	0.033	Symmetrical
KURTOSIS (K):	7.086	12.34	12.34	0.774	0.774	Platykurtic

GRAIN SIZE DISTRIBUTION

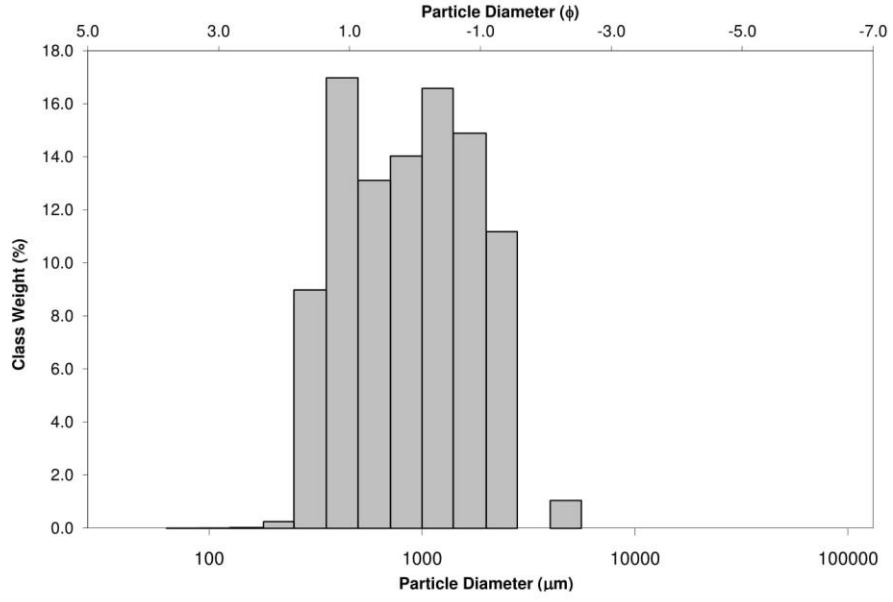

SAMPLE STATISTICS

SAMPLE IDENTITY: **OF 3** ANALYST & DATE: ,

SAMPLE TYPE: Unimodal, Moderately Sorted TEXTURAL GROUP: Slightly Gravelly Sand

SEDIMENT NAME: Slightly Very Fine Gravelly Coarse Sand

	μm	ϕ
MODE 1:	427.5	1.247
MODE 2:		
MODE 3:		
D_{10}:	335.3	-0.280
MEDIAN or D_{50}:	566.4	0.820
D_{90}:	1214.5	1.576
(D_{90} / D_{10}):	3.622	-5.622
(D_{90} - D_{10}):	879.2	1.857
(D_{75} / D_{25}):	2.047	5.321
(D_{75} - D_{25}):	433.3	1.033

GRAIN SIZE DISTRIBUTION

GRAVEL:	1.5%	COARSE SAND:	42.5%
SAND:	96.9%	MEDIUM SAND:	39.7%
MUD:	1.6%	FINE SAND:	0.2%
		V FINE SAND:	0.0%
V COARSE GRAVEL:	0.0%	V COARSE SILT:	0.3%
COARSE GRAVEL:	0.0%	COARSE SILT:	0.3%
MEDIUM GRAVEL:	0.0%	MEDIUM SILT:	0.3%
FINE GRAVEL:	0.2%	FINE SILT:	0.3%
V FINE GRAVEL:	1.3%	V FINE SILT:	0.3%
V COARSE SAND:	14.6%	CLAY:	0.3%

	METHOD OF MOMENTS			FOLK & WARD METHOD		
	Arithmetic μm	Geometric μm	Logarithmic ϕ	Geometric μm	Logarithmic ϕ	Description
MEAN ($\bar{x}$) :	697.0	571.0	0.808	596.3	0.746	Coarse Sand
SORTING (σ):	433.6	2.071	1.051	1.645	0.718	Moderately Sorted
SKEWNESS (Sk):	2.826	-2.941	2.941	0.154	-0.154	Coarse Skewed
KURTOSIS (K):	19.39	19.86	19.86	0.948	0.948	Mesokurtic

GRAIN SIZE DISTRIBUTION

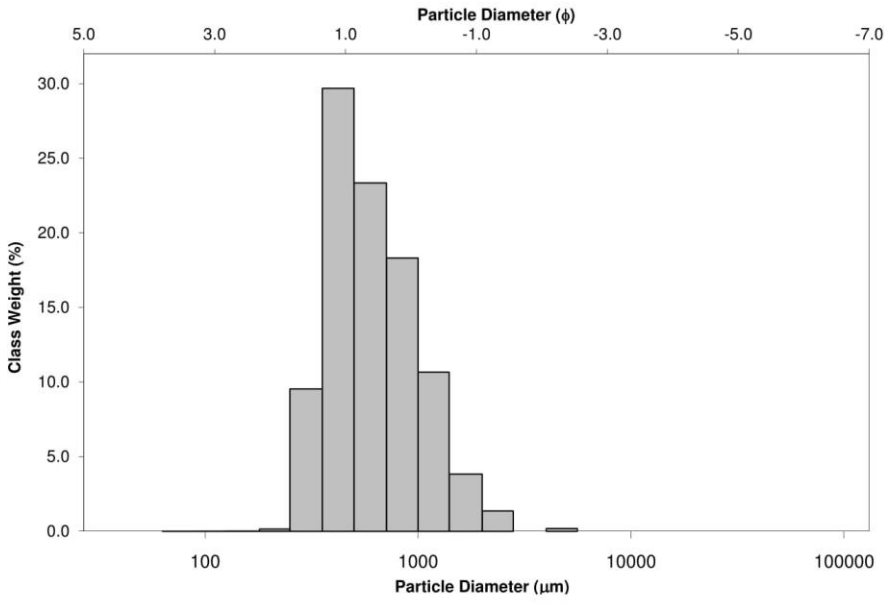

SAMPLE STATISTICS

SAMPLE IDENTITY: **OF 4** ANALYST & DATE: ,

SAMPLE TYPE: Unimodal, Moderately Well Sorted TEXTURAL GROUP: Slightly Gravelly Sand

SEDIMENT NAME: Slightly Fine Gravelly Medium Sand

	µm	ϕ
MODE 1:	427.5	1.247
MODE 2:		
MODE 3:		
D_{10}:	314.9	0.342
MEDIAN or D_{50}:	477.8	1.065
D_{90}:	789.0	1.667
(D_{90} / D_{10}):	2.506	4.876
(D_{90} - D_{10}):	474.1	1.325
(D_{75} / D_{25}):	1.600	1.993
(D_{75} - D_{25}):	233.6	0.678

GRAIN SIZE DISTRIBUTION

GRAVEL:	0.5%	COARSE SAND:	42.1%
SAND:	96.8%	MEDIUM SAND:	52.7%
MUD:	2.7%	FINE SAND:	0.2%
		V FINE SAND:	0.0%
V COARSE GRAVEL:	0.0%	V COARSE SILT:	0.4%
COARSE GRAVEL:	0.0%	COARSE SILT:	0.4%
MEDIUM GRAVEL:	0.0%	MEDIUM SILT:	0.4%
FINE GRAVEL:	0.4%	FINE SILT:	0.4%
V FINE GRAVEL:	0.0%	V FINE SILT:	0.4%
V COARSE SAND:	1.8%	CLAY:	0.4%

	METHOD OF MOMENTS			FOLK & WARD METHOD		
	Arithmetic µm	Geometric µm	Logarithmic ϕ	Geometric µm	Logarithmic ϕ	Description
MEAN ($\bar{x}$) :	541.3	452.0	1.146	492.1	1.023	Medium Sand
SORTING (σ):	350.0	2.134	1.093	1.417	0.503	Moderately Well Sorted
SKEWNESS (Sk):	8.073	-3.863	3.863	0.100	-0.100	Symmetrical
KURTOSIS (K):	96.46	22.49	22.49	1.077	1.077	Mesokurtic

GRAIN SIZE DISTRIBUTION

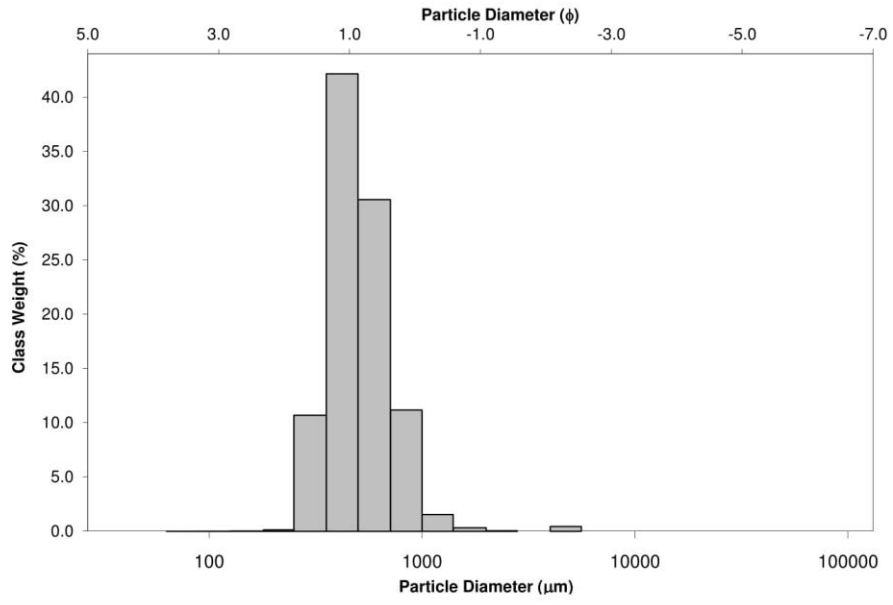

SAMPLE STATISTICS

SAMPLE IDENTITY: **OF 5** ANALYST & DATE: ,

SAMPLE TYPE: Trimodal, Poorly Sorted TEXTURAL GROUP: Gravelly Sand

SEDIMENT NAME: Very Fine Gravelly Medium Sand

	μm	ϕ
MODE 1:	427.5	1.247
MODE 2:	2400.0	-1.243
MODE 3:	4800.0	-2.243
D_{10}:	357.5	-1.483
MEDIAN or D_{50}:	709.5	0.495
D_{90}:	2794.4	1.484
(D_{90} / D_{10}):	7.816	-1.001
(D_{90} - D_{10}):	2436.9	2.966
(D_{75} / D_{25}):	4.323	-1.238
(D_{75} - D_{25}):	1478.7	2.112

GRAIN SIZE DISTRIBUTION

GRAVEL:	24.2%	COARSE SAND:	28.7%
SAND:	75.7%	MEDIUM SAND:	32.7%
MUD:	0.0%	FINE SAND:	0.3%
		V FINE SAND:	0.0%
V COARSE GRAVEL:	0.0%	V COARSE SILT:	0.0%
COARSE GRAVEL:	0.0%	COARSE SILT:	0.0%
MEDIUM GRAVEL:	0.0%	MEDIUM SILT:	0.0%
FINE GRAVEL:	9.9%	FINE SILT:	0.0%
V FINE GRAVEL:	14.3%	V FINE SILT:	0.0%
V COARSE SAND:	14.1%	CLAY:	0.0%

	METHOD OF MOMENTS			FOLK & WARD METHOD		
	Arithmetic μm	Geometric μm	Logarithmic ϕ	Geometric μm	Logarithmic ϕ	Description
MEAN ($\bar{x}$) :	1354.9	902.4	0.148	875.9	0.191	Coarse Sand
SORTING (σ):	1332.7	2.345	1.230	2.399	1.263	Poorly Sorted
SKEWNESS (Sk):	1.620	0.534	-0.534	0.360	-0.360	Very Coarse Skewed
KURTOSIS (K):	4.593	2.261	2.261	0.773	0.773	Platykurtic

GRAIN SIZE DISTRIBUTION

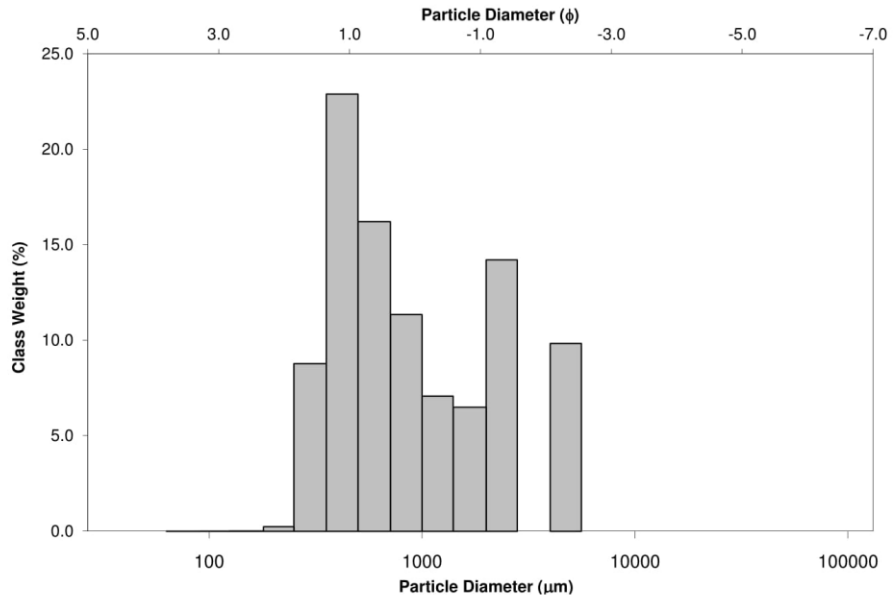

SAMPLE STATISTICS

SIEVING ERROR: 1.8%

SAMPLE IDENTITY: **OF 6A**

ANALYST & DATE: ,

SAMPLE TYPE: Bimodal, Poorly Sorted

TEXTURAL GROUP: Gravelly Sand

SEDIMENT NAME: Very Fine Gravelly Very Coarse Sand

	μm	ϕ
MODE 1:	1200.0	-0.243
MODE 2:	4800.0	-2.243
MODE 3:		
D_{10}:	405.2	-1.310
MEDIAN or D_{50}:	1018.3	-0.026
D_{90}:	2479.3	1.303
(D_{90} / D_{10}):	6.119	-0.995
(D_{90} - D_{10}):	2074.1	2.613
(D_{75} / D_{25}):	2.611	-0.951
(D_{75} - D_{25}):	1008.9	1.384

GRAIN SIZE DISTRIBUTION

GRAVEL:	16.9%	COARSE SAND:	32.5%
SAND:	83.1%	MEDIUM SAND:	15.8%
MUD:	0.0%	FINE SAND:	0.5%
		V FINE SAND:	0.1%
V COARSE GRAVEL:	0.0%	V COARSE SILT:	0.0%
COARSE GRAVEL:	0.0%	COARSE SILT:	0.0%
MEDIUM GRAVEL:	0.0%	MEDIUM SILT:	0.0%
FINE GRAVEL:	6.1%	FINE SILT:	0.0%
V FINE GRAVEL:	10.8%	V FINE SILT:	0.0%
V COARSE SAND:	34.2%	CLAY:	0.0%

	METHOD OF MOMENTS			FOLK & WARD METHOD		
	Arithmetic μm	Geometric μm	Logarithmic ϕ	Geometric μm	Logarithmic ϕ	Description
MEAN ($\bar{x}$) :	1340.5	1026.3	-0.037	1010.0	-0.014	Very Coarse Sand
SORTING (σ):	1070.3	2.021	1.015	2.102	1.072	Poorly Sorted
SKEWNESS (Sk):	1.990	0.083	-0.083	0.053	-0.053	Symmetrical
KURTOSIS (K):	6.927	3.386	3.386	1.087	1.087	Mesokurtic

GRAIN SIZE DISTRIBUTION

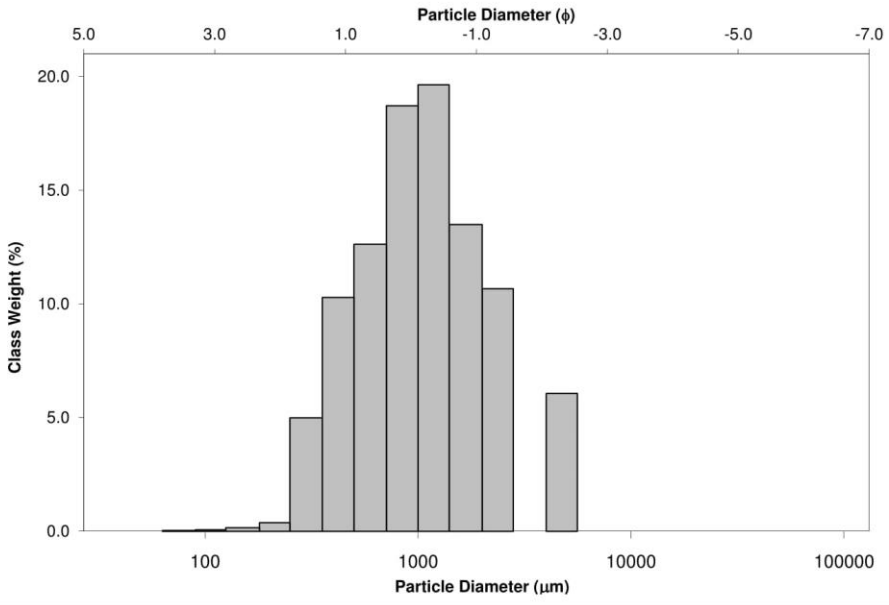

SAMPLE STATISTICS

SIEVING ERROR: 2.0%

SAMPLE IDENTITY: **OF 7A**

ANALYST & DATE: ,

SAMPLE TYPE: Unimodal, Moderately Sorted

TEXTURAL GROUP: Gravelly Sand

SEDIMENT NAME: Very Fine Gravelly Coarse Sand

	μm	ϕ
MODE 1:	855.0	0.247
MODE 2:		
MODE 3:		
D_{10}:	441.7	-0.940
MEDIAN or D_{50}:	833.8	0.262
D_{90}:	1919.2	1.179
(D_{90} / D_{10}):	4.345	-1.254
(D_{90} - D_{10}):	1477.5	2.119
(D_{75} / D_{25}):	2.079	-2.600
(D_{75} - D_{25}):	636.0	1.056

GRAIN SIZE DISTRIBUTION

GRAVEL:	8.9%	COARSE SAND:	50.3%
SAND:	91.1%	MEDIUM SAND:	14.3%
MUD:	0.0%	FINE SAND:	0.1%
		V FINE SAND:	0.0%
V COARSE GRAVEL:	0.0%	V COARSE SILT:	0.0%
COARSE GRAVEL:	0.0%	COARSE SILT:	0.0%
MEDIUM GRAVEL:	0.0%	MEDIUM SILT:	0.0%
FINE GRAVEL:	2.1%	FINE SILT:	0.0%
V FINE GRAVEL:	6.8%	V FINE SILT:	0.0%
V COARSE SAND:	26.4%	CLAY:	0.0%

	METHOD OF MOMENTS			FOLK & WARD METHOD		
	Arithmetic μm	Geometric μm	Logarithmic ϕ	Geometric μm	Logarithmic ϕ	Description
MEAN ($\bar{x}$) :	1059.9	878.5	0.187	867.2	0.206	Coarse Sand
SORTING (σ):	760.4	1.745	0.804	1.737	0.797	Moderately Sorted
SKEWNESS (Sk):	2.784	0.550	-0.550	0.133	-0.133	Coarse Skewed
KURTOSIS (K):	13.12	3.807	3.807	1.034	1.034	Mesokurtic

GRAIN SIZE DISTRIBUTION

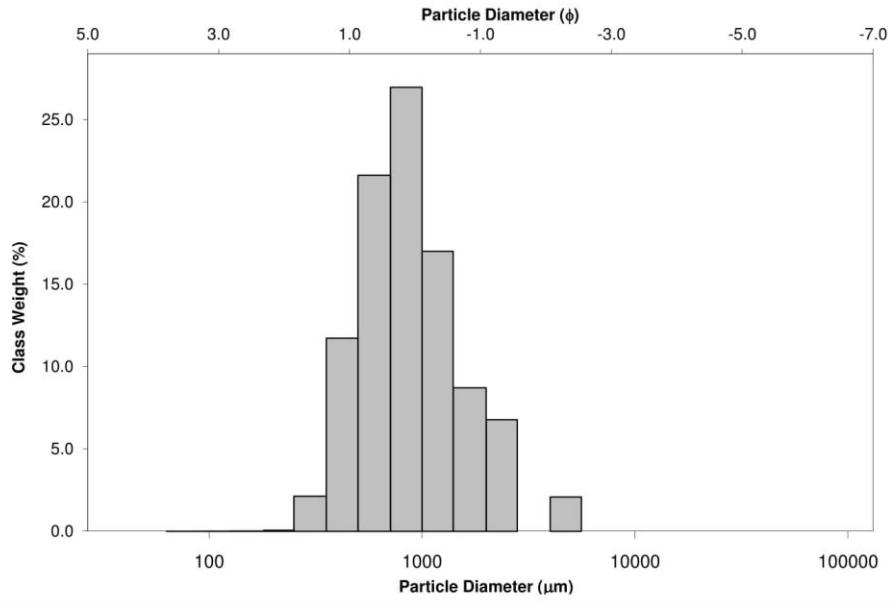

SAMPLE STATISTICS

SAMPLE IDENTITY: **OF 8**

ANALYST & DATE: ,

SAMPLE TYPE: Trimodal, Poorly Sorted

TEXTURAL GROUP: Sandy Gravel

SEDIMENT NAME: Sandy Fine Gravel

	μm	ϕ
MODE 1:	4800.0	-2.243
MODE 2:	855.0	0.247
MODE 3:	2400.0	-1.243
D_{10}:	565.3	-2.343
MEDIAN or D_{50}:	1786.8	-0.837
D_{90}:	5072.6	0.823
(D_{90} / D_{10}):	8.973	-0.351
(D_{90} - D_{10}):	4507.3	3.166
(D_{75} / D_{25}):	5.184	-0.115
(D_{75} - D_{25}):	3529.5	2.374

GRAIN SIZE DISTRIBUTION

GRAVEL:	47.2%	COARSE SAND:	26.4%
SAND:	52.8%	MEDIUM SAND:	5.8%
MUD:	0.0%	FINE SAND:	0.1%
		V FINE SAND:	0.0%
V COARSE GRAVEL:	0.0%	V COARSE SILT:	0.0%
COARSE GRAVEL:	0.0%	COARSE SILT:	0.0%
MEDIUM GRAVEL:	0.0%	MEDIUM SILT:	0.0%
FINE GRAVEL:	34.0%	FINE SILT:	0.0%
V FINE GRAVEL:	13.2%	V FINE SILT:	0.0%
V COARSE SAND:	20.5%	CLAY:	0.0%

	METHOD OF MOMENTS			FOLK & WARD METHOD		
	Arithmetic μm	Geometric μm	Logarithmic ϕ	Geometric μm	Logarithmic ϕ	Description
MEAN ($\bar{x}$) :	2459.6	1760.7	-0.816	1794.3	-0.843	Very Coarse Sand
SORTING (σ):	1769.3	2.336	1.224	2.357	1.237	Poorly Sorted
SKEWNESS (Sk):	0.401	-0.198	0.198	-0.047	0.047	Symmetrical
KURTOSIS (K):	1.424	1.977	1.977	0.605	0.605	Very Platykurtic

GRAIN SIZE DISTRIBUTION

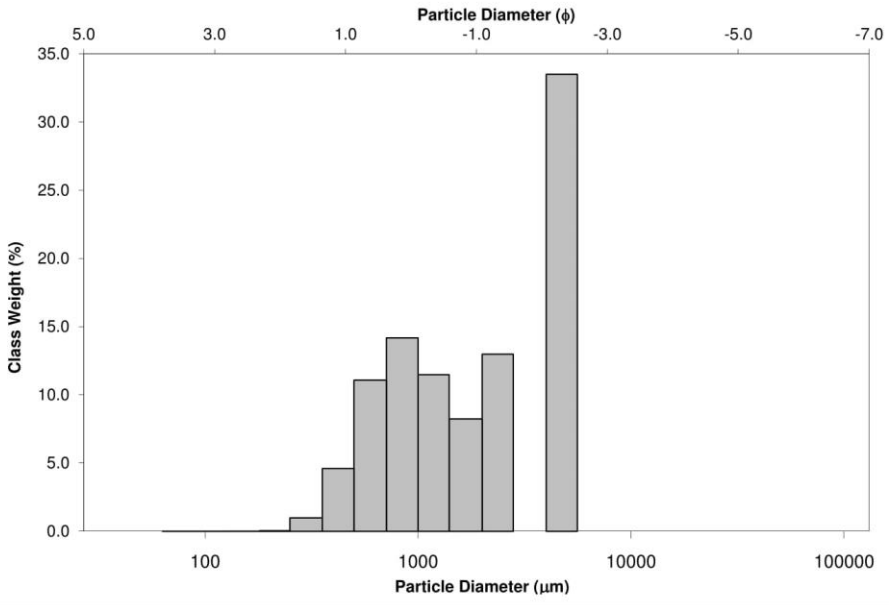

SAMPLE STATISTICS

SIEVING ERROR: 4.2%

SAMPLE IDENTITY: **OF 9**

ANALYST & DATE: ,

SAMPLE TYPE: Unimodal, Moderately Sorted

TEXTURAL GROUP: Gravelly Sand

SEDIMENT NAME: Very Fine Gravelly Coarse Sand

	μm	ϕ
MODE 1:	855.0	0.247
MODE 2:		
MODE 3:		
D_{10}:	482.8	-0.969
MEDIAN or D_{50}:	893.6	0.162
D_{90}:	1957.9	1.051
(D_{90} / D_{10}):	4.055	-1.084
(D_{90} - D_{10}):	1475.1	2.020
(D_{75} / D_{25}):	2.075	-1.657
(D_{75} - D_{25}):	681.7	1.053

GRAIN SIZE DISTRIBUTION

GRAVEL:	9.3%	COARSE SAND:	48.0%
SAND:	90.7%	MEDIUM SAND:	10.9%
MUD:	0.0%	FINE SAND:	0.1%
		V FINE SAND:	0.0%
V COARSE GRAVEL:	0.0%	V COARSE SILT:	0.0%
COARSE GRAVEL:	0.0%	COARSE SILT:	0.0%
MEDIUM GRAVEL:	0.0%	MEDIUM SILT:	0.0%
FINE GRAVEL:	1.2%	FINE SILT:	0.0%
V FINE GRAVEL:	8.1%	V FINE SILT:	0.0%
V COARSE SAND:	31.7%	CLAY:	0.0%

	METHOD OF MOMENTS			FOLK & WARD METHOD		
	Arithmetic μm	Geometric μm	Logarithmic ϕ	Geometric μm	Logarithmic ϕ	Description
MEAN ($\bar{x}$) :	1096.4	931.0	0.103	927.8	0.108	Coarse Sand
SORTING (σ):	682.2	1.701	0.766	1.726	0.787	Moderately Sorted
SKEWNESS (Sk):	2.355	0.273	-0.273	0.103	-0.103	Coarse Skewed
KURTOSIS (K):	11.70	3.644	3.644	1.001	1.001	Mesokurtic

GRAIN SIZE DISTRIBUTION

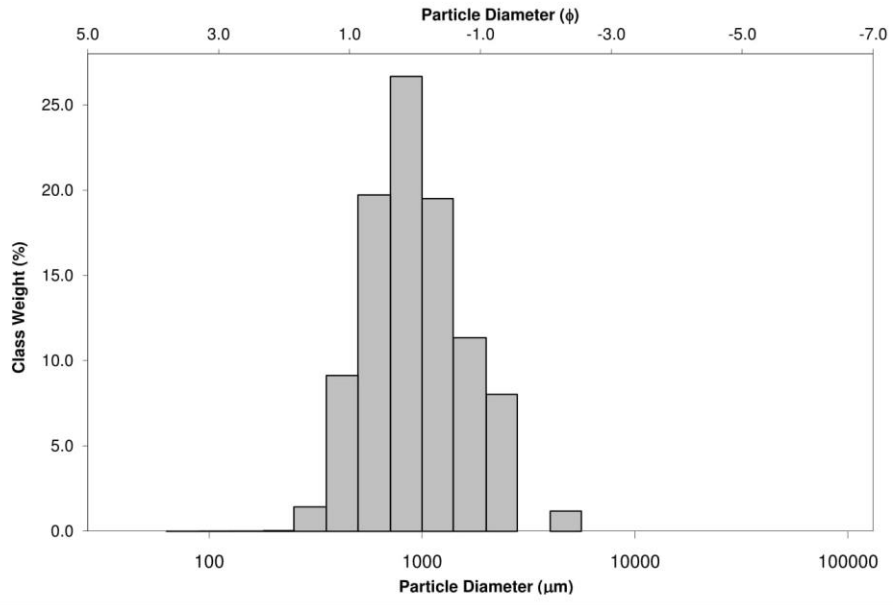

SAMPLE STATISTICS

SIEVING ERROR: 4.2%

SAMPLE IDENTITY: **OF 10A** ANALYST & DATE: ,

SAMPLE TYPE: Unimodal, Moderately Sorted TEXTURAL GROUP: Slightly Gravelly Sand

SEDIMENT NAME: Slightly Very Fine Gravelly Coarse Sand

	μm	ϕ
MODE 1:	855.0	0.247
MODE 2:		
MODE 3:		
D_{10}:	394.0	-0.509
MEDIAN or D_{50}:	766.9	0.383
D_{90}:	1423.4	1.344
(D_{90} / D_{10}):	3.613	-2.639
(D_{90} - D_{10}):	1029.4	1.853
(D_{75} / D_{25}):	1.989	-10.118
(D_{75} - D_{25}):	529.1	0.992

GRAIN SIZE DISTRIBUTION

GRAVEL:	2.6%	COARSE SAND:	51.1%
SAND:	97.4%	MEDIUM SAND:	20.4%
MUD:	0.0%	FINE SAND:	0.2%
		V FINE SAND:	0.0%
V COARSE GRAVEL:	0.0%	V COARSE SILT:	0.0%
COARSE GRAVEL:	0.0%	COARSE SILT:	0.0%
MEDIUM GRAVEL:	0.0%	MEDIUM SILT:	0.0%
FINE GRAVEL:	0.1%	FINE SILT:	0.0%
V FINE GRAVEL:	2.6%	V FINE SILT:	0.0%
V COARSE SAND:	25.7%	CLAY:	0.0%

	METHOD OF MOMENTS			FOLK & WARD METHOD		
	Arithmetic μm	Geometric μm	Logarithmic ϕ	Geometric μm	Logarithmic ϕ	Description
MEAN ($\bar{x}$) :	872.0	761.5	0.393	758.1	0.400	Coarse Sand
SORTING (σ):	456.3	1.633	0.708	1.659	0.730	Moderately Sorted
SKEWNESS (Sk):	1.685	-0.012	0.012	-0.001	0.001	Symmetrical
KURTOSIS (K):	8.629	3.704	3.704	0.980	0.980	Mesokurtic

GRAIN SIZE DISTRIBUTION

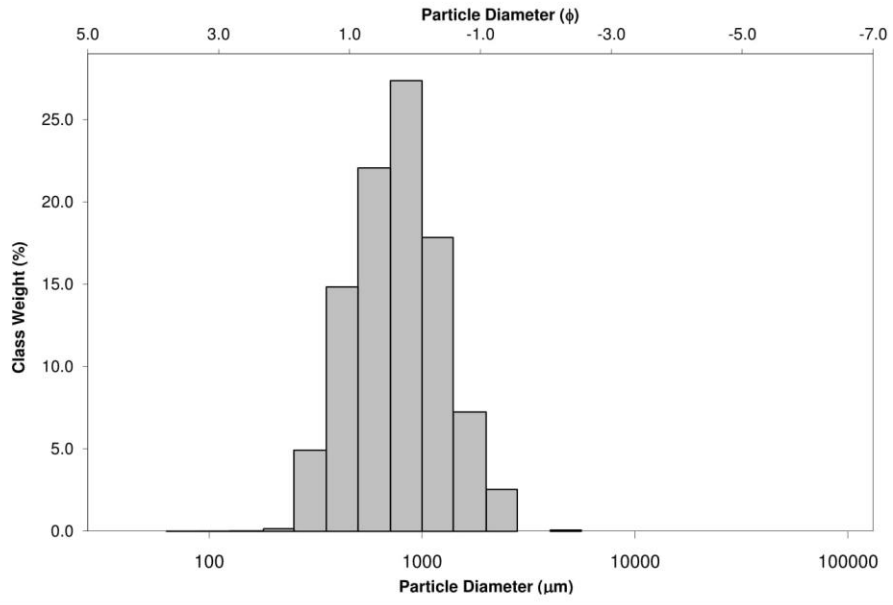

SAMPLE STATISTICS

SAMPLE IDENTITY: **OF 11** ANALYST & DATE: ,

SAMPLE TYPE: Polymodal, Poorly Sorted TEXTURAL GROUP: Sandy Gravel

SEDIMENT NAME: Sandy Fine Gravel

	µm	ϕ
MODE 1:	4800.0	-2.243
MODE 2:	427.5	1.247
MODE 3:	855.0	0.247
D_{10}:	380.0	-2.374
MEDIAN or D_{50}:	2094.3	-1.066
D_{90}:	5182.8	1.396
(D_{90} / D_{10}):	13.64	-0.588
(D_{90} - D_{10}):	4802.8	3.770
(D_{75} / D_{25}):	7.276	-0.298
(D_{75} - D_{25}):	3980.3	2.863

GRAIN SIZE DISTRIBUTION

GRAVEL:	51.0%	COARSE SAND:	18.0%
SAND:	48.9%	MEDIUM SAND:	18.3%
MUD:	0.0%	FINE SAND:	0.6%
		V FINE SAND:	0.1%
V COARSE GRAVEL:	0.0%	V COARSE SILT:	0.0%
COARSE GRAVEL:	0.0%	COARSE SILT:	0.0%
MEDIUM GRAVEL:	0.0%	MEDIUM SILT:	0.0%
FINE GRAVEL:	43.5%	FINE SILT:	0.0%
V FINE GRAVEL:	7.6%	V FINE SILT:	0.0%
V COARSE SAND:	12.0%	CLAY:	0.0%

	METHOD OF MOMENTS			FOLK & WARD METHOD		
	Arithmetic µm	Geometric µm	Logarithmic ϕ	Geometric µm	Logarithmic ϕ	Description
MEAN ($\bar{x}$) :	2639.2	1684.4	-0.752	1678.3	-0.747	Very Coarse Sand
SORTING (σ):	1963.7	2.843	1.507	2.798	1.484	Poorly Sorted
SKEWNESS (Sk):	0.086	-0.389	0.389	-0.309	0.309	Very Fine Skewed
KURTOSIS (K):	1.164	1.776	1.776	0.590	0.590	Very Platykurtic

GRAIN SIZE DISTRIBUTION

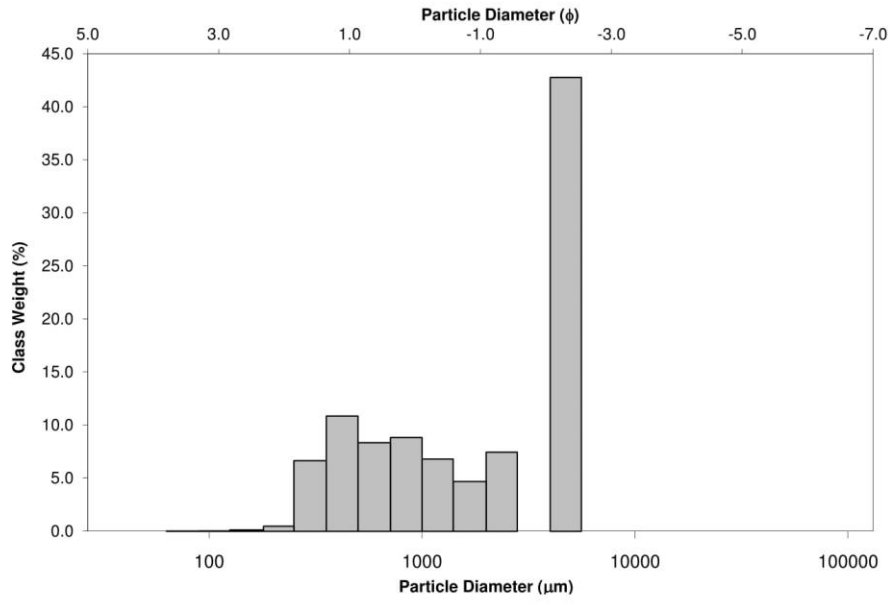

SAMPLE STATISTICS

SAMPLE IDENTITY: **OF 12A** ANALYST & DATE: ,

SAMPLE TYPE: Bimodal, Moderately Sorted TEXTURAL GROUP: Gravel

SEDIMENT NAME: Fine Gravel

	μm	ϕ
MODE 1:	4800.0	-2.243
MODE 2:	2400.0	-1.243
MODE 3:		
D_{10}:	1240.0	-2.412
MEDIAN or D_{50}:	4341.3	-2.118
D_{90}:	5322.0	-0.310
(D_{90} / D_{10}):	4.292	0.129
(D_{90} - D_{10}):	4082.0	2.102
(D_{75} / D_{25}):	2.107	0.533
(D_{75} - D_{25}):	2591.0	1.075

GRAIN SIZE DISTRIBUTION

GRAVEL:	82.8%	COARSE SAND:	2.3%
SAND:	17.1%	MEDIUM SAND:	4.7%
MUD:	0.1%	FINE SAND:	1.4%
		V FINE SAND:	0.2%
V COARSE GRAVEL:	0.0%	V COARSE SILT:	0.0%
COARSE GRAVEL:	0.0%	COARSE SILT:	0.0%
MEDIUM GRAVEL:	0.0%	MEDIUM SILT:	0.0%
FINE GRAVEL:	66.1%	FINE SILT:	0.0%
V FINE GRAVEL:	16.7%	V FINE SILT:	0.0%
V COARSE SAND:	8.6%	CLAY:	0.0%

	METHOD OF MOMENTS			FOLK & WARD METHOD		
	Arithmetic μm	Geometric μm	Logarithmic ϕ	Geometric μm	Logarithmic ϕ	Description
MEAN ($\bar{x}$) :	3744.6	3062.7	-1.615	3473.1	-1.796	Very Fine Gravel
SORTING (σ):	1549.7	2.186	1.128	1.916	0.938	Moderately Sorted
SKEWNESS (Sk):	-1.003	-2.308	2.308	-0.742	0.742	Very Fine Skewed
KURTOSIS (K):	2.452	9.169	9.169	1.438	1.438	Leptokurtic

GRAIN SIZE DISTRIBUTION

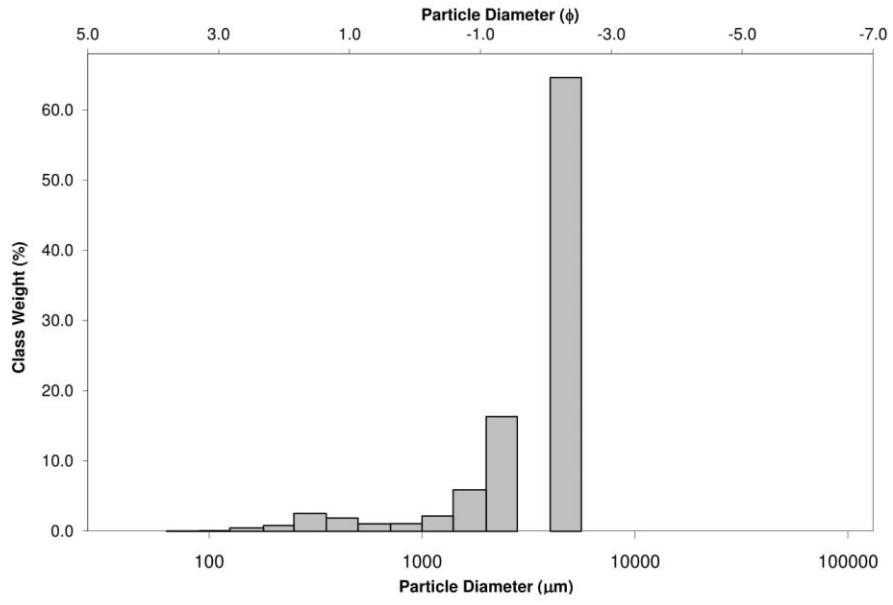

SAMPLE STATISTICS

SAMPLE IDENTITY: **OF 13** ANALYST & DATE: ,

SAMPLE TYPE: Unimodal, Very Well Sorted TEXTURAL GROUP: Gravel

SEDIMENT NAME: Fine Gravel

	μm	ϕ
MODE 1:	4800.0	-2.243
MODE 2:		
MODE 3:		
D_{10}:	4018.6	-2.432
MEDIAN or D_{50}:	4657.2	-2.219
D_{90}:	5397.3	-2.007
(D_{90} / D_{10}):	1.343	0.825
(D_{90} - D_{10}):	1378.7	0.426
(D_{75} / D_{25}):	1.202	0.887
(D_{75} - D_{25}):	859.8	0.266

GRAIN SIZE DISTRIBUTION

GRAVEL:	95.9%	COARSE SAND:	0.5%
SAND:	3.9%	MEDIUM SAND:	0.5%
MUD:	0.2%	FINE SAND:	0.2%
		V FINE SAND:	0.2%
V COARSE GRAVEL:	0.0%	V COARSE SILT:	0.0%
COARSE GRAVEL:	0.0%	COARSE SILT:	0.0%
MEDIUM GRAVEL:	0.0%	MEDIUM SILT:	0.0%
FINE GRAVEL:	91.3%	FINE SILT:	0.0%
V FINE GRAVEL:	4.6%	V FINE SILT:	0.0%
V COARSE SAND:	2.4%	CLAY:	0.0%

	METHOD OF MOMENTS			FOLK & WARD METHOD		
	Arithmetic μm	Geometric μm	Logarithmic ϕ	Geometric μm	Logarithmic ϕ	Description
MEAN ($\bar{x}$) :	4530.9	4208.1	-2.073	4657.2	-2.219	Fine Gravel
SORTING (σ):	902.1	1.670	0.740	1.229	0.298	Very Well Sorted
SKEWNESS (Sk):	-3.331	-7.234	7.234	-0.325	0.325	Very Fine Skewed
KURTOSIS (K):	13.12	71.04	71.04	2.109	2.109	Very Leptokurtic

GRAIN SIZE DISTRIBUTION

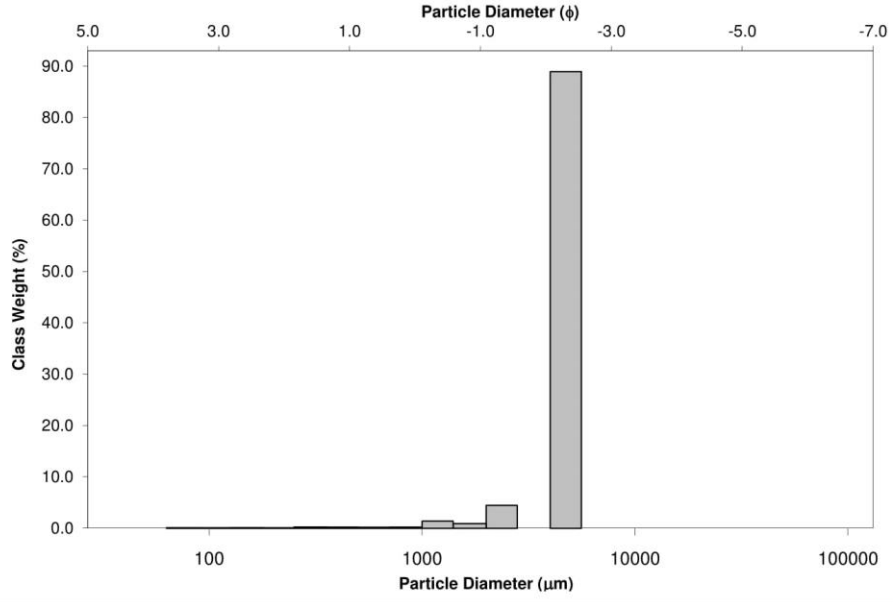

SAMPLE STATISTICS

SIEVING ERROR: 4.2%

SAMPLE IDENTITY: **OF 14**

ANALYST & DATE: ,

SAMPLE TYPE: Bimodal, Moderately Sorted

TEXTURAL GROUP: Gravelly Sand

SEDIMENT NAME: Very Fine Gravelly Very Coarse Sand

	μm	ϕ
MODE 1:	1200.0	-0.243
MODE 2:	4800.0	-2.243
MODE 3:		
D_{10}:	411.2	-1.276
MEDIAN or D_{50}:	1097.1	-0.134
D_{90}:	2421.2	1.282
(D_{90} / D_{10}):	5.889	-1.005
(D_{90} - D_{10}):	2010.0	2.558
(D_{75} / D_{25}):	2.829	-0.808
(D_{75} - D_{25}):	1149.4	1.500

GRAIN SIZE DISTRIBUTION

GRAVEL:	19.3%	COARSE SAND:	28.1%
SAND:	80.7%	MEDIUM SAND:	16.6%
MUD:	0.0%	FINE SAND:	0.2%
		V FINE SAND:	0.0%
V COARSE GRAVEL:	0.0%	V COARSE SILT:	0.0%
COARSE GRAVEL:	0.0%	COARSE SILT:	0.0%
MEDIUM GRAVEL:	0.0%	MEDIUM SILT:	0.0%
FINE GRAVEL:	3.0%	FINE SILT:	0.0%
V FINE GRAVEL:	16.3%	V FINE SILT:	0.0%
V COARSE SAND:	35.8%	CLAY:	0.0%

	METHOD OF MOMENTS			FOLK & WARD METHOD		
	Arithmetic μm	Geometric μm	Logarithmic ϕ	Geometric μm	Logarithmic ϕ	Description
MEAN ($\bar{x}$) :	1324.4	1052.4	-0.074	1046.5	-0.066	Very Coarse Sand
SORTING (σ):	905.8	1.955	0.967	1.965	0.974	Moderately Sorted
SKEWNESS (Sk):	1.686	-0.161	0.161	-0.105	0.105	Fine Skewed
KURTOSIS (K):	7.005	3.089	3.089	0.796	0.796	Platykurtic

GRAIN SIZE DISTRIBUTION

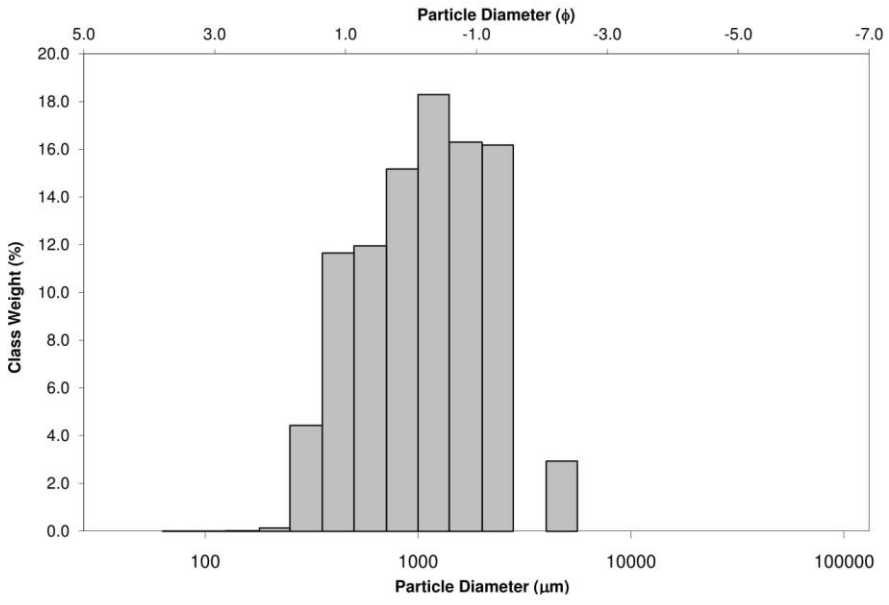

SAMPLE STATISTICS

SIEVING ERROR: 3.0%

SAMPLE IDENTITY: **OF 15**

ANALYST & DATE: ,

SAMPLE TYPE: Unimodal, Moderately Sorted

TEXTURAL GROUP: Slightly Gravelly Sand

SEDIMENT NAME: Slightly Very Fine Gravelly Coarse Sand

	μm	ϕ
MODE 1:	855.0	0.247
MODE 2:		
MODE 3:		
D_{10}:	389.0	-0.561
MEDIAN or D_{50}:	758.4	0.399
D_{90}:	1475.7	1.362
(D_{90} / D_{10}):	3.794	-2.427
(D_{90} - D_{10}):	1086.7	1.924
(D_{75} / D_{25}):	2.051	-10.585
(D_{75} - D_{25}):	545.3	1.037

GRAIN SIZE DISTRIBUTION

GRAVEL:	3.8%	COARSE SAND:	49.2%
SAND:	96.2%	MEDIUM SAND:	22.5%
MUD:	0.0%	FINE SAND:	0.2%
		V FINE SAND:	0.0%
V COARSE GRAVEL:	0.0%	V COARSE SILT:	0.0%
COARSE GRAVEL:	0.0%	COARSE SILT:	0.0%
MEDIUM GRAVEL:	0.0%	MEDIUM SILT:	0.0%
FINE GRAVEL:	0.4%	FINE SILT:	0.0%
V FINE GRAVEL:	3.4%	V FINE SILT:	0.0%
V COARSE SAND:	24.4%	CLAY:	0.0%

	METHOD OF MOMENTS			FOLK & WARD METHOD		
	Arithmetic μm	Geometric μm	Logarithmic ϕ	Geometric μm	Logarithmic ϕ	Description
MEAN ($\bar{x}$) :	884.5	759.5	0.397	750.1	0.415	Coarse Sand
SORTING (σ):	526.4	1.672	0.742	1.687	0.755	Moderately Sorted
SKEWNESS (Sk):	2.550	0.187	-0.187	0.021	-0.021	Symmetrical
KURTOSIS (K):	15.27	3.875	3.875	0.967	0.967	Mesokurtic

GRAIN SIZE DISTRIBUTION

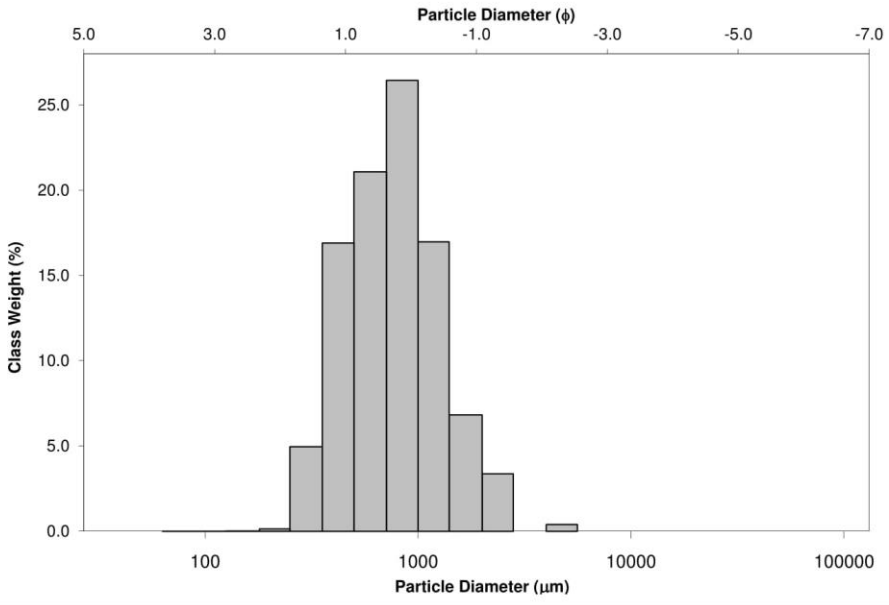

SAMPLE STATISTICS

SIEVING ERROR: 2.9%

SAMPLE IDENTITY: **OF 16**

ANALYST & DATE: ,

SAMPLE TYPE: Unimodal, Moderately Well Sorted TEXTURAL GROUP: Slightly Gravelly Sand

SEDIMENT NAME: Slightly Very Fine Gravelly Coarse Sand

	μm	ϕ
MODE 1:	427.5	1.247
MODE 2:		
MODE 3:		
D_{10}:	364.1	0.072
MEDIAN or D_{50}:	546.3	0.872
D_{90}:	951.4	1.458
(D_{90} / D_{10}):	2.613	20.26
(D_{90} - D_{10}):	587.3	1.386
(D_{75} / D_{25}):	1.671	2.486
(D_{75} - D_{25}):	284.2	0.741

GRAIN SIZE DISTRIBUTION

GRAVEL: 0.9%	COARSE SAND: 51.1%
SAND: 99.1%	MEDIUM SAND: 41.3%
MUD: 0.0%	FINE SAND: 0.1%
	V FINE SAND: 0.0%
V COARSE GRAVEL: 0.0%	V COARSE SILT: 0.0%
COARSE GRAVEL: 0.0%	COARSE SILT: 0.0%
MEDIUM GRAVEL: 0.0%	MEDIUM SILT: 0.0%
FINE GRAVEL: 0.1%	FINE SILT: 0.0%
V FINE GRAVEL: 0.8%	V FINE SILT: 0.0%
V COARSE SAND: 6.6%	CLAY: 0.0%

	METHOD OF MOMENTS			FOLK & WARD METHOD		
	Arithmetic μm	Geometric μm	Logarithmic ϕ	Geometric μm	Logarithmic ϕ	Description
MEAN ($\bar{x}$) :	631.3	568.8	0.814	562.9	0.829	Coarse Sand
SORTING (σ):	325.9	1.490	0.575	1.487	0.573	Moderately Well Sorted
SKEWNESS (Sk):	3.627	0.729	-0.729	0.144	-0.144	Coarse Skewed
KURTOSIS (K):	29.09	5.362	5.362	1.063	1.063	Mesokurtic

GRAIN SIZE DISTRIBUTION

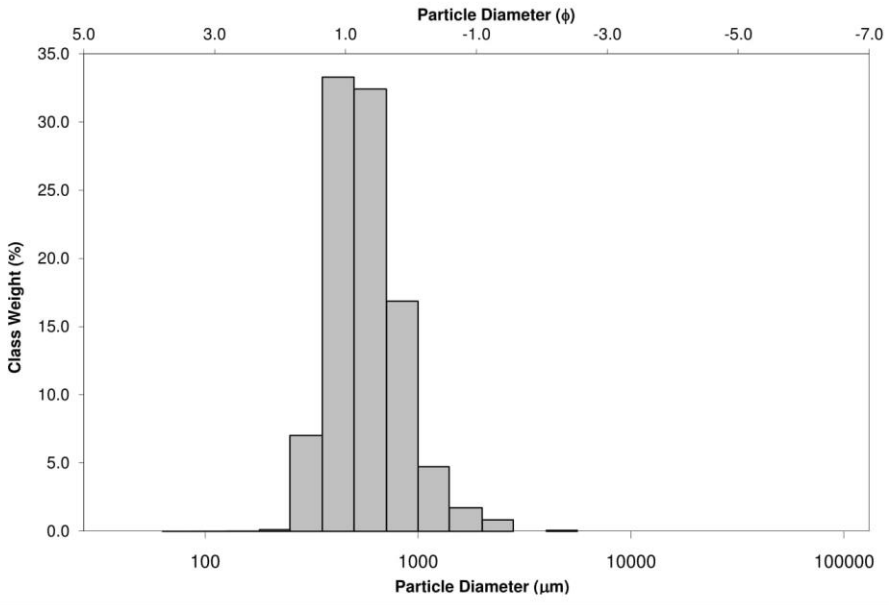

SAMPLE STATISTICS

SAMPLE IDENTITY: **OF 17**

ANALYST & DATE: ,

SAMPLE TYPE: Trimodal, Poorly Sorted

TEXTURAL GROUP: Sandy Gravel

SEDIMENT NAME: Sandy Very Fine Gravel

	μm	ϕ
MODE 1:	2400.0	-1.243
MODE 2:	427.5	1.247
MODE 3:	4800.0	-2.243
D_{10}:	355.3	-1.423
MEDIAN or D_{50}:	1237.7	-0.308
D_{90}:	2682.3	1.493
(D_{90} / D_{10}):	7.549	-1.049
(D_{90} - D_{10}):	2327.0	2.916
(D_{75} / D_{25}):	4.061	-0.826
(D_{75} - D_{25}):	1623.5	2.022

GRAIN SIZE DISTRIBUTION

GRAVEL:	30.1%	COARSE SAND:	19.0%
SAND:	69.9%	MEDIUM SAND:	23.1%
MUD:	0.0%	FINE SAND:	0.4%
		V FINE SAND:	0.0%
V COARSE GRAVEL:	0.0%	V COARSE SILT:	0.0%
COARSE GRAVEL:	0.0%	COARSE SILT:	0.0%
MEDIUM GRAVEL:	0.0%	MEDIUM SILT:	0.0%
FINE GRAVEL:	7.1%	FINE SILT:	0.0%
V FINE GRAVEL:	23.0%	V FINE SILT:	0.0%
V COARSE SAND:	27.5%	CLAY:	0.0%

	METHOD OF MOMENTS			FOLK & WARD METHOD		
	Arithmetic μm	Geometric μm	Logarithmic ϕ	Geometric μm	Logarithmic ϕ	Description
MEAN ($\bar{x}$) :	1525.8	1110.7	-0.151	1079.6	-0.110	Very Coarse Sand
SORTING (σ):	1176.8	2.246	1.168	2.351	1.233	Poorly Sorted
SKEWNESS (Sk):	1.329	-0.125	0.125	-0.145	0.145	Fine Skewed
KURTOSIS (K):	4.568	2.055	2.055	0.790	0.790	Platykurtic

GRAIN SIZE DISTRIBUTION